ON THE DYNAMICS OF SPACECRAFT WITH FLEXIBLE, DEPLOYABLE AND SLEWING APPENDAGES

by

Qianruo Shen

B.Sc., Peking University, 1970

M.Eng., Beijing University of Aeronautics and Astronautics, 1983

A THESIS SUBMITTED IN PARTIAL FULFILLMENT
OF THE REQUIREMENTS FOR THE DEGREE OF
DOCTOR OF PHILOSOPHY
in the Department
of
Mathematics & Statistics

SIMON FRASER UNIVERSITY

August 1993

APPROVAL

Name: Qianruo Shen

Degree: Doctor of Philosophy

Title of thesis: On the Dynamics of Spacecraft with Flexible, Deployable and Slewing Appendages

Examining Committee:

Chairman: Dr. S. K. Thomason

Dr. V. J. Modi
Senior Supervisor

Dr. M. Singh
Supervisor

Dr. C. Y. Shen
Supervisor

Dr. G. A. C. Graham

Dr. B. Tabarrok
Department of Mechanical Engineering
University of Victoria
External Examiner

Date Approved: August 13, 1993

PARTIAL COPYRIGHT LICENSE

I hereby grant to Simon Fraser University the right to lend my thesis, project or extended essay (the title of which is shown below) to users of the Simon Fraser University Library, and to make partial or single copies only for such users or in response to a request from the library of any other university, or other educational institution, on its own behalf or for one of its users. I further agree that permission for multiple copying of this work for scholarly purposes may be granted by me or the Dean of Graduate Studies. It is understood that copying or publication of this work for financial gain shall not be allowed without my written permission.

Title of Thesis/Project/Extended Essay

On the Dynamics of Spacecraft with Flexible, Deployable and Slewing Appendages

Author:

(signature)

Qianrao Shen

(name)

June 21, 1993

(date)

ABSTRACT

A relatively general dynamical formulation applicable to a large class of systems, characterized by a rigid central body with flexible, deployable and slewing appendages, is presented. In general, the extremely lengthy, highly nonlinear, nonautonomous and coupled equations of motion are not amenable to any closed-form solution. A general purpose computer code is developed, in a modular fashion, to help undertake a parametric study of the system dynamics. Validity of the formulation and the computer code are assessed through comparison with known particular cases.

Versatility of this formulation is illustrated through its application to a variety of spacecraft configurations of contemporary interest. To that end, two distinctly different approaches are used:

I. Analytical procedures for simple rigid as well as flexible systems. This involves stability study using the Liapunov method; and planar dynamics of a satellite with a flexible slewing appendage.

II. Numerical simulation of the complete nonlinear, nonautonomous and coupled equations of motion to study dynamics of:

   (a) a Japanese spacecraft called the Space Flyer Unit (SFU) to be launched in February 1994;

   (b) the Space Shuttle based slewing mast, similar to the experiment once proposed by NASA;

   (c) the Two-Dimensionally Deployable Array, an experiment that will be carried out using the SFU.

Besides showing the potential of the methodology developed, the results obtained are of fundamental character and have long range value to spacecraft design engineers.

TO THE MEMORY OF MY FATHER

ZUXIAN SHEN

—A GREAT AERONAUTICAL ENGINEER

ACKNOWLEDGEMENT

I would like to thank Professor V. J. Modi for his ingenious guidance during the preparation of the thesis.

I would also like to thank Professor M. Singh for his help throughout my Ph.D. program and the financial support by his NSERC grant.

The research project has been supported by the Department of Mathematics and Statistics, Simon Fraser University. A special thank goes to Professors A. H. Lachlan and S. Thomason for their effort in the completion of this project.

Mr. Lixin Liu provided valuable assistance with computer work, his time and effort are appreciated.

TABLE OF CONTENTS

LIST OF SYMBOLS

$[A]$	transformation matrix from the coordinate system $C - X, Y, Z$ to $C - x_c, y_c, z_c$
$[\ a_i\ ]$	transposition of the i-th column of $[A]$
$\overline{\overline{AB}}$	$\overline{A} \cdot \overline{B}\ \overline{\overline{I}} - \overline{B}\ \overline{A}$, a tensor composed of two vectors
$[B_i]$	a matrix relating components of the angular velocity of body i with the angular rates $\dot{\alpha}_i$; $\overline{\omega}_i = [\ \dot{\alpha}_i\ ]\,[B_i]\,[\ \overline{e}_i\ ]^T$
C	mass center of the spacecraft
$C - X, Y, Z$	orbiting coordinate system with origin at the center of mass of the spacecraft
$C - x_c, y_c, z_c$	coordinate system with the origin at the center of mass of the spacecraft and the directions of its axes fixed on the central body, referred to as 'system frame' and used to identify the libration of the spacecraft
$[C_i]$	transformation matrix from the coordinate system $o_o - x_o, y_o, z_o$ to $o_i - x_i, y_i, z_i$
d_i	half-width of the appendage i
dm_i	mass element of body i
dv_i	volume element of body i
$\overline{d}_i$	direction vector for the velocity of dm_i due to deployment or retrieval
$[\ d_i\ ]$	row matrix of components of $\overline{d}_i$; $\overline{d}_i = [\ \overline{e}_i\ ][\ d_i\ ]^T$
$\overline{D}_i$	$\int \overline{r}_i \times \overline{d}_i\ dm_i$
$[\ D_i\ ]$	row matrix of components of $\overline{D}_i$; $\overline{D}_i = [\ \overline{e}_i\ ][\ D_i\ ]^T$
$[\ \overline{e}_i\ ]$	$[\overline{i}_i\ \ \overline{j}_i\ \ \overline{k}_i]$
$[f_i]$	matrix of modal functions for appendage i
$[\ \overline{f}_i\ ]$	$[\ \overline{e}_i\ ][f_i]$
$[\ f_i\ ]$	row matrix of modal functions for appendage i
$[f_i']$	$[\frac{\partial f_i}{\partial \xi_i}]$
$[F_i]$	$\int [f_i] dm_i$
$[\ \overline{F}_i\ ]$	$[\ \overline{e}_i\ ][F_i]$

$[F_i^1]$	$\int [x_i\ y_i\ z_i][f_i]dm_i$
$[F_i^2]$	$\int [f_i]^T[f_i]dm_i$
$[F_i^3]$	$\int [\ f_i\ ]^T[\ f_i\ ]dm_i$
$[F_i^{11}]$	$\int [x_i\ y_i\ z_i]^T[\ f_i\ ]dm_i$
$[F_i^{1*}]$	$\int [x_i\ y_i\ z_i]^*[f_i]dm_i$
$[F_i^p]$	$\int \frac{l_i - z_i}{l_i^2}\,[f_i']\,dm_i$
$[F_i^4]$	$\int \frac{l_i - z_i}{l_i^2}\,[f_i']\,[f_i]\,dm_i$
$[F_i^5]$	$\int (\frac{l_i - z_i}{l_i^2})^2\,[f_i']^T\,[f_i']\,dm_i$
$[F_i^6]$	$\int \frac{l_i - z_i}{l_i^2}[x_i\ y_i\ z_i]^*\,[f_i']\,dm_i$
$[F_i^u]$	$\int ([\ u_i\ ]\,[f_i]^T)^*\,[f_i]\,dm_i$
$[F_i^{u1}]$	$\int \frac{l_i - z_i}{l_i^2}([\ u_i\ ]\,[f_i]^T)^*\,[f_i']\,dm_i$
$\overline{G}$	relative angular momentum of the spacecraft w.r.t. the system frame due to relative motions
$\overline{H}_i$	$\int \overline{r}_i dm_i$
$[\ H_i\ ]$	row matrix of components of $\overline{H}_i$; $\overline{H}_i = [\ \overline{e}_i\ ][\ H_i\ ]^T$
$\overline{H}_i'$	$\frac{\partial \overline{H}_i}{\partial l_i} = \int \overline{d}_i dm_i$
$[\ H_i'\ ]$	row matrix of components of $\overline{H}_i'$; $\overline{H}_i' = [\ \overline{e}_i\ ][\ H_i'\ ]^T$
$\overline{\overline{I}}$	unit tensor
$[I]$	unit matrix
$[\overline{i}\ \ \overline{j}\ \ \overline{k}]$	unit vectors along the axes of the orbiting coordinate system
$[\overline{i}_i\ \overline{j}_i\ \overline{k}_i]$	unit vectors along the axes of the body i fixed system
$\overline{\overline{J}}_i$	inertia tensor of body i at hinge o_i, $\overline{\overline{J}}_i = \int (\overline{r}_i \cdot \overline{r}_i \overline{\overline{I}} - \overline{r}_i \overline{r}_i) dm_i$
$[J_i]$	coordinate matrix of $\overline{\overline{J}}_i$, $\overline{\overline{J}}_i = [\ \overline{e}_i\ ]\,[J_i]\,[\ \overline{e}_i\ ]^T$
J_i^0, $[J_i^1]$	$[J_i] = J_i^0\,[I] - [J_i^1]$
J_{iu}^0, $[J_{iu}^1]$	$[J_{iu}] = J_{iu}^0\,[I] - [J_{iu}^1]$, where $[J_{iu}]$ is the coordinate matrix of the inertia tensor of the undeformed appendage i
$\overline{\overline{J}}$	instantanius inertia tensor of the whole system
$[J]$	coordinate matrix of $\overline{\overline{J}}$, $\overline{\overline{J}} = [\ \overline{e}_o\ ]\,[J]\,[\ \overline{e}_o\ ]^T$
J^0, $[J^1]$	$[J] = J^0\,[I] - [J^1]$
K	constant of earth's gravitational field
l_i	length of the deployed part of appendage i
$\overline{L}_i$	vector from the mass center of the central body to hinge o_i
L_i	magnitude of $\overline{L}_i$

$[\ L_i\ ]$	row matrix of components of $\overline{L}_i$
$\overline{L}_o$	$\frac{1}{M}\sum_{i=1}^{n}\overline{L}_i$
L_o	magnitude of $\overline{L}_o$
$[\ L_o\ ]$	row matrix of components of $\overline{L}_o$
$[L_i - L_o]$	row matrix of components of $\overline{L}_i - \overline{L}_o$
$\overline{L}_{i1}$	$\overline{L}_i - \overline{L}_o - \frac{1}{M}\sum_{j=1}^{n}\overline{H}_j$
$[\ L_{i1}\ ]$	$[L_i - L_o] - \frac{1}{M}\sum_{j=1}^{n}[\ H_j\ ][C_j]$
m_i	mass of body i
M	total mass of the spacecraft
$(m_d)_i$	$\int \overline{d}_i \cdot \overline{d}_i dm_i$
$[m_{ds}]_i$	$\int \overline{d}_i \cdot [\ \overline{f}_i\ ] dm_i$
$[m_s]_i$	$\int [\ \overline{f}_i\ ]^T \cdot [\ \overline{f}_i\ ] dm_i = \int [f_i]^T\,[f_i]\,dm_i$
$[M_{12}]_i$	inertia matrix associated with the coupling between the librational motion and rotation of the appendage i
$[M_{13}]_i$	inertia matrix associated with the coupling between the librational motion and deployment or retrieval of the appendage i
$[M_{14}]_i$	inertia matrix associated with the coupling between the librational motion and elastic vibration of the appendage i
$[M_{22}]_{ij}$	inertia matrix associated with the coupling between rotations of the appendages i and j
$[M_{23}]_{ij}$	inertia matrix associated with the coupling between rotation of the appendage i and deployment or retrieval of the appendage j
$[M_{24}]_{ij}$	inertia matrix associated with the coupling between rotation of the appendage i and vibration of the appendage j
$[M_{33}]_{ij}$	inertia matrix associated with the coupling between deployment and /or retrieval maneuvers of the appendages i and j
$[M_{34}]_{ij}$	inertia matrix associated with the coupling between deployment or retrieval of the appendage i and vibration of the appendage j
$[M_{44}]_{ij}$	inertia matrix associated with the coupling between vibration of the appendages i and j
n	number of appendages of the spacecraft
O	earth's center
$O - X_o, Y_o, Z_o$	inertia coordinate system at the earth's center

o_o	mass center of the central body
o_i	position of the hinge connecting the appendage i to the central body
$o_o - x_o, y_o, z_o$	coordinate system fixed on the central body with the origin at its mass center and the three axes along its principal axes of inertia
$o_i - x_i, y_i, z_i$	coordinate system fixed on the undeformed appendage i and centered at o_i
$[\ q\ ]$	row matrix of a group of generalized coordinates
$[\ Q_q\ ]$	row matrix of generalized forces corresponding to $[\ q\ ]$
$\overline{r}_i$	vector from o_i to dm_i
$\overline{R}_o$	vector from the center of mass C of the spacecraft to the center of mass o_o of the central body
$[\ \overline{S}_i\ ]$	$\int \overline{r}_i \times [\ \overline{f}_i\ ] dm_i$
$[S_i]$	$[\ \overline{S}_i\ ] = [\ \overline{e}_i\ ][S_i]$
T	total kinetic energy of the spacecraft
T_{orb}	kinetic energy due to orbital motion of the spacecraft considered as a mass point
T_{lib}	kinetic energy of the system rotation of the spacecraft as a rigid body
T_{coup}	kinetic energy due to coupling between system rotation and appendage slew or free rotation, deployment or retrieval, and vibration
T_{rel}	kinetic energy due to relative motions
$tr.(\ldots)$	trace of tensor or square matrix
$\overline{u}_i$	elastic displacement of the mass element dm_i of the appendage i
$[\ u_i\ ]$	row matrix of the time varying generalized coordinates associated with vibration of the appendage i
$[U_i^s]$	matrix of time varying generalized coordinates associated with vibration of the appendage i
v_i	deployment (or retrieval) velocity of the appendage i
V_g	gravitational potential energy of the spacecraft
V_s	strain energy of the spacecraft
V_{si}	strain energy of the appendage i
$[\ \alpha_o\ ]$	$[\lambda,\ \phi,\ \psi]$, row matrix of the librational angles
$[\ \alpha_i\ ]$	row matrix of slew or free rotation of the appendage i
Ω	angular velocity of the orbital motion of the spacecraft

$\overline{\omega}_o$	angular velocity of libration of the spacecraft
$\overline{\omega}_i$	angular velocity of slew or free rotation of the appendage i
ν_i	density per unit length along the z_i axis of the deployed part of the appendage i
ξ	z_i/l_i
η	y_i/d_i
δ_{ij}	Kronecker deltas, $\delta_{ij} = 0$, for $i \neq j$; $\delta_{ij} = 1$, if $i = j$
$[\ \Psi(\xi)\ ]$	$[\Psi_1(\xi), \ldots, \Psi_k(\xi)]$, a row of the modal functions for bending of a cantilever beam
$[\ \Phi(\eta)\ ]$	$[\Phi_1(\eta), \ldots, \Phi_k(\eta)]$, a row of the modal functions for bending of a free-free beam
$(\dot{})$	derivative w.r.t. time; absolute time rate of change w.r.t. the inertial frame $O - X_o, Y_o, Z_o$
$(^\circ)$	relative time rate of change w.r.t. the system frame $C - x_c, y_c, z_c$
$(')$	derivative with respect to the true anomaly
$[\ ]^T$	transpose of a matrix
$[\ ]^*$	skew-symmetric matrix corresponding to the vector within the bracket
$\{\}$	column matrix

LIST OF TABLES

LIST OF FIGURES

1. INTRODUCTION

1.1 Preliminary Remarks

The motion of spacecraft presents two aspects of interest: the orbital motion of the center of mass, nominally governed by the classical Keplerian relations; and the attitude motion about its mass center referred to as libration. It is desirable for scientific and application satellites to maintain a fixed orientation with respect to the earth for successful completion of their intended objectives. Hence the spacecraft attitude dynamics has become a very active field of study since the launching of the first artificial satellite in 1957.

To maintain the satellite in a fixed orientation, active as well as passive control techniques have been adopted [1–3]. Active control procedures involve large expenditure of energy in the form of microthruster units, momentum gyros and reaction control wheels. On the other hand, the passive control aims at designing satellites with proper inertia distribution (using physical characteristics like booms, solar panels, flaps, etc.), to generate stabilizing moment in the gravity gradient field thus maintaining a specified orientation. Passive control demands very little or virtually no power consumption, however the pointing accuracy that can be achieved is limited to a few degrees. In general, communication satellites demand stationkeeping precision of around 1/10 to 1/100 of a degree. This can be achieved only through active control.

With the evolution of spacecraft in size, power and mission capabilities, dynamicists are facing increasingly challenging problems. Two major contributing issues are described below:

(a) In the early stages of space exploration, satellites were usually small in size, consisting of only a few, essentially rigid, interconnected bodies. For modern spacecraft with their large, light weight appendages in the form of solar panels, antennas, booms, masts, etc., it is no longer true. These significant changes are brought about by the following factors:

- The increasing demand on power for operation of the on board instrumentation, scientific experiments, communication systems, etc. has

been reflected in the size of the solar panels. For example, the communication satellite 'Olympus' of the European Space Agency (ESA) has two solar panels extending to 33 m for generation of 7 kW of power (Figure 1-1).

- Large members are essential in some missions. For example, the Radio Astronomy Explorer (RAE) satellite used four 228.8m antennas to detect low frequency signals.
- The U. S. proposed space station 'Freedom', to be operational towards the end of this century, will be a gigantic structure about the size of a soccer field. Serving as a multimission platform with permanent human presence on board (4–6 astronauts), it will be a multibody system with interconnected flexible (main truss, solar panels, radiators, etc.) and rigid (habitat, experiment, laboratory, etc. modules) members (Figure 1-2). The space station represents a highly flexible system with the fundamental system frequency of around 0.1 Hz.

(b) There are several other factors of importance besides flexibility. They lead to changes in shape, mass and inertia of the system.

- Depending on the spacecraft mission, often slew maneuvers are required to reorient antennas, telescopes and other scientific instruments. Manipulators mounted on the spacecraft, e.g. the Canadian built Remote Manipulator System (RMS) on the Space Shuttle, have slewing capability for launching and retrieval of spacecraft, repositioning of the payload, etc. The proposed Mobile Serving System (MSS) will assist in construction, operation and maintenance of the Space Station.
- Large and complex space structures are stored in compact forms during launch. Later, they evolve like a butterfly coming out of its cocoon. The Solar Array Flight Experiment (SAFE, 1984) involved deployment and retrieval of a solar array for testing its dynamical characteristics (Figure 1-3).
- The Space Station will be constructed using around 17 to 22 flights of the Shuttle. The structural components will be integrated using the MSS and extravehicular activities of the astronauts. Thus the Space

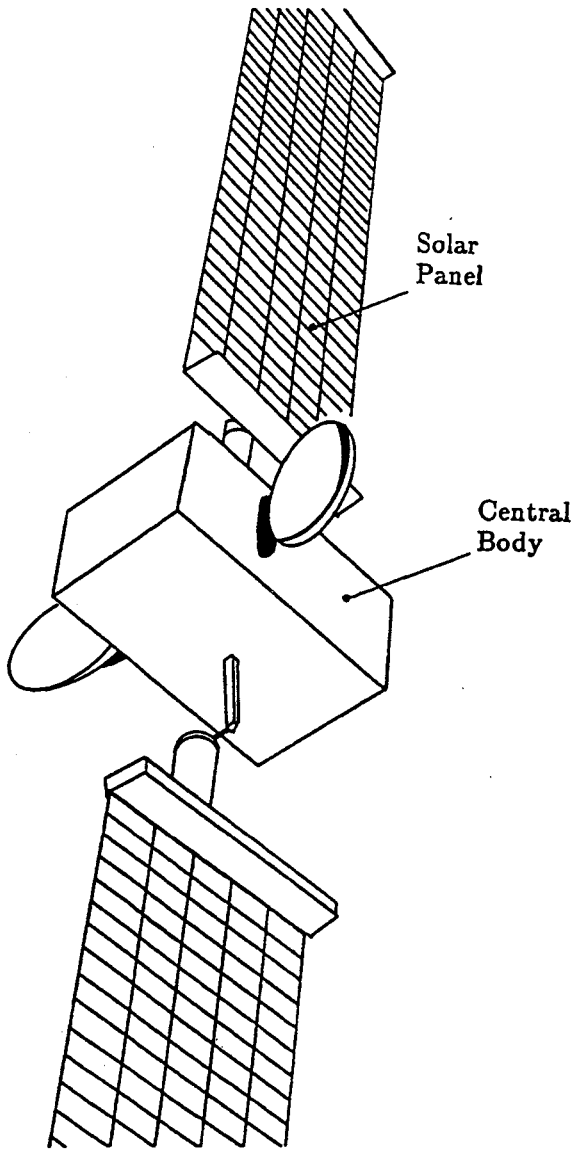

Figure 1-1 ESA's communications satellite 'Olympus'. Note the large solar panels extending to 33m.

(Provided by the Department of Mechanical Engineering, University of British Columbia)

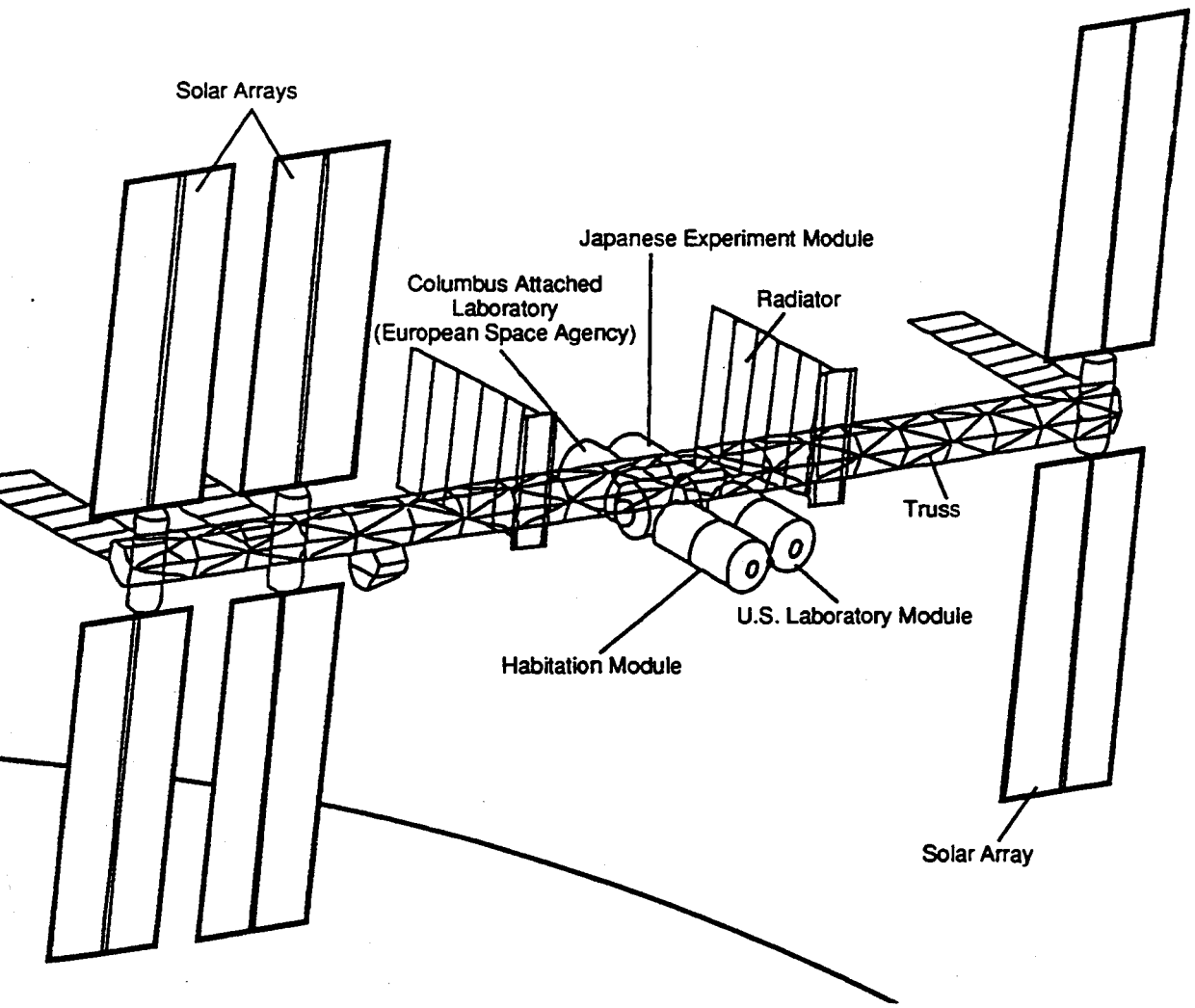

Figure 1-2 A schematic diagram of the U.S. proposed Space Station Freedom representing a system with rigid and flexible interconnected bodies.

(Provided by the Department of Mechanical Engineering, University of British Columbia)

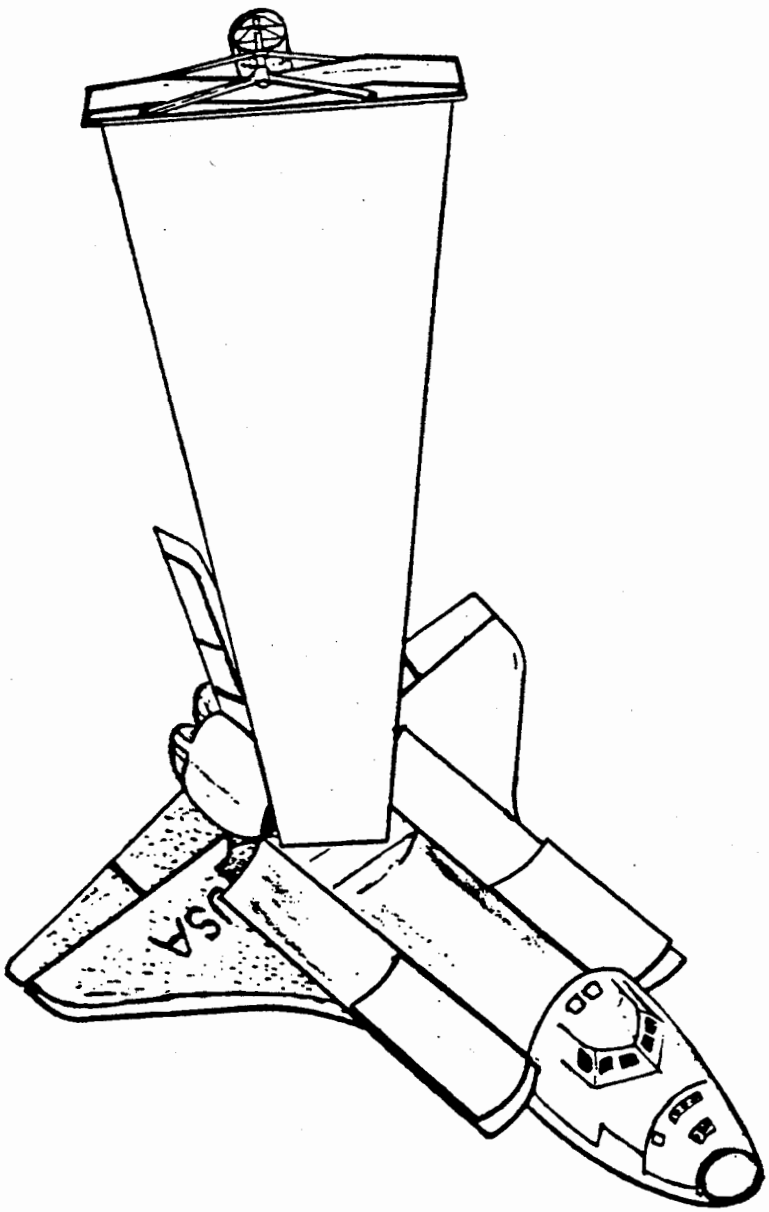

Figure 1-3 Orbiter based deployment of a 4×31 m solar array

(Provided by the Department of Mechanical Engineering, University of British Columbia)

Station represents an evolving structure with its geometry, mass, inertia, flexibility, damping, etc. characteristics changing with time. Docking of the Space Shuttle and even movement of the astronauts contribute to these effects.

Thus multi-body character, flexibility, deployment and retrieval, and slew maneuvers make the dynamical analyses of spacecraft a challenging task. Various environmental disturbances contributed by gravitational and magnetic forces of the earth, free molecular effects, solar pressure, thermal radiation, etc. add to the problem [Figure 1-4, 3].

In the early stages of the space age, when the spacecraft were small in size and essentially rigid, ground based tests proved to be adequate [3]. However, this is no longer true for modern satellites. It is commonly agreed that gravitational, magnetic, plasma, solar radiation and free molecular forces cannot be modeled precisely with the ground based simulation facilities. Hence carefully planned space based experiments are the only means of checking dynamical simulations through mathematical modeling. To that end, the NASA proposed experiment SCOLE (Spacecraft COntrol Laboratory Experiment) involves prescribed slewing maneuver of a reflector plate type antenna, attached to a flexible mast, supported by the Space Shuttle [Figure 1-5; 4,5]. Another joint experiment by NASA and the Italian Space Agency (PSN) involves deployment of a 20 km long electrodynamic tether from the Space Shuttle and its subsequent retrieval (Figure 1-6).

However, these experiments still remain proposals for the future. In fact, since launching of the Sputnik in 1957, there has not been a single successful experiment aimed at dynamics and control of flexible structures in space. The only attempt to-date has been the SAFE mentioned before which, unfortunately, failed due to the instrumentation malfunction. Furthermore, the space based experiments tend to be enormously costly. Thus the emphasis has been, and will continue to be so in future, on the development of more sophisticated and reliable mathematical models for dynamical and control analyses of such complex structures.

A comment concerning the effect of the librational and vibrational motions on the spacecraft orbit would be appropriate. It has been established that, for most practical purposes, the influence is negligible [6]. Only when the satellite dimensions become comparable to the orbital distance, the coupling effects become noticeable. In other

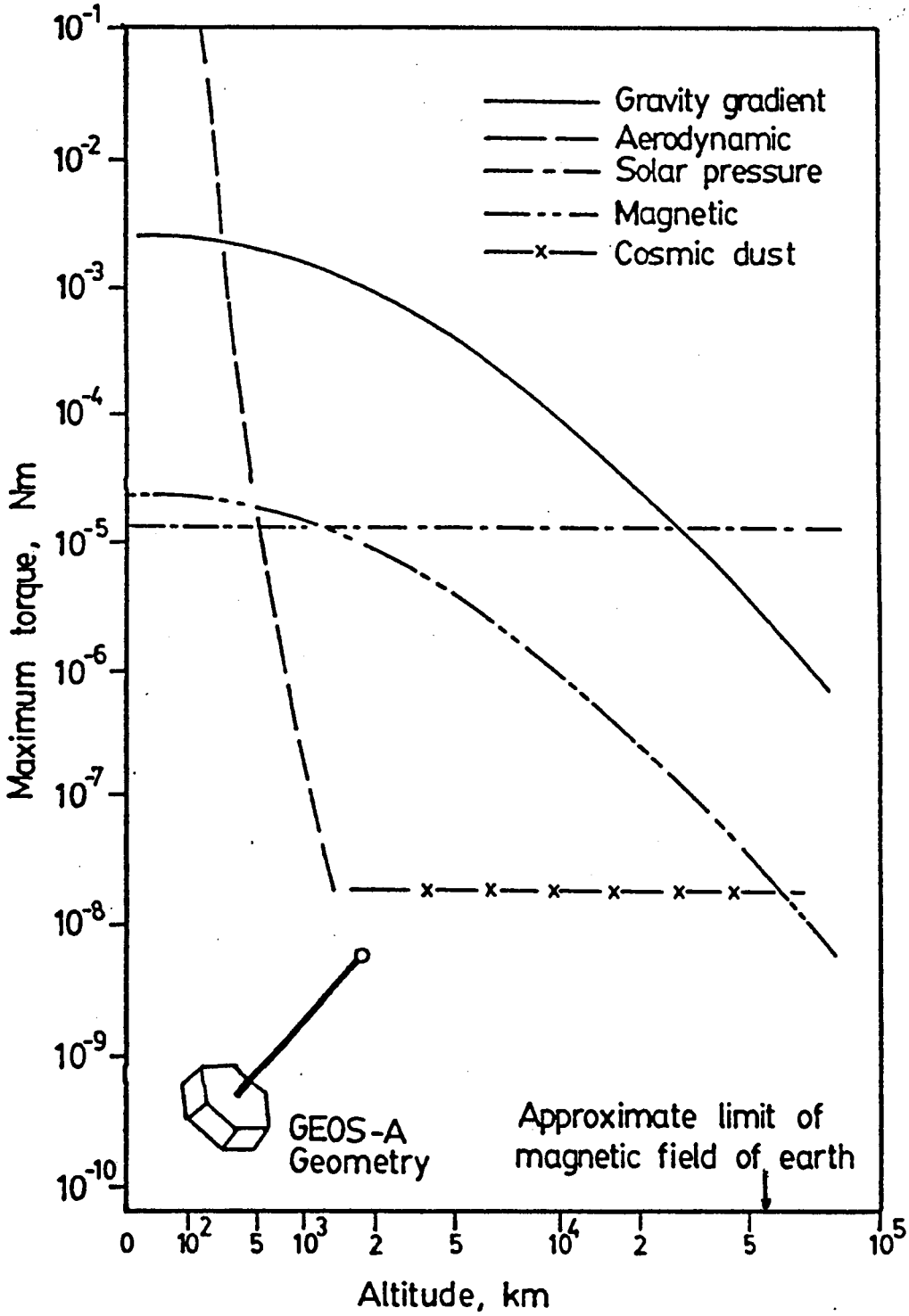

Figure 1-4 A chart showing the variation of environmental torques with altitude on the GEOS-A satellite.

(Provided by the Department of Mechanical Engineering, University of British Columbia)

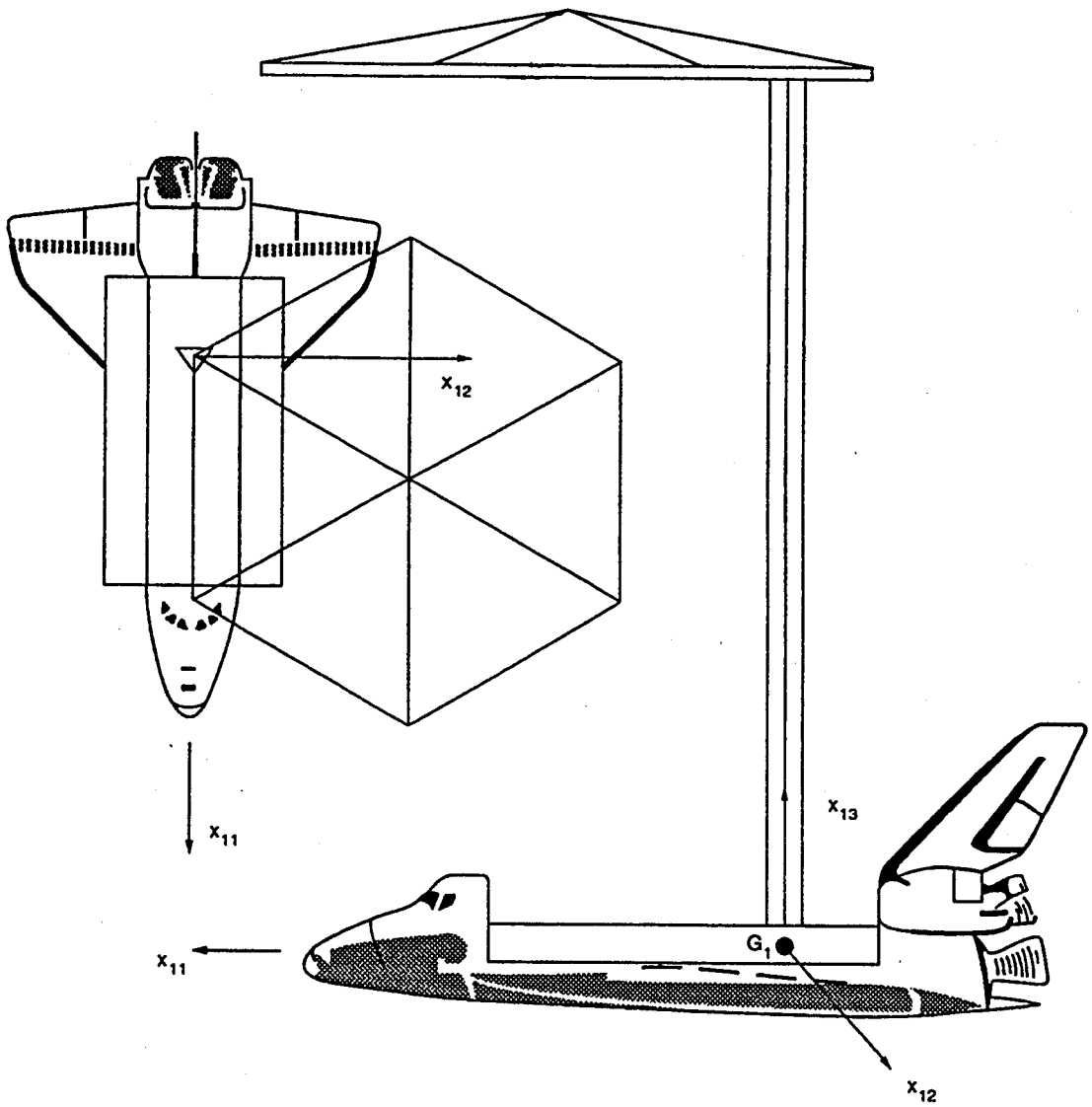

Figure 1-5 The SCOLE configuration consisting of the Space Shuttle based slewing mast asymmetrically supporting a reflector plate.

(Provided by the Department of Mechanical Engineering, University of British Columbia)

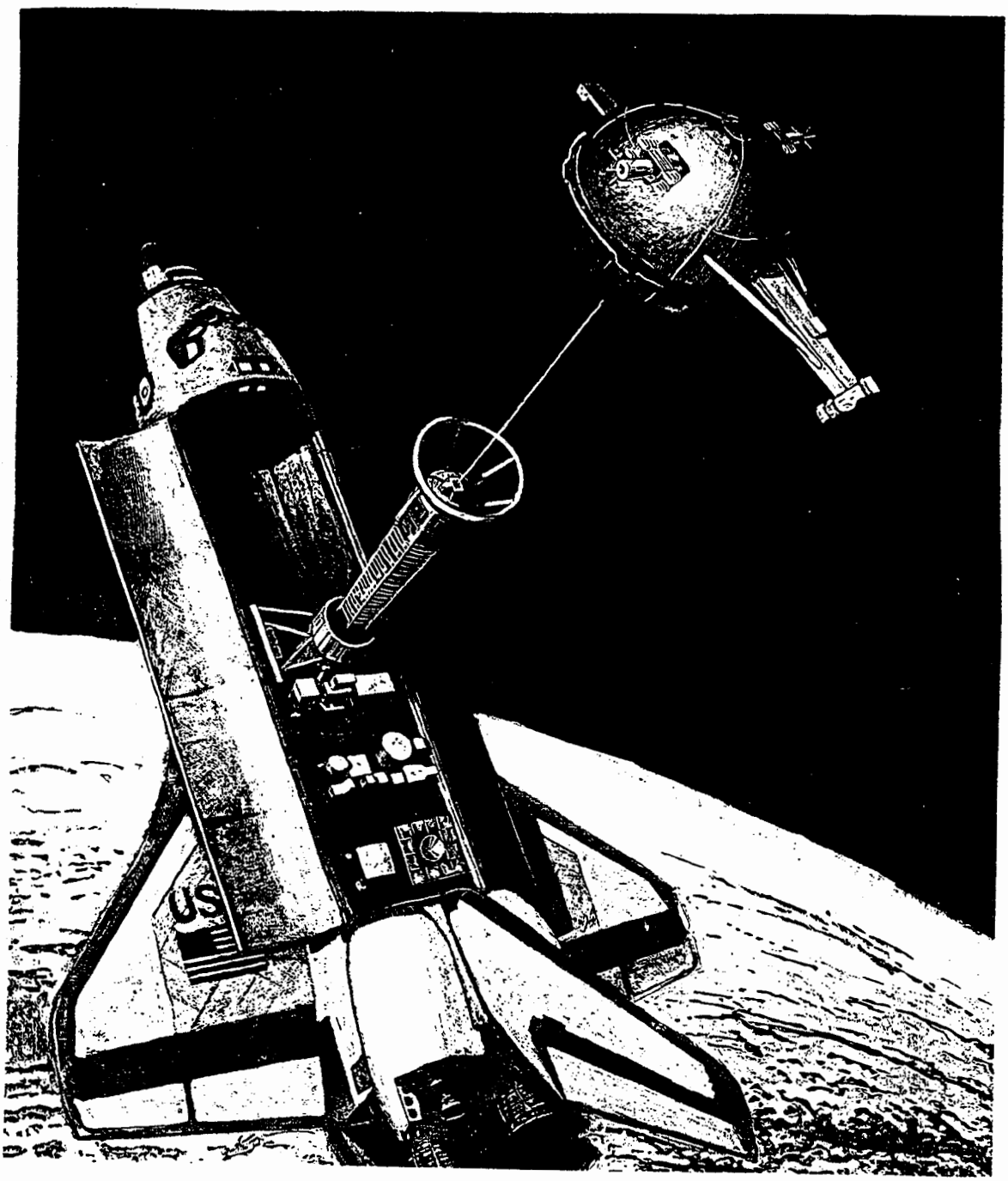

Figure 1-6 Electrodynamic tether experiment to be conducted jointly by NASA and PSN.

(Provided by the Department of Mechanical Engineering, University of British Columbia)

words, the Keplerian equations can be used to predict the trajectory.

1.2 A Brief Review of the Relevant Literature

Multibody dynamics is a vast area with several branches including machine dynamics, ground vehicle motion, robotics, biosystem kinetics and others. A common feature is the interconnection of rigid and/or flexible bodies through joints, which themselves may be flexible and dissipative. Compared to other fields, the study of spacecraft dynamics has proved to be particularly challenging because of the highly flexible character of the structures, operating in the presence of environmental disturbances and demanding a high level of accuracy in design, never encountered before.

Comprehensive reviews of the vast body of literature on spacecraft attitude dynamics have been presented by Likins, Modi, Bainum and others [7–11]. Theses by Ibrahim, Ng, and others [12–15] have also surveyed contributions aimed at specific problems of deployment, thermal deformations, slewing, etc. at considerable lengths. Some aspects regarding the modeling, formulation and computer implementation approaches are briefly touched upon here.

1.2.1 Model evolution

The model for multibody systems is generally described by a tree topology [16] as shown in Figure 1-7. One of the bodies is selected as the central body. The bodies are connected through joints which, in general, can be elastic and dissipative.

One of the early contributions to the multibody spacecraft dynamics is attributed to Fletcher, Rongved and Yu [17], who studied the behavior of a satellite composed of two interconnected rigid bodies. With the evolution of the spacecraft, the field of study has also shown the corresponding growth.

Hooker and Margulies [18] in 1965, and Roberson and Wittenburg [19] in 1966, independently derived the dynamical equations for satellites composed of n interconnected rigid bodies. Until early 1980's, the attention was primarily focused on rigid systems [20, 21], although there were some efforts at understanding the flexibility effects by Hooker [22, 23], Likins [24, 25], Ho [26] and others [27]. By early 1980's, the multi-rigid-body dynamics was well established, and the analysis of flexible-multibody systems became a problem of major concern.

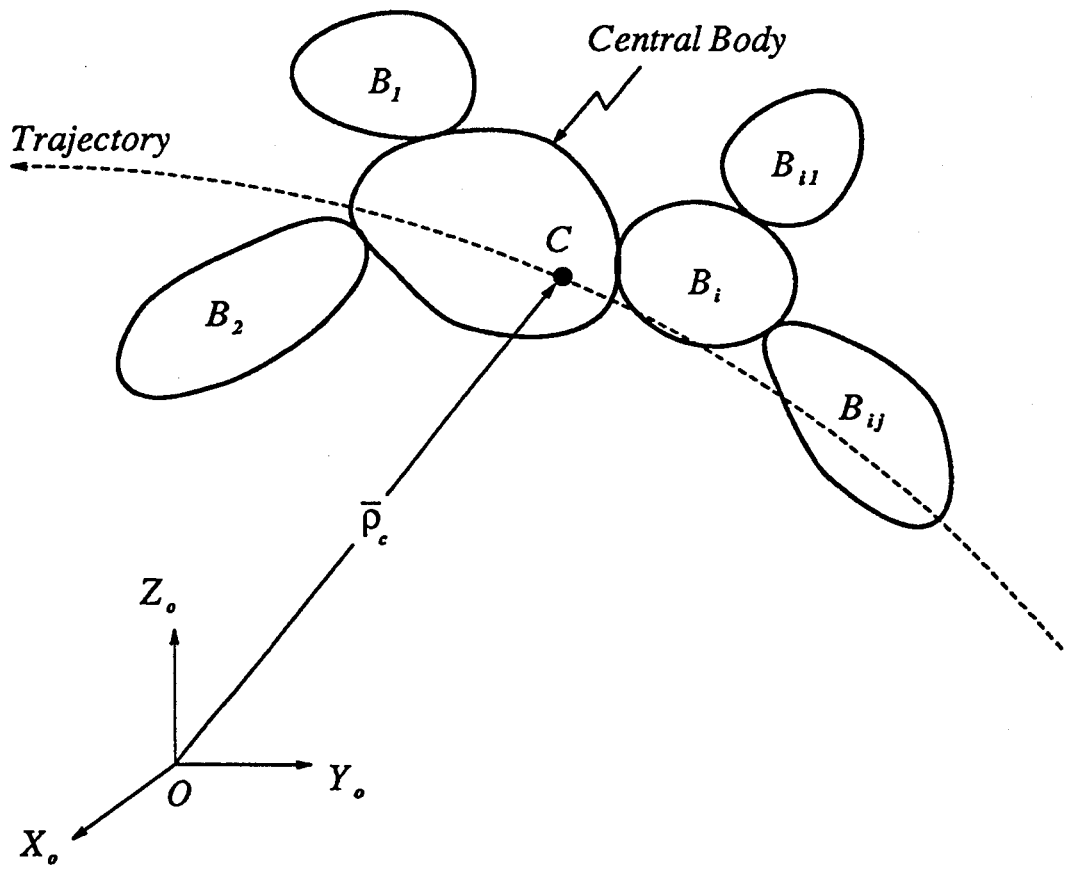

Figure 1-7 A tree topology model for multibody systems.

The dynamical study during appendage deployment and slew maneuver was initiated in the 1970's. Hughes [28] studied the deployment dynamics of a communication satellite in 1976, while Lips and Modi [29] provided a relatively general formulation, in 1978, applicable to a large class of systems involving deployment of beam type appendages. Ibrahim and Misra [30], in 1982, and Modi and Ibrahim [31, 32], in 1984, investigated the dynamics during plate and beam-type appendage deployment. Turner and Junkins studied the large angle, single axis rotational maneuver of flexible spacecraft [33], while Mah and Modi [34] investigated the dynamical response during slewing and translational maneuvers of the Space Station based MRMS. Meirovitch and associates have also studied the maneuver of flexible spacecraft using simpler models [35, 36].

The relative translations between members of the spacecraft has also received some attention [37]. Dynamics of the Orbiter based construction of structural components for the space platform was investigated by Modi and Ibrahim [38]. Some attention has also been directed towards the effect of the motion of the internal objects on the dynamics of a rigid space platform [39].

1.2.2 Dynamical approaches

Methodologies for deriving the equations of motion of multibody systems may be classified in a number of ways. One division may be based on the vectorial or analytical approaches used.

Vectorial approaches refer to the Newton-Euler method and apply theorems of linear and angular momenta, to individual parts of the system, to arrive at the equations of motion. Characterization of the subsystems affects the efficiency with which the equations of motion can be obtained.

In the beginning, the choice of individual bodies as objective parts was quite common [18, 19]. The difficulty in doing so lies in the constraint torques at the joints. To eliminate them from the equations, Hooker suggested to take the sum of all the equations of bodies outside some particular joint [40]. On the other hand, Russel adopted a straightforward method which takes the subsystem of all the bodies outside some joint as an objective part to apply theorems of linear and angular momenta [41]. By doing so, the treatment of joint constraint torques is essentially avoided and the equations are formulated efficiently with clear physical appreciation. This method

was called 'Momentum Approach' by Russel, or 'Nested Bodies Method' by Frisch [42], and was accepted by Hooker and other researchers later. The procedure may be referred to as the 'Subsystem Method'.

Procedures which use the principles in analytical dynamics, such as the Lagrangian, Hamilton, or Kane's approach, are termed analytical methods [43]. Note, Kane's approach [44] is essentially the generalization of Lagrangian form of the D'Alembert Principle. As the entire system is considered, the constraint forces and moments do not appear. The analytical method leads to true coordinate equations for holonomic systems; and quasi-coordinate equations of non-holonomic systems. From the point of view of the formulation complexity, some authors have shown preference for Kane's approach [45, 16]. This is because the components of absolute or relative angular velocities can be chosen as generalized velocities, and the orientation parameters, such as the Euler Angles, are not involved in the first stage of the formulation. It is argued that Kane's Equation combine the advantages of both vectorial and analytical approaches; however, this is a controversial point that has aroused considerable debate.

On the other hand, the Lagrangian procedure has its own unique advantages. At the outset it must be recognized that the methodology has served us well in tackling a wide variety of problems for more than 200 years. It satisfies holonomic constraints implicitly as pointed out before, and provides useful functions of energy, Lagrangian, Hamiltonian, conjugate momenta, etc. The kinetic and potential energy functions have been used in stability studies. Note, differentiation of the scalar energy functions can be accomplished by a computer. Judicious application of the symbolic manipulation in conjunction with the Lagrange principle can provide equations of motion applicable to a wide class of systems. For example, Ibrahim and Modi [46] established equations of motion for spacecraft with arbitrary number of flexible deployable appendages; while Modi and Ng [47] formulated the dynamical and control problem for a system of interconnected flexible members accounting for the solar radiation induced thermal effects.

A systematic comparison of several dynamical methods has been presented by Kane and Levinson, as well as Shen [48, 49]. It is pointed out that different identification of subsystems in vectorial approaches corresponds to different selection of generalized velocities in analytical methods. The equations formulated by the Newton-Euler method applying the theorems of linear and angular momenta to individual bodies,

and those by Kane's approach using absolute angular velocities, have the same form. On the other hand, the equations established by the 'Subsystem Method' and the Kane procedure using relative angular velocities have different forms [49].

1.2.3 Matrix notation

Matrix notation plays an important role in the formulation of the equations of motion. In the early days, the equations were obtained and then cast into a matrix form to look compact. Later, Ho [26] designed an incidence matrix describing the topological structure of multibody systems. For instance, the incidence matrix for the system in Figure 1-7 takes the following form:

$$\begin{bmatrix} 1 & 1 & 1 & 1 & 1 & 1 \\ 0 & 1 & 0 & 0 & 0 & 0 \\ 0 & 0 & 1 & 0 & 0 & 0 \\ 0 & 0 & 0 & 1 & 1 & 1 \\ 0 & 0 & 0 & 0 & 1 & 0 \\ 0 & 0 & 0 & 0 & 0 & 1 \end{bmatrix}.$$

Introduction of incidence matrix has contributed significantly to the development of multibody dynamics. With such a tool in hand, some researchers have started to derive the equations of motion as a whole in matrix form [20]. Adopting Ho's incidence matrix, Shen [21] designed 'Position Vector Matrix' and 'Rotating Axes Matrix' to obtain equations of motion for multi-rigid-body systems through Kane's approach.

It should be noted that, for using matrix manipulations, analytical approaches must be adopted. As pointed out before, analytical approaches treat the system as a whole instead of its individual parts. Matrices describe integral structure of the system and hence they are consistent. The use of matrices during formulation renders the process relatively simple, more efficient, and idealy suited for computer simulation.

1.2.4 Discretization

One of the important aspects in the study of the flexible body dynamics is the representation of the elastic deformations. A literature review suggests that this is normally accomplished through the use of admissible or assumed mode functions [15, 31]

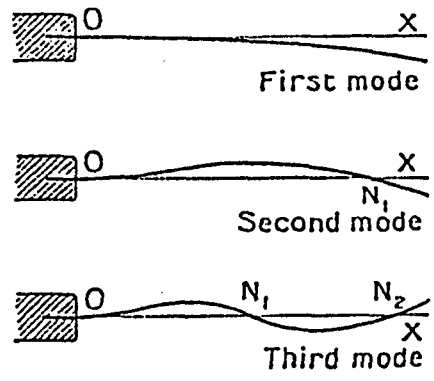

Figure 1-8 The first three modes of a cantilever beam. N_i refers to nodes.

$$\bar{u}_i = \sum_{j=1}^{\infty} \bar{\Phi}_{ij}(\bar{x}_i)\delta_{ij}(t) \ ,$$

where $\bar{u}_i$ is the elastic displacement of the i-th body; $\bar{\Phi}_{ij}(\bar{x}_i)$ is the j-the mode function of the i-th body satisfying the end conditions; and $\delta_{ij}(t)$ is the generalized coordinate associated with the $\bar{\Phi}_{ij}$. In practical applications only finite number of terms are taken.

For simple isotropic structures, such as homogeneous beams and plates, closed form expressions are available for frequencies and shape functions. For the interconnected bodies, 'free-free' modes are usually chosen; while for terminal bodies, 'fixed-free' modes are preferred. The first three modes of a cantilever beam are shown in Figure 1-8 [50].

For complex and nonisotropic systems, a finite element method is usually used to obtain this information. This is a subject in itself and there is an extensive literature available; only a small sample of it is cited here [51–54].

1.2.5 Computer simulation

Based on the formalisms, several computer codes simulating multibody systems have been developed commercially. Some of them are listed below:

Code	Contributors
ADAMS	R.R.Ryan [55]
ALLFLEX	J.Y.L.Ho,D.R.Herber,B.R.Clapp,R.J.Schultz [56]
AUTOLEV	D.A.Levinson, T.R.Kane [55]
MESA VERDE	J.Wittenburg, U.Wolz, A.Schmidt [55]
NBOD and DISCOS	H.P.Frisch [57]
SD/FAST	M.Sherman [58]
TREETOPS	R.P.Singh, R.J.VanderVoort, P.W.Likins [59]
UCIN-DYNOCOMBS	R.L.Huston, T.P.King, J.W.Kamman [55]

They accommodate mechanisms, robots, manipulators, spacecraft, rail and road vehicles, as well as biosystems. They are written in FORTRAN and the numerical integration generally requires methods for nonstiff differential equations. The standard output is time history plots of motion.

As can be expected, each one claims some distinctive advantage; and there are limitations peculiar to a specific program. Furthermore, it takes enormous time and effort to render the program operational, and the user end modifications are virtually impossible. The program packages often become "black boxes", thus impeding in physical appreciation of the system behavior at the fundamental level. This has motivated many researchers in development of their own programs which are often more versatile and efficient [60–65].

1.3 Purpose and Scope of the Investigation

With this as background, the thesis focuses on a large class of problems, of contemporary and future interests, characterized by a central rigid body, in orbit, supporting an arbitrary number of beam and plate type slewing, deployable structural members. The joint between the central body and the flexible member permits rotations (slew or free) about the three orthogonal axes. Besides a large family of satellites which conform to this geometry as shown in Figure 1-9 [3], the configuration exhibits a degree of versatility that is attractive and has never been studied before. It is applicable to the dynamical simulations of:

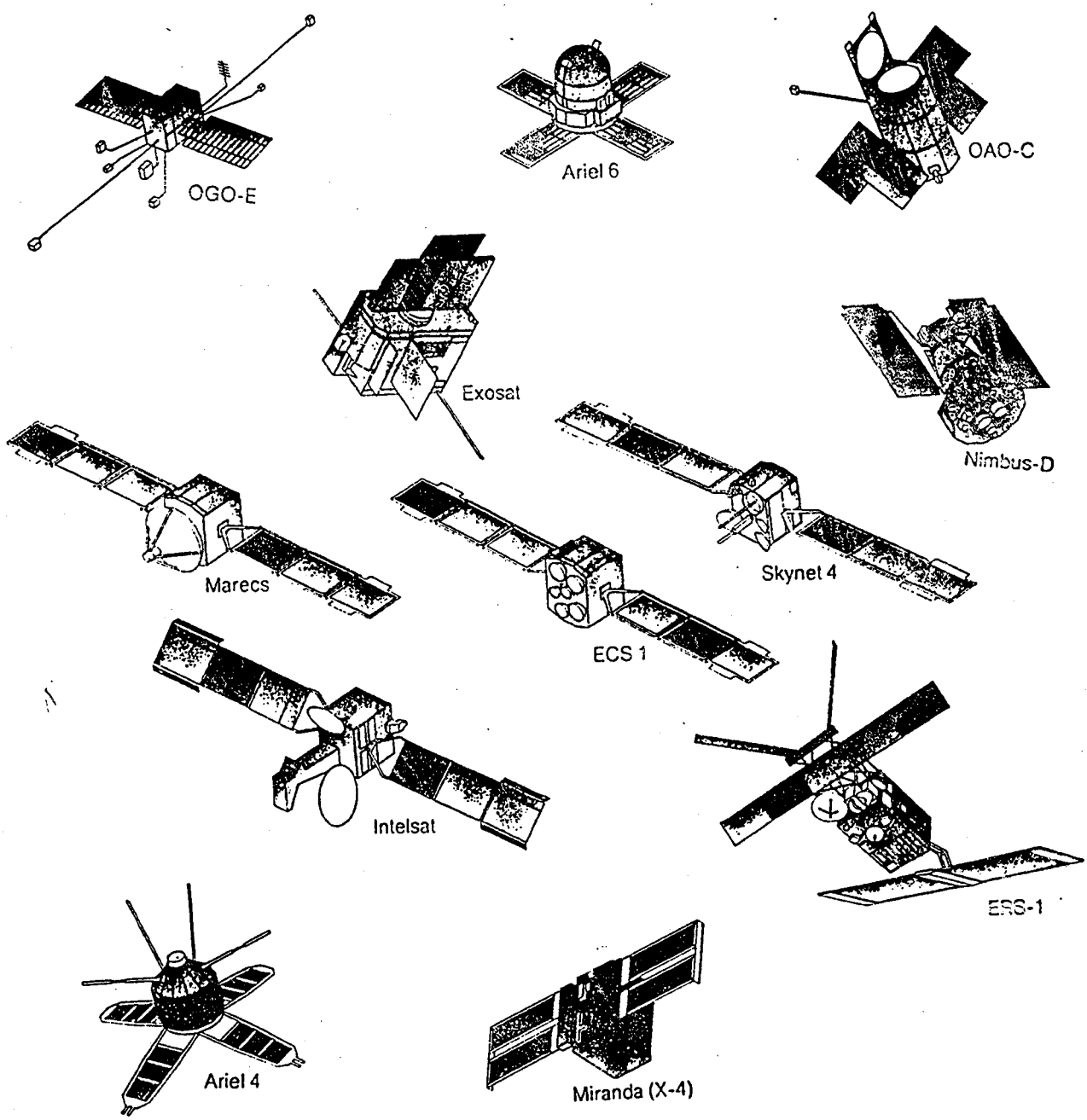

Figure 1-9 Several examples of spacecraft with flexible appendages connected to an essentially rigid central body.

(Adopted from *Satellite Technology and its Application*, by P.R.K. Chetty)

(a) communications and scientific satellites, which normally have central rigid body, with deployable solar panels, antennas and booms;

(b) the space shuttle based robotic manipulator useful in relocating the payload along a prescribed trajectory; and capturing of a disabled satellite or a stranded astronaut;

(c) the multi-arm robotic manipulators;

(d) the evolving Space Station Freedom with the cluster of modules representing the central rigid body, and the main truss as a pair of flexible beams;

(e) experiments involving slewing motion of the on board equipment such as telescope, armament, etc.;

(f) the offset control strategy for space manufacturing in the desired microgravity environment;

and many other situations. Some of the above mentioned applications are schematically shown in Figure 1-10.

Development of a relatively general formulation for studying dynamics of this class of problems, as given in Chapter 2, forms the backbone of the thesis. The derivation of the equations of motion for such a complex system is so formidable that the assessment of its validity becomes a challenge. This issue is addressed in Chapter 3. This is followed by the stability study of a particular simple configuration representing a rigid satellite with two rigid appendages, each free to rotate about one axis. This study in Chapter 4 also helps towards the validating efforts, as the system behaviour must conform to the physical reality.

Encouraged by the stability results for the rigid system, attention is now directed towards the analytical, closed-form solution for a relatively difficult particular case involving the planar dynamics of a satellite with a flexible, slewing, beam type appendage. The nonlinear analysis is based on the variation of parameter method as suggested by Butenin [66]. Accuracy of the solution is assessed through comparison with numerical solution of the exact equations of motion. Finally, in Chapter 6, the 'backbone' meets the 'head' of the thesis. The original highly nonlinear, nonautonomous and coupled equations of motion are computer coded through a general purpose program "Dynamics of Spacecraft with Deployable and Slewing Appendages" (DSDSA, 23 subroutines). Accuracy of the program is checked through comparison

(Provided by the Department of Mechanical Engineering, University of British Columbia)

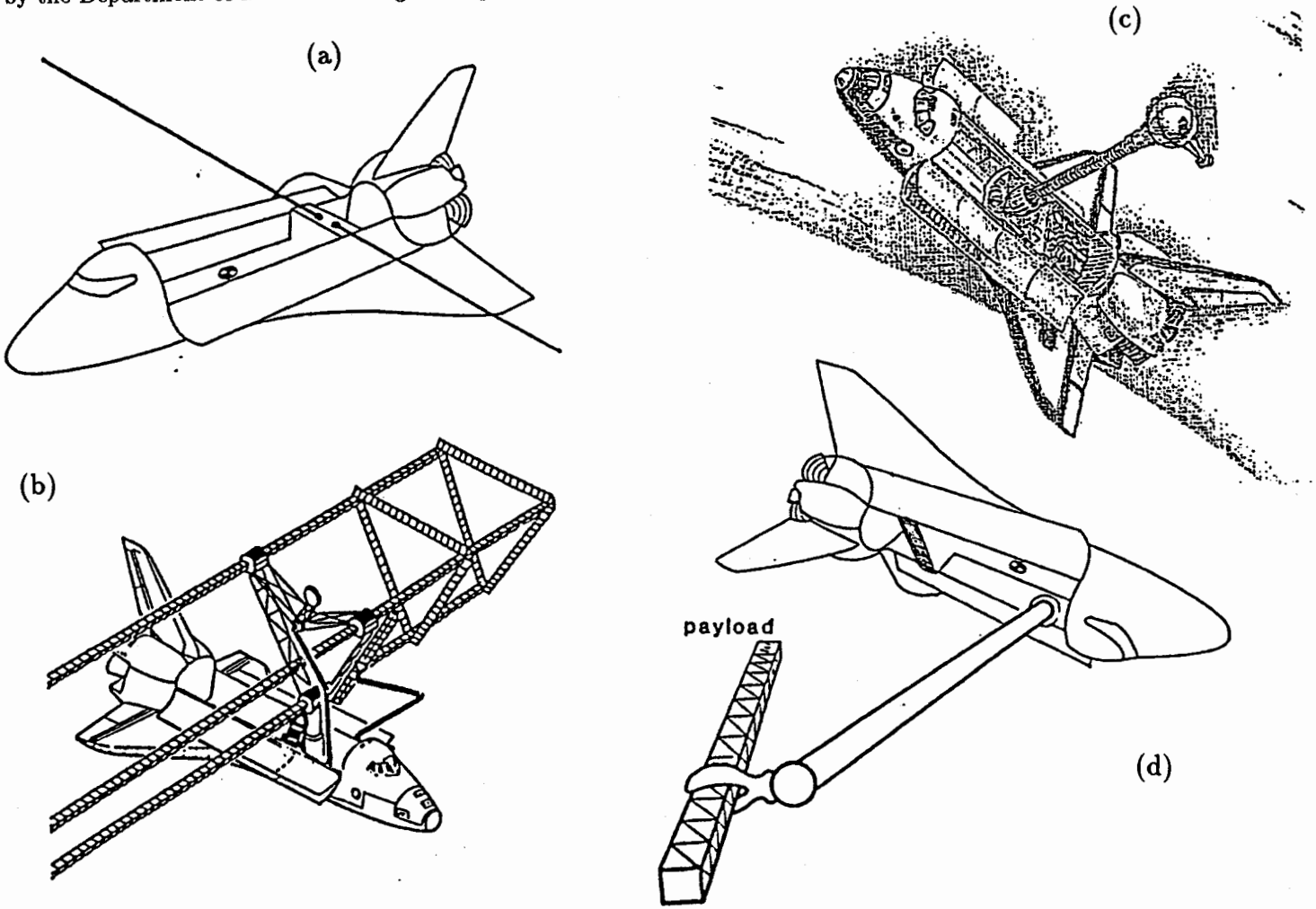

Figure 1-10 Proposed experiments using the Space Shuttle: (a) Waves in Space Plasma (WISP) involves two 150 m long dipole antennae; (b) manufacturing of truss-type structures for construction of the Space Station; (c) a mast supporting the subsatellite during the Electrodynamic Tether Experiment (TSS-1); (d) Canadarm supporting a payload.

of results for a known particular case. Now the general purpose program is applied to study dynamics of three different systems of contemporary interest:

- Japan's Space Flyer Unit (SFU) to be launched in 1994;
- Space Shuttle based articulating appendage;
- the Two-Dimensionally Deployable Array Experiment.

The objective is to study the effects of deployment, slew maneuver and flexibility. The thesis ends with concluding remarks and recommendations for future extensions to the study.

2. FORMULATION OF THE PROBLEM

2.1 System Description

As pointed out before and indicated in Figure 1-9, a wide variety of scientific, application and military satellites are characterized by a rigid central body with an arbitrary number (n) of flexible beam and plate type appendages attached to it. That is the model considered here for study (Figure 2-1). To make it more versatile, the appendages can undergo prescribed deployment or retrieval along some specified direction and have three degrees of freedom for slewing maneuvers or free rotations w.r.t. the central body. The central rigid body is numbered '0', and the appendages are referred to as body '1', '2', ..., 'n'. The spacecraft is free to negotiate any specified trajectory.

The inertial coordinate system $O - X_o, Y_o, Z_o$ has its origin at the earth centre. An orbiting frame $C - X, Y, Z$ is located at the instantaneous centre of mass of the system with X axis along the local vertical, Y axis normal to the local vertical in the plane of the orbit, and Z axis perpendicular to the orbital plane. There are also body fixed frames $o_i - x_i, y_i, z_i$ (i=0, 1, 2,....., n) with their origins o_i at the centre of mass of the central body (o_o) and at the hinges for the appendages. The axes x_o, y_o and z_o are aligned with the principal axes of inertia of the central body. For the beam-type appendage i, the z_i-axis is along the beam; while for the plate-type appendage i, the origin of the plate-fixed frame is at the midpoint of the edge attached to the central body with the z_i-axis along the plate and perpendicular to the edge. The y_i-axis is perpendicular to z_i in the plane of the plate, and the x_i-axis is normal to the y_i, z_i-plane.

At the instantaneous mass centre of the spacecraft, 'system frame' $C - x_c, y_c, z_c$ is located (not shown to retain clarity of the figure) with the direction of its axes fixed on the central body; and in any nominal orientation, the x_c, y_c and z_c axes are aligned with X, Y and Z axes of the orbital frame, respectively.

General motion of the spacecraft has contributions from the following sources:

- Orbital motion—translation of the spacecraft as a point mass w.r.t. the inertial frame.

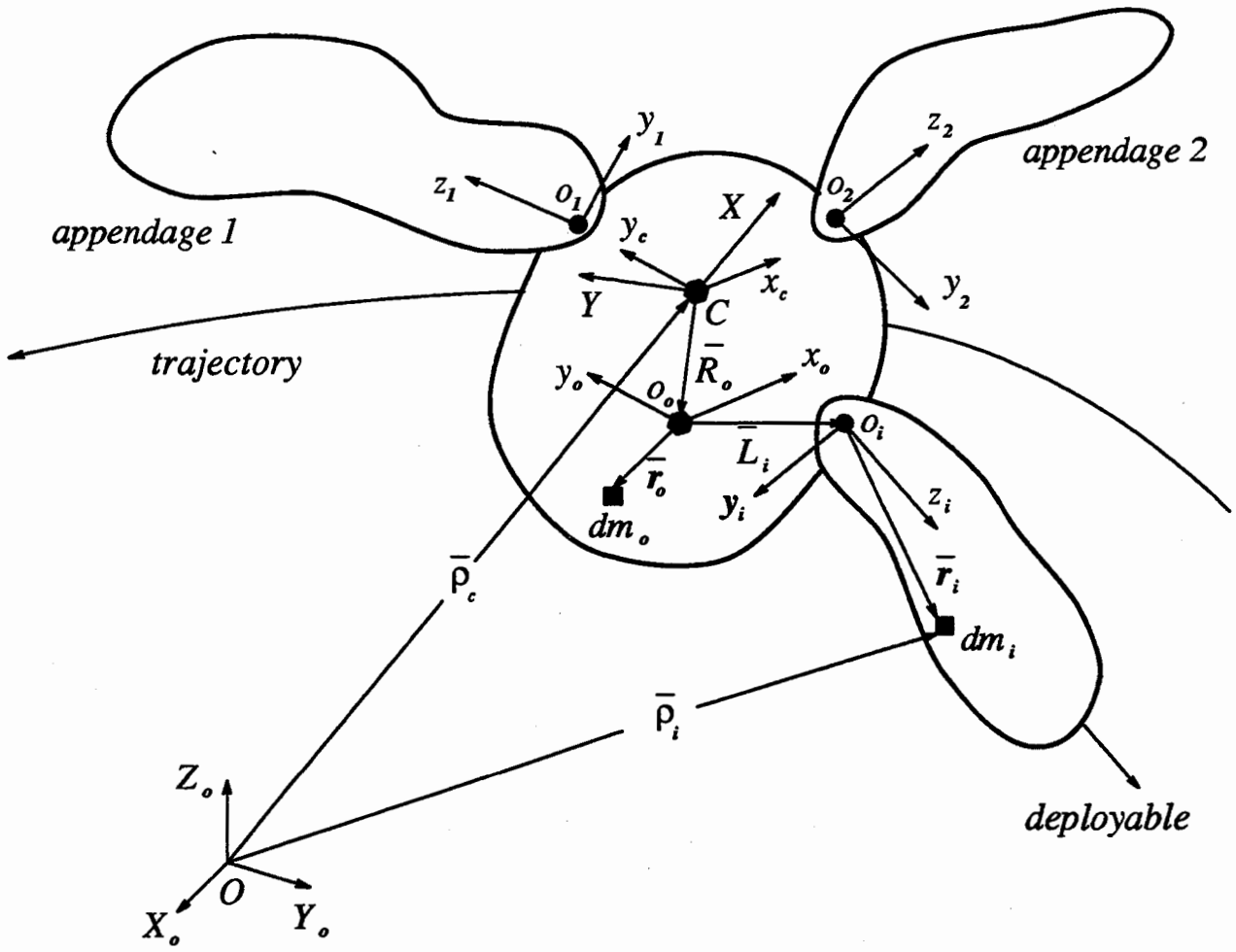

Figure 2-1 Model of the spacecraft considered for investigation. It consists of a central rigid body with flexible, deployable, and slewing appendages having beam and/or plate-type character.

- Librational motion—angular motion of the spacecraft as a rigid body about the system c.m. represented by the relative motion of the system frame w.r.t. the orbital frame.

- System rotation—angular motion of the spacecraft as a rigid body w.r.t. the inertial frame, i.e. the angular motion of the orbital frame w.r.t. the inertial frame plus the librational motion.

- Appendage rotation—slew maneuver or free rotation of an appendage w.r.t. the central body.

- Relative motions—motions of individual parts or mass elements of the spacecraft w.r.t. the system frame including appendage rotation, deployment or retrieval, and vibrations.

The librational motion of the spacecraft is described by a set of three orientation angles (λ, ϕ, ψ). The row matrix $[\ \alpha_o\ ] = [\lambda \quad \phi \quad \psi]$ defines motion of the system frame $C - x_c, y_c, z_c$ w.r.t. the orbital frame $C - X, Y, Z$. Euler angles or modified Euler angles (Bryant angles) [67] are often used as the orientation angles with the rotation sequences shown in Figures 2-2 and 2-3.

Consider the orbital frame $C - X, Y, Z$ as indicated in the diagram. Objective is to provide any arbitrary orientation to the system through three successive rotations λ, ϕ and ψ. Let the initial position of the system frame, coincident with the orbital frame, be designated as a_o, b_o, c_o as shown in the figure. By definition, rotation about the local vertical is referred to as yaw, about the 'local horizontal' as roll, and about the 'orbit normal' as pitch. The Eulerian or Bryant rotations may represent yaw, roll and pitch but not necessarily so. In the classical Eulerian case, λ about $X = a_o$ gives a_1, b_1, c_1; rotation ϕ about b_1 yields a_2, b_2, c_2; and finally ψ about a_2 leads to $a_3, b_3, c_3 \equiv x_c, y_c, z_c$. In the Bryant rotations, the sequence is the same as before (λ, ϕ, ψ); however, now the rotations are applied about a different set of axes: λ about $X \equiv a_o$ as before; ϕ about b_1; and ψ about c_2. Note, for the modified Euler angles (Bryant case), λ being about the local vertical represents yaw. However, ϕ and ψ are not about the local horizontal and orbit normal, respectively. One may look upon them as modified or approximate roll and pitch, respectively, if the rotations are small.

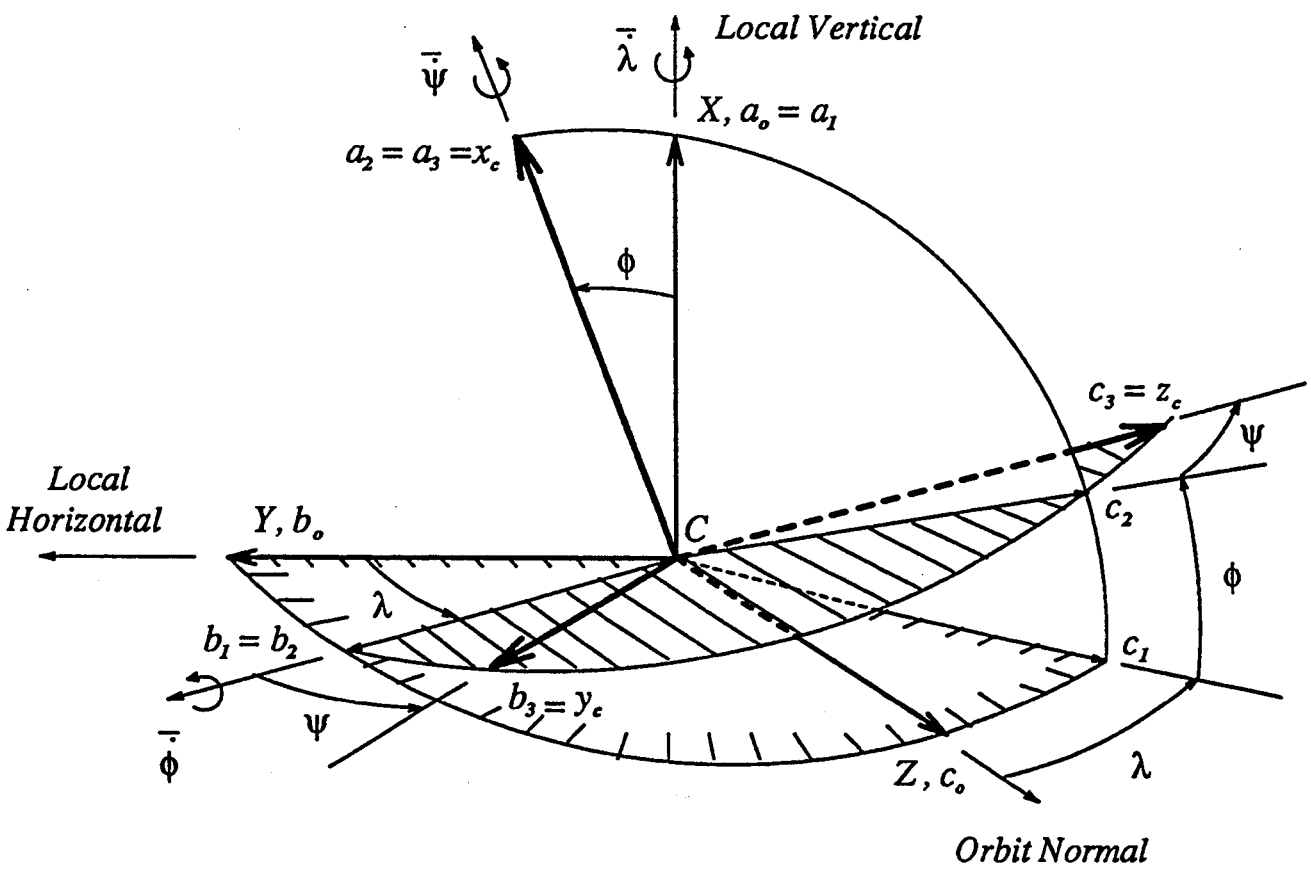

Figure 2-2 The classical Euler angles

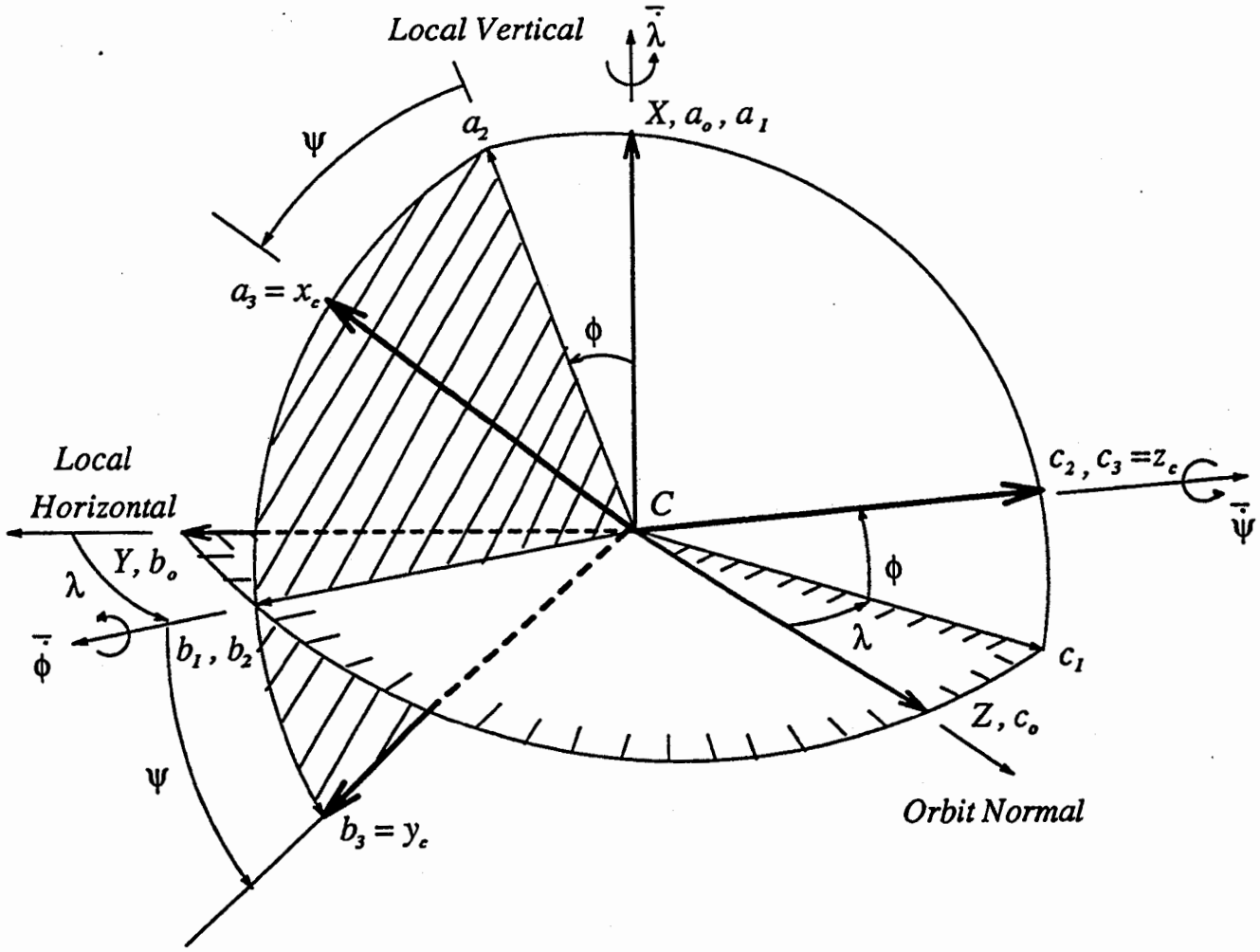

Figure 2-3 The modified Euler angles (Bryant angles)

Using Bryant angles, the transformation matrix from the $C-X,Y,Z$ frame to the frame $C-x_c,y_c,z_c$ (or the central-body-fixed frame o_o-x_o,y_o,z_o) is

$$[A]=\begin{bmatrix} cos\phi cos\psi & cos\lambda sin\psi+sin\lambda sin\phi cos\psi & sin\lambda sin\psi-cos\lambda sin\phi cos\psi \\ -cos\phi sin\psi & cos\lambda cos\psi-sin\lambda sin\phi sin\psi & sin\lambda cos\psi+cos\lambda sin\phi sin\psi \\ sin\phi & -sin\lambda cos\phi & cos\lambda cos\phi \end{bmatrix}. \tag{2.1}$$

The general three dimensional slewing or free rotation of the 'i'-th appendage is represented by three angles α_{i1}, α_{i2}, α_{i3} of the system o_i-x_i,y_i,z_i w.r.t. its nominal position on the central body. The deployment or retrieval of the 'i'th appendage is taken to be along the z_i axis.

The vibratory displacement of a mass element (on the flexible appendage) is represented by sets of admissible modal functions associated with time-varying generalized coordinates,

$$\overline{u}_i=[\,\overline{e}_i\,][f_i][\,u_i\,]^T. \tag{2.2}$$

For the beam-type appendages, displacements in x and y directions are considered,

$$[f_i]=\begin{bmatrix} \Psi_1(\xi)\ldots & 0 \\ 0 & \Psi_1(\xi)\ldots \\ 0 & 0 \end{bmatrix}, \tag{2.3}$$

and

$$[\,u_i\,]=[u_{ix1}(t),\ldots,u_{iy1}(t),\ldots]\,. \tag{2.4}$$

For the plate type appendages, only the displacement in x_i direction normal to the plate is usually significant, hence

$$[f_i]=\begin{bmatrix} \Phi_1(\eta)\Psi_1(\xi),\ldots \\ 0 \\ 0 \end{bmatrix}, \tag{2.5}$$

and

$$[\,u_i\,]=[u_{ix1}(t),\ldots\,]\,, \tag{2.6}$$

where $\Psi_j(\xi)$ is the j-th bending mode of a cantilever beam:

$$\begin{aligned}\Psi_j(\xi) \;=\; & [cosh(\lambda_j\xi)-cos(\lambda_j\xi)]-\sigma_j[sinh(\lambda_j\xi)-sin(\lambda_j\xi)] \\ & (0\le\xi\le 1,\ j=1,2,...)\,;\end{aligned} \tag{2.7}$$

and $\Phi_j(\eta)$ is the j-th bending mode of a free-free beam:

$$\begin{aligned}
\Phi_1(\eta) &= 1 \qquad (\textit{rigid body translation}) ; \\
\Phi_2(\eta) &= 1 - \sqrt{3}\eta/2 \qquad (\textit{rigid body rotation}) ; \\
\Phi_{j+2}(\eta) &= [cosh(\mu_j(\eta+1)/2) + cos(\mu_j(\eta+1)/2)] \\
&\quad -\delta_j[sinh(\mu_j(\eta+1)/2) + sin(\mu_j(\eta+1)/2)] , \\
&\qquad (-1 \le \eta \le 1, j = 1, 2, ...) . \qquad (2.8)
\end{aligned}$$

In equations (2.7) and (2.8), λ_j and μ_j are the roots of the transcendental equations:

$$1 + cosh(\lambda)cos(\lambda) = 0 ; \qquad (2.9)$$

$$1 - cosh(\mu)cos(\mu) = 0 ; \qquad (2.10)$$

respectively; and σ_j, δ_j are constants depending on λ_j and μ_j.

2.2 Kinematics

The position vector of an arbitrary mass element dm_o on the central body is expressed as the sum of three vectors,

$$\overline{\rho}_o = \overline{\rho}_c + \overline{R}_o + \overline{r}_o \ , \qquad (2.11)$$

where $\overline{\rho}_c$ is the vector from the centre of the earth 'O' to the instantaneous centre of mass 'C' of the system; $\overline{R}_o$ is the vector from C to the mass center of the central body o_o; and $\overline{r}_o$ extends from o_o to the mass element dm_o.

The position vector of a mass element dm_i on the 'i'-th appendage is expressed as the sum of four vectors,

$$\overline{\rho}_i = \overline{\rho}_c + \overline{R}_o + \overline{L}_i + \overline{r}_i \ , \qquad (2.12)$$

where $\overline{L}_i$ is a vector from the mass centre of the central body to the hinge connecting the appendage i and

$$\overline{r}_i = \overline{r}_{io} + \overline{u}_i \ , \qquad (2.13)$$

with $\overline{r}_{io}$ representing the position vector of dm_i for the undeformed appendage.

As 'C' is the centre of mass of the entire spacecraft, the following identity holds,

$$\int (\overline{R}_o + \overline{r}_o) dm_o + \sum_{i=1}^{n} \int (\overline{R}_o + \overline{L}_i + \overline{r}_i) dm_i = \overline{0} \ , \qquad (2.14)$$

i.e.

$$M\overline{R}_o + \sum_{i=1}^{n}(m_i\overline{L}_i + \int \overline{r}_i dm_i) = \overline{0}\ , \tag{2.15}$$

where: 'M' is the total mass of the system; m_i, the mass of the 'i'-th appendage; and $\int \overline{r}_o dm_o$ vanishes since o_o is the centre of mass of the rigid central body.

Let:

$$\overline{L}_o = \frac{1}{M}\sum_{i=1}^{n} m_i\overline{L}_i\ ; \tag{2.16}$$

$$\begin{aligned}\overline{H}_i &= [\ \overline{e}_i\ ][\ H_i\ ]^T = \int \overline{r}_i dm_i\ , \\ &= [\ \overline{e}_i\ ]\left([0 \quad 0 \quad \int \nu_i z_i dz_i] + [F_i][\ u_i\ ]^T\right).\end{aligned} \tag{2.17}$$

Note, ν_i is the density per unit length of the appendage i along the z_i direction. It is assumed that the undeployed part is concentrated at line $x_i = z_i = 0$. Substituting equations (2.16) and (2.17) into (2.15) gives

$$\overline{R}_o = -\overline{L}_o - \frac{1}{M}\sum_{i=1}^{n}\overline{H}_i\ . \tag{2.18}$$

The angular velocity of the orbital frame w.r.t. the inertial system is $\Omega\overline{k}$, where $\overline{k}$ is the unit vector perpendicular to the orbital plane. The angular velocity of the central body w.r.t. the orbiting system is giving by

$$\overline{\omega}_o = [\ \dot{\alpha}_o\ ]\,[B_o]\,[\ \overline{e}_o\ ]^T. \tag{2.19}$$

Using Bryant angles,

$$[B_o] = \begin{bmatrix} cos\phi cos\psi & -cos\phi sin\psi & sin\phi \\ sin\psi & cos\psi & 0 \\ 0 & 0 & 1 \end{bmatrix}. \tag{2.20}$$

The angular velocity of the appendage i, w.r.t. the central body, is

$$\overline{\omega}_i = [\ \dot{\alpha}_i\ ]\,[B_i]\,[\ \overline{e}_i\ ]^T, \tag{2.21}$$

where the dimensions of $[\ \dot{\alpha}_i\ ]$ and $[B_i]$ depend on the dimension of slewing (or free rotation) of the appendage i.

The time derivatives of the position vectors are as follows:

$$\dot{\overline{L}}_i = (\Omega\overline{k} + \overline{\omega}_o) \times \overline{L}_i\ , \qquad i = 0, 1, ..., n; \tag{2.22}$$

$$\dot{\overline{r}}_o = (\Omega\overline{k} + \overline{\omega}_o) \times \overline{r}_o\ ; \tag{2.23}$$

$$\dot{\overline{r}}_i = (\Omega\overline{k} + \overline{\omega}_o) \times \overline{r}_i + \overset{\circ}{\overline{r}}_i\ , \qquad i = 1, ..., n. \tag{2.24}$$

The second part in equation (2.24) is due to slewing, deployment and elastic vibration of the appendage. In case $\overline{r}_i$ corresponds to the rigid (or undeployed) part of the appendage,

$$\overset{\circ}{\overline{r}}_i = \overline{\omega}_i \times \overline{r}_i \ . \tag{2.25}$$

For a flexible, deploying and slewing appendage,

$$\overset{\circ}{\overline{r}}_i = \overline{\omega}_i \times \overline{r}_i + \overline{d}_i v_i + [\ \overline{f}_i\ ][\ \dot{u}_i\ ]^T, \tag{2.26}$$

where v_i is the deployment rate and $\overline{d}_i$ defines the direction of motion of dm_i due to the deployment,

$$\overline{d}_i = [\ \overline{e}_i\ ]\left([0\ \ 0\ \ 1]^T + \frac{1-\xi}{l_i}[f_i'][\ u_i\ ]^T\right). \tag{2.27}$$

Thus when $\overline{r}_i$ refers to an undeployed mass element, both v_i and $\dot{u}_i$ vanish.

The deployment and slewing of the appendages, as well as their vibration, affect the system center of mass. This can be evaluated quite readily. Recognizing that $\overline{H}$ represents the first moment of the mass (2.17),

$$\begin{aligned} \dot{\overline{H}}_i &= \left(\Omega\overline{k} + \overline{\omega}_o\right) \times \overline{H}_i + \overset{\circ}{\overline{H}}_i \ , \\ &= \left(\Omega\overline{k} + \overline{\omega}_o\right) \times \overline{H}_i + \overline{\omega}_i \times \overline{H}_i + \overline{H}_i' v_i + [\ \overline{e}_i\ ][F_i][\ \dot{u}_i\ ]^T, \end{aligned} \tag{2.28}$$

with

$$\begin{aligned} \overline{H}_i' &= \int \overline{d}_i dm_i \ , \\ &= [\ \overline{e}_i\ ]\left([0\ \ 0\ \ m_i^*]^T + [F_i^p][\ u_i\ ]^T\right), \end{aligned} \tag{2.29}$$

where m_i^* is the mass of the deployed part of the appendage i.

Now $\overline{R}_o$ represents the position vector between the c.m. of the spacecraft and c.m. of the central body. Therefore,

$$\begin{aligned} \dot{\overline{R}}_o &= \left(\Omega\overline{k} + \overline{\omega}_o\right) \times \overline{R}_o + \overset{\circ}{\overline{R}}_o \ , \\ &= \left(\Omega\overline{k} + \overline{\omega}_o\right) \times \overline{R}_o - \frac{1}{M}\sum_{i=1}^{n} \overset{\circ}{\overline{H}}_i \ . \end{aligned} \tag{2.30}$$

Note, $\overset{\circ}{\overline{R}}_o$ describes movement of the centre of mass of the spacecraft due to its deformation.

2.3 Kinetic Energy

2.3.1 Composition of the kinetic energy

The total kinetic energy of the spacecraft is the sum of the contributions from the constituent bodies,

$$
\begin{aligned}
T &= \frac{1}{2}\int \dot{\bar{\rho}}_o \cdot \dot{\bar{\rho}}_o \, dm_o + \frac{1}{2}\sum_{i=1}^{n}\int \dot{\bar{\rho}}_i \cdot \dot{\bar{\rho}}_i \, dm_i \\
&= \frac{1}{2}\int \left(\dot{\bar{\rho}}_c + \dot{\bar{R}}_o + \dot{\bar{r}}_o\right)\cdot\left(\dot{\bar{\rho}}_c + \dot{\bar{R}}_o + \dot{\bar{r}}_o\right) dm_o \\
&+ \frac{1}{2}\sum_{i=1}^{n}\int \left(\dot{\bar{\rho}}_c + \dot{\bar{R}}_o + \dot{\bar{L}}_i + \dot{\bar{r}}_i\right)\cdot\left(\dot{\bar{\rho}}_c + \dot{\bar{R}}_o + \dot{\bar{L}}_i + \dot{\bar{r}}_i\right) dm_i \\
&= \frac{1}{2}M\,\dot{\bar{\rho}}_c \cdot \dot{\bar{\rho}}_c + \frac{1}{2}(\Omega\bar{k} + \bar{\omega}_o)\cdot \\
&\quad \left\{\bar{\bar{J}}_o - M\overline{\overline{R_oR_o}} + \sum_{i=1}^{n}\left(m_i\overline{\overline{L_iL_i}} + \overline{\overline{L_iH_i}} + \overline{\overline{H_iL_i}} + \bar{\bar{J}}_i\right)\right\}\cdot(\Omega\bar{k} + \bar{\omega}_o) \\
&+ (\Omega\bar{k} + \bar{\omega}_o)\cdot\left\{\sum_{i=1}^{n}\left(\bar{L}_i \times \overset{\circ}{\bar{H}}_i + \int \bar{r}_i \times \overset{\circ}{\bar{r}}_i \, dm_i\right) - M\bar{R}_o \times \overset{\circ}{\bar{R}}_o\right\} \\
&+ \frac{1}{2}\left(\sum_{i=1}^{n}\int \overset{\circ}{\bar{r}}_i \cdot \overset{\circ}{\bar{r}}_i \, dm_i - M\,\overset{\circ}{\bar{R}}_o \cdot \overset{\circ}{\bar{R}}_o\right),
\end{aligned}
\tag{2.31}
$$

where $\bar{\bar{J}}_o$ and $\bar{\bar{J}}_i$ are inertia tensors of the central body and appendage i, respectively. Note:

$$\overline{\overline{R_oR_o}} = \bar{R}_o\cdot\bar{R}_o\bar{\bar{I}} - \bar{R}_o\bar{R}_o \; ; \tag{2.32}$$

$$\overline{\overline{L_iL_i}} = \bar{L}_i\cdot\bar{L}_i\bar{\bar{I}} - \bar{L}_i\bar{L}_i \; ; \tag{2.33}$$

$$\overline{\overline{L_iH_i}} = \bar{L}_i\cdot\bar{H}_i\bar{\bar{I}} - \bar{H}_i\bar{L}_i \; ; \tag{2.34}$$

$$\overline{\overline{H_iL_i}} = \bar{H}_i\cdot\bar{L}_i\bar{\bar{I}} - \bar{L}_i\bar{H}_i \; ; \tag{2.35}$$

with $\bar{\bar{I}}$ as the unit tensor.

In expression (2.31), the first term represents the kinetic energy contribution due to motion of the spacecraft as a point mass. The second term is the kinetic energy of the rotational motion of the whole spacecraft as a rigid body about its mass center C (system rotation). As shown in the next section, terms in the first pair of curly braces correspond to the instantaneous inertia tensor of the spacecraft about its centre of mass. The last term is the kinetic energy of the spacecraft due to relative motions, including slewing, deployment and vibrations. The third term represents the kinetic

energy due to coupling between the system rotation and relative motions. The terms in the second pair of curly braces express relative angular momentum of the spacecraft w.r.t. the system frame.

Putting:

$$\overline{\overline{J}} = \overline{\overline{J}}_o - M\overline{\overline{R_o R_o}} + \sum_{i=1}^{n}\left(m_i\overline{\overline{L_i L_i}} + \overline{\overline{L_i H_i}} + \overline{\overline{H_i L_i}} + \overline{\overline{J}}_i\right); \tag{2.36}$$

$$\overline{G} = \sum_{i=1}^{n}\left(\overline{L}_i \times \overset{\circ}{\overline{H}}_i + \int \overline{r}_i \times \overset{\circ}{\overline{r}}_i \, dm_i\right) - M\overline{R}_o \times \overset{\circ}{\overline{R}}_o \; ; \tag{2.37}$$

the kinetic energy expression can be rewritten as

$$\begin{aligned} T &= \frac{1}{2}M\,\dot{\overline{\rho}}_c \cdot \dot{\overline{\rho}}_c + \frac{1}{2}(\Omega\overline{k} + \overline{\omega}_o)\cdot\overline{\overline{J}}\cdot(\Omega\overline{k} + \overline{\omega}_o) \\ &+ (\Omega\overline{k} + \overline{\omega}_o)\cdot\overline{G} + \frac{1}{2}\left(\sum_{i=1}^{n}\int \overset{\circ}{\overline{r}}_i \cdot \overset{\circ}{\overline{r}}_i \, dm_i - M\,\overset{\circ}{\overline{R}}_o \cdot \overset{\circ}{\overline{R}}_o\right) \\ &= T_{orb} + T_{lib} + T_{coup} + T_{rel} \; . \end{aligned} \tag{2.38}$$

2.3.2 Inertia tensor and energy of the system rotation

To determine the total inertia tensor $\overline{\overline{J}}$, the inertia tensor of the appendage i is derived first. From

$$\overline{\overline{J}}_i = \int \left(\overline{r}_i \cdot \overline{r}_i \overline{\overline{I}} - \overline{r}_i \overline{r}_i\right) dm_i \; , \tag{2.39}$$

it can be shown that

$$\overline{\overline{J}}_i = [\,\overline{e}_i\,]\left(J_i^o\,[\,I\,] - \left[J_i^1\right]\right)[\,\overline{e}_i\,]^T , \tag{2.40}$$

where:

$$J_i^o = J_{iu}^o + 2\left[F_i^1\right][\,u_i\,]^T + [\,u_i\,]\left[F_i^2\right][\,u_i\,]^T ; \tag{2.41}$$

$$\left[J_i^1\right] = \left[J_{iu}^1\right] + \left[U_i^S\right]\left[F_i^{11}\right]^T + \left[F_i^{11}\right]\left[U_i^S\right]^T + \left[U_i^S\right]\left[F_i^3\right]\left[U_i^S\right]^T . \tag{2.42}$$

For a beam-type appendage,

$$\left[U_i^S\right] = \begin{bmatrix} u_{ix1(t)}, \cdots & 0 \\ 0 & u_{iy1(t)}, \cdots \\ 0 & 0 \end{bmatrix} ; \tag{2.43}$$

and for a plate-type structural member,

$$\left[U_i^S\right] = \begin{bmatrix} u_{ix1}(t), \ldots \\ 0 \\ 0 \end{bmatrix} . \tag{2.44}$$

Next, expanding $\overline{\overline{R_oR_o}}$ and using equation (2.18),

$$M\overline{\overline{R_oR_o}} = M\overline{\overline{L_oL_o}} + \sum_{i=1}^{n}\left(\overline{\overline{L_oH_i}} + \overline{\overline{H_iL_o}}\right) + \frac{1}{M}\sum_{i=1}^{n}\sum_{i=1}^{n}\overline{\overline{H_iH_j}}\,. \tag{2.45}$$

Now the inertia tensor of the entire system can be written as

$$\begin{aligned}\overline{\overline{J}} &= \overline{\overline{J}}_o - M\overline{\overline{L_oL_o}} - \frac{1}{M}\sum_{i=1}^{n}\sum_{j=1}^{n}\overline{\overline{H_iH_j}} \\ &+ \sum_{i=1}^{n}\left(m_i\overline{\overline{L_iL_i}} + \overline{\overline{(L_i-L_o)\,H_i}} + \overline{\overline{H_i\,(L_i-L_o)}} + \overline{\overline{J}}_i\right).\end{aligned} \tag{2.46}$$

Let $[C_i]$ be the matrix for transformation from system $o_o - x_o, y_o, z_o$ to $o_i - x_i, y_i, z_i$. Putting:

$$\begin{aligned}J^o &= J_o^o - ML_o^2 + \sum_{i=1}^{n}\left(J_i^o + m_iL_i^2 + 2\,[L_i - L_o]\,[C_i]^T\,[\,H_i\,]^T\right) \\ &\quad -\frac{1}{M}\sum_{i=1}^{n}\sum_{j=1}^{n}[\,H_i\,]\,[C_i]\,[C_j]^T\,[\,H_j\,]^T;\end{aligned} \tag{2.47}$$

$$\begin{aligned}\left[J^1\right] &= \left[J_o^1\right] - M\,[\,L_o\,]^T\,[\,L_o\,] - \frac{1}{M}\sum_{i=1}^{n}\sum_{j=1}^{n}[C_i]^T\,[\,H_i\,]^T\,[H_j\,]\,[C_j] \\ &\quad +\sum_{i=1}^{n}\Big([C_i]^T\left[J_i^1\right][C_i] + m_i\,[\,L_i\,]^T\,[\,L_i\,] \\ &\quad + [C_i]^T\,[\,H_i\,]^T\,[L_i - L_o] + [L_i - L_o]^T\,[\,H_i\,]\,[C_i]\Big);\end{aligned} \tag{2.48}$$

gives

$$\overline{\overline{J}} = [\,\overline{e}_o\,]\left(J^o\,[I] - \left[J^1\right]\right)[\,\overline{e}_o\,]^T = [\,\overline{e}_o\,]\,[J]\,[\,\overline{e}_o\,]^T. \tag{2.49}$$

Let $[\,a_1\,]^T$, $[\,a_2\,]^T$ and $[\,a_3\,]^T$ be columns of the transformation matrix A (2.1), then the angular velocity of the system rotation is given by

$$\Omega\overline{k} + \overline{\omega}_o = ([\,a_3\,]\Omega + [\,\dot{\alpha}_o\,]\,[B_o])[\,\overline{e}_o\,]^T. \tag{2.50}$$

Therefore the kinetic energy of system rotation, i.e. the librational contribution in equation (2.38), takes the form

$$\begin{aligned}T_{lib} &= \frac{1}{2}(\Omega\overline{k} + \overline{\omega}_o)\cdot\overline{\overline{J}}\cdot(\Omega\overline{k} + \overline{\omega}_o)\,, \\ &= \frac{1}{2}([\,a_3\,]\Omega + [\,\dot{\alpha}_o\,]\,[B_o])\,[J]\,([\,a_3\,]\Omega + [\,\dot{\alpha}_o\,]\,[B_o])^T\,, \\ &= \frac{1}{2}J^o(\Omega^2 + 2\Omega[\,a_3\,]\,[B_o]^T\,[\,\dot{\alpha}_o\,]^T + [\,\dot{\alpha}_o\,]\,[B_o]\,[B_o]^T\,[\,\dot{\alpha}_o\,]^T) \\ &\quad -\frac{1}{2}([\,a_3\,]\Omega + [\,\dot{\alpha}_o\,]\,[B_o])\left[J^1\right]([\,a_3\,]\Omega + [\,\dot{\alpha}_o\,]\,[B_o])^T.\end{aligned} \tag{2.51}$$

2.3.3 Relative angular momentum; energy of coupling between the system rotation and relative motions

Substituting from equation (2.26), the integral $\int \overline{r}_i \times \overset{\circ}{\overline{r}}_i \, dm_i$ appearing in the expression for $\overline{G}$ (2.37) can be expressed as

$$\int \overline{r}_i \times \overset{\circ}{\overline{r}}_i \, dm_i = \overline{\overline{J}}_i \cdot \overline{\omega}_i + \overline{D}_i v_i + [\, \overline{S}_i \,][\, \dot{u}_i \,]^T, \tag{2.52}$$

where:

$$\begin{aligned} \overline{D}_i &= \int \overline{r}_i \times \overline{d}_i dm_i = [\, \overline{e}_i \,][\, D_i \,]^T, \\ &= [\, \overline{e}_i \,] \left(\left[F_i^6 \right] [\, u_i \,]^T + \left([\, u_i \,] [F_i]^T \right)^* [0 \;\; 0 \;\; 1]^T \right. \\ &\quad \left. + \left[F_i^{u1} \right] [\, u_i \,]^T \right); \end{aligned} \tag{2.53}$$

$$[\, \overline{S}_i \,] = \int \overline{r}_i \times [\, \overline{f}_i \,] dm_i = [\, \overline{e}_i \,] [S_i] = [\, \overline{e}_i \,] \left(\left[F_i^{1*} \right] + [F_i^u] \right). \tag{2.54}$$

Expanding $M\overline{R}_o \times \overset{\circ}{\overline{R}}_o$ as

$$M\overline{R}_o \times \overset{\circ}{\overline{R}}_o = \sum_{i=1}^{n} \left(\overline{L}_o + \frac{1}{M} \sum_{j=1}^{n} \overline{H}_j \right) \times \overset{\circ}{\overline{H}}_i \,, \tag{2.55}$$

and substituting from equation (2.52), (2.55) and (2.28) gives

$$\begin{aligned} \overline{G} &= \sum_{i=1}^{n} \left(\overline{L}_{i1} \times \overset{\circ}{\overline{H}}_i + \overline{\overline{J}}_i \cdot \overline{\omega}_i + \overline{D}_i v_i + [\, \overline{S}_i \,][\, \dot{u}_i \,]^T \right), \\ &= \sum_{i=1}^{n} \left(\left(\overline{\overline{J}}_i + \overline{\overline{L_{i1} H_i}} \right) \cdot \overline{\omega}_i + \left(\overline{L}_{i1} \times \overline{H}'_i + \overline{D}_i \right) v_i + \left(\overline{L}_{i1} \times [\, \overline{F}_i \,] + [\, \overline{S}_i \,] \right) [\, \dot{u}_i \,]^T \right), \\ &= [\, \overline{e}_o \,] \sum_{i=1}^{n} \left([M_{12}]_i [B_i]^T [\, \dot{\alpha}_i \,]^T + [\, M_{13} \,]_i^T v_i + [M_{14}]_i [\, \dot{u}_i \,]^T \right), \end{aligned} \tag{2.56}$$

where:

$$\begin{aligned} \overline{L}_{i1} &= \overline{L}_i - \overline{L}_o - \frac{1}{M} \sum_{j=1}^{n} \overline{H}_j \,, \\ &= [\, \overline{e}_o \,][\, L_{i1} \,]^T = [\, \overline{e}_o \,] \left([L_i - L_o] - \frac{1}{M} \sum_{j=1}^{n} [\, H_j \,] [C_j] \right)^T ; \end{aligned} \tag{2.57}$$

$$\begin{aligned} [M_{12}]_i &= [C_i]^T \left(\left(J_i^o + [\, L_{i1} \,] [C_i]^T [\, H_i \,]^T \right) [I] - \left[J_i^1 \right] \right. \\ &\quad \left. - [\, H_i \,]^T [\, L_{i1} \,] [C_i]^T \right); \end{aligned} \tag{2.58}$$

$$[M_{13}]_i = [D_i] [C_i] - [\, H'_i \,] [C_i] [\, L_{i1} \,]^* ; \tag{2.59}$$

$$[M_{14}]_i = [C_i]^T [S_i] + [\, L_{i1} \,]^* [C_i]^T [F_i] \,. \tag{2.60}$$

Here '*' implies skew-symmetric matrix associated with the vector inside the braket.

Now the kinetic energy due to coupling between the system rotation and relative motions can be written as

$$\begin{aligned} T_{coup} &= \left(\Omega\overline{k} + \overline{\omega}_o\right) \cdot \overline{G} \,, \\ &= \left([\, a_3 \,]\Omega + [\, \dot{\alpha}_o \,][B_o] \right) \sum_{i=1}^{n} \Big([M_{12}]_i [B_i]^T \left[\, \dot{\alpha}_i \,\right]^T \\ &\quad + [\, M_{13} \,]_i^T v_i + [M_{14}]_i [\, \dot{u}_i \,]^T \Big) \,. \end{aligned} \tag{2.61}$$

It is clear that $[M_{12}]_i$, $[M_{13}]_i$ and $[M_{14}]_i$ are inertia matrices associated with the coupling between the system rotation and slew, deployment or retrival, and appendage vibration, respectively.

2.3.4 Energy due to relative motions

From equation (2.38),

$$T_{rel} = \frac{1}{2} \left(\sum_{i=1}^{n} \int \overset{\circ}{\overline{r}}_i \cdot \overset{\circ}{\overline{r}}_i \, dm_i - M \, \overset{\circ}{\overline{R}}_o \cdot \overset{\circ}{\overline{R}}_o \right). \tag{2.62}$$

The integral $\int \overset{\circ}{\overline{r}}_i \cdot \overset{\circ}{\overline{r}}_i \, dm_i$ can be expressed as

$$\begin{aligned} \int \overset{\circ}{\overline{r}}_i \cdot \overset{\circ}{\overline{r}}_i \, dm_i &= \overline{\omega}_i \cdot \overline{\overline{J}}_i \cdot \overline{\omega}_i + 2\overline{\omega}_i \cdot \left(\overline{D}_i v_i + [\, S_i \,][\, \dot{u}_i \,]^T \right) \\ &\quad + (m_d)_i v_i^2 + 2 v_i [m_{ds}]_i [\, \dot{u}_i \,]^T + [\, \dot{u}_i \,] \left[F_i^2 \right] [\, \dot{u}_i \,]^T, \end{aligned} \tag{2.63}$$

with:

$$(m_d)_i = \int \overline{d}_i \cdot \overline{d}_i dm_i = m_i^* + 2[0 \;\; 0 \;\; 1] [F_i^p] [\, u_i \,]^T + [\, u_i \,] \left[F_i^5 \right] [\, u_i \,]^T; \tag{2.64}$$

$$[m_{ds}]_i = \int \overline{d}_i \cdot [\, \overline{f}_i \,] dm_i = [0 \;\; 0 \;\; 1] [F_i] + [\, u_i \,] \left[F_i^4 \right]. \tag{2.65}$$

The remaining part can be expressed as

$$\begin{aligned} M \, \overset{\circ}{\overline{R}}_o \cdot \overset{\circ}{\overline{R}}_o &= \frac{1}{M} \sum_{i=1}^{n} \sum_{j=1}^{n} \Big(\overline{\omega}_i \cdot \overline{\overline{H_i H_j}} \cdot \overline{\omega}_j + 2\overline{\omega}_i \cdot \overline{H}_i \times \left(\overline{H}'_j v_j + [\, \overline{F}_j \,][\, \dot{u}_j \,]^T \right) \cdot \\ &\quad + v_i \overline{H}'_i \cdot \overline{H}'_j v_j + 2 v_i \overline{H}'_i \cdot [\, \overline{F}_j \,][\, \dot{u}_j \,]^T + [\, \dot{u}_i \,][\, \overline{F}_i \,]^T \cdot [\, \overline{F}_j \,][\, \dot{u}_j \,]^T \Big) \,. \end{aligned} \tag{2.66}$$

Combining equations(2.63) and (2.66), the kinetic energy of relative motions is obtained as

$$T_{rel} = \frac{1}{2} \sum_{i=1}^{n} \sum_{j=1}^{n} \Big([\, \dot{\alpha}_i \,] [B_i] \left([M_{22}]_{ij} [B_j]^T [\, \dot{\alpha}_j \,]^T + 2 [\, M_{23} \,]_{ij}^T v_j \right.$$

$$+2\,[M_{24}]_{ij}\,[\dot{u}_j\,]^T\Big) + v_i\Big\{(M_{33})_{ij}v_j + 2[\,M_{34}\,]_{ij}[\,\dot{u}_j\,]^T\Big\}$$
$$+[\,\dot{u}_i\,]\,[M_{44}]_{ij}\,[\,\dot{u}_j\,]^T\Big)\,, \tag{2.67}$$

where:

$$[M_{22}]_{ij} = \Big\{\Big(\delta_{ij}J_i^\circ - \frac{1}{M}[\,H_i\,]\,[C_i]\,[C_j]^T\,[\,H_j\,]^T\Big)\,[I] - \Big(\delta_{ij}\,\big[J_i^1\big] - \frac{1}{M}\,[C_i]\,[C_j]^T\,[\,H_j\,]^T[\,H_i\,]\Big)\Big\}\,[C_i]\,[C_j]^T\,; \tag{2.68}$$

$$[M_{23}]_{ij}^T = \delta_{ij}[\,D\,]_j^T - \frac{1}{M}[\,H_i\,]^*\,[C_i]\,[C_j]^T\,[\,H_j'\,]^T; \tag{2.69}$$

$$[M_{24}]_{ij} = \delta_{ij}\,[S]_j - \frac{1}{M}[\,H_i\,]^*\,[C_i]\,[C_j]^T\,[F_j]\,; \tag{2.70}$$

$$(m_{33})_{ij} = \delta_{ij}\,(m_d)_j - \frac{1}{M}[\,H_i'\,]\,[C_i]\,[C_j]^T\,[\,H_j'\,]^T; \tag{2.71}$$

$$[M_{34}]_{ij} = \delta_{ij}\,[m_{ds}]_j - \frac{1}{M}[\,H_i'\,]\,[C_i]\,[C_j]^T\,[F_j]\,; \tag{2.72}$$

$$[M_{44}]_{ij} = \delta_{ij}\,\big[F_j^2\big] - \frac{1}{M}[F_i]^T\,[C_i]\,[C_j]^T\,[F_j]\,. \tag{2.73}$$

Note, $[M_{22}]_{ij}$, $[M_{23}]_{ij}$ and $[M_{24}]_{ij}$ are the inertia matrices associated with the coupling between rotation of the appendage i and slew, deployment (or retrival), as well as vibration of the appendage j, respectively. $(M_{33})_{ij}$ and $[M_{34}]_{ij}$ represent coupling between deployment of the appendage i, and deployment as well as elastic vibration of the appendage j, respectively. Similarly, $[M_{44}]_{ij}$ is associated with the coupling between vibrations of the appendages i and j.

2.4 Potential Energy

The potential energy of the system is composed of two contributions: gravitational potential energy; and elastic strain energy.

2.4.1 Gravitational potential energy

For a spacecraft with mass M and inertia tensor $\overline{\overline{J}}$, the gravitational potential energy is given by

$$V_g = -\frac{KM}{\rho_c} - \frac{K}{2\rho_c^3}\left(tr.\overline{\overline{J}} - 3\bar{i}.\overline{\overline{J}}.\bar{i}\right), = -\frac{KM}{\rho_c} - \frac{1}{6}\epsilon_g\Omega^2\left(tr.\overline{\overline{J}} - 3\bar{i}.\overline{\overline{J}}.\bar{i}\right), \tag{2.74}$$

where 'K' is the gravitational constant of the earth, ρ_c is the distance from the center of the earth to the center of mass of the spacecraft; '$\vec{i}$', the unit vector along $\overline{\rho}_c$; and

$$\epsilon_g = \frac{3}{1 + \epsilon cos\theta} , \tag{2.75}$$

with θ representing the true anomaly. For the spacecraft under consideration, the inertia tensor about its center of mass is

$$\begin{aligned}
\overline{\overline{J}} &= \int \overline{\overline{(R_o + r_o)(R_o + r_o)}} dm_o + \sum_{i=1}^{n} \int \overline{\overline{(R_o + L_i + r_i)(R_o + L_i + r_i)}} dm_i , \\
&= \overline{\overline{J}} - M\overline{\overline{L_o L_o}} - \frac{1}{M}\sum_{i=1}^{n}\sum_{i=1}^{n}\overline{\overline{H_i H_j}} \\
&\quad + \sum_{i=1}^{n}\left(\overline{\overline{J}}_i + m_i\overline{\overline{L_i L_i}} + \overline{\overline{(L_i - L_o)H_i}} + \overline{\overline{H_i(L_i - L_o)}}\right).
\end{aligned} \tag{2.76}$$

Note, equations (2.76) and (2.46) are identical. It can be shown that:

$$tr.\overline{\overline{J}} = 2J^o ; \tag{2.77}$$

$$\vec{i}.\overline{\overline{J}}.\vec{i} = J^o - [\ a_1\ ]\left[J^1\right][\ a_1\ ]^T. \tag{2.78}$$

Therefore the gravitational potential energy expression takes the form as

$$V_g = -\frac{KM}{\rho_c} + \frac{1}{6}\epsilon_g\Omega^2 J^o - \frac{1}{2}\epsilon_g\Omega^2[\ a_1\ ]\left[J^1\right][\ a_1\ ]^T. \tag{2.79}$$

2.4.2 Elastic strain energy

The strain energy expressions for a beam and a plate are:

$$V_{s,beam} = \frac{E}{2}\int\left\{I_{yy}\left(\frac{\partial^2 u_x}{\partial z^2}\right)^2 + I_{xx}\left(\frac{\partial^2 u_y}{\partial z^2}\right)^2\right\}dz ; \tag{2.80}$$

$$\begin{aligned}
V_{s,plate} &= \frac{D}{2}\int\int\left\{\left(\frac{\partial^2 u}{\partial y^2}\right)^2 + 2\nu\left(\frac{\partial^2 u}{\partial y^2}\right)\left(\frac{\partial^2 u}{\partial z^2}\right) + \left(\frac{\partial^2 u}{\partial z^2}\right)^2\right. \\
&\quad \left. + 2(1-\nu)\left(\frac{\partial^2 u}{\partial y \partial z}\right)^2\right\}dydz ;
\end{aligned} \tag{2.81}$$

where D and ν are the flexural rigidity and Poisson's ratio of the plate material, respectively; and EI_{xx}, EI_{yy} are the bending rigidity of the beam about the y and x axes, respectively. Substituting for the elastic deflections (2.2–2.6) into equation

(2.81), the strain energy for a plate is obtained as

$$V_{s,plate} = \frac{D}{2}\sum_p\sum_q\sum_r\sum_s u_{pq}(t)u_{rs}(t)\left\{\mu_p^2\mu_r^2\Pi^{ww}_{pqrs} + 2\nu\mu_p^2\lambda_s^2\Pi^{wl}_{pqrs} + \lambda_q^2\lambda_s^2\Pi^{ll}_{pqrs} + 2(1-\nu)\mu_p\lambda_q\mu_r\lambda_s\Pi^{wlwl}_{pqrs}\right\}, \quad (2.82)$$

with:

$$\Pi^{ww}_{pqrs} = \int \frac{l}{d^3}\Phi_p''\Psi_q\Phi_r''\Psi_s d\eta d\xi \; ; \quad (2.83)$$

$$\Pi^{wl}_{pqrs} = \int \frac{1}{dl}\Phi_p''\Psi_q\Phi_r\Psi_s'' d\eta d\xi \; ; \quad (2.84)$$

$$\Pi^{ll}_{pqrs} = \int \frac{d}{l^3}\Phi_p\Psi_q''\Phi_r\Psi_s'' d\eta d\xi \; ; \quad (2.85)$$

$$\Pi^{wlwl}_{pqrs} = \int \frac{1}{dl}\Phi_p'\Psi_q'\Phi_r'\Psi_s' d\eta d\xi \; . \quad (2.86)$$

For a rectangular plate with the width 'd' and the length 'l', the expression takes the form as follows,

$$V_{s,plate} = \frac{D}{2}\sum_p\sum_q\sum_r\sum_s u_{pq}(t)u_{rs}(t)\left\{\mu_p^2\mu_r^2\delta_{qs}\frac{l}{d^3}\Gamma^{wpp}_{pr} + \frac{2\nu}{dl}\mu_p^2\lambda_s^2\Gamma^{wp}_{pr}\Gamma^{lp}_{sq} + \lambda_q^2\lambda_s^2\frac{d}{l^3}\delta_{pr}\Gamma^{lpp}_{qs} + \frac{2(1-\nu)}{dl}\mu_p\lambda_q\mu_r\lambda_s\Gamma^{w}_{pr}\Gamma^{l}_{qs}\right\}. \quad (2.87)$$

Here:

$$\Gamma^{wpp}_{pr} = \int \Phi_p''\Phi_r'' d\eta \; ; \quad (2.88)$$

$$\Gamma^{wp}_{pr} = \int \Phi_p''\Phi_r d\eta \; ; \quad (2.89)$$

$$\Gamma^{lp}_{sq} = \int \Psi_s''\Psi_q d\xi \; ; \quad (2.90)$$

$$\Gamma^{lpp}_{qs} = \int \Psi_q''\Psi_s'' d\xi \; ; \quad (2.91)$$

$$\Gamma^{w}_{pr} = \int \Phi_p'\Phi_r' d\eta \; ; \quad (2.92)$$

$$\Gamma^{l}_{qs} = \int \Psi_q'\Psi_s' d\xi \; . \quad (2.93)$$

The strain energy for a beam can be written as

$$V_{s,beam} = \frac{E}{2l^3}\left\{\sum_p\sum_q I_{yy}\lambda_p^2\lambda_q^2 u_{xp}(t)u_{xq}(t)\Gamma^{lpp}_{pq} + \sum_r\sum_s I_{xx}\lambda_r^2\lambda_s^2 u_{yr}(t)u_{ys}(t)\Gamma^{lpp}_{rs}\right\}. \quad (2.94)$$

The expressions (2.87) and (2.94) can be written in a compact matrix form as

$$V_{si} = \frac{1}{2}[\ u_i\ ]\,[K_i]\,[\ u_i\ ]^T. \tag{2.95}$$

Here $[K_i]$ is the stiffness matrix of the appendage i. For example, assuming i to be a beam and taking two modes in x_i and y_i directions, the stiffness matrix can be written as

$$[K_i] = \begin{bmatrix} k^i_{11} & k^i_{12} & 0 & 0 \\ k^i_{21} & k^i_{22} & 0 & 0 \\ 0 & 0 & k^i_{33} & k^i_{34} \\ 0 & 0 & k^i_{43} & k^i_{44} \end{bmatrix}, \tag{2.96}$$

with:

$$\begin{aligned} k^i_{11} &= E_i I_{iyy} \lambda_1^4 \Gamma^{lpp}_{11} / l_i^3\ ; \\ k^i_{12} &= k^i_{21} = E_i I_{iyy} \lambda_1^2 \lambda_2^2 \Gamma^{lpp}_{12} / l_i^3\ ; \\ k^i_{22} &= E_i I_{iyy} \lambda_2^4 \Gamma^{lpp}_{22} / l_i^3\ ; \\ k^i_{33} &= E_i I_{ixx} \lambda_1^4 \Gamma^{lpp}_{11} / l_i^3\ ; \\ k^i_{34} &= k^i_{43} = E_i I_{ixx} \lambda_1^2 \lambda_2^2 \Gamma^{lpp}_{12} / l_i^3\ ; \\ k^i_{44} &= E_i I_{ixx} \lambda_2^4 \Gamma^{lpp}_{22} / l_i^3\ . \end{aligned}$$

The associated generalized coordinates are

$$[\ u_i\ ] = [u_{ix1}(t)\ u_{ix2}(t)\ u_{iy1}(t)\ u_{iy2}(t)]\ .$$

For a rectangular plate appendage, with three modes in the z_i direction and two in the y_i direction, the stiffness matrix is

$$[K_i] = \begin{bmatrix} k^i_{11} & k^i_{12} & k^i_{13} & 0 & 0 & 0 \\ k^i_{21} & k^i_{22} & k^i_{23} & 0 & 0 & 0 \\ k^i_{31} & k^i_{32} & k^i_{33} & 0 & 0 & 0 \\ 0 & 0 & 0 & k^i_{44} & k^i_{45} & k^i_{46} \\ 0 & 0 & 0 & k^i_{54} & k^i_{55} & k^i_{56} \\ 0 & 0 & 0 & k^i_{64} & k^i_{65} & k^i_{66} \end{bmatrix}, \tag{2.97}$$

with:

$$k^i_{11} = D_i \lambda_1^4 \frac{d_i}{l_i^3} \Gamma^{lpp}_{11}\ ;$$

$$
\begin{aligned}
k^i_{12} &= k^i_{21} = D_i\lambda_1^2\lambda_2^2\frac{d_i}{l_i^3}\Gamma^{lpp}_{12}\ ;\\
k^i_{13} &= k^i_{31} = D_i\lambda_1^2\lambda_3^2\frac{d_i}{l_i^3}\Gamma^{lpp}_{13}\ ;\\
k^i_{22} &= D_i\lambda_2^4\frac{d_i}{l_i^3}\Gamma^{lpp}_{22}\ ;\\
k^i_{23} &= k^i_{32} = D_i\lambda_2^2\lambda_3^2\frac{d_i}{l_i^3}\Gamma^{lpp}_{23}\ ;\\
k^i_{33} &= D_i\lambda_3^4\frac{d_i}{l_i^3}\Gamma^{lpp}_{33}\ ;\\
k^i_{44} &= D_i\lambda_1^4\frac{d_i}{l_i^3}\Gamma^{lpp}_{11} + \frac{2D_i(1-\nu_i)}{d_il_i}\mu_2^2\lambda_1^2\Gamma^w_{22}\Gamma^l_{11}\ ;\\
k^i_{45} &= k^i_{54} = D_i\lambda_1^2\lambda_2^2\frac{d_i}{l_i^3}\Gamma^{lpp}_{12} + \frac{2D_i(1-\nu_i)}{d_il_i}\mu_2^2\lambda_1\lambda_2\Gamma^w_{22}\Gamma^l_{12}\ ;\\
k^i_{46} &= k^i_{64} = D_i\lambda_1^2\lambda_3^2\frac{d_i}{l_i^3}\Gamma^{lpp}_{13} + \frac{2D_i(1-\nu_i)}{d_il_i}\mu_2^2\lambda_1\lambda_3\Gamma^w_{22}\Gamma^l_{13}\ ;\\
k^i_{55} &= D_i\lambda_2^4\frac{d_i}{l_i^3}\Gamma^{lpp}_{22} + \frac{2D_i(1-\nu_i)}{d_il_i}\mu_2^2\lambda_2^2\Gamma^w_{22}\Gamma^l_{22}\ ;\\
k^i_{56} &= k^i_{65} = D_i\lambda_2^2\lambda_3^2\frac{d_i}{l_i^3}\Gamma^{lpp}_{23} + \frac{2D_i(1-\nu_i)}{d_il_i}\mu_2^2\lambda_2\lambda_3\Gamma^w_{22}\Gamma^l_{23}\ ;\\
k^i_{66} &= D_i\lambda_3^4\frac{d_i}{l_i^3}\Gamma^{lpp}_{33} + \frac{2D_i(1-\nu_i)}{d_il_i}\mu_2^2\lambda_3^2\Gamma^w_{22}\Gamma^l_{33}\ .
\end{aligned}
$$

Now the generalized coordinates are given as

$$[\ u_i\ ] = [u_{i11}(t),\ u_{i12}(t),\ u_{i13}(t),\ u_{i21}(t),\ u_{i22}(t),\ u_{i23}(t)]\ .$$

2.5 Governing Equations of Motion

The governing equations of motion were obtained using the Lagrangian formulation procedure,

$$\frac{d}{dt}\frac{\partial T}{\partial[\ \dot{q}\ ]} - \frac{\partial T}{\partial[\ q\ ]} + \frac{\partial V_g}{\partial[\ q\ ]} + \frac{\partial V_s}{\partial[\ q\ ]} = [Q]\,, \tag{2.98}$$

where $[Q]$ is a column matrix of generalized forces corresponding to the group of generalized coordinates $[\ q\ ]$. The generalized coordinates are divided into three groups:

- librational motion: λ, ϕ, ψ;
- appendage vibrational coordinates: $[\ u_k\ ]$, $\quad k = 1, 2, \cdots, n$;

- free rotation of the appendages (as against the prescribed slew) : $[\ \alpha_k\ ]$.

2.5.1 Librational equations

Librational velocities $[\ \dot{\alpha}_o\ ] = [\dot{\lambda}\ \ \dot{\phi}\ \ \dot{\psi}]$, being contained in T_{lib} and T_{coup} , give

$$\frac{\partial T}{\partial[\ \dot{\alpha}_o\ ]} = [B_o]\Big\{[J]\left([\ a_3\ ]^T\Omega + [B_o]^T[\ \dot{\alpha}_o\ ]^T\right) + \sum_{i=1}^{n}\left([M_{12}]_i\,[B_i]^T[\ \dot{\alpha}_i\ ]^T + [M_{13}]_i\,v_i + [M_{14}]_i[\ \dot{u}_i\ ]^T\right)\Big\}. \quad (2.99)$$

Similarly, librational angles appear in T_{lib}, T_{coup} and V_g resulting in:

$$\frac{\partial T}{\partial[\ \alpha_o\ ]} = \left(\frac{\partial[\ a_3\ ]}{\partial[\ \alpha_o\ ]}\Omega + \frac{\partial}{\partial[\ \alpha_o\ ]}[\ \dot{\alpha}_o\ ][B_o]\right)\Big\{[J]\left([\ a_3\ ]^T\Omega + [B_o]^T[\ \dot{\alpha}_o\ ]^T\right) + \sum_{i=1}^{n}\left([M_{12}]_i\,[B_i]^T[\ \dot{\alpha}_i\ ]^T + [M_{13}]_i\,v_i + [M_{14}]_i[\ \dot{u}_i\ ]^T\right)\Big\}; \quad (2.100)$$

$$\frac{\partial V_g}{\partial[\ \alpha_o\ ]} = -\epsilon_g\Omega^2\frac{\partial[\ a_1\ ]}{\partial[\ \alpha_o\ ]}\left[J^1\right][\ a_1\ ]^T. \quad (2.101)$$

Substituting from equations (2.99)–(2.101) into the Lagrangian equation (2.98), the librational equations of motion are obtained as

$$\begin{aligned}
&\left(\left[\dot{B}_o\right] - \frac{\partial[\ a_3\ ]}{\partial[\ \alpha_o\ ]}\Omega - \frac{\partial}{\partial[\ \alpha_o\ ]}[\ \dot{\alpha}_o\ ][B_o]\right)\Big\{[J]\left([\ a_3\ ]^T\Omega + [B_o]^T[\ \dot{\alpha}_o\ ]^T\right) \\
&+ \sum_{i=1}^{n}\left([M_{12}]_i\,[B_i]^T[\ \dot{\alpha}_i\ ]^T + [M_{13}]_i\,v_i + [M_{14}]_i[\ \dot{u}_i\ ]^T\right)\Big\} \\
&+ [B_o]\Big\{\left[\dot{J}\right]\left([\ a_3\ ]^T\Omega + [B_o]^T[\ \dot{\alpha}_o\ ]^T\right) + [J]\left(\left(\frac{\partial[\ a_3\ ]}{\partial[\ \alpha_o\ ]}\right)^T\Omega + \left[\dot{B}_o\right]^T\right)[\ \dot{\alpha}_o\ ]^T \\
&+ [J]\left([\ a_3\ ]^T\dot{\Omega} + [B_o]^T[\ \ddot{\alpha}_o\ ]^T\right) + \sum_{i=1}^{n}\Big(\left(\left[\dot{M}_{12}\right]_i[B_i]^T + [M_{12}]_i\left[\dot{B}_i\right]^T\right)[\ \dot{\alpha}_i\ ]^T \\
&+ [M_{12}]_i\,[B_i]^T[\ \ddot{\alpha}_i\ ]^T + \left[\dot{M}_{13}\right]_i v_i + [M_{13}]_i\,\dot{v}_i + \left[\dot{M}_{14}\right]_i[\ \dot{u}_i\ ]^T \\
&+ [M_{14}]_i[\ \ddot{u}_i\ ]^T\Big)\Big\} - \epsilon_g\Omega^2\frac{\partial[\ a_1\ ]}{\partial[\ \alpha_o\ ]}\left[J^1\right][\ a_1\ ]^T = [Q_{\alpha o}].
\end{aligned} \quad (2.102)$$

It is convenient and more meaningful in practice to use true anomaly θ as the independent variable instead of time. Using the relations:

$$\begin{aligned}
\frac{d}{dt} &= \dot{\theta}\,\frac{d}{d\theta} = \Omega\frac{d}{d\theta}\ ; \\
\frac{d^2}{dt^2} &= \dot{\theta}^2\left(\frac{d^2}{d\theta^2} - \epsilon_c\frac{d}{d\theta}\right) = \Omega^2\left(\frac{d^2}{d\theta^2} - \epsilon_c\frac{d}{d\theta}\right),
\end{aligned} \quad (2.103)$$

with

$$\epsilon_c = \frac{2\epsilon sin\theta}{1+\epsilon cos\theta} \quad ,$$

the equations of librational motion become:

$$\begin{aligned}
& [B_o][J]\left\{[B_o]^T[\,\alpha_o''\,]^T + \left(\left(\frac{\partial[\,a_3\,]}{\partial[\,\alpha_o\,]}\right)^T + [B_o']^T\right)[\,\alpha_o'\,]\right\} \\
+\ & ([D^*][J] + [B_o][J'])\left([\,a_3\,]^T\Omega + [B_o]^T[\,\alpha_o'\,]^T\right) \\
+\ & \sum_{i=1}^{n}\left\{[B_o][M_{12}]_i\left([B_i]^T[\,\alpha_i''\,]^T + [B_i']^T[\,\alpha_i'\,]^T\right) + ([D^*][M_{12}]_i + [B_o][M_{12}']_i)\right. \\
& \left.[B_i]^T[\,\alpha_i'\,]^T\right\} + \sum_{i=1}^{n}\left\{\,[B_o][M_{13}]_i\,l_i'' + ([D^*][M_{13}]_i + [B_o][M_{13}']_i)\,l_i'\,\right\} \\
+\ & \sum_{i=1}^{n}\left\{[B_o][M_{14}]_i[\,u_i''\,]^T + ([D^*][M_{14}]_i + [B_o][M_{14}']_i)[\,u_i'\,]^T\right\} \\
-\ & \epsilon_g\frac{\partial[\,a_1\,]}{\partial[\,\alpha_o\,]}\left[J^1\right][\,a_1\,]^T \;=\; \frac{1}{\Omega^2}[Q_{ao}]\,, \qquad (2.104)
\end{aligned}$$

where the primes represent the derivative with respect to the true anomaly , and

$$[D^*] = [B_o'] - \frac{\partial[\,a_3\,]}{\partial[\,\alpha_o\,]} - \frac{\partial}{\partial[\,\alpha_o\,]}[\,\alpha_o'\,][B_o] - \epsilon_c[B_o]\,. \qquad (2.105)$$

2.5.2 Vibrational equations

The equations corresponding to vibration of the elastic appendage k are derived as follows:

$$\begin{aligned}
\frac{\partial T}{\partial[\,\dot{u}_k\,]} &= [M_{14}]_k^T\left([\,a_3\,]^T\Omega + [B_o]^T[\,\dot{\alpha}_o\,]^T\right) \\
&+ \sum_{i=1}^{n}\left([M_{24}]_{ik}^T[B_i]^T[\,\dot{\alpha}_i\,]^T + [M_{34}]_{ik}^T v_i + [M_{44}]_{ki}[\,\dot{u}_i\,]^T\right); \qquad (2.106) \\
\frac{\partial T}{\partial[\,u_k\,]} &= \frac{1}{2}\frac{\partial J^o}{\partial[\,u_k\,]}\left(\Omega^2 + 2\Omega[\,a_3\,][B_o]^T[\,\dot{\alpha}_o\,]^T + [\,\dot{\alpha}_o\,][B_o][B_o]^T[\,\dot{\alpha}_o\,]^T\right) \\
&- \frac{1}{2}\frac{\partial}{\partial[\,u_k\,]}\left([\,a_3\,]\Omega + [\,\dot{\alpha}_o\,[B_o]\right)\left[J^1\right]\left([\,a_3\,]^T\Omega + [B_o]^T[\,\dot{\alpha}_o\,]^T\right) \\
&+ \frac{1}{2}\frac{\partial}{\partial[\,u_k\,]}\sum_{i=1}^{n}\sum_{j=1}^{n}\left\{[\,\dot{\alpha}_i\,][B_i]\left([M_{22}]_{ij}[B_j]^T[\,\dot{\alpha}_j\,]^T + 2[M_{23}]_{ij}v_j + 2[M_{24}]_{ij}[\,\dot{u}_j\,]^T\right)\right. \\
&+ \left. v_i\left((M_{33})_{ij}v_j + 2[M_{34}]_{ij}[\,\dot{u}_j\,]^T\right) + [\,\dot{u}_i\,][M_{44}]_{ij}[\,\dot{u}_j\,]^T\right\}; \qquad (2.107) \\
\frac{\partial V_g}{\partial[\,u_k\,]} &= \frac{1}{6}\epsilon_g\Omega^2\frac{\partial J^o}{\partial[\,u_k\,]} - \frac{1}{2}\epsilon_g\Omega^2[\,a_1\,]\frac{\partial}{\partial[\,u_k\,]}\left[J^1\right][\,a_1\,]^T; \qquad (2.108) \\
\frac{\partial V_s}{\partial[\,u_k\,]} &= \frac{\partial V_{sk}}{\partial[\,u_k\,]} = [K_k][\,u_k\,]^T. \qquad (2.109)
\end{aligned}$$

Combining the above contributions leads to the vibrational equations of the appendage k as

$$
\begin{aligned}
& [M_{14}]_k^T \left\{ [B_o]^T [\, \ddot{\alpha}_o \,]^T + [\, a_3 \,]^T \dot{\Omega} + \left(\left(\frac{\partial [\, a_3 \,]}{\partial [\, \alpha_o \,]} \right)^T \Omega + \left[\dot{B}_o \right]^T \right) [\, \dot{\alpha}_o \,]^T \right\} \\
+ & \left\{ \left[\dot{M}_{14} \right]_k^T + \frac{1}{2} \frac{\partial}{\partial [\, u_k \,]} \left([\, a_3 \,] \Omega + [\, \dot{\alpha}_o \,] [B_o] \right) \left[J^1 \right] \right. \\
- & \left. \frac{\partial}{\partial [\, u_k \,]} \sum_{i=1}^{n} \left([\, \dot{\alpha}_i \,] [B_i] [M_{12}]_i^T + [M_{13}]_i^T v_i + [\, \dot{u}_i \,] [M_{14}]_i^T \right) \right\} \left([\, a_3 \,]^T \Omega + [B_o]^T [\, \dot{\alpha}_o \,]^T \right) \\
+ & \frac{\partial J^o}{\partial [\, u_k \,]} \left(\frac{1}{6} \epsilon_g \Omega^2 - \frac{1}{2} \Omega^2 - \Omega [\, a_3 \,] [B_o]^T [\, \dot{\alpha}_o \,]^T - \frac{1}{2} [\, \dot{\alpha}_o \,] [B_o] [B_o]^T [\, \dot{\alpha}_o \,]^T \right) \\
- & \frac{1}{2} \epsilon_g \Omega^2 [\, a_1 \,] \frac{\partial}{\partial [\, u_k \,]} \left[J^1 \right] [\, a_1 \,]^T \\
+ & \sum_{i=1}^{n} \left([M_{24}]_{ik}^T [B_i]^T [\, \ddot{\alpha}_i \,]^T + [M_{24}]_{ik}^T \left[\dot{B}_i \right]^T [\, \dot{\alpha}_i \,]^T + \left[\dot{M}_{24} \right]_{ik}^T [B_i]^T [\, \dot{\alpha}_i \,]^T \right. \\
+ & \left. [M_{34}]_{ik}^T \dot{v}_i + \left[\dot{M}_{34} \right]_{ik}^T v_i + [M_{44}]_{ki} [\, \ddot{u}_i \,] + \left[\dot{M}_{44} \right]_{ki} [\, \dot{u}_i \,]^T \right) \\
- & \frac{\partial}{\partial [\, u_k \,]} \sum_{i=1}^{n} \sum_{j=1}^{n} \left\{ \left(\frac{1}{2} [\, \dot{\alpha}_i \,] [B_i] [M_{22}]_{ij}^T + [M_{23}]_{ij}^T v_j + [\, \dot{u}_j \,] [M_{24}]_{ij}^T \right) [B_i]^T [\, \dot{\alpha}_i \,]^T \right. \\
+ & \left. \frac{1}{2} (M_{33})_{ij} v_i v_j + [\, \dot{u}_j \,] [M_{34}]_{ij}^T v_i \right\} + [K_k] [\, u_k \,]^T \;=\; [Q_{uk}] . \qquad (2.110)
\end{aligned}
$$

In terms of the true anomaly θ as the independent variable, the equations take the form

$$
\begin{aligned}
& [M_{14}]_k^T [B_o]^T [\, \alpha_o'' \,]^T + \left([M_{14}']_k^T - \epsilon_c [M_{14}]_k^T \right) \left([\, a_3 \,]^T + [B_o]^T [\, \alpha_o' \,]^T \right) \\
+ & [M_{14}]_k^T \left(\left(\frac{\partial [\, a_3 \,]}{\partial [\, \alpha_o \,]} \right)^T + [B_o'] \right) [\, \alpha_o' \,]^T - \frac{1}{2} \epsilon_g \frac{\partial}{\partial [\, u_k \,]} [\, a_1 \,] \left[J^1 \right] [\, a_1 \,]^T \\
+ & \frac{1}{2} \frac{\partial}{\partial [\, u_k \,]} \left([\, a_3 \,] + [\, \alpha_o' \,] [B_o] \right) \left[J^1 \right] \left([\, a_3 \,]^T + [B_o]^T [\, \alpha_o' \,]^T \right) \\
+ & \frac{\partial J^o}{\partial [\, u_k \,]} \left(\frac{1}{6} \epsilon_g - \frac{1}{2} - [\, a_3 \,] [B_o]^T [\, \alpha_o' \,]^T - \frac{1}{2} [\, \alpha_o' \,] [B_o] [B_o]^T [\, \alpha_o' \,]^T \right) \\
- & \frac{\partial}{\partial [\, u_k \,]} \sum_{i=1}^{n} \left([\, \alpha_i' \,] [B_i] [M_{12}]_i^T + [M_{13}]_i^T l_i' + [\, u_i' \,] [M_{14}]_i^T \right) \\
& \left([\, a_3 \,]^T + [B_o]^T [\, \alpha_o' \,]^T \right) + \sum_{i=1}^{n} \left\{ [M_{24}]_{ik}^T [B_i]^T [\, \alpha_i'' \,]^T \right. \\
+ & \left. \left([M_{24}]_{ik}^T [B_i']^T + [M_{24}']_{ik}^T [B_i]^T - \epsilon_c [M_{24}]_{ik}^T [B_i]^T \right) [\, \alpha_i' \,]^T \right\} \\
- & \frac{\partial}{\partial [\, u_k \,]} \sum_{i=1}^{n} \sum_{j=1}^{n} \left(\frac{1}{2} [\, \alpha_j' \,] [B_j] [M_{22}]_{ij}^T + l_j' [M_{23}]_{ij}^T + [\, u_j' \,] [M_{24}]_{ij}^T \right) [B_i]^T [\, \alpha_i' \,]^T
\end{aligned}
$$

$$+ \sum_{i=1}^{n} \left\{ [M_{34}]_{ik}^T \, l_i'' + \left([M_{34}']_{ik}^T - \epsilon_c \, [M_{34}]_{ik}^T \right) l_i' \right\}$$

$$- \frac{\partial}{\partial [\, u_k \,]} \sum_{i=1}^{n} \sum_{j=1}^{n} \left\{ \frac{1}{2} \, (M_{33})_{ij} \, l_i' l_j' + [\, u_j' \,] \, [M_{34}]_{ij}^T \, l_i' \right\}$$

$$+ \sum_{i=1}^{n} \left\{ [M_{44}]_{ki} \, [\, u_i'' \,]^T + ([M_{44}']_{ki} - \epsilon_c \, [M_{44}]_{ki}) \, [\, u_i' \,]^T \right\}$$

$$+ \frac{1}{\Omega^2} \, [K_k] \, [\, u_k \,]^T = \frac{1}{\Omega^2} \, [Q_{uk}] \, . \qquad (2.111)$$

2.5.3 Equations of motion for free rotation of the appendage

If the appendage k is permitted to rotate freely with respect to the central body, the corresponding equations of motion can be derived as follows:

$$\frac{\partial T}{\partial [\, \dot{\alpha}_k \,]} = [B_k] \, [M_{12}]_k^T \left([\, a_3 \,]^T \Omega + [B_o]^T \, [\, \dot{\alpha}_o \,]^T \right)$$

$$+ [B_k] \sum_{j=1}^{n} \left([M_{22}]_{kj} \, [B_j]^T \, [\, \dot{\alpha}_j \,]^T + [M_{23}]_{kj} \, v_j + [M_{24}]_{kj} \, [\, \dot{u}_j \,]^T \right) ; \qquad (2.112)$$

$$\frac{\partial T}{\partial [\, \alpha_k \,]} = \frac{1}{2} \frac{\partial J^o}{\partial [\, \alpha_k \,]} \left(\Omega^2 + 2\Omega [\, a_3 \,] \, [B_o]^T \, [\, \dot{\alpha}_o \,]^T + [\, \dot{\alpha}_o \,] \, [B_o] \, [B_o]^T \, [\, \dot{\alpha}_o \,]^T \right)$$

$$- \frac{1}{2} \frac{\partial}{\partial [\, \alpha_k \,]} \left([\, a_3 \,] \Omega + [\, \dot{\alpha}_o \,] \, [B_o] \right) \left[J^1 \right] \left([\, a_3 \,] \Omega + [\, \dot{\alpha}_o \,] \, [B_o] \right)^T$$

$$+ \frac{\partial}{\partial [\, \alpha_k \,]} \sum_{i=1}^{n} \left([\, \dot{\alpha}_i \,] \, [B_i] \, [M_{12}]_i^T + v_i \, [\, M_{13} \,]_i^T + [\, \dot{u}_i \,] \, [M_{14}]_i^T \right) \left([\, a_3 \,] \Omega + [\, \dot{\alpha}_o \,] \, [B_o] \right)^T$$

$$+ \frac{\partial}{\partial [\, \alpha_k \,]} \sum_{i=1}^{n} \sum_{j=1}^{n} \left\{ \left(\frac{1}{2} [\, \dot{\alpha}_j \,] \, [B_j] \, [M_{22}]_{ji} + v_j \, [M_{23}]_{ij}^T + [\, \dot{u}_j \,] \, [M_{24}]_{ij}^T \right) [B_i]^T \, [\, \dot{\alpha}_i \,]^T \right.$$

$$\left. + \frac{1}{2} \, (M_{33}) \, v_i v_j + v_i \, [M_{34}]_{ij} \, [\, \dot{u}_j \,]^T + \frac{1}{2} [\, \dot{u}_i \,] \, [M_{44}] \, [\, \dot{u}_i \,]^T \right\} ; \qquad (2.113)$$

$$\frac{\partial V_g}{\partial [\, \alpha_k \,]} = \frac{1}{6} \epsilon_g \Omega^2 \frac{\partial J^o}{\partial [\, \alpha_k \,]} - \frac{1}{2} \epsilon_g \Omega^2 \frac{\partial}{\partial [\, \alpha_k \,]} [\, a_1 \,] \left[J^1 \right] [\, a_1 \,]^T . \qquad (2.114)$$

Combining the above contributions, the equations corresponding to free rotation of the appendage k are:

$$[B_k] \left\{ [M_{12}]_k^T \left([B_o]^T \, [\, \ddot{\alpha}_o \,]^T + \left(\left(\frac{\partial [\, a_3 \,]}{\partial [\, \alpha_o \,]} \right)^T \Omega + \left[\dot{B}_o \right] \right) [\, \dot{\alpha}_o \,]^T + [\, a_3 \,]^T \, \dot{\Omega} \right) \right.$$

$$\left. + \sum_{j=1}^{n} \left([M_{22}]_{kj} \, [B_j]^T \, [\, \ddot{\alpha}_j \,]^T + [M_{24}]_{kj} \, [\, \ddot{u}_j \,]^T \right) \right\}$$

$$+ \left(\left[\dot{B}_k \right] [M_{12}]_k^T + [B_k] \left[\dot{M}_{12} \right]_k^T \right) \left([\, a_3 \,]^T \Omega + [B_o]^T \, [\, \dot{\alpha}_o \,]^T \right)$$

$$
\begin{aligned}
&+ \left[\dot{B}_k\right]\sum_{j=1}^{n}\left([M_{22}]_{kj}\,[B_j]^T\,[\,\dot{\alpha}_j\,]^T + [M_{23}]_{kj}\,v_j + [M_{24}]_{kj}\,[\,\dot{u}_j\,]^T\right)\\
&+ [B_k]\sum_{j=1}^{n}\left\{\left(\left[\dot{M}_{22}\right]_{kj}[B_j]^T + [M_{22}]_{kj}\left[\dot{B}_j\right]^T\right)[\,\dot{\alpha}_j\,]^T + \left[\dot{M}_{23}\right]_{kj}v_j\right.\\
&+ \left.[M_{23}]_{kj}\,\dot{v}_j + \left[\dot{M}_{24}\right]_{kj}[\,\dot{u}_j\,]^T\right\} - \frac{1}{2}\epsilon_g\Omega^2\frac{\partial}{\partial[\,\alpha_k\,]}[\,a_1\,]\left[J^1\right][\,a_1\,]^T\\
&+ \frac{\partial J^o}{\partial[\,\alpha_k\,]}\left(\frac{1}{6}\epsilon_g\Omega^2 - \frac{1}{2}\Omega^2 - \Omega[\,a_3\,][B_o]^T[\,\dot{\alpha}_o\,]^T - \frac{1}{2}[\,\dot{\alpha}_o\,][B_o][B_o]^T[\,\dot{\alpha}_o\,]^T\right)\\
&+ \frac{\partial}{\partial[\,\alpha_k\,]}\left\{\frac{1}{2}\left([\,a_3\,]\Omega + [\,\dot{\alpha}_o\,][B_o]\right)\left[J^1\right]\right.\\
&- \left.\sum_{i=1}^{n}\left([\,\dot{\alpha}_i\,][B_i][M_{12}]_i^T + v_i[\,M_{13}\,]_i^T + [\,\dot{u}_i\,][M_{14}]_i^T\right)\right\}\left([\,a_3\,]\Omega + [\,\dot{\alpha}_o\,][B_o]\right)^T\\
&+ \frac{\partial}{\partial[\,\alpha_k\,]}\sum_{i=1}^{n}\sum_{j=1}^{n}\left\{\left(\frac{1}{2}[\,\dot{\alpha}_j\,][B_j][M_{22}]_{ji} + v_j\,[M_{23}]_{ij}^T + [\,\dot{u}_j\,][M_{24}]_{ij}^T\right)[B_i]^T[\,\dot{\alpha}_i\,]^T\right.\\
&+ \left.\frac{1}{2}\,(M_{33})_{ij}\,v_iv_j + v_i\,[M_{34}]_{ij}\,[\,\dot{u}_j\,]^T + \frac{1}{2}[\,\dot{u}_i\,][M_{44}]_{ij}\,[\,\dot{u}_j\,]^T\right\} \;=\; [Q_{\alpha k}]\;. \qquad (2.115)
\end{aligned}
$$

As before, with the true anomaly as the independent variable, the equations for free rotation of appendage k take the form:

$$
\begin{aligned}
&[B_k]\left\{[M_{12}]_k^T\,[B_o]^T[\,\alpha_o''\,] + \sum_{j=1}^{n}\left([M_{22}]_{kj}\,[B_j]^T[\,\alpha_j''\,]^T + [M_{24}]_{kj}[\,u_j''\,]^T\right)\right\}\\
&+ \left([B_k'][M_{12}]_k^T + [B_k][M_{12}']_k^T - \epsilon_c\,[B_k][M_{12}]_k^T\right)([\,a_3\,] + [\,\alpha_o'\,][B_o])^T\\
&+ [B_k][M_{12}]_k^T\left\{\left(\frac{\partial[\,a_3\,]}{\partial[\,\alpha_o\,]}\right)^T + [B_o']^T\right\}[\,\alpha_o'\,]^T\\
&+ [B_k']\sum_{j=1}^{n}\left([M_{22}]_{kj}\,[B_j]^T[\,\alpha_j'\,]^T + [M_{23}]_{kj}\,l_j' + [M_{24}]_{kj}[\,u_j'\,]^T\right)\\
&+ [B_k]\sum_{j=1}^{n}\left\{\left([M_{22}']_{kj}\,[B_j]^T + [M_{22}]_{kj}\left[B_j'\right]^T - \epsilon_c\,[M_{22}]_{kj}\,[B_j]^T\right)[\,\alpha_j'\,]^T\right.\\
&+ \left.[M_{23}']_{kj}\,l_j' + [M_{23}]_{kj}\left(l_j'' - \epsilon_c l_j'\right) + \left([M_{24}']_{kj} - \epsilon_c\,[M_{24}]_{kj}\right)[\,u_j'\,]^T\right\}\\
&+ \frac{\partial J^o}{\partial[\,\alpha_k\,]}\left(\frac{1}{6}\epsilon_g - \frac{1}{2} - [\,a_3\,][B_o]^T[\,\alpha_o'\,]^T - \frac{1}{2}[\,\alpha_o'\,][B_o][B_o]^T[\,\alpha_o'\,]^T\right)\\
&- \frac{1}{2}\epsilon_g\frac{\partial}{\partial[\,\alpha_k\,]}[\,a_1\,]\left[J^1\right][\,a_1\,]^T + \frac{\partial}{\partial[\,\alpha_k\,]}\left\{\frac{1}{2}\left([\,a_3\,] + [\,\alpha_o'\,][B_o]\right)\left[J^1\right]\right.\\
&- \left.\sum_{j=1}^{n}\left([\,\alpha_j'\,][B_j][M_{12}]_j^T + l_j'\,[M_{13}]_j^T + [\,u_j'\,][M_{14}]_j^T\right)\right\}\left([\,a_3\,] + [\,\alpha_o'\,][B_o]\right)^T
\end{aligned}
$$

$$- \frac{\partial}{\partial[\ \alpha_k\ ]} \sum_{i=1}^{n} \sum_{j=1}^{n} \left\{ \left(\frac{1}{2} [\ \alpha_i'\ ]\,[B_i]\,[M_{22}]_{ij} + l_i'[M_{23}]_{ji}^T + [\ u_i'\ ]\,[M_{24}]_{ji}^T \right) [B_j]^T [\ \alpha_j'\ ]^T \right.$$

$$+ \left. \frac{1}{2} (M_{33})_{ij}\, l_i' l_j' + l_i' [M_{34}]_{ij} [\ u_j'\ ]^T + \frac{1}{2} [\ u_i'\ ]\,[M_{44}]_{ij} [\ u_j'\ ]^T \right\} \ = \ \frac{1}{\Omega^2} [Q_{\alpha k}] \quad (2.116)$$

3. CHECKS ON THE FORMULATION METHODOLOGY

In order to assess validity of the formulation, two particular configurations were selected and the corresponding specific equations of motion, as given by the Lagrangian procedure, obtained. These equations were compared with those obtained independently using a different approach or by a different researcher.

3.1 Test Configuration 1

The first configuration selected for comparison consists of three interconnected rigid bodies as shown in Figure 3-1. The governing linearized equations of motion for this particular case have been obtained by Shen [49] using Kane's approach. They are compared with those given by the Lagrangian method. Of course, the present approach, being quite general, treats the system as a particular case. Furthermore, the equations are linearized to permit comparison. The independent variable is taken to be time.

3.1.1 System description

A three-body rigid satellite, composed of a central body with two rectangular plate shaped appendages, is taken to be in a circular orbit around the earth. The appendages are considered identical, each with mass 'm', length 'l' and width '2d'. The dotted straight line $c_1 - o_1 - o_o - o_2 - c_2$ is a principal axis of inertia for each of the three bodies, and the hinge position parameters $L_1 = L_2 = L$. The appendages are free to undergo rotations (α_1, α_2) about the principal axis. Note, the body fixed coordinate systems are such that x_o, z_1 and z_2 are aligned with the principal axis, with $\overline{i}_o = \overline{k}_1 = -\overline{k}_2$. The system has five degrees of freedom: the librational angles λ, ϕ, ψ and the appendage rotations α_1, α_2.

To facilitate comparison of the particular set of equations of motion for the system under consideration, the first step is to linearize the equations of motion, as given by the Lagrangian procedure, about the system's equilibrium position $\lambda = \phi = \psi = \alpha_1 = \alpha_2 = 0$. To that end, all the angles and their time derivatives are considered small.

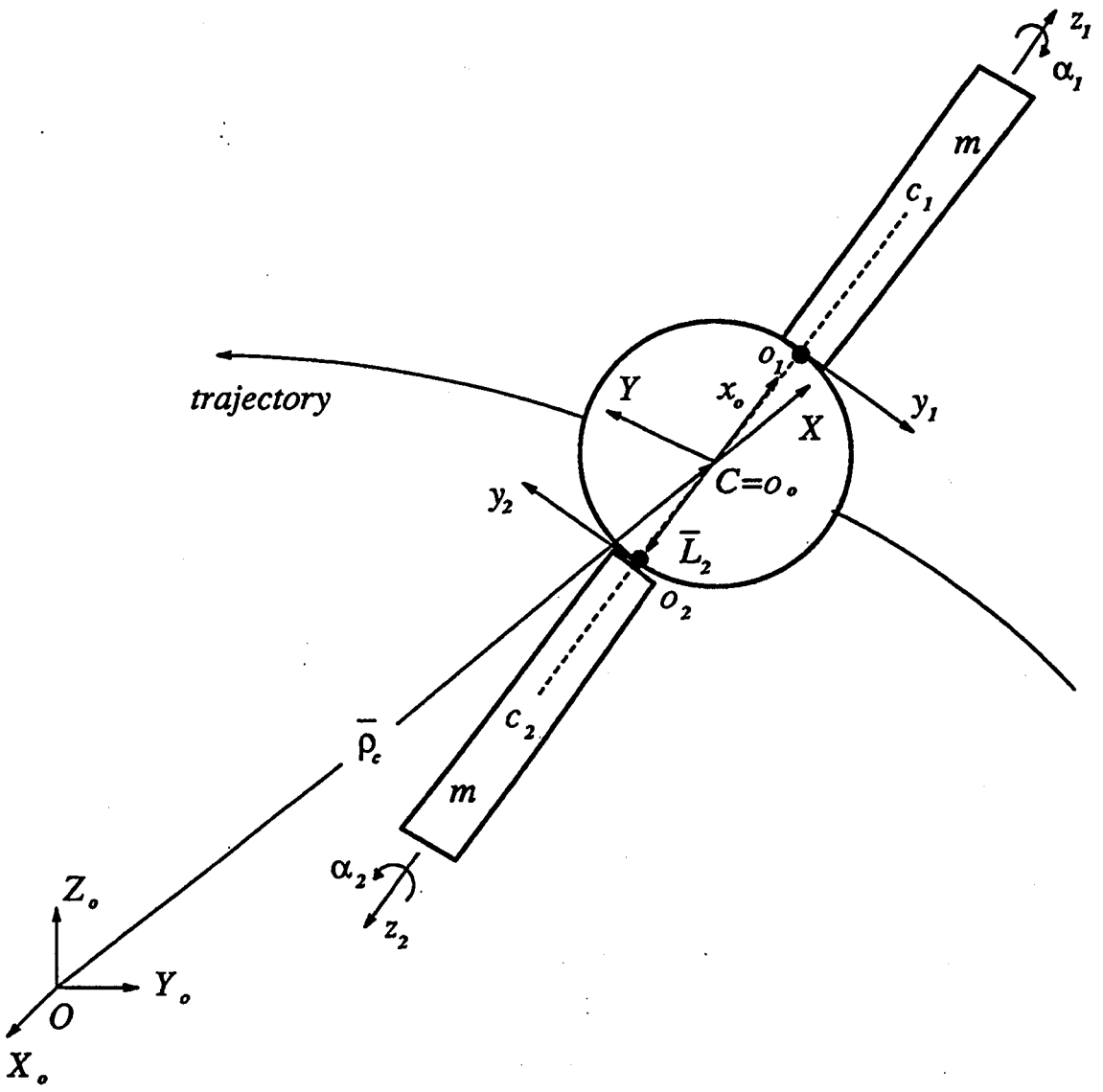

Figure 3-1 A satellite configuration, with three interconnected rigid bodies, considered to check the equations of motion.

For the particular configuration under consideration:

$$
\begin{aligned}
[L_1] &= [L \;\; 0 \;\; 0]\,; \\
[L_2] &= [-L \;\; 0 \;\; 0]\,; \\
[H_1] &= [H_2] = [0 \;\; 0 \;\; \frac{1}{2}ml]\,; \\
J_1^o &= J_2^o = \frac{1}{3}m\left(d^2 + l^2\right)\,; \\
\left[J_1^1\right] &= \left[J_2^1\right] = \begin{bmatrix} 0 & & \\ & \frac{1}{3}md^2 & \\ & & \frac{1}{3}ml^2 \end{bmatrix}.
\end{aligned}
$$

The transformation matrices are:

$$
[A] \approx \begin{bmatrix} 1 & \psi & -\phi \\ -\psi & 1 & \lambda \\ \phi & -\lambda & 1 \end{bmatrix};
$$

$$
[B_o] \approx \begin{bmatrix} 1 & -\psi & \phi \\ \psi & 1 & 0 \\ 0 & 0 & 1 \end{bmatrix};
$$

$$
[C_1] = \begin{bmatrix} 0 & -sin\alpha_1 & cos\alpha_1 \\ 0 & -cos\alpha_1 & -sin\alpha_1 \\ 1 & 0 & 0 \end{bmatrix} \approx \begin{bmatrix} 0 & -\alpha_1 & 1 \\ 0 & -1 & -\alpha_1 \\ 1 & 0 & 0 \end{bmatrix};
$$

$$
[C_2] = \begin{bmatrix} 0 & sin\alpha_2 & cos\alpha_2 \\ 0 & cos\alpha_2 & -sin\alpha_2 \\ -1 & 0 & 0 \end{bmatrix} \approx \begin{bmatrix} 0 & \alpha_2 & 1 \\ 0 & 1 & -\alpha_2 \\ -1 & 0 & 0 \end{bmatrix};
$$

$$
[B_1] = [B_2] = [0 \;\; 0 \;\; 1]\,.
$$

3.1.2 Librational equations of motion

Neglecting the nonlinear terms, librational equation (2.102) reduces to:

$$
\left(\left[\dot{B}_o\right] - \frac{\partial[\,a_3\,]}{\partial[\,\alpha_o\,]}\Omega - \frac{\partial}{\partial[\,\alpha_o\,]}[\,\dot{\alpha}_o\,][B_o]\right)[J][\,a_3\,]^T\Omega
$$

$$
- \frac{\partial[\,a_3\,]}{\partial[\,\alpha_o\,]}\Omega\left([J][B_o]^T[\,\dot{\alpha}_o\,]^T + \sum_{i=1}^{2}[M_{12}]_i[B_i]^T\,\dot{\alpha}_i\right)
$$

$$+ \quad [B_o]\left\{\left[\dot{J}\right]\left[\ a_3\ \right]^T\Omega + [J]\left(\frac{\partial[\ a_3\ ]}{\partial[\ \alpha_o\ ]}\right)^T \Omega[\ \dot{\alpha}_o\ ]^T + [J]\,[B_o]^T\,[\ \ddot{\alpha}_o\ ]^T\right.$$

$$\left. + \quad \sum_{i=1}^{2}[M_{12}]_i\,[B_i]^T\,\ddot{\alpha}_i\right\} - \epsilon_g\Omega^2\frac{\partial[\ a_1\ ]}{\partial[\ \alpha_o\ ]}\left[J^1\right]\left[\ a_1\ \right]^T = [0]\ . \qquad (3.1)$$

From the expressions obtained in the last section, the following relation involving inertia matrices can be derived:

$$J^o \ = \ \tilde{J} + J_1^o + J_2^o + \frac{1}{2}\left(J_{01} + J_{02} + J_{03}\right)\ ;$$

with

$$\tilde{J} = 2mL\left(L + l\right)\ ;$$

and

$$\left[J^1\right] \approx \begin{bmatrix} \frac{1}{2}\left(J_{02} + J_{03} - J_{01}\right) + \frac{2}{3}ml^2 + \tilde{J} & 0 & 0 \\ 0 & \frac{1}{2}\left(J_{01} + J_{03} - J_{02}\right) + \frac{2}{3}md^2 & \frac{1}{3}md^2\left(\alpha_1 - \alpha_2\right) \\ 0 & \frac{1}{3}md^2\left(\alpha_1 - \alpha_2\right) & \frac{1}{2}\left(J_{01} + J_{02} - J_{03}\right) \end{bmatrix}\ ; \qquad (3.2)$$

$$[M_{12}]_1 \ = \ [C_1]^T\begin{bmatrix} \frac{1}{3}m\left(d^2 + l^2\right) + \frac{1}{2}mLl & 0 & 0 \\ 0 & \frac{1}{3}ml^2 + \frac{1}{2}mLl & 0 \\ 0 & 0 & \frac{1}{3}md^2 \end{bmatrix}\ ;$$

$$[M_{12}]_2 \ = \ [C_2]^T\begin{bmatrix} \frac{1}{3}m\left(d^2 + l^2\right) + \frac{1}{2}mLl & 0 & 0 \\ 0 & \frac{1}{3}ml^2 + \frac{1}{2}mLl & 0 \\ 0 & 0 & \frac{1}{3}md^2 \end{bmatrix}\ .$$

Substituting the above expressions and their derivatives in equation (3.1), and omitting the nonlinear terms, the following equations are obtained:

$$J_1\,\ddot{\lambda} + \left(J_3 - J_1 - J_2\right)\dot{\phi}\,\Omega + \left(J_3 - J_2\right)\lambda\Omega^2$$
$$+\frac{1}{3}md^2\left\{\ddot{\alpha}_1 - \ddot{\alpha}_2 + \Omega^2\left(\alpha_1 - \alpha_2\right)\right\} \ = \ 0\ ; \qquad (3.3)$$

$$J_2\,\ddot{\phi} - \left(J_3 - J_1 - J_2\right)\dot{\lambda}\,\Omega + 4\left(J_3 - J_1\right)\phi\Omega^2 \ = \ 0\ ; \qquad (3.4)$$

$$J_3\,\ddot{\psi} + 3\left(J_2 - J_1\right)\psi\Omega^2 \ = \ 0; \qquad (3.5)$$

with:

$$J_1 \ = \ J_{01} + \frac{2}{3}md^2\ ;$$

$$J_2 = J_{02} + \tilde{J} + \frac{2}{3} m l^2 ;$$
$$J_3 = J_{03} + \frac{2}{3} m \left(d^2 + l^2 \right) + \tilde{J} .$$

These equations are the same as those obtained by the Kane procedure in reference [49]. Note, with $\alpha_1 = \alpha_2 = 0$, and $\ddot{\alpha}_1 = \ddot{\alpha}_2 = 0$, equations (3.3) – (3.5) represent the classical librational cases for a single rigid body.

3.1.3 Equations of motion for the appendage rotation

For the particular configuration, equation (2.115), when linearized, reduces to

$$[B_k]\,[M_{12}]_k^T \left\{ [B_o]^T [\,\ddot{\alpha}_o\,]^T + \Omega \left(\frac{\partial [\,a_3\,]}{\partial [\,\alpha_o\,]} \right)^T [\,\dot{\alpha}_o\,]^T \right\} + [B_k] \sum_{i=1}^{2} \left([M_{22}]_{ki}\, [B_i]^T\, \ddot{\alpha}_i \right)$$
$$+ \frac{\partial}{\partial \alpha_k} [\,a_3\,] \left[J^1 \right] [B_o]^T [\,\dot{\alpha}_o\,]^T \Omega + \left([B_k] \left[\dot{M}_{12} \right]_k^T - \frac{\partial}{\partial \alpha_k} \sum_{i=1}^{2} \dot{\alpha}_i\, [B_i]\, [M_{12}]_i^T \right) [\,a_3\,]^T \Omega$$
$$+ \frac{1}{2} \frac{\partial}{\partial \alpha_k} [\,a_3\,] \left[J^1 \right] [\,a_3\,]^T \Omega^2 - \frac{1}{2} \epsilon_g \Omega^2 \frac{\partial}{\partial \alpha_k} [\,a_1\,] \left[J^1 \right] [\,a_1\,]^T = 0 . \qquad (3.6)$$

Here:

$$[M_{22}]_{11} = [M_{22}]_{22} = \begin{bmatrix} \frac{1}{3} m \left(d^2 + l^2 \right) - \frac{m^2}{4M} l^2 & 0 & 0 \\ 0 & \frac{1}{3} m l^2 - \frac{m^2}{4M} l^2 & 0 \\ 0 & 0 & \frac{1}{3} m d^2 \end{bmatrix} ;$$

$$[M_{22}]_{12} = [M_{22}]_{21} = \frac{m^2}{4M} l^2 \begin{bmatrix} 1 & -\alpha_1 - \alpha_2 & 0 \\ -\alpha_1 - \alpha_2 & -1 & 0 \\ 0 & 0 & 0 \end{bmatrix} \approx \frac{m^2}{4M} l^2 \begin{bmatrix} -1 & 0 & 0 \\ 0 & 1 & 0 \\ 0 & 0 & 0 \end{bmatrix} .$$

Substituting the inertia matrices and their time derivatives as well as partial derivatives w.r.t. α_k in equation (3.6), followed by considerable amount of algebraic manipulations eventually lead to the equations corresponding to free rotations of appendages 1 and 2 as:

$$\frac{1}{3} m d^2 \left\{ \left(\ddot{\lambda} + \ddot{\alpha}_1 \right) + \left(\lambda + \alpha_1 \right) \Omega^2 \right\} = 0 ; \qquad (3.7)$$
$$\frac{1}{3} m d^2 \left\{ \left(\ddot{\lambda} - \ddot{\alpha}_2 \right) + \left(\lambda - \alpha_2 \right) \Omega^2 \right\} = 0 ; \qquad (3.8)$$

respectively.

Note, equations (3.7) and (3.8) are exactly the same as those obtained in reference [49].

3.2 Test Configuration 2

Ng et al. [72] have investigated planar dynamics of a spacecraft, with two beam type appendages, orbiting along an elliptic trajectory around the earth. The equations of pitch motion and appendage vibration in the orbital plane were obtained. The same spacecraft is selected to compare the equations of motion obtained as a particular case here.

A comment concerning the planar motions of spacecraft, i.e., motions in the orbital plane corresponding to pitch, deployment or retrieval, slewing, and vibrations of the appendages, would be appropriate. Note, the spacecraft is not constrained to move in the orbital plane but can respond in three dimensions. However, as is known, a planar disturbance does not excite the out-of-plane motion. Only in this sense, there exists the so called "planar motion". Of course, the original nonlinear equations for planar and out-of-plane motions are coupled as shown in the formulation.

3.2.1 System description

The spacecraft is composed of a circular cylindrical shaped rigid body with two flexible beam-type appendages fixed at centres of its two ends. The two appendages are identical in geometry and attached at the same distance from the centre of the central body, i.e. $m_1 = m_2 = m$; $l_1 = l_2 = l$; and $L_1 = L_2 = L$. Here m is the mass of the appendage; l, its length; and L, the distance to the attachment point. The cylinder being axisymmetric, its transverse moments of inertia about the y_o and z_o axes are the same, i.e. $J_{02} = J_{03}$. Transverse vibrations of appendage 1 in the x_1 direction and of appendage 2 in the x_2 direction are considered. The system is discretized using the first bending mode of a cantilever beam. $2u_1$ and $2u_2$ represent tip deflections of the upper and lower beams, respectively.

Figure 3-2 shows a typical orientation of the spacecraft. For the present case, the transformation matrices take the form as follows:

$$[A] = \begin{bmatrix} cos\psi & sin\psi & 0 \\ -sin\psi & cos\psi & 0 \\ 0 & 0 & 1 \end{bmatrix};$$

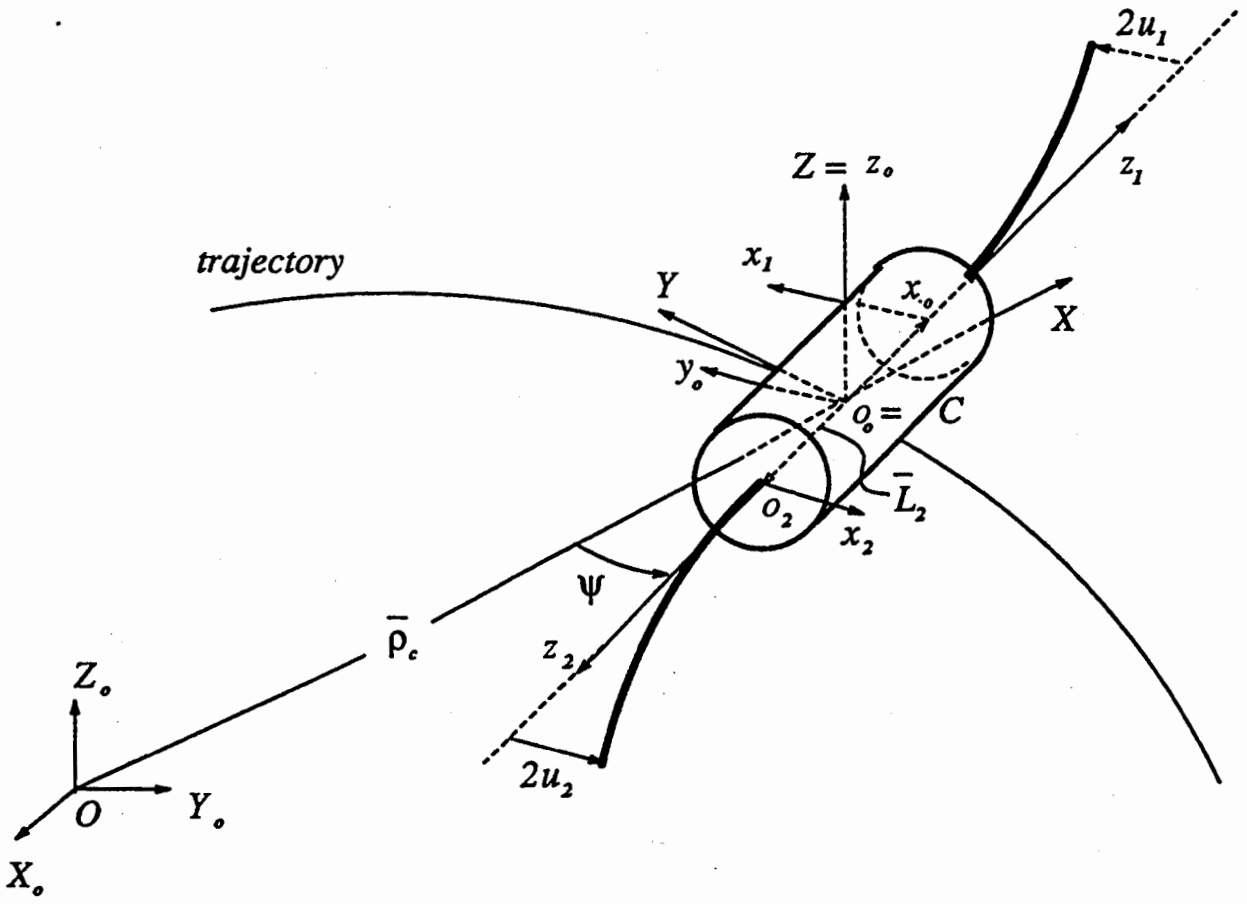

Figure 3-2 A satellite with two beam type appendages considered to check the equations of motion

$$[B_o] = \begin{bmatrix} cos\psi & -sin\psi & 0 \\ sin\psi & cos\psi & 0 \\ 0 & 0 & 1 \end{bmatrix};$$

$$[C_1] = \begin{bmatrix} 0 & 1 & 0 \\ 0 & 0 & 1 \\ 1 & 0 & 0 \end{bmatrix};$$

$$[C_2] = \begin{bmatrix} 0 & -1 & 0 \\ 0 & 0 & 1 \\ -1 & 0 & 0 \end{bmatrix}.$$

The basic inertia elements are:

$$[L_1] = [L_1 - L_o] = [L \;\; 0 \;\; 0];$$
$$[L_2] = [L_2 - L_o] = [-L \;\; 0 \;\; 0];$$
$$[H_1] = [\beta_1 m u_1 \;\; 0 \;\; 0.5ml];$$
$$[H_2] = [\beta_1 m u_2 \;\; 0 \;\; 0.5ml];$$

and the integral matrices associated with the vibration take the form:

$$[F_1] = [F_2] = \begin{bmatrix} \beta_1 m \\ 0 \\ 0 \end{bmatrix};$$

$$\left[F_1^2\right] = \left[F_2^2\right] = \left[F_1^3\right] = \left[F_2^3\right] = m;$$

$$\left[F_1^{11}\right] = \left[F_2^{11}\right] = \begin{bmatrix} 0 \\ 0 \\ \beta_2 ml \end{bmatrix};$$

$$\left[F_1^{1*}\right] = \left[F_2^{1*}\right] = \begin{bmatrix} 0 \\ 0 \\ \beta_2 ml \end{bmatrix};$$

with

$$\beta_1 = \int_0^1 \Psi_1(\xi) d\xi = 0.7830\,, \quad \beta_2 = \int_0^1 \xi\, \Psi_1(\xi)\, d\xi = 0.5688\,. \tag{3.9}$$

All other matrices are zero.

3.2.2 Librational equations

For the particular system under consideration, the librational equations (2.104) now reduce to:

$$
\begin{aligned}
& [B_o]\,[J]\left\{[B_o]^T\,[\,\alpha_o''\,]^T + \left(\left(\frac{\partial[\,a_3\,]}{\partial[\,\alpha_o\,]}\right)^T + [B_o']^T\right)[\,\alpha_o'\,]\right\} \\
+ \;& \left([D^*]\,[J] + [B_o]\,[J']\right)\left([\,a_3\,]^T\Omega + [B_o]^T\,[\,\alpha_o'\,]^T\right) \\
+ \;& \sum_{i=1}^{n}\left\{[B_o]\,[M_{14}]_i\,u_i'' + \left([D^*]\,[M_{14}]_i + [B_o]\,[M_{14}']_i\right)u_i'\right\} \\
- \;& \epsilon_g \frac{\partial[\,a_1\,]}{\partial[\,\alpha_o\,]}\left[J^1\right][\,a_1\,]^T = \frac{1}{\Omega^2}\,[Q_{\alpha o}]\ . \qquad (3.10)
\end{aligned}
$$

From the basic inertia elements and integral matrices, the following inertia matrices can be obtained:

$$
\begin{aligned}
J_1^o &= \frac{1}{3}ml^2 + mu_1^2\ ; \\
J_2^o &= \frac{1}{3}ml^2 + mu_2^2\ ;
\end{aligned}
$$

$$
\left[J_1^1\right] = \begin{bmatrix} mu_1^2 & 0 & \beta_2 mlu_1 \\ 0 & 0 & 0 \\ \beta_2 mlu_1 & 0 & \frac{1}{3}ml^2 \end{bmatrix}\ ;
$$

$$
\left[J_2^1\right] = \begin{bmatrix} mu_2^2 & 0 & \beta_2 mlu_2 \\ 0 & 0 & 0 \\ \beta_2 mlu_2 & 0 & \frac{1}{3}ml^2 \end{bmatrix}\ ;
$$

$$
J^o \approx J_{03} + \frac{1}{2}J_{01} + \tilde{J} + m\left(u_1^2 + u_2^2\right)\ ;
$$

$$
\left[J^1\right] = \begin{bmatrix} J_{03} - \frac{1}{2}J_{01} + \tilde{J} & m\left(\beta_2 l + \beta_1 L\right)(u_1 + u_2) & 0 \\ m\left(\beta_2 l + \beta_1 L\right)(u_1 + u_2) & \frac{1}{2}J_{01} + m(u_1^2 + u_2^2) & 0 \\ 0 & 0 & \frac{1}{2}J_{01} \end{bmatrix}\ ;
$$

$$
[M_{14}]_1 = \begin{bmatrix} \beta_2 ml \\ 0 \\ \beta_1 mL \end{bmatrix}\ ;
$$

$$[M_{14}]_2 = \begin{bmatrix} -\beta_2 ml \\ 0 \\ \beta_1 mL \end{bmatrix} .$$

$\tilde{J}$ in J^o and $[J^1]$ is:

$$\tilde{J} = 2mL^2 + 2mlL + \frac{2}{3}ml^2 .$$

Substituting the above expressions and their derivatives in equation (3.10), the following equations are obtained:

$$\begin{aligned}
&\lambda'' = 0 ; \\
&\phi'' = 0 ; \\
&\left\{1 + K_a\left(u_1^2 + u_2^2\right)\right\}\left(\psi'' - \epsilon_c\psi' - \epsilon_c\right) + 2K_a\left(u_1u_2' + u_1'u_2\right)\left(\psi' + 1\right) \\
&+\epsilon_g\left\{K_i sin\psi cos\psi + K_a\alpha\left(u_1 + u_2\right)\left(cos^2\psi - sin^2\psi\right)\right. \\
&\left. - K_a\left(u_1^2 + u_2^2\right) sin\psi cos\psi\right\} + K_a\alpha\left\{u_1'' + u_2'' - \epsilon_c\left(u_1' + u_2'\right)\right\} = 0 ; \qquad (3.11)
\end{aligned}$$

with:

$$K_i = 1 - \frac{J_{01}}{J_{03} + \tilde{J}} ;$$

$$K_a = \frac{m}{J_{03} + \tilde{J}} ;$$

$$\alpha = \beta_2 l + \beta_1 L .$$

The first two equations for yaw and roll show that they are not excited by inplane disturbances. The pitch equation is the same as that given in reference [72].

3.2.3 Vibrational equations

For the particular configuration under consideration, vibrational equations (**??**) reduce to

$$\begin{aligned}
&[M_{14}]_k^T\,[B_o]^T\,[\,\alpha_o''\,]^T + \left([M_{14}']_k^T - \epsilon_c\,[M_{14}]_k^T\right)\left([\,a_3\,]^T + [B_o]^T\,[\,\alpha_o'\,]^T\right) \\
+\;&[M_{14}]_k^T\left\{\left(\frac{\partial[\,a_3\,]}{\partial[\,\alpha_o\,]}\right)^T + [B_o']\right\}[\,\alpha_o'\,]^T - \frac{1}{2}\epsilon_g\frac{\partial}{\partial u_k}[\,a_1\,]\left[J^1\right][\,a_1\,]^T
\end{aligned}$$

$$
\begin{aligned}
&+ \frac{1}{2}\frac{\partial}{\partial u_k}\left([\,a_3\,]+[\,\alpha_o'\,][B_o]\right)\left[J^1\right]\left([\,a_3\,]^T+[B_o]^T[\,\alpha_o'\,]^T\right)\\
&+ \frac{\partial J^o}{\partial u_k}\left(\frac{1}{6}\epsilon_g-\frac{1}{2}-[\,a_3\,][B_o]^T[\,\alpha_o'\,]^T-\frac{1}{2}[\,\alpha_o'\,][B_o][B_o]^T[\,\alpha_o'\,]^T\right)\\
&- \frac{\partial}{\partial u_k}\sum_{i=1}^{2}u_i'[M_{14}]_i^T\left([\,a_3\,]^T+[B_o]^T[\,\alpha_o'\,]^T\right)\\
&+ \sum_{i=1}^{2}\left([M_{44}]_{ki}\,u_i''-\epsilon_c[M_{44}]_{ki}\,u_i'\right)+\frac{1}{\Omega^2}K_k u_k=\frac{1}{\Omega^2}Q_{uk}\ . \qquad (3.12)
\end{aligned}
$$

Now:

$$
\begin{aligned}
(m_s)_1 &= (m_s)_2 = m\ ;\\
[M_{44}]_{11} &= [M_{44}]_{22} = m\left(1-\beta_1^2\frac{m}{M}\right)\ ;\\
[M_{44}]_{12} &= [M_{44}]_{21} = \beta_1^2\frac{m^2}{M}\ ;\\
K_1 &= K_2 = k = EI_{yy}\lambda_1^4\Gamma_{11}^{lpp}/l^3\ .
\end{aligned}
$$

Neglecting terms of higher order of smallness, the following vibrational equations are obtained:

$$
\begin{aligned}
u_1''-\epsilon_c u_1'+\alpha\left(\psi''-\epsilon_c\psi'-\epsilon_c\right)-u_1\left(1+\psi'\right)^2+\epsilon_v u_1&\\
+\epsilon_g\left\{u_1\left(\frac{1}{3}-sin^2\psi\right)+\alpha sin\psi cos\psi\right\} &= 0\ ;\\
u_2''-\epsilon_c u_2'+\alpha\left(\psi''-\epsilon_c\psi'-\epsilon_c\right)-u_2\left(1+\psi'\right)^2+\epsilon_v u_2&\\
+\epsilon_g\left\{u_2\left(\frac{1}{3}-sin^2\psi\right)+\alpha sin\psi cos\psi\right\} &= 0\ ;
\end{aligned}
$$

with

$$
\epsilon_v=\frac{k}{m\Omega^2}=\frac{EI_{yy}\lambda_1^4\Gamma_{11}^{lpp}}{ml^3\Omega^2}\ .
$$

These are identical to the vibrational equations in reference [72].

4. STABILITY STUDY

In the absence of any internal or external disturbances, including appendage maneuvers and dissipation, a spacecraft in a circular orbit attains a fixed orientation w.r.t. the earth. In other words, motion of the spacecraft with respect to the orbiting frame is absent: no librational motions, no appendage rotation, no vibration. Such fixed orientation is designated variously as: equilibrium orientation; torque free equilibrium; relative equilibrium; stationary orientation; etc. For a single rigid body, it is well known that, when the three principal inertia axes at the mass centre of the body are parallel to the orbital frame, the earth-oriented equilibrium persists [1, 68].

Among the relative equilibria, only a few are stable. For a single rigid body, only when its major axis is normal to the orbital plane and the minor axis along the local vertical, the equilibrium state is stable, referred to as the 'Lagrange Configuration'. The moon is in the Lagrange configuration and hence presents one side facing the earth all the time.

For a multibody, multidegrees of freedom spacecraft, determination of the relative equilibria and their stability properties remains a field that has received relatively less attention [69, 70]. This chapter studies stability of the relative equilibria associated with the particular configuration considered in Chapter 3 (Test Case 1). To recapitulate, the system consists of three interconnected rigid bodies and has five degrees of freedom: pitch, roll and yaw librational motions; and rotation of the individual appendage about an axis.

4.1 Methodology

As in the case of the general formulation, effect of the attitude motion on the spacecraft trajectory is neglected. The librational motion is the relative motion with respect to the orbiting frame, which is a noninertial reference having a prescribed motion. In the situation of a circular orbit, the orbiting frame rotates at a constant angular velocity Ω. The system operates in the gravitational potential field. The independent variable 't' or 'θ' does not appear explicitly in the kinetic energy 'T'

or the potential energy 'V', hence there exists the generalized energy integral (also referred to as the 'Jacobi-Poincaré integral'),

$$H = T_2 - T_o + V = T_2 + V_e = constant, \tag{4.1}$$

where $V_e = V - T_o$ is called the 'equivalent potential energy' or 'dynamical potential energy'. Here T_o is the part of the kinetic energy without the generalized velocities, and T_2 represents quadratic part of the kinetic energy.

For a conservative system, it is wellknown that equilibrium state corresponds to the stationary point of the potential energy. Furthermore, stable equilibrium represents the state of minimum potential energy. For the relative motion under consideration here, one arrives at a similar conclusion with the 'potential energy' replaced by the 'equivalent potential energy' [43]. This can be expressed in the form of a theorem as follows:

Theorem:

For relative motion of a mechanical system with respect to a noninertial coordinate frame, when only the potential forces exist and the independent variable is not contained explicitly in the Lagrangian function of the system:

(a) a relative equilibrium is attained at the stationary point of the equivalent potential energy;

(b) a stable relative equilibrium is attained at the minimum point of the equivalent potential energy.

To prove the part (a), let the Lagrange equation be rewritten as

$$\frac{d}{dt}\frac{\partial(T_2+T_1)}{\partial[\,\dot{q}\,]} - \frac{\partial(T_2+T_1)}{\partial[\,q\,]} + \frac{\partial(V-T_o)}{\partial[\,q\,]} = \{0\}\ , \tag{4.2}$$

where T_2 is as defined before; and T_1, the linear part in the kinetic energy expression. If the relative motions are quiescent, i.e. all $\dot{q}$= 0, then the first two terms in equation (4.2) vanish giving

$$\frac{\partial V_e}{\partial[\,q\,]} = \frac{\partial(V-T_o)}{\partial[\,q\,]} = \{0\}\ . \tag{4.3}$$

Thus equation (4.3) governs the relative equilibrium. It shows that when the equivalent potential energy reaches its stationary value, a relative equilibrium persists.

To prove the stability part of the theorem in (b), a Liapunov function is used. At a relative equilibrium:

$$T_2 = 0 \; ; \quad and \quad V_e = V_{eo} \; ;$$

where V_{eo} is a constant. In the neighbourhood of the equilibrium, let

$$H^* = T_2 + V_e - V_{eo}; \tag{4.4}$$

then from equation (4.1), H^* is also a constant.

It is known that T_2 has a positive definite quadratic form. If $V_e - V_{eo}$ is a positive definite function too, or in other words, if V_e reaches its minimum at the relative equilibrium, then H^* can be used as a Liapunov function to demonstrate the stability of the said equilibrium.

To show that the equivalent potential energy reaches its minimum value at some relative equilibrium, a sufficient condition is: for the following matrix, with the second partial derivatives of V_e at the said equilibrium as entries, to be positive definite:

$$[D] = \begin{bmatrix} \frac{\partial^2 V_e}{\partial q_1^2} & \cdots & \frac{\partial^2 V_e}{\partial q_1 \partial q_r} \\ \vdots & & \vdots \\ \frac{\partial^2 V_e}{\partial q_r \partial q_1} & \cdots & \frac{\partial^2 V_e}{\partial q_r^2} \end{bmatrix} . \tag{4.5}$$

Note, here 'r' generalized coordinates are taken for the system.

Another approach to the stability study would be through linearization of the equations in the neighbourhood of the equilibrium. The linearized equations may be cast into the standard form as

$$[M]\left\{\ddot{q}\right\} + [G]\left\{\dot{q}\right\} + [K]\left\{q - q_o\right\} = \{0\} \; , \tag{4.6}$$

where: $[M]$ is a positive definite, symmetric inertia matrix; and $[G]$ is a gyroscopic skew-symmetric matrix. For the linearized system, the necessary and sufficient condition for equilibrium $[\, q \,] = [\, q_o \,]$ to be stable is the stiffness matrix $[K]$ to be positive definite. However, this is only a necessary condition for the original nonlinear system to be stable [71].

If one investigates the equilibrium condition by the above two methods, an interesting identity emerges,

$$[D] \equiv [K] \; . \tag{4.7}$$

This is not surprising. Comparing equations (4.6) and (4.2), it can be seen that the term $[K]\{q - q_o\}$ arises from $\partial V_e/\partial[\ q\ ]$. Now $\partial V_e/\partial[q]$ is a set of functions of the generalized coordinates:

$$\frac{\partial V_e}{\partial[\ q]} = \begin{bmatrix} \frac{\partial V_e}{\partial q_1} \\ \vdots \\ \frac{\partial V_e}{\partial q_r} \end{bmatrix} = \begin{bmatrix} f_1(q_1, \ldots, q_r) \\ \vdots \\ f_r(q_1, \ldots, q_r) \end{bmatrix} .$$

Expanding $f_k(q_1, \ldots, q_r)$ for $k = 1, \ldots, r$ into the Taylor series around $\{q\} = \{q_o\}$,

$$f_k(q_1, \ldots, q_r) = f_k(q_{1o}, \ldots, q_{ro}) + \sum_{i=1}^{r} \frac{\partial f_k}{\partial q_i} \Big|_{q=q_o} (q_i - q_{io}) + \ldots \quad .$$

But at the relative equilibrium,

$$\frac{\partial V_e}{\partial q_k} = f_k(q_{10}, \ldots, q_{r0}) = 0 \quad for \quad k = 1, \ldots, r.$$

Therefore

$$f_k(q_1, \ldots, q_r) \approx \sum_{i=1}^{r} \frac{\partial f_k}{\partial q_i} \Big|_{q=q_o} (q_i - q_{io}) \quad for \quad k = 1, \ldots, r.$$

In the matrix form,

$$\begin{aligned} \frac{\partial V_e}{\partial[q]} &\approx \begin{bmatrix} \frac{\partial f_1}{\partial q_1} & \cdots & \frac{\partial f_1}{\partial q_r} \\ \vdots & & \vdots \\ \frac{\partial f_r}{\partial q_1} & \cdots & \frac{\partial f_r}{\partial q_r} \end{bmatrix} \begin{bmatrix} q_1 - q_{1o} \\ \vdots \\ q_r - q_{ro} \end{bmatrix} \\ &= \begin{bmatrix} \frac{\partial^2 V_e}{\partial q_1^2} & \cdots & \frac{\partial^2 V_e}{\partial q_r \partial q_1} \\ \vdots & & \vdots \\ \frac{\partial^2 V_e}{\partial q_1 \partial q_r} & \cdots & \frac{\partial^2 V_e}{\partial q_r^2} \end{bmatrix} \begin{bmatrix} q_1 - q_{1o} \\ \vdots \\ q_r - q_{ro} \end{bmatrix} \\ &= [K]\{q - q_o\} \end{aligned} \tag{4.8}$$

From the above derivation, it can be seen that $[D] \equiv [K]$. Two apparently different methods are intrinsically consistent.

Just as the V_e is called the 'equivalent potential energy', $\partial V_e/\partial[q]$ can be referred to as the 'equivalent potential force', i.e. a sum of the ordinary potential force and the centrifugal inertia force. Equation (4.8) suggests that, when the equivalent potential force is a restoring force (or torque) near some relative equilibrium state, the equilibrium is stable.

In summary, to investigate stability conditions of a relative equilibrium, one only needs to find the stiffness matrix and then determine the conditions for the matrix to be positive definite. The conditions obtained are both necessary and sufficient for the equilibrium to be stable.

4.2 Determination of the Stationary Orientations

For the particular configuration,

$$V_e = -\frac{KM}{\rho_c} - \frac{3}{2}\Omega^2[\ a_1\ ]\left[J^1\right]\{a_1\} + \frac{1}{2}\Omega^2[\ a_3\ ]\left[J^1\right]\{a_3\} - \frac{1}{2}M\,\dot{\bar{\rho}}_c \cdot \dot{\bar{\rho}}_c\ . \qquad (4.9)$$

Differentiating equation (4.9) w.r.t. $[\ \alpha_o\ ]$,

$$\frac{\partial V_e}{\partial[\ \alpha_o\ ]} = -3\Omega^2\frac{\partial[\ a_1\ ]}{\partial[\ \alpha_o\ ]}\left[J^1\right]\{a_1\} + \Omega^2\frac{\partial[\ a_3\ ]}{\partial[\ \alpha_o\ ]}\left[J^1\right]\{a_3\} = 0\ . \qquad (4.10)$$

Differentiating equation (4.9) w.r.t. α_k,

$$\frac{\partial V_e}{\partial \alpha_k} = -\frac{3}{2}\Omega^2[\ a_1\ ]\frac{\partial}{\partial \alpha_k}\left[J^1\right]\{a_1\} + \frac{1}{2}\Omega^2[\ a_3\ ]\frac{\partial}{\partial \alpha_k}\left[J^1\right]\{a_3\} = 0\ , \quad k = 1,2. \qquad (4.11)$$

The stationary orientation or relative equilibrium is governed by five equations represented in (4.10) and (4.11). The six orientations shown in Figure 4-1 satisfy them, i.e., they are relative equilibria as explained before.

The relative equilibria are represented by the three Bryant angles $[\lambda_o,\ \phi_o,\ \psi_o]$ of the central-body-fixed frame $o_o - x_o, y_o, z_o$ with respect to the orbital frame $C - X, Y, Z$. The transformation matrix 'A' (Chapter 2, p.24) and its partial derivatives $\partial[\ a_1\ ]/\partial[\ \alpha_o\ ]$ and $\partial[\ a_3\ ]/\partial[\ \alpha_o\ ]$ in the six orientations are listed in Table 4-1.

The other two partial derivatives are:

$$\frac{\partial}{\partial \alpha_1}\left[J^1\right] = \frac{1}{3}md^2\begin{bmatrix} 0 & 0 & 0 \\ 0 & -sin2\alpha_1 & cos2\alpha_1 \\ 0 & cos2\alpha_1 & sin2\alpha_1 \end{bmatrix} \approx \frac{1}{3}md^2\begin{bmatrix} 0 & 0 & 0 \\ 0 & -2\alpha_1 & 1 \\ 0 & 1 & 2\alpha_1 \end{bmatrix}; \qquad (4.12)$$

$$\frac{\partial}{\partial \alpha_2}\left[J^1\right] = \frac{1}{3}md^2\begin{bmatrix} 0 & 0 & 0 \\ 0 & -sin2\alpha_2 & -cos2\alpha_2 \\ 0 & -cos2\alpha_2 & sin2\alpha_2 \end{bmatrix} \approx \frac{1}{3}md^2\begin{bmatrix} 0 & 0 & 0 \\ 0 & -2\alpha_2 & -1 \\ 0 & -1 & 2\alpha_2 \end{bmatrix} \qquad (4.13)$$

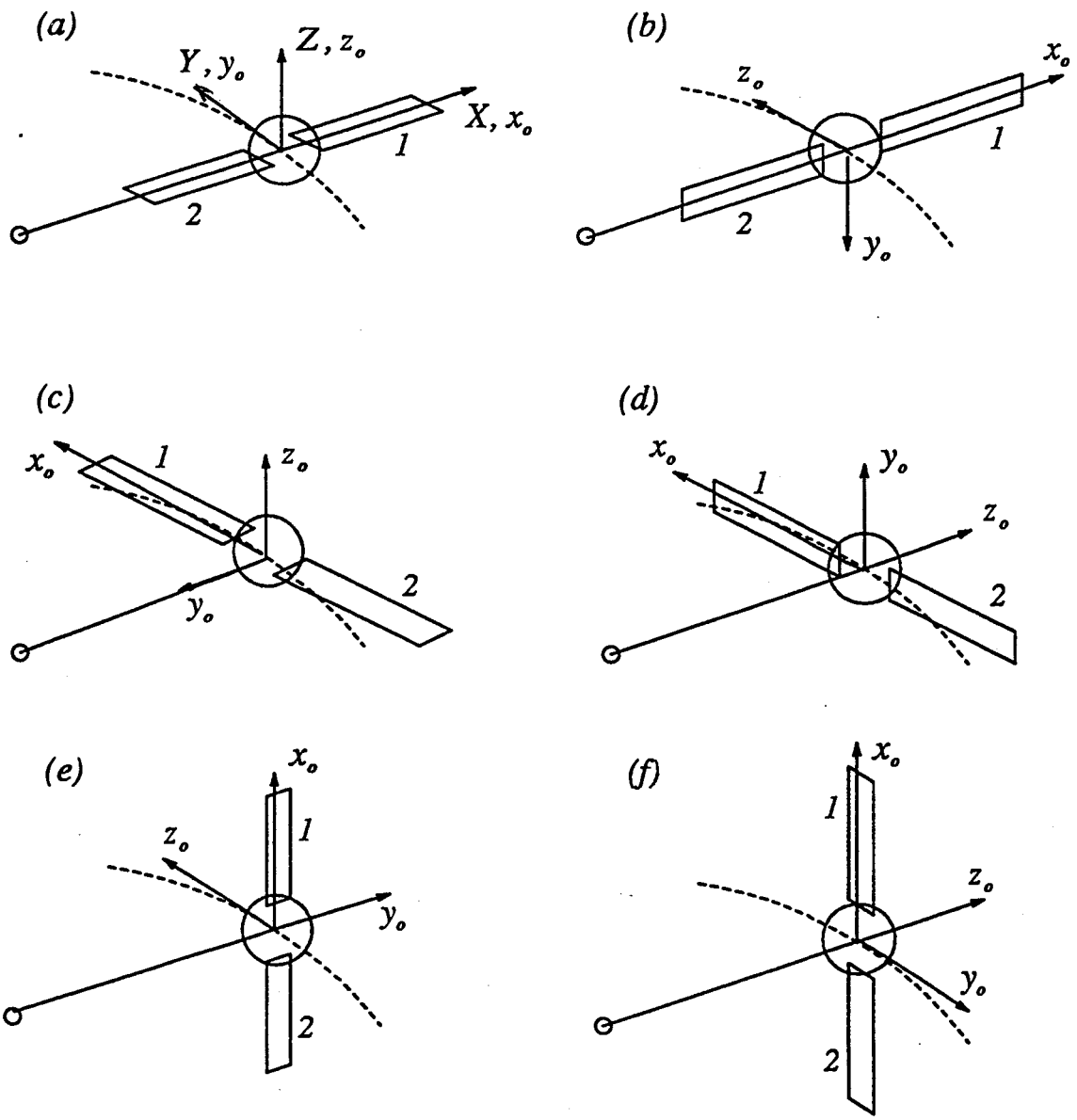

Figure 4-1 Stationary orientations of a rigid spacecraft with two plate type appendages free to rotate about the x_o-axis.

Table 4-1 Transformation matrices in the stationary orientations.

Orientation	*Definition*	$[A]$	$\partial[\,a_1\,]/\partial[\,\alpha_o\,]$	$\partial[\,a_3\,]/\partial[\,\alpha_o\,]$
(a)	$\lambda_o = 0$ $\phi_o = 0$ $\psi_o = 0$	$\begin{bmatrix} 1 & 0 & 0 \\ 0 & 1 & 0 \\ 0 & 0 & 1 \end{bmatrix}$	$\begin{bmatrix} 0 & 0 & 0 \\ 0 & 0 & 1 \\ 0 & -1 & 0 \end{bmatrix}$	$\begin{bmatrix} 0 & 1 & 0 \\ -1 & 0 & 0 \\ 0 & 0 & 0 \end{bmatrix}$
(b)	$\lambda_o = \frac{\pi}{2}$ $\phi_o = 0$ $\psi_o = 0$	$\begin{bmatrix} 1 & 0 & 0 \\ 0 & 0 & -1 \\ 0 & 1 & 0 \end{bmatrix}$	$\begin{bmatrix} 0 & 0 & 0 \\ 0 & 0 & 1 \\ 0 & -1 & 0 \end{bmatrix}$	$\begin{bmatrix} 0 & 0 & 1 \\ 0 & 0 & 0 \\ -1 & 0 & 0 \end{bmatrix}$
(c)	$\lambda_o = 0$ $\phi_o = 0$ $\psi_o = \frac{\pi}{2}$	$\begin{bmatrix} 0 & 1 & 0 \\ -1 & 0 & 0 \\ 0 & 0 & 1 \end{bmatrix}$	$\begin{bmatrix} 0 & 0 & 0 \\ 0 & 0 & 1 \\ -1 & 0 & 0 \end{bmatrix}$	$\begin{bmatrix} 1 & 0 & 0 \\ 0 & 1 & 0 \\ 0 & 0 & 0 \end{bmatrix}$
(d)	$\lambda_o = \frac{\pi}{2}$ $\phi_o = \frac{\pi}{2}$ $\psi_o = 0$	$\begin{bmatrix} 0 & 1 & 0 \\ 0 & 0 & 1 \\ 1 & 0 & 0 \end{bmatrix}$	$\begin{bmatrix} -1 & 0 & 0 \\ 0 & 1 & 0 \\ 0 & 0 & 0 \end{bmatrix}$	$\begin{bmatrix} 0 & 0 & 0 \\ 0 & 0 & -1 \\ 1 & 0 & 0 \end{bmatrix}$
(e)	$\lambda_o = -\frac{\pi}{2}$ $\phi_o = 0$ $\psi_o = -\frac{\pi}{2}$	$\begin{bmatrix} 0 & 0 & 1 \\ 1 & 0 & 0 \\ 0 & 1 & 0 \end{bmatrix}$	$\begin{bmatrix} 0 & 0 & 0 \\ 0 & 0 & 1 \\ 1 & 0 & 0 \end{bmatrix}$	$\begin{bmatrix} 0 & 0 & 1 \\ 0 & 0 & 0 \\ 0 & -1 & 0 \end{bmatrix}$
(f)	$\lambda_o = \frac{\pi}{2}$ $\phi_o = \frac{\pi}{2}$ $\psi_o = \frac{\pi}{2}$	$\begin{bmatrix} 0 & 0 & 1 \\ 0 & -1 & 0 \\ 1 & 0 & 0 \end{bmatrix}$	$\begin{bmatrix} 0 & 1 & 0 \\ 1 & 0 & 0 \\ 0 & 0 & 0 \end{bmatrix}$	$\begin{bmatrix} 0 & 0 & 0 \\ 0 & 0 & -1 \\ 0 & -1 & 0 \end{bmatrix}$

In all the six orientations, $\alpha_1 = \alpha_2 = 0$, hence:

$$\frac{\partial}{\partial \alpha_1}\left[J^1\right] = \frac{1}{3}md^2\begin{bmatrix} 0 & 0 & 0 \\ 0 & 0 & 1 \\ 0 & 1 & 0 \end{bmatrix}; \tag{4.14}$$

$$\frac{\partial}{\partial \alpha_2}\left[J^1\right] = \frac{1}{3}md^2\begin{bmatrix} 0 & 0 & 0 \\ 0 & 0 & -1 \\ 0 & -1 & 0 \end{bmatrix}. \tag{4.15}$$

With the matrices determined, it is easy to verify that equations (4.10) and (4.11) are satisfied by the six orientations.

4.3 Stability

The stability properties for the six orientations are considered in this section.

The linearized equations for the motion around the orientation (a) were presented in Chapter 3. The stiffness matrix can now be obtained as,

$$[K] = \Omega^2 \begin{bmatrix} J_3 - J_2 & 0 & 0 & \frac{1}{3}md^2 & -\frac{1}{3}md^2 \\ 0 & 4(J_3 - J_1) & 0 & 0 & 0 \\ 0 & 0 & 3(J_2 - J_1) & 0 & 0 \\ \frac{1}{3}md^2 & 0 & 0 & \frac{1}{3}md^2 & 0 \\ -\frac{1}{3}md^2 & 0 & 0 & 0 & \frac{1}{3}md^2 \end{bmatrix} . \qquad (4.16)$$

The necessary and sufficient condition for a square matrix to be positive definite is to have all the principal minor determinants to be positive. This leads to stability conditions for the orientation (a) as:

$$\begin{aligned} J_2 &> J_1 ; \\ J_3 &> J_2 + \tfrac{2}{3}md^2 ; \end{aligned}$$

i.e.,

$$\begin{aligned} J_{02} + \tilde{J} + \tfrac{2}{3}ml^2 &> J_{01} + \tfrac{2}{3}md^2 ; \\ J_{03} &> J_{02} . \end{aligned} \qquad (4.17)$$

These conditions are verified by the plots in Figures 4-2 and 4-3. Geometric and inertia parameter values used in the simulation are indicated in the diagram. In Figure 4-2, both the conditions in equation (4.17) are satisfied, hence the stationary orientation is stable. Note, the system is subjected to an initial disturbance of $\phi = \alpha_1 = 3°$. Through coupling, pitch and yaw of the central body are excited, however, appendage 2 remains unaffected. Figure 4-3 considers the case where the second condition of eq. (4.17) is not satisfied. The system is now subjected only to the roll disturbance of 3°, however it becomes unstable in yaw. Note, the yaw of the central body and the rotation of the appendages are all in the range of 0° to 180°, but in the opposite sense.

Next, consider the stability of motion around the equilibrium orientation in (b). To find the stiffness matrix, the linear part of equations (4.10) and (4.11) are taken. From equation (3.2), the following expressions can be obtained:

$$\frac{\partial V_e}{\partial[\,\alpha_o\,]} \approx \Omega^2 \begin{bmatrix} (J_2 - J_3)\lambda + \frac{1}{3}md^2(\alpha_2 - \alpha_1) \\ 4(J_2 - J_1)\phi \\ 3(J_3 - J_1)\psi \end{bmatrix} ;$$

$$\frac{\partial V_e}{\partial \alpha_1} \approx -\frac{1}{3}\Omega^2 md^2(\lambda + \alpha_1) ;$$

$$\frac{\partial V_e}{\partial \alpha_2} \approx \frac{1}{3}\Omega^2 md^2(\lambda - \alpha_2) .$$

$$J_{01} = 3.75kg \cdot m^2 \quad J_{02} = 18.75kg \cdot m^2 \quad J_{03} = 22.5kg \cdot m^2$$

$$m = 10kg \quad L = 2.5m \quad l = 5m \quad d = 1m$$

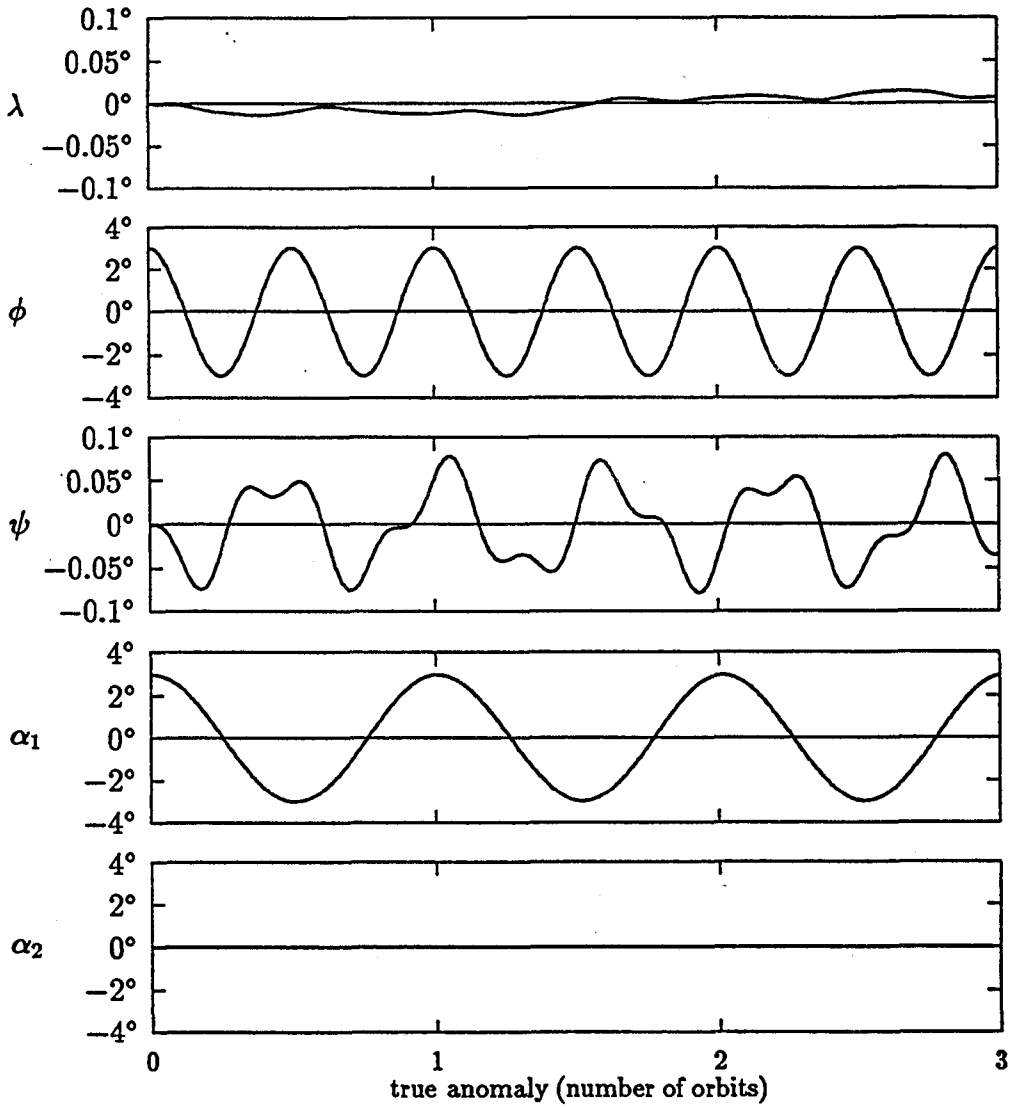

Figure 4-2 Stable response of the system around the equilibrium orientation (a) when both the conditions in eq. (4.17) are satisfied. Note the initial conditions are: $\phi(0) = \alpha_1(0) = 3°$.

$$J_{01} = 3.75kg \cdot m^2 \quad J_{02} = 22.5kg \cdot m^2 \quad J_{03} = 18.75kg \cdot m^2$$

$$m = 10kg \quad L = 2.5m \quad l = 5m \quad d = 1m$$

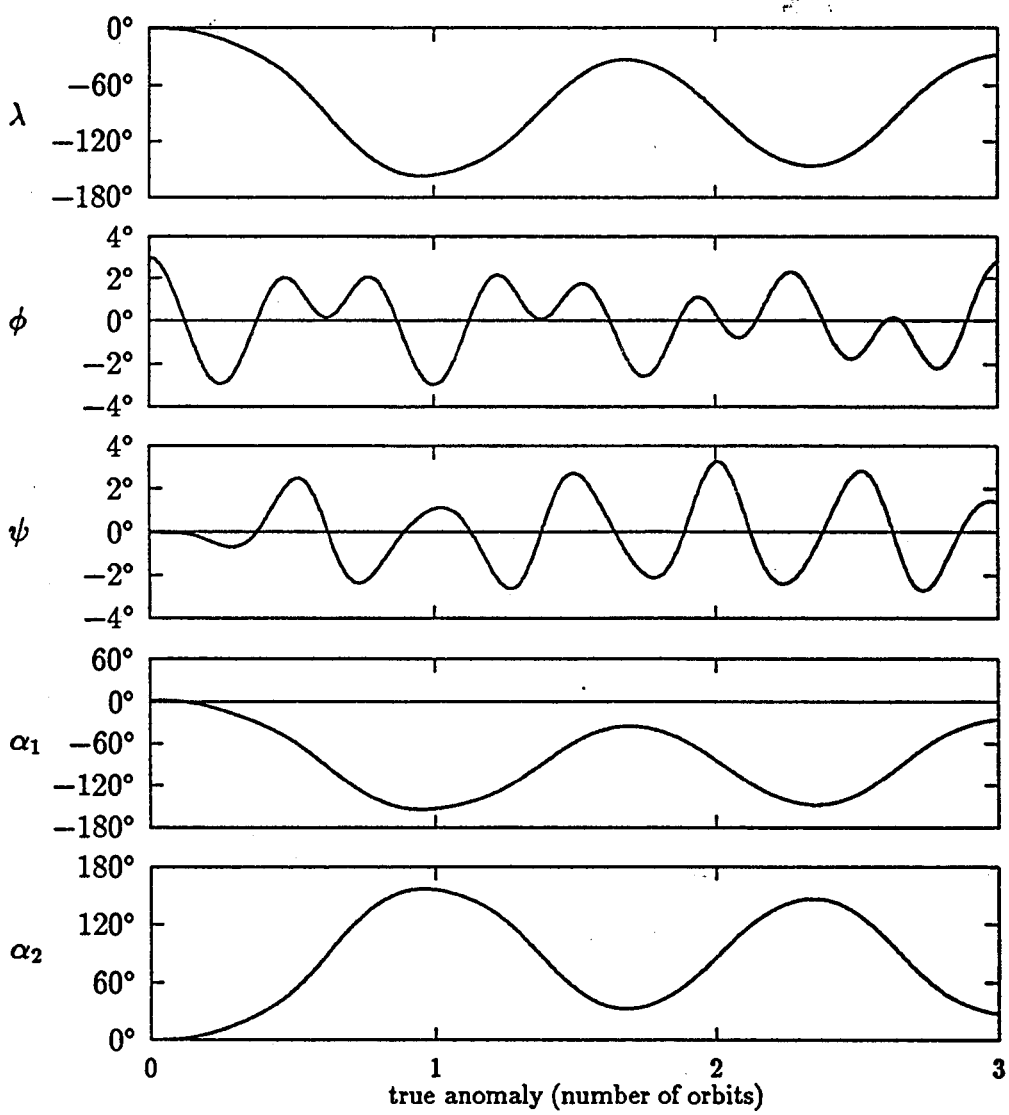

Figure 4-3 Unstable response around the equilibrium in (a) when one of the stability conditions in eq. (4.17) is not satisfied. The system is initially subjected to a roll disturbance of 3°.

The stiffness matrix can now be written as

$$[K] = \Omega^2 \begin{bmatrix} J_2 - J_3 & 0 & 0 & -\frac{1}{3}md^2 & \frac{1}{3}md^2 \\ 0 & 4(J_2 - J_1) & 0 & 0 & 0 \\ 0 & 0 & 3(J_3 - J_1) & 0 & 0 \\ -\frac{1}{3}md^2 & 0 & 0 & -\frac{1}{3}md^2 & 0 \\ \frac{1}{3}md^2 & 0 & 0 & 0 & -\frac{1}{3}md^2 \end{bmatrix} . \qquad (4.18)$$

This is not a positive definite matrix, i.e., the orientation in (b) is always unstable. This is substantiated by the plots in Figure 4-4 where the parameters are the same as in Figure 4-3.

For the orientation (c):

$$\frac{\partial V_e}{\partial [\ \alpha_o\ ]} \approx \Omega^2 \begin{bmatrix} (J_3 - J_1)\lambda \\ 4(J_3 - J_2)\phi + \frac{4}{3}md^2(\alpha_1 - \alpha_2) \\ 3(J_1 - J_2)\psi \end{bmatrix} ;$$

$$\frac{\partial V_e}{\partial \alpha_1} \approx \frac{4}{3}\Omega^2 md^2(\phi + \alpha_1) ;$$

$$\frac{\partial V_e}{\partial \alpha_2} \approx \frac{4}{3}\Omega^2 md^2(\alpha_2 - \phi) ;$$

with the stiffness matrix

$$[K] = \Omega^2 \begin{bmatrix} J_3 - J_1 & 0 & 0 & 0 & 0 \\ 0 & 4(J_3 - J_2) & 0 & \frac{4}{3}md^2 & -\frac{4}{3}md^2 \\ 0 & 0 & 3(J_1 - J_2) & 0 & 0 \\ 0 & \frac{4}{3}md^2 & 0 & \frac{4}{3}md^2 & 0 \\ 0 & -\frac{4}{3}md^2 & 0 & 0 & \frac{4}{3}md^2 \end{bmatrix} . \qquad (4.19)$$

The stability conditions are:

$$\begin{aligned} J_{01} + \tfrac{2}{3}md^2 &> J_{02} + \tfrac{2}{3}ml^2 + \tilde{J} ; \\ J_{03} + \tfrac{2}{3}ml^2 + \tilde{J} &> J_{01} ; \\ J_{03} &> J_{02} . \end{aligned} \qquad (4.20)$$

The stable response with all the three conditions satisfied is presented in Figure 4-5. It can be seen that the appendages are short and wide. However, with the first condition unsatisfied (larger size and mass of the appendages), the system becomes unstable in pitch (Figure 4-6). In fact, the motion is a $\pm 90°$ oscillation around the stable equilibrium orientation in (a).

$$J_{01} = 3.75kg \cdot m^2 \quad J_{02} = 22.5kg \cdot m^2 \quad J_{03} = 18.75kg \cdot m^2$$

$$m = 10kg \quad L = 2.5m \quad l = 5m \quad d = 1m$$

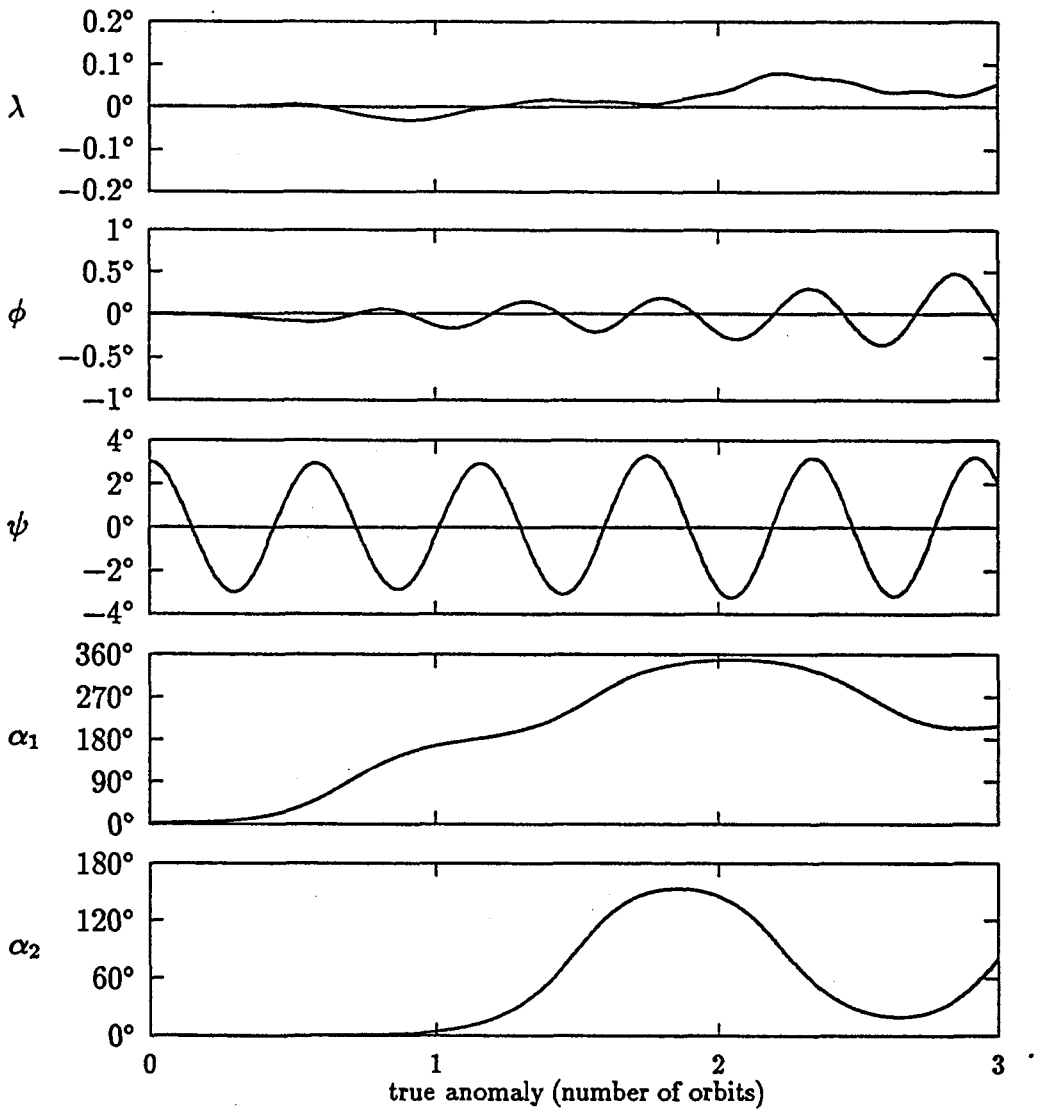

Figure 4-4 Unstable response around the equilibrium orienration (b). The configuration is always unstable irrespective of the parameters' values.

$$J_{01} = 18.75kg \cdot m^2 \quad J_{02} = 3.75kg \cdot m^2 \quad J_{03} = 22.5kg \cdot m^2$$

$$m = 3kg \quad L = 1m \quad l = 1m \quad d = 2m$$

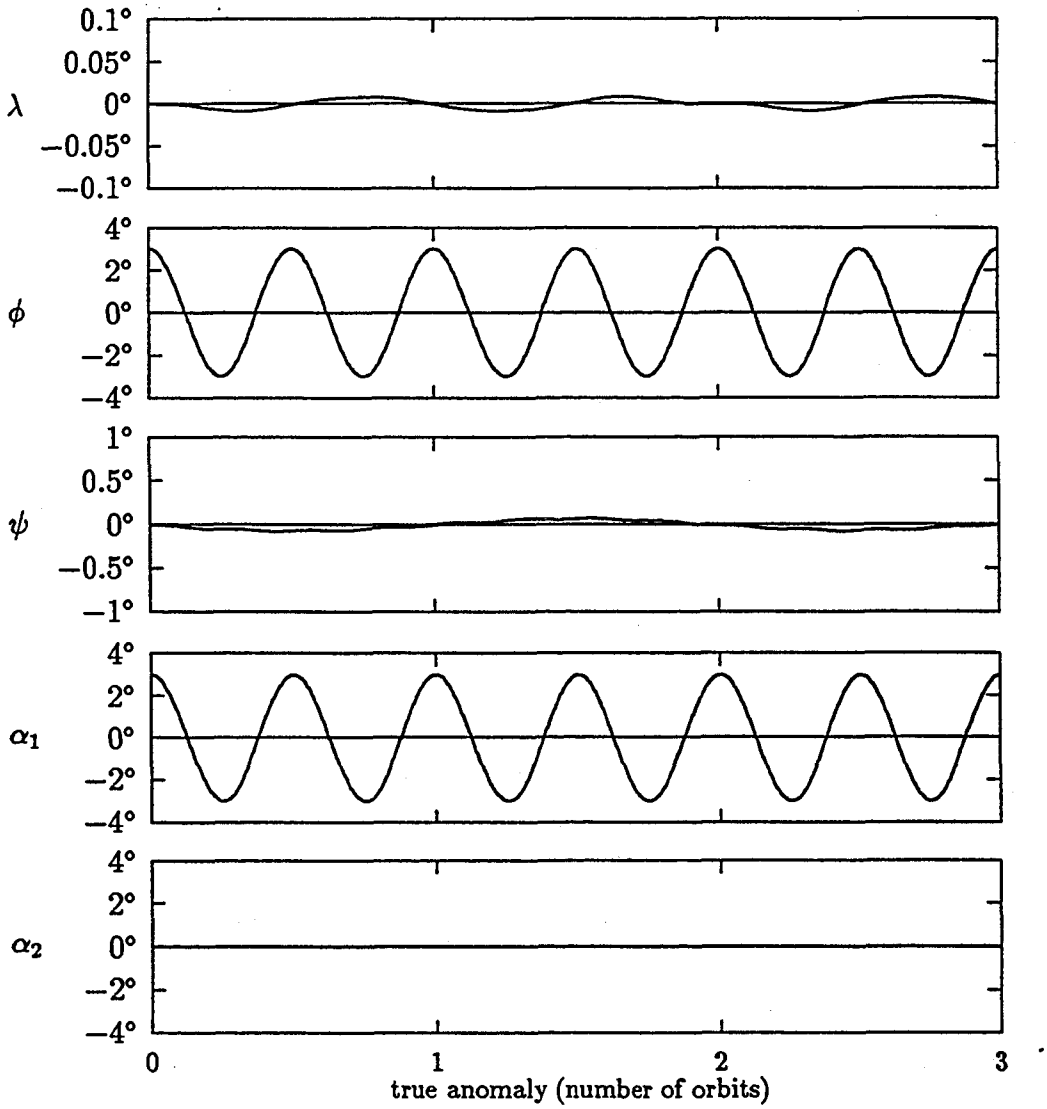

Figure 4-5 Typical response plots showing stable character of the equilibrium orientation in (c) when the appendages are short and wide.

$$J_{01} = 18.75kg \cdot m^2 \quad J_{02} = 3.75kg \cdot m^2 \quad J_{03} = 22.5kg \cdot m^2$$

$$m = 10kg \quad L = 2.5m \quad l = 5m \quad d = 1m$$

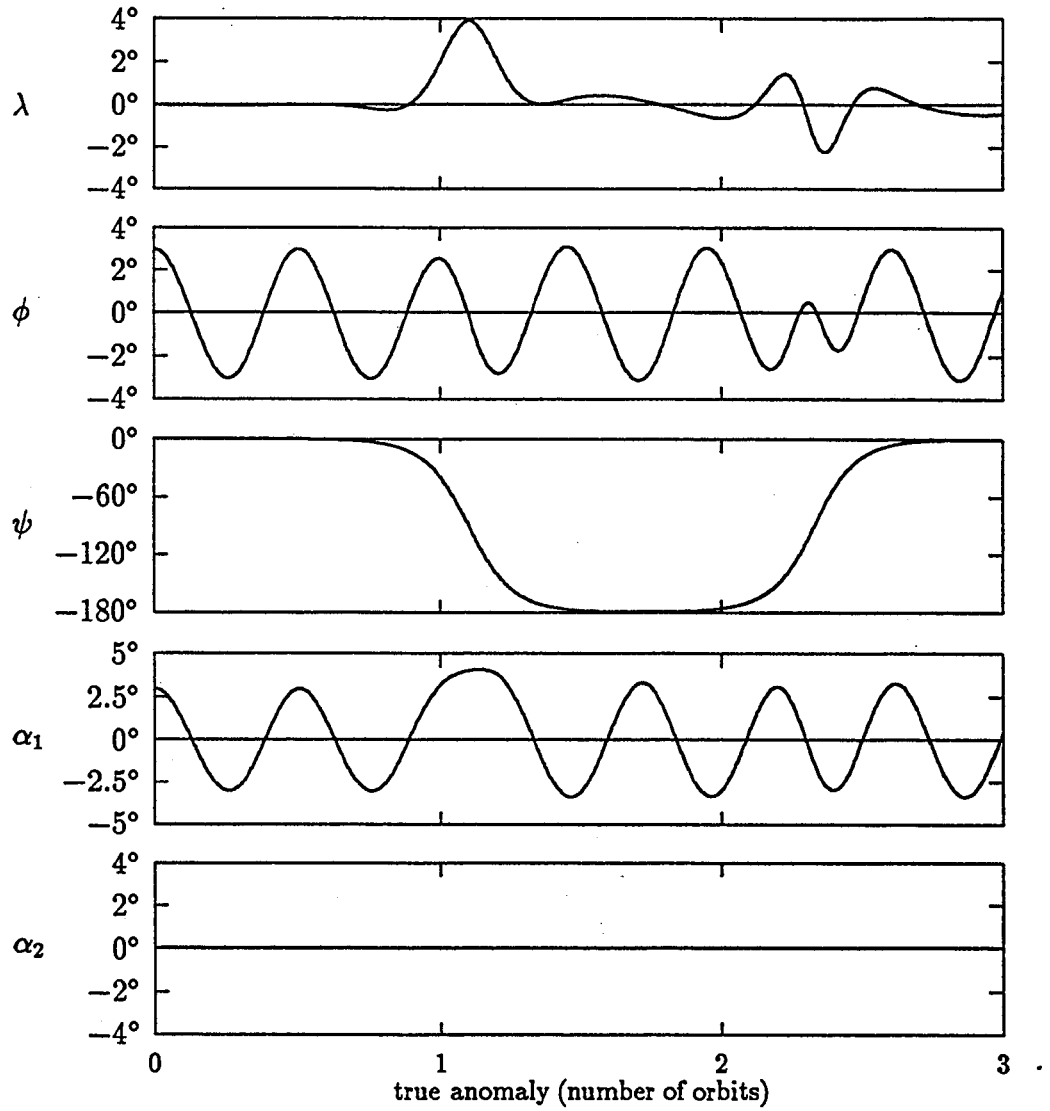

Figure 4-6 Unstable motion around the orientation (c) when one of the stability conditions in (4.20) is not satisfied. Note, the unstable degree of freedom is pitch.

Following the same procedure, the stiffness matrix for orientation (d) is obtained as

$$[K] = \Omega^2 \begin{bmatrix} (J_2 - J_1) & 0 & 0 & 0 & 0 \\ 0 & 4(J_2 - J_3) & 0 & -\frac{4}{3}md^2 & \frac{4}{3}md^2 \\ 0 & 0 & 3(J_1 - J_3) & 0 & 0 \\ 0 & -\frac{4}{3}md^2 & 0 & -\frac{4}{3}md^2 & 0 \\ 0 & \frac{4}{3}md^2 & 0 & 0 & -\frac{4}{3}md^2 \end{bmatrix} . \qquad (4.21)$$

Obviously it is impossible for the matrix to be positive definite. The equilibrium orientation is unstable as shown in Figure 4-7.

The stiffness matrix for motion around the orientation (e) was found to be:

$$[K] = \Omega^2 \begin{bmatrix} (J_1 - J_3) & 0 & 0 & 0 & 0 \\ 0 & 4(J_1 - J_2) & 0 & 0 & 0 \\ 0 & 0 & 3(J_3 - J_2) & -md^2 & md^2 \\ 0 & 0 & -md^2 & md^2 & 0 \\ 0 & 0 & md^2 & 0 & md^2 \end{bmatrix} , \qquad (4.22)$$

with conditions for stability as:

$$\begin{aligned} J_{01} &> J_{03} + \tfrac{2}{3}ml^2 + \tilde{J} \; ; \\ J_{03} &> J_{02} \; . \end{aligned} \qquad (4.23)$$

Short and wide appendages would help satisfy the conditions rendering the system stable as shown in Figure 4-8. Figure 4-9 shows the unstable motion when these conditions are not met.

The stiffness matrix for motion around the orientation (f) is

$$[K] = \Omega^2 \begin{bmatrix} (J_1 - J_2) & 0 & 0 & 0 & 0 \\ 0 & 4(J_1 - J_3) & 0 & 0 & 0 \\ 0 & 0 & 3(J_2 - J_3) & -md^2 & md^2 \\ 0 & 0 & -md^2 & -md^2 & 0 \\ 0 & 0 & md^2 & 0 & -md^2 \end{bmatrix} . \qquad (4.24)$$

Obviously the matrix can not be positive definite, and the equilibrium orientation is always unstable (Figure 4-10).

$$J_{01} = 22.5kg \cdot m^2 \quad J_{02} = 18.75kg \cdot m^2 \quad J_{03} = 3.75kg \cdot m^2$$

$$m = 10kg \quad L = 2.5m \quad l = 5m \quad d = 1m$$

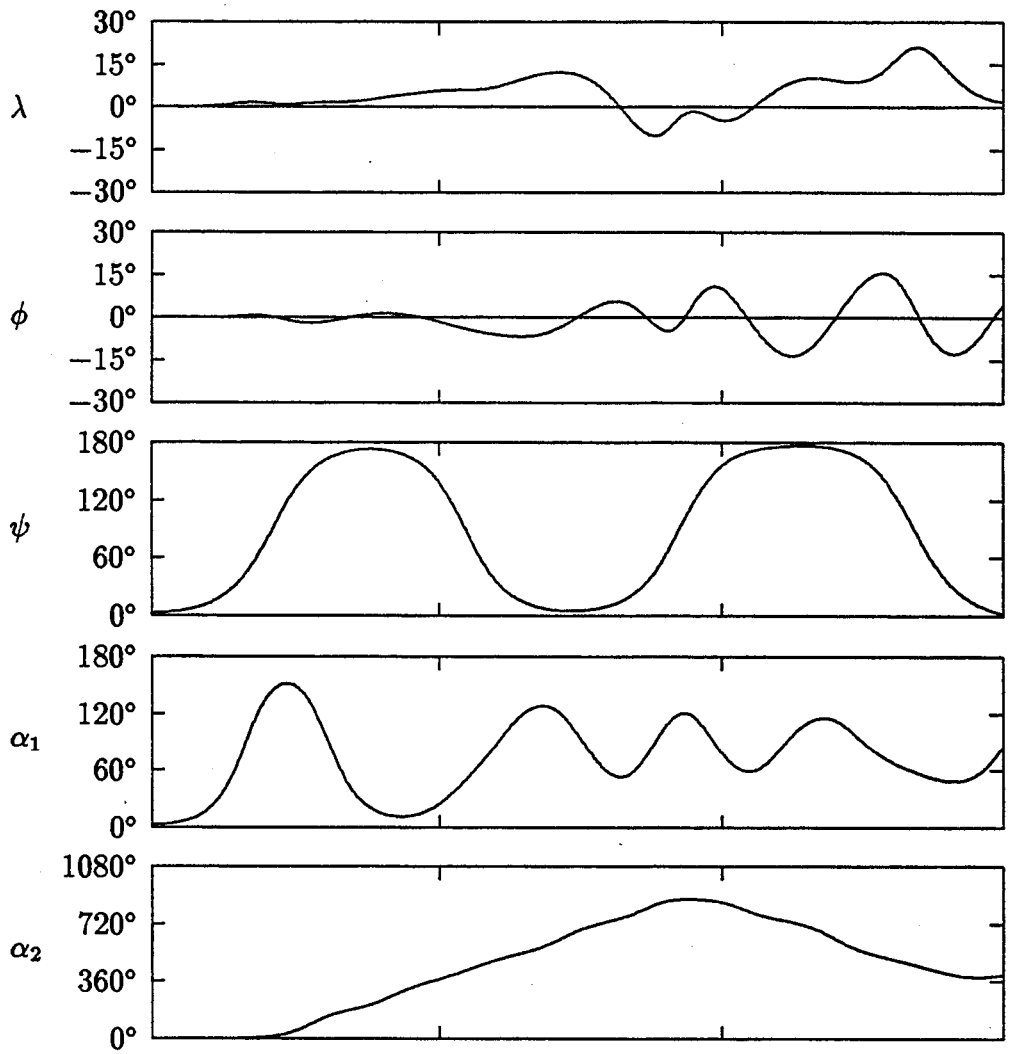

Figure 4-7 Response plots showing unsatble character of the equilibrium orienration (d) presented in Figure 4-1.

$$J_{01} = 22.5kg \cdot m^2 \quad J_{02} = 3.75kg \cdot m^2 \quad J_{03} = 6kg \cdot m^2$$

$$m = 3kg \quad L = 1m \quad l = 1m \quad d = 2m$$

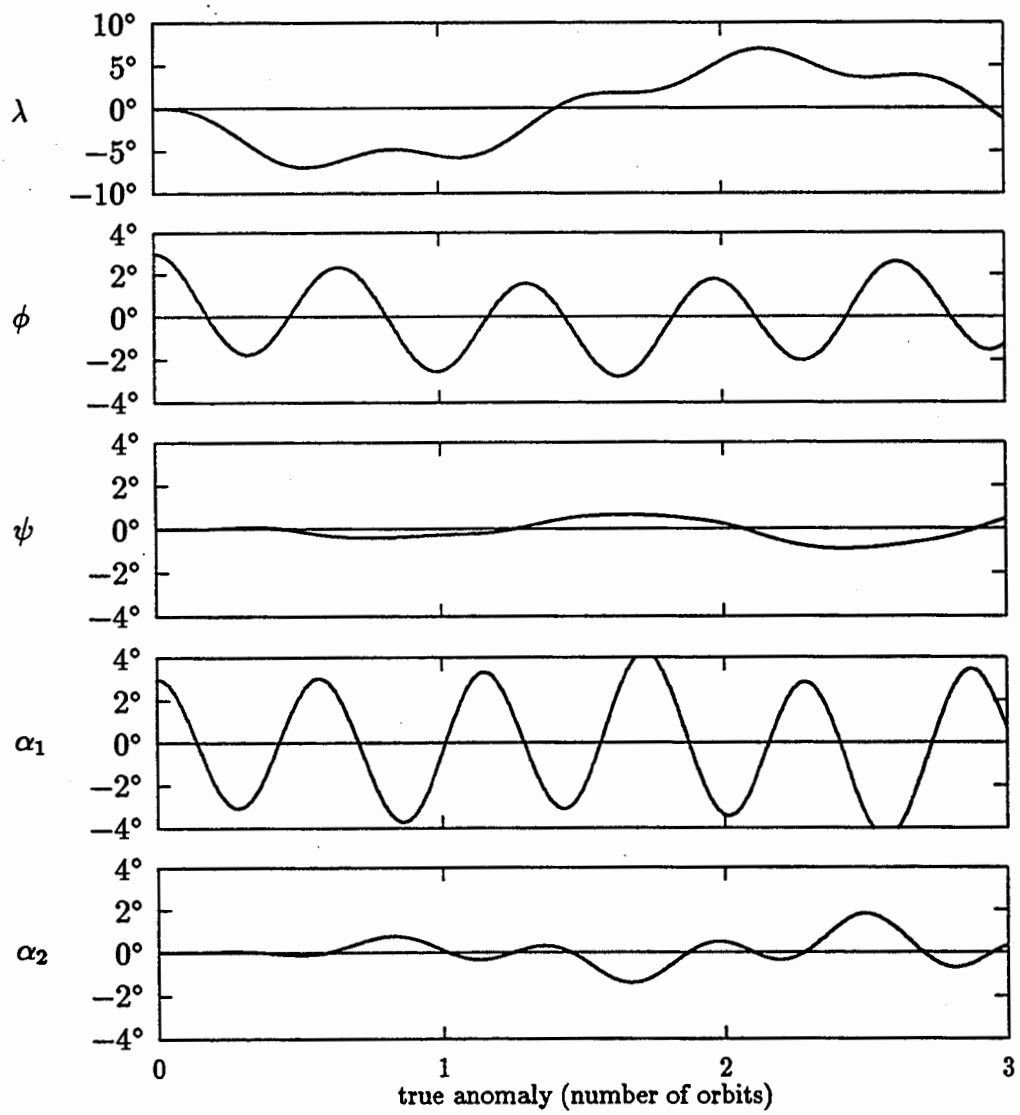

Figure 4-8 Response plots showing stable character of the equilibrium orientation (e) when the conditions in eq. (4.23) are satisfied. Note the appendages are short and wide.

$$J_{01} = 22.5kg \cdot m^2 \quad J_{02} = 18.75kg \cdot m^2 \quad J_{03} = 3.75kg \cdot m^2$$

$$m = 10kg \quad L = 2.5m \quad l = 5m \quad d = 1m$$

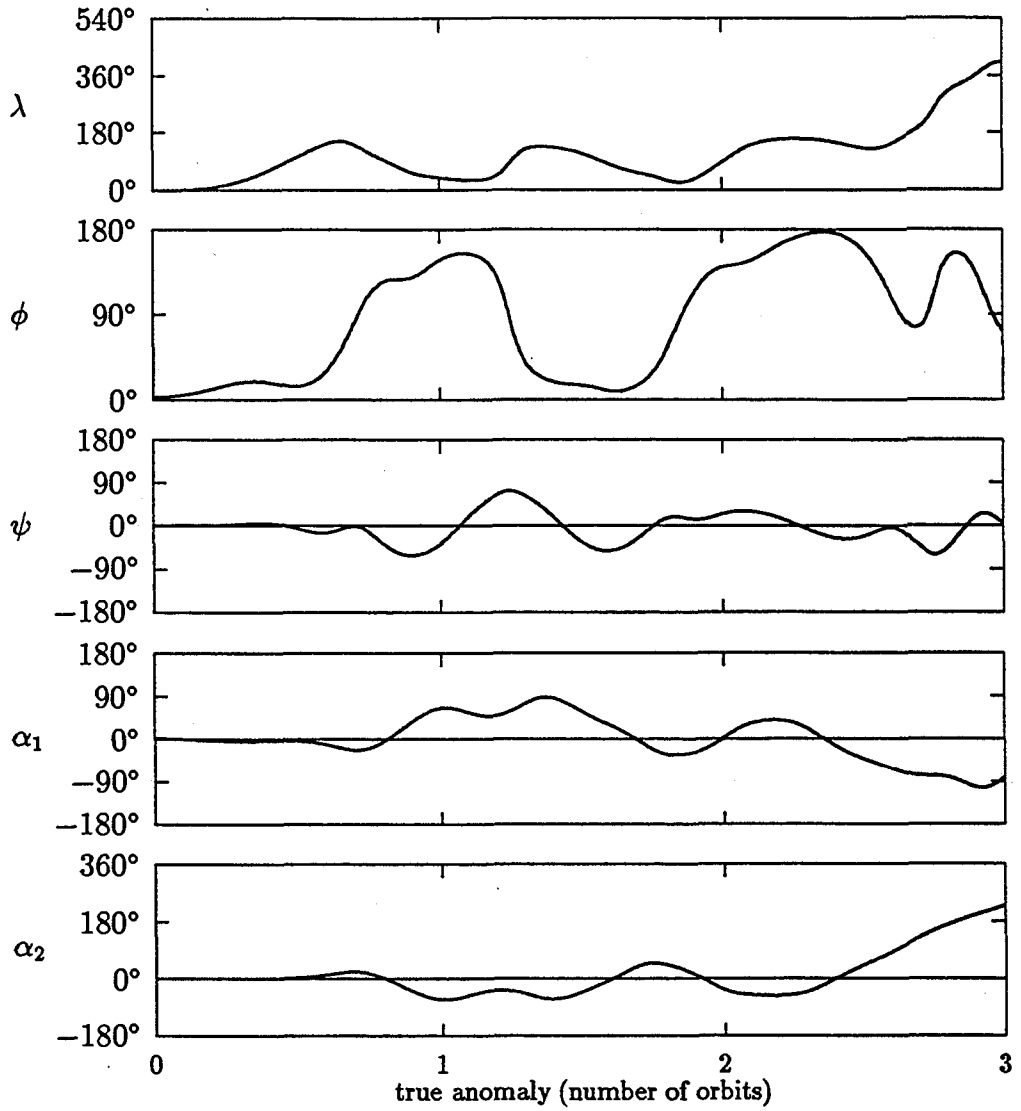

Figure 4-9 Unstable response around the orientation (e) when the conditions in eq. (4.23) are not met. Note, all the five degrees of freedom are unstable in this particular case.

$$J_{01} = 22.5kg \cdot m^2 \quad J_{02} = 18.75kg \cdot m^2 \quad J_{03} = 3.75kg \cdot m^2$$

$$m = 10kg \quad L = 2.5m \quad l = 5m \quad d = 1m$$

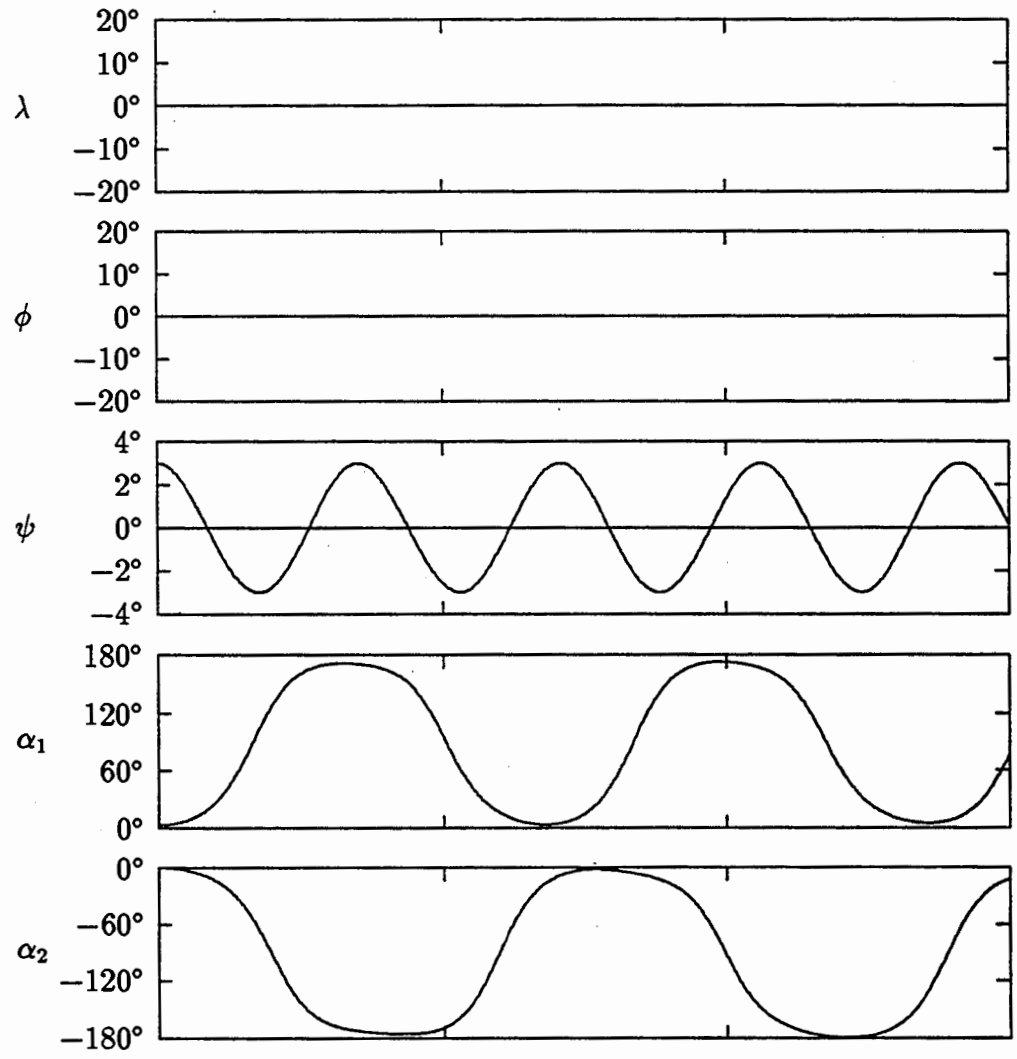

Figure 4-10 Response plots showing unstable character of the equilibrium orientation (f). Note, the instability is limited to the free rotations of the appendages and the motion of the central body is stable for this particular case.

5. APPROXIMATE ANALYTICAL SOLUTION

Approximate analytical solutions, if able to capture essence of the problem, often provide better physical appreciation and insight into the system behavior at a considerable saving in time, effort and computational cost. It can thus complement numerical analysis of complex problems, such as the present one, in a useful way. To that end, Modi et al. have studied dynamics of spacecraft with two beam–type appendages [72, 47] using the K-B [73] and Butenin's method [66]. Modi and Misra [61] have presented an approximate analytical solution for a tethered satellite system during deployment and retrieval, while Kalaycioglu and Misra [74] obtained a simple closed-form solution for the system dynamics during deployment of flexible appendages.

This chapter investigates dynamics of spacecraft with a beam-type appendage, free to undergo librational and vibrational motions in the orbital plane, during a prescribed slew maneuver. The governing equations are first simplified to confirm to the standard nonlinear form and then solved by Butenin's method. Validity of the analytical solution is assessed over a range of system parameters and initial conditions by comparing it with numerical integration of the exact equations of motion. The results show good correlation and provide better insight into the dynamical behavior of the system.

5.1 System Description and the Equations of Motion

The spacecraft consists of a triaxial rigid central body and a beam-type appendage undergoing a prescribed slew maneuver, as shown in Figure 5-1. It has the following features:

- a circular orbit around the earth;
- the mass and inertia of the beam are much smaller than those of the central body;

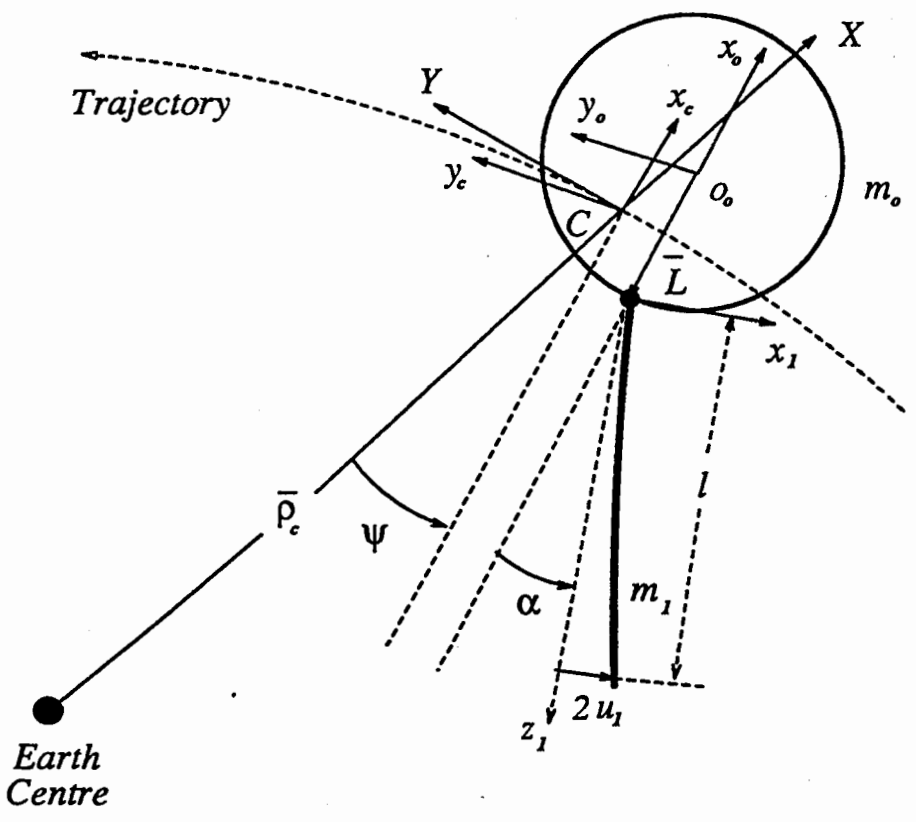

Figure 5-1 A satellite with the beam-type slewing appendage, undergoing planar motion, considered for the study using Butenin's method.

- the beam is aligned with one of the principal axes at the mass centre of the central body and attached to it by a joint permitting slew as a cantilevered appendage;

- the time history of the slew maneuver is taken to be sinusoidal [63],

$$\alpha = \alpha_0 + \frac{\Delta\alpha}{\Delta\theta}\left\{\theta - \frac{\Delta\theta}{2\pi} sin(\frac{2\pi}{\Delta\theta}\theta)\right\} . \tag{5.1}$$

  Magnitude of the maneuver $\Delta\alpha$ is 30°, and the slewing time, in terms of true anomaly, $\Delta\theta$, is varied in the interval of $5° - 10°$. The system response during and after the slew maneuver is determined.

- the fundamental cantilever mode is used to discretize the vibratory motion. The flexural rigidity of the beam is varied with the corresponding frequencies in the range of 60-120 cycles per orbit.

- the scope of this investigation includes assessment of the pitch motion and elastic vibration of the beam in the orbital plane.

For the planar motion:

$$\lambda = \phi = 0; \quad and \quad \dot{\lambda}=\dot{\phi}= 0 .$$

The transformation matrices are:

$$[A] = \begin{bmatrix} cos\psi & sin\psi & 0 \\ -sin\psi & cos\psi & 0 \\ 0 & 0 & 1 \end{bmatrix};$$

$$[B_o] = \begin{bmatrix} cos\psi & -sin\psi & 0 \\ sin\psi & cos\psi & 0 \\ 0 & 0 & 1 \end{bmatrix};$$

$$[C_1] = \begin{bmatrix} sin\alpha & -cos\alpha & 0 \\ 0 & 0 & 1 \\ -cos\alpha & -sin\alpha & 0 \end{bmatrix};$$

$$[B_1] = [0 \quad 1 \quad 0] .$$

The integral matrices associated with the elastic vibration, and the inertia matrices of the appendage, are the same as in Test Configuration 2 of Chapter 3. The other

matrices are:

$$
\begin{aligned}
[\,L_1\,] &= [-L \quad 0 \quad 0]\,; \\
J^o &= \frac{1}{2}(J_{03}+J_{02}+J_{01}) + m_1\left(\frac{1}{3}-\frac{m_1}{4M}\right)l^2 + \frac{m_o m_1}{M}L\,(L+l cos\alpha - 2\beta_1 u_1 sin\alpha)\,; \\
\left[J^1\right] &= \begin{bmatrix} j^1_{xx} & j^1_{yx} & 0 \\ j^1_{yx} & j^1_{yy} & 0 \\ 0 & 0 & j^1_{zz} \end{bmatrix};
\end{aligned}
$$

with:

$$
\begin{aligned}
j^1_{xx} &= \frac{1}{2}(J_{02}+J_{03}-J_{01}) + m_1\left(\frac{1}{3}-\frac{m_1}{4M}\right)l^2 cos^2\alpha + \frac{m_o m_1}{M}L\,(L+l cos\alpha - 2\beta_1 u_1 sin\alpha) \\
&\quad -m_1 l u_1\left(\beta_2 - \frac{m_1}{2M}\beta_1\right) sin2\alpha\,; \\
j^1_{yy} &= \frac{1}{2}(J_{03}+J_{01}-J_{02}) + m_1\left(\frac{1}{3}-\frac{m_1}{4M}\right)l^2 sin^2\alpha + m_1 l u_1\left(\beta_2 - \frac{m_1}{2M}\beta_1\right) sin2\alpha\,; \\
j^1_{zz} &= \frac{1}{2}(J_{01}+J_{02}-J_{03})\,; \\
j^1_{yx} &= -\frac{1}{2}m_1 l^2\left(\frac{1}{3}-\frac{m_1}{4M}\right) sin2\alpha - m_1 l u_1\left(\beta_2 - \frac{2m_1}{M}\beta_1\right) cos2\alpha \\
&\quad -\frac{m_o m_1}{M}L\,(\beta_1 u_1 cos\alpha + 0.5 l sin\alpha)\,;
\end{aligned}
$$

and

$$
[M_{12}]_1 = \begin{bmatrix} m_{xx} & 0 & m_{xz} \\ 0 & m_{yy} & 0 \\ m_{xx} & 0 & m_{zz} \end{bmatrix}.
$$

Here:

$$
\begin{aligned}
m_{xx} &= -m_1 l u_1\left(\beta_2 - \frac{2m_1}{M}\beta_1\right) sin\alpha - \frac{m_o m_1}{M}L l cos^2\alpha\,; \\
m_{yy} &= -m_1\left(\frac{1}{3}-\frac{m_1}{4M}\right)l^2 cos\alpha + m_1 l u_1\left(\beta_2 - \frac{2m_1}{M}\beta_1\right) sin\alpha - \frac{m_o m_1}{2M}L l\,; \\
m_{zz} &= m_1\left(\frac{1}{3}-\frac{m_1}{4M}\right)l^2 - \frac{m_o m_1}{M}L\,(\beta_1 u_1 sin\alpha - 0.5 l cos\alpha)\,; \\
m_{yx} &= m_1 l u\left(\beta_2 - \frac{2m_1}{M}\beta_1\right) cos\alpha - \frac{m_o m_1}{M}L\,(\beta_1 u + 0.5 l sin2\alpha)\,; \\
m_{xy} &= m_1\left(\frac{1}{3}-\frac{m_1}{4M}\right)l^2 sin^2\alpha + m_1 l u_1\left(\beta_2 - \frac{2m_1}{M}\beta_1\right) cos\alpha\,.
\end{aligned}
$$

Similarly:

$$
[M_{14}]_1 = \begin{bmatrix} 0 \\ 0 \\ m_1 l\left(\beta_2 - \frac{m_1}{M}\beta_1\right) + \frac{m_o m_1}{M}L\beta_1 \end{bmatrix};
$$

$$[M_{22}]_{11} = m_1 l \begin{bmatrix} \left(\frac{1}{3} - \frac{m_1}{4M}\right) l & 0 & -\left(\beta_2 - \frac{2m_1}{M}\beta_1\right) u_1 \\ 0 & \left(\frac{1}{3} - \frac{m_1}{4M}\right) l & 0 \\ -\left(\beta_2 - \frac{2m_1}{M}\beta_1\right) u_1 & 0 & 0 \end{bmatrix} ;$$

$$[M_{24}]_{11} = \begin{bmatrix} 0 \\ m_1 l \left(\beta_2 - \frac{2m_1}{M}\beta_1\right) \\ 0 \end{bmatrix} ;$$

$$(M_{44})_{11} = m_1 \left(1 - \frac{m_1}{M}\beta_1^2\right) .$$

Substituting the above expressions into equations (2.104) and (2.111), and taking the nondimensionized variable $u = u_1/l$ for the elastic vibration, where u represents ratio of half the tip deflection over its length; the governing equations during a specified slewing maneuver are obtained as follows:

$$\lambda'' = 0 ; \tag{5.2}$$

$$\phi'' = 0 ; \tag{5.3}$$

$$\left\{\tilde{J}_{03} + \epsilon_m \beta_3 \epsilon_l^2 + \frac{\epsilon_m}{1+\epsilon_m}(1 + \epsilon_l cos\alpha - \epsilon_l \beta_1 u sin\alpha)\right\} \psi''$$
$$+\frac{\epsilon_m \epsilon_l}{2}\left\{\epsilon_l \beta_2 + \frac{1 - \epsilon_m \epsilon_l}{1+\epsilon_m}\beta_1\right\} u'' + \epsilon_m \epsilon_l \left\{\beta_3 \epsilon_l - \frac{1}{2(1+\epsilon_m)}(\beta_1 u sin\alpha - cos\alpha)\right\} \alpha''$$
$$-\frac{\epsilon_m \epsilon_l}{1+\epsilon_m}\left\{\beta_1 sin\alpha\, u' + (\beta_1 cos\alpha\, u + sin\alpha)\alpha'\right\}(1 + \psi' + \frac{\alpha'}{2})$$
$$+\frac{3}{2}\left\{\tilde{J}_{02} - \tilde{J}_{01} + \frac{\epsilon_m}{1+\epsilon_m}(1 + \epsilon_l cos\alpha - \epsilon_l \beta_1 u sin\alpha)\right.$$
$$\left. + \epsilon_m \epsilon_l^2(\beta_3 cos2\alpha - \beta_4 sin2\alpha\, u)\right\} sin2\psi + \frac{3}{2}\epsilon_m \epsilon_l \left\{\frac{1}{1+\epsilon_m}(\beta_1 u cos\alpha + sin\alpha)\right.$$
$$\left. + \epsilon_l(\beta_3 sin2\alpha + \beta_4 cos2\alpha\, u)\right\} cos2\psi = 0 ; \tag{5.4}$$

$$\left\{\frac{\beta_1}{1+\epsilon_m} + \epsilon_l(\beta_2 - \frac{\epsilon_m}{1+\epsilon_m}\beta_1)\right\} \psi'' + \frac{\epsilon_l}{2}(1 - \frac{\epsilon_m}{1+\epsilon_m}\beta_1^2) u'' + \frac{\epsilon_l}{2} r_v^2 u$$
$$+\epsilon_l \beta_4 \alpha'' + \frac{\beta_1}{1+\epsilon_m} sin\alpha \left\{1.5 + \alpha' + \alpha'\psi' + 2\psi' + \psi'^2\right\}$$
$$+\frac{3}{2}\left\{\epsilon_l \beta_4 sin2\alpha + \frac{\beta_1}{1+\epsilon_m} sin\alpha\right\} cos2\psi$$
$$+\frac{3}{2}\left\{\epsilon_l \beta_4 cos2\alpha + \frac{\beta_1}{1+\epsilon_m} cos\alpha\right\} sin2\psi = 0. \tag{5.5}$$

In equations (5.2) to (5.5), $\epsilon_m = m_1/m_0$; $\epsilon_l = l/L$; $r_v = \frac{1}{\Omega}\sqrt{k/m_1}$, with '$k$', the bending rigidity of the beam and 'Ω', the angular velocity of the orbital motion;

$\tilde{J}_{0i} = J_{0i}/(m_0 L^2)$, $i = 1, 2, 3$; and

$$\beta_3 = \frac{1}{3} - \frac{\epsilon_m}{4(1+\epsilon_m)}; \qquad \beta_4 = \beta_2 - \frac{\epsilon_m}{2(1+\epsilon_m)}\beta_1 \ .$$

Equations (5.2) and (5.3) show that yaw and roll are not excited by the pitch and vibrations in the orbital plane if they are initially quiescent.

Note , α' and α'' vanish at the beginning ($\theta = 0°$) and at the end ($\theta = \Delta\theta$) of the slew due to the sinusoidal character. However during the slew they are varying. After the slew, since α is fixed at $\alpha_f = \alpha_0 + \Delta\alpha$, α' and α'' vanish, and the equations become simpler:

$$\begin{aligned}
&\left\{\tilde{J}_{03} + \epsilon_m\,\beta_3\epsilon_l^2 + \frac{\epsilon_m}{1+\epsilon_m}(\,1 + \epsilon_l\,cos\alpha_f - \epsilon_l\,\beta_1 u\,sin\alpha_f)\right\}\psi'' \\
&+\frac{\epsilon_m\,\epsilon_l}{2}\left\{\epsilon_l\beta_2 + \frac{\beta_1(1-\epsilon_m\epsilon_l)}{1+\epsilon_m}\right\}u'' - \frac{\epsilon_m\,\epsilon_l}{1+\epsilon_m}\,\beta_1\,sin\alpha_f\,u'\,(\,1+\psi') \\
&+\frac{3}{2}\left\{\tilde{J}_{02} - \tilde{J}_{01} + \frac{\epsilon_m}{1+\epsilon_m}\,(\,1 + \epsilon_l\,cos\alpha_f - \epsilon_l\beta_1\,u\,sin\alpha_f)\right. \\
&\left.+\ \epsilon_m\,\epsilon_l^2(\,\beta_3\,cos2\alpha_f - \beta_4 sin2\alpha_f\,u\,)\right\}sin2\psi + \frac{3}{2}\,\epsilon_m\,\epsilon_l\left\{\frac{1}{1+\epsilon_m}(\,\beta_1\,u\,cos\alpha_f + sin\alpha_f)\right. \\
&\left.+\ \epsilon_l\,(\,\beta_3\,sin2\alpha_f + \beta_4\,cos2\alpha_f\,u\,)\right\}cos2\psi = 0, \qquad (5.6)
\end{aligned}$$

$$\begin{aligned}
&\left\{\frac{\beta_1}{1+\epsilon_m} + \epsilon_l\,(\,\beta_2 - \frac{\epsilon_m}{1+\epsilon_m}\beta_1)\right\}\psi'' + \frac{\epsilon_l}{2}(1 - \frac{\epsilon_m}{1+\epsilon_m}\beta_1^2)\,u'' + \frac{\epsilon_l}{2}\,r_v^2\,u \\
&+\frac{\beta_1}{1+\epsilon_m}sin\alpha_f\left\{1.5 + 2\psi' + \psi'^2\right\} + \frac{3}{2}\left\{\epsilon_l\,\beta_4\,sin2\alpha_f + \frac{\beta_1}{1+\epsilon_m}\,sin\alpha_f\right\}cos2\psi \\
&+\frac{3}{2}\left\{\epsilon_l\,\beta_4\,cos2\alpha_f + \frac{\beta_1}{1+\epsilon_m}\,cos\alpha_f\right\}sin2\psi = 0. \qquad (5.7)
\end{aligned}$$

5.2 Simplification of the Equations

Equations (5.4)–(5.7) are highly nonlinear, nonautonomous and coupled. To determine their approximate analytical solution, they were simplified using the following assumptions:

- the coefficients in the equations are either constants or vary slowly over a small range with respect to the independent variable;
- the dependent variables and their first derivatives are small.

The first assumption implies that ϵ_m is small and $\Delta\alpha$ is not large. To ensure the second condition, the dependent variables must be selected carefully. The problem may occur with ψ since the equilibrium of ψ may not be zero because of the orientation change of the beam with respect to the central body. Consider $\psi = \psi_0 + \tilde{\psi}$, where ψ_0 is a constant angle representing the equilibrium and $\tilde{\psi}$ is the new variable replacing ψ. To determine ψ_0 during a slewing maneuver, set the 'average gravitational moment' (with the small terms having 'u' ignored) to zero,

$$\frac{3}{2}\left\{\tilde{J}_{02} - \tilde{J}_{01} + \frac{\epsilon_m}{1+\epsilon_m}(1 + \epsilon_l\overline{cos\alpha}) + \epsilon_m\epsilon_l^2\beta_3\overline{cos2\alpha}\right\} sin2\psi_o$$
$$+\frac{3}{2}\left\{\frac{\epsilon_m\epsilon_l}{1+\epsilon_m}\overline{sin\alpha} + \epsilon_m\epsilon_l^2\beta_3\overline{sin2\alpha}\right\} cos2\psi_o \;=\; 0\,.$$

Then

$$tan2\psi_0 = -\frac{\frac{\epsilon_m\,\epsilon_l}{1+\epsilon_m}\overline{sin\alpha} + \epsilon_m\,\epsilon_l^2\,\beta_3\,\overline{sin2\alpha}}{\tilde{J}_{02} - \tilde{J}_{01} + \frac{\epsilon_m}{1+\epsilon_m}(1 + \epsilon_l\,\overline{cos\alpha}) + \epsilon_m\,\epsilon_l^2\,\beta_3\,\overline{cos2\alpha}}\,, \tag{5.8}$$

where the overline represents average value of the function beneath it during slewing:

$$\overline{sin\alpha} = \frac{1}{\Delta\alpha}(cos\alpha_0 - cos\alpha_f)\;;$$
$$\overline{cos\alpha} = \frac{1}{\Delta\alpha}(sin\alpha_f - \sin\alpha_0)\;.$$

To determine ψ_0 after the slewing, formula (5.8) is still applicable with:

$$\overline{sin\alpha} = sin\alpha_f\;; \quad \overline{cos\alpha} = cos\alpha_f\;.$$

Butenin's Method deals with equations of the form

$$\begin{bmatrix} C_{11} & C_{12} \\ C_{21} & C_{22} \end{bmatrix}\begin{bmatrix} \tilde{\psi}'' \\ u'' \end{bmatrix} + \begin{bmatrix} C_{13} & C_{14} \\ C_{23} & C_{24} \end{bmatrix}\begin{bmatrix} \tilde{\psi} \\ u \end{bmatrix}$$
$$= \Sigma_i \begin{bmatrix} D_{1i} \\ D_{2i} \end{bmatrix} sin(\omega_i\,\theta + \gamma_i) + \begin{bmatrix} f(\theta, \tilde{\psi}, \tilde{\psi}', \tilde{\psi}'', u, u') \\ g(\theta, \tilde{\psi}, \tilde{\psi}', u, u') \end{bmatrix}\,. \tag{5.9}$$

In equation (5.9), all the entries in the inertia and stiffness matrices are constants. The frequency ω_i, the initial phase γ_i and amplitudes D_{1i}, D_{2i} of the forcing terms are constants too. The functions f and g have small values. To solve equations (5.4), (5.5) and (5.6), (5.7) by the Butenin method, the first step would be to transform them into the required form (5.9). Consider equations (5.4) and (5.5) first.

Entries of the inertia matrix are easy to obtain except for C_{11}. To get an accurate value of C_{11}, the term involving 'u' in the coefficient of $\psi''(=\tilde{\psi}'')$ is introduced into the function f and the average value of $cos\alpha$ taken. Thus:

$$\begin{aligned}
C_{11} &= \tilde{J}_{03} + \epsilon_m\,\beta_3\,\epsilon_l^2 + \frac{\epsilon_m}{1+\epsilon_m}\,(1+\epsilon_l\,\overline{cos\alpha})\;;\\
C_{12} &= \frac{\epsilon_m\,\epsilon_l}{2}\left\{\epsilon_l\,\beta_2 + \frac{\beta_1\,(1-\epsilon_m\,\epsilon_l)}{1+\epsilon_m}\right\}\;;\\
C_{21} &= \frac{\beta_1}{1+\epsilon_m} + \epsilon_l\,(\beta_2 - \frac{\epsilon_m}{l+\epsilon_m}\,\beta_1)\;;\\
C_{22} &= \frac{1}{2}\epsilon_l\,(1 - \frac{\epsilon_m}{1+\epsilon_m}\beta_1^2)\;.
\end{aligned}$$

Entries for the stiffness matrix (except C_{24}) have terms involving $sin2\psi$ and $cos2\psi$. Using the following formulas:

$$sin2\psi = sin2\psi_0\,cos2\tilde{\psi} + cos2\psi_0\,sin2\tilde{\psi}\;;$$

$$cos2\psi = cos2\psi_0\,cos2\tilde{\psi} - sin2\psi_0\,sin2\tilde{\psi}\;;$$

and approximating:

$$cos2\tilde{\psi} \approx 1 - 2\,\tilde{\psi}^2\;; \qquad sin2\tilde{\psi} \approx 2\,\tilde{\psi} - \frac{4}{3}\,\tilde{\psi}^3\;;$$

the terms involving $sin2\psi$ and $cos2\psi$ in equation (5.4) become

$$\begin{aligned}
&\frac{3}{2}\left\{(\tilde{J}_{02} - \tilde{J}_{01} + \frac{\epsilon_m}{1+\epsilon_m})\,sin2\psi_0 + \frac{\epsilon_m\,\epsilon_l}{1+\epsilon_m}\,sin(2\psi_0+\alpha)\right.\\
+\;&\left.\epsilon_m\,\epsilon_l^2\,\beta_3\,sin2\,(\psi_0+\alpha)\right\}(1-2\,\tilde{\psi}^2)\\
+\;&\frac{3}{2}\left\{\frac{\epsilon_m\,\epsilon_l}{1+\epsilon_m}\,\beta_1\,cos(2\psi_0+\alpha) + \epsilon_m\,\epsilon_l^2\,\beta_4\,cos2\,(\psi_0+\alpha)\right\}\,u\,(1-2\,\tilde{\psi}^2)\\
+\;&3\left\{(\tilde{J}_{02} - \tilde{J}_{01} + \frac{\epsilon_m}{1+\epsilon_m})\,cos2\psi_0 + \frac{\epsilon_m\,\epsilon_l}{1+\epsilon_m}\,cos(2\psi_0+\alpha)\right.\\
+\;&\left.\epsilon_m\,\epsilon_l^2\,\beta_3\,cos2\,(\psi_0+\alpha)\right\}(\tilde{\psi} - \frac{2}{3}\tilde{\psi}^3)\\
-\;&3\left\{\frac{\epsilon_m\,\epsilon_l}{1+\epsilon_m}\,\beta_1\,sin(2\psi_0+\alpha) + \epsilon_m\,\epsilon_l^2\,\beta_4\,sin2\,(\psi_0+\alpha)\right\}\,\tilde{\psi}\,u\;.
\end{aligned} \tag{5.10}$$

Similarly, the terms involving $sin2\psi$ and $cos2\psi$ in equation (5.5) become

$$\begin{aligned}
&\frac{3}{2}\left\{\frac{\beta_1}{1+\epsilon_m}sin(2\,\psi_0+\alpha) + \epsilon_l\,\beta_4\,sin2\,(\psi_0+\alpha)\right\}(1-2\,\tilde{\psi}^2)\\
+\;&3\left\{\frac{\beta_1}{1+\epsilon_m}cos(2\psi_0+\alpha) + \epsilon_l\,\beta_4\,cos2\,(\psi_0+\alpha)\right\}(\tilde{\psi} - \frac{2}{3}\tilde{\psi}^3)\;.
\end{aligned} \tag{5.11}$$

Thus, the stiffness constants C_{13}, C_{14}, and C_{23} are obtained as the coefficients of $\tilde{\psi}$ and u in expressions (5.10) and (5.11):

$$
\begin{aligned}
C_{13} &= 3\left\{(\tilde{J}_{02}-\tilde{J}_{01}+\frac{\epsilon_m}{1+\epsilon_m})\,cos2\psi_0+\frac{\epsilon_m\,\epsilon_l}{1+\epsilon_m}\,\overline{cos(2\psi_0+\alpha)}+\epsilon_m\,\epsilon_l^2\,\beta_3\,\overline{cos2\,(\psi_0+\alpha)}\right\}\;;\\
C_{14} &= \frac{3}{2}\left\{\frac{\epsilon_m\,\epsilon_l}{1+\epsilon_m}\,\beta_1\,\overline{cos(2\psi_0+\alpha)}+\epsilon_m\,\epsilon_l^2\,\beta_4\,\overline{cos2\,(\psi_0+\alpha)}\right\}\;;\\
C_{23} &= 3\left\{\frac{\beta_1}{1+\epsilon_m}\overline{cos(2\psi_0+\alpha)}+\epsilon_l\,\beta_4\,\overline{cos2\,(\psi_0+\alpha)}\right\}\;;\\
C_{24} &= 0.5\,\epsilon_l\,r_v^2\;.
\end{aligned}
$$

Now, the terms without the dependent variables are treated as forcing functions and the nonlinear terms are included in the functions f and g. From equation (5.1):

$$\alpha'=\frac{\Delta\alpha}{\Delta\theta}\left\{1-cos(\frac{2\pi}{\Delta\theta}\,\theta)\right\}\;;\quad \alpha''=\frac{2\pi\,\Delta\alpha}{\Delta\theta^2}sin(\frac{2\pi}{\Delta\theta}\,\theta)\;. \tag{5.12}$$

Since $\frac{\Delta\theta}{2\,\pi}\ll 1$: $\quad \alpha\approx\alpha_0+\frac{\Delta\alpha}{\Delta\theta}\,\theta$;

$$sin\alpha\approx sin(\frac{\Delta\alpha}{\Delta\theta}\,\theta+\alpha_0)\;;\qquad cos\alpha\approx cos(\frac{\Delta\alpha}{\Delta\theta}\,\theta+\alpha_0)\;. \tag{5.13}$$

Collecting and arranging terms in equations (5.4) and (5.5), seven forcing components can be identified. Their frequencies, initial phases and amplitudes are:

$$
\begin{array}{llll}
\omega_3=0, & \gamma_3=2\psi_0, & D_{13}=-\frac{3}{2}\,(\tilde{J}_{02}-\tilde{J}_{01}+\frac{\epsilon_m}{1+\epsilon_m}), & D_{23}=0,\\
\omega_4=\frac{\Delta\alpha}{\Delta\theta}, & \gamma_4=\alpha_0, & D_{14}=\frac{\epsilon_m\,\epsilon_l}{1+\epsilon_m}\frac{\Delta\alpha}{\Delta\theta}(1+\frac{3}{4}\,\frac{\Delta\alpha}{\Delta\theta}), & D_{24}=-\frac{\beta_1}{1+\epsilon_m}(\frac{3}{2}+\frac{\Delta\alpha}{\Delta\theta}),\\
\omega_5=\frac{2\pi}{\Delta\theta}, & \gamma_5=0, & D_{15}=-\epsilon_m\epsilon_l^2\,\beta_3\,\frac{2\pi\,\Delta\alpha}{\Delta\theta^2}, & D_{25}=-\epsilon_l\beta_4\,\frac{2\pi\,\Delta\alpha}{\Delta\theta^2},\\
\omega_6=\frac{\Delta\alpha}{\Delta\theta}, & \gamma_6=2\,(\psi_o+\alpha_o), & D_{16}=-\frac{3}{2}\frac{\epsilon_m\,\epsilon_l}{1+\epsilon_m}, & D_{26}=-\frac{3}{2}\frac{\beta_1}{1+\epsilon_m},\\
\omega_7=2\frac{\Delta\alpha}{\Delta\theta}, & \gamma_7=2(\psi_o+\alpha_o), & D_{17}=-\frac{3}{2}\epsilon_m\,\epsilon_l^2\,\beta_3, & D_{27}=-\frac{3}{2}\,\epsilon_l\,\beta_4,\\
\omega_8=\frac{2\pi+\Delta\alpha}{\Delta\theta}, & \gamma_8=\alpha_0, & D_{18}=-\frac{1}{2}\frac{\epsilon_m\,\epsilon_l}{1+\epsilon_m}\frac{\Delta\alpha}{\Delta\theta}(1+\frac{\Delta\alpha}{\Delta\theta}+\frac{\pi}{\Delta\theta}), & D_{28}=\frac{1}{2}\frac{\beta_1}{1+\epsilon_m}\frac{\Delta\alpha}{\Delta\theta},\\
\omega_9=\frac{2\pi-\Delta\alpha}{\Delta\theta}, & \gamma_9=-\alpha_0, & D_{19}=\frac{1}{2}\frac{\epsilon_m\,\epsilon_l}{1+\epsilon_m}\frac{\Delta\alpha}{\Delta\theta}(1+\frac{\Delta\alpha}{\Delta\theta}-\frac{\pi}{\Delta\theta}), & D_{29}=-\frac{1}{2}\frac{\beta_1}{1+\epsilon_m}\frac{\Delta\alpha}{\Delta\theta}.
\end{array}
\tag{5.14}
$$

The frequency $\frac{2\pi}{\Delta\theta}$ is due to the inertia force caused by the slew.

The nonlinear functions $f(\theta,\tilde{\psi},\tilde{\psi}',\tilde{\psi}'',u,u')$ and $g(\theta,\tilde{\psi},\tilde{\psi}',u,u')$ up to the third degree can be written as:

$$
\begin{aligned}
f &= 3\left\{\frac{\epsilon_m\,\epsilon_l}{1+\epsilon_m}\,\beta_1\,sin(2\psi_0+\alpha)+\epsilon_m\,\epsilon_l^2\,\beta_4\,sin2\,(\psi_0+\alpha)\right\}\,\tilde{\psi}\,u\\
&\quad +3\left\{(\tilde{J}_{02}-\tilde{J}_{01}+\frac{\epsilon_m}{1+\epsilon_m})\,sin2\psi_0+\frac{\epsilon_m\,\epsilon_l}{1+\epsilon_m}\,sin(2\psi_0+\alpha)+\epsilon_m\,\epsilon_l^2\,\beta_3\,sin2\,(\psi_0+\alpha)\right\}\tilde{\psi}^2
\end{aligned}
$$

$$
\begin{aligned}
&+3\left\{\frac{\epsilon_m\,\epsilon_l}{1+\epsilon_m}\,\beta_1\,cos(2\psi_0+\alpha)+\epsilon_m\,\epsilon_l^2\,\beta_4\,cos2\,(\psi_0+\alpha)\right\}\tilde{\psi}^2\,u\\
&+2\left\{(\tilde{J}_{02}-\tilde{J}_{01}+\frac{\epsilon_m}{1+\epsilon_m})\,cos2\psi_0+\frac{\epsilon_m\,\epsilon_l}{1+\epsilon_m}\,cos(2\psi_0+\alpha)+\epsilon_m\,\epsilon_l^2\,\beta_3\,cos2\,(\psi_0+\alpha)\right\}\tilde{\psi}^3\\
&+\frac{\epsilon_m}{1+\epsilon_m}\,\epsilon_l^2\,sin\alpha\,\alpha'\,\tilde{\psi}'+\frac{\epsilon_m}{1+\epsilon_m}\,\epsilon_l\,\beta_1\left\{(1+\frac{\alpha'}{2})\,cos\alpha\,\alpha'+\frac{1}{2}sin\alpha\,\alpha''+sin\alpha\,\tilde{\psi}''\right\}u\\
&+\frac{\epsilon_m}{1+\epsilon_m}\,\epsilon_l\,\beta_1(1+\frac{\alpha'}{2}+\tilde{\psi}')\,sin\alpha\,u'+\frac{\epsilon_m}{1+\epsilon_m}\epsilon_l\,\beta_1\,cos\alpha\,\alpha'\,\tilde{\psi}'u\;; \qquad (5.15)
\end{aligned}
$$

$$
\begin{aligned}
g \;=\;& 3\left\{\frac{\beta_1}{1+\epsilon_m}sin(2\,\psi_0+\alpha)+\epsilon_l\,\beta_4\,sin2\,(\psi_0+\alpha)\right\}\tilde{\psi}^2\\
&+2\left\{\frac{\beta_1}{1+\epsilon_m}cos(2\psi_0+\alpha)+\epsilon_l\,\beta_4\,cos2\,(\psi_0+\alpha)\right\}\tilde{\psi}^3\\
&-\frac{\beta_1}{1+\epsilon_m}\,sin\alpha\,(2\,\tilde{\psi}'+\alpha'\,\tilde{\psi}'+\tilde{\psi}'^2)\;. \qquad (5.16)
\end{aligned}
$$

Following the similar procedure, the simplified equations (5.6) and (5.7) for the system motion after the slew take the form:

$$
\begin{bmatrix} C_{11}^* & C_{12}^* \\ C_{21}^* & C_{22}^* \end{bmatrix}\begin{bmatrix} \tilde{\psi}'' \\ u'' \end{bmatrix}+\begin{bmatrix} C_{13}^* & C_{14}^* \\ C_{23}^* & C_{24}^* \end{bmatrix}\begin{bmatrix} \tilde{\psi} \\ u \end{bmatrix}
$$

$$
=\begin{bmatrix} 0 \\ D_{23}^* \end{bmatrix}+\begin{bmatrix} f^*(\theta,\tilde{\psi},\tilde{\psi}',\tilde{\psi}'',u,u') \\ g^*(\theta,\tilde{\psi},\tilde{\psi}',u,u') \end{bmatrix}\;, \qquad (5.17)
$$

where:

$$
\begin{aligned}
C_{11}^* &= \tilde{J}_{02}+\epsilon_m\,\beta_3\,\epsilon_l^2+\frac{\epsilon_m}{1+\epsilon_m}\,(1+\epsilon_l\,cos\alpha_f)\;;\\
C_{13}^* &= 3\left\{(\tilde{J}_{02}-\tilde{J}_{01}+\frac{\epsilon_m}{1+\epsilon_m})\,cos2\psi_0+\frac{\epsilon_m\,\epsilon_l}{1+\epsilon_m}\,cos(2\psi_0+\alpha_f)\right.\\
&\quad\left.+\,\epsilon_m\,\epsilon_l^2\,\beta_3\,cos2\,(\psi_0+\alpha_f)\right\}\;;\\
C_{14}^* &= \frac{3}{2}\left\{\frac{\epsilon_m\,\epsilon_l}{1+\epsilon_m}\,\beta_1\,cos(2\psi_0+\alpha_f)+\epsilon_m\,\epsilon_l^2\,\beta_4\,cos2\,(\psi_0+\alpha_f)\right\}\;;\\
C_{23}^* &= 3\left\{\frac{\beta_1}{1+\epsilon_m}cos(2\psi_0+\alpha_f)+\epsilon_l\,\beta_4\,cos2\,(\psi_0+\alpha_f)\right\}\;;\\
C_{24}^* &= 0.5\,\epsilon_l\,r_v^2\;;\\
D_{23}^* &= -\frac{3}{2}\left\{\frac{\beta_1}{1+\epsilon_m}sin(2\,\psi_0+\alpha_f)+\epsilon_l\,\beta_4\,sin2(\psi_0+\alpha_f)\right\}-\frac{3\,\beta_1}{2(1+\epsilon_m)}sin\alpha_f\;;
\end{aligned}
$$

and

$$
C_{12}^*=C_{12}\;;\quad C_{21}^*=C_{21}\;;\quad C_{22}^*=C_{22}.
$$

The nonlinear functions can be written as:

$$
\begin{aligned}
f^* &= 3\left\{\frac{\epsilon_m\,\epsilon_l}{1+\epsilon_m}\,\beta_1\,sin(2\psi_0+\alpha_f)+\epsilon_m\,\epsilon_l^2\,\beta_4\,sin2\,(\psi_0+\alpha_f)\right\}\tilde{\psi}\,u \\
&\quad +3\left\{\frac{\epsilon_m\,\epsilon_l}{1+\epsilon_m}\,\beta_1\,cos(2\psi_0+\alpha_f)+\epsilon_m\,\epsilon_l^2\,\beta_4\,cos2\,(\psi_0+\alpha_f)\right\}\tilde{\psi}^2\,u \\
&\quad +2\left\{(\tilde{J}_{02}-\tilde{J}_{01}+\frac{\epsilon_m}{1+\epsilon_m})\,cos2\psi_0+\frac{\epsilon_m\,\epsilon_l}{1+\epsilon_m}\,cos(2\psi_0+\alpha_f)\right. \\
&\quad \left.+\,\epsilon_m\,\epsilon_l^2\,\beta_3\,cos2\,(\psi_0+\alpha_f)\right\}\tilde{\psi}^3+\frac{\epsilon_m}{1+\epsilon_m}\,\epsilon_l\,\beta_1\,sin\alpha_f(u'+\tilde{\psi}'\,u'+\tilde{\psi}''\,u) \qquad (5.18)
\end{aligned}
$$

$$
\begin{aligned}
g^* &= 3\left\{\frac{\beta_1}{1+\epsilon_m}sin(2\,\psi_0+\alpha_f)+\epsilon_l\,\beta_4\,sin2\,(\psi_0+\alpha_f)\right\}\tilde{\psi}^2 \\
&\quad +2\left\{\frac{\beta_1}{1+\epsilon_m}cos(2\psi_0+\alpha_f)+\epsilon_l\,\beta_4\,cos2\,(\psi_0+\alpha_f)\right\}\tilde{\psi}^3 \\
&\quad -\frac{\beta_1}{1+\epsilon_m}\,sin\alpha_f\,(2\,\tilde{\psi}'+\tilde{\psi}'^2)\,. \qquad (5.19)
\end{aligned}
$$

5.3 Solution of the Equations of Motion

The equations of motion during slewing are solved first. For the linearized equation with f and g ignored, the solution can be written as

$$
\begin{bmatrix}\tilde{\psi}\\ u\end{bmatrix}=A_p\begin{bmatrix}1\\ \alpha_v\end{bmatrix}sin(\omega_p\,\theta+\gamma_p)+A_v\begin{bmatrix}\alpha_p\\ 1\end{bmatrix}sin(\omega_v\,\theta+\gamma_v)
+\sum_{i=3}^{9}\begin{bmatrix}A_{1i}\\ A_{2i}\end{bmatrix}sin(\omega_i\,\theta+\gamma_i)\,, \qquad (5.20)
$$

where:

$$
\begin{aligned}
\omega_p &= \left\{\frac{1}{2(C_{11}C_{22}-C_{12}C_{21})}\left\{C_{11}C_{24}+C_{13}C_{22}-C_{12}C_{23}-C_{14}C_{21}\right.\right. \\
&\quad -\left\{(C_{12}C_{23}+C_{14}C_{21}-C_{11}C_{24}-C_{13}C_{22})^2\right. \\
&\quad \left.\left.\left.-4\;(C_{11}C_{22}-C_{12}C_{21})(C_{13}C_{24}-C_{14}C_{23})\right\}^{0.5}\right\}\right\}^{\frac{1}{2}}\;; \qquad (5.21)
\end{aligned}
$$

$$
\begin{aligned}
\omega_v &= \left\{\frac{1}{2(C_{11}C_{22}-C_{12}C_{21})}\left\{C_{11}C_{24}+C_{13}C_{22}-C_{12}C_{23}-C_{14}C_{21}\right.\right. \\
&\quad +\left\{(C_{12}C_{23}+C_{14}C_{21}-C_{11}C_{24}-C_{13}C_{22})^2\right. \\
&\quad \left.\left.\left.-4\;(C_{11}C_{22}-C_{12}C_{21})(C_{13}C_{24}-C_{14}C_{23})\right\}^{0.5}\right\}\right\}^{\frac{1}{2}}\;; \qquad (5.22)
\end{aligned}
$$

$$\alpha_p = -\frac{C_{14} - \omega_v^2 C_{12}}{C_{13} - \omega_v^2 C_{11}} \; ; \qquad \alpha_v = -\frac{C_{23} - \omega_p^2 C_{21}}{C_{24} - \omega_p^2 C_{22}} \; ; \tag{5.23}$$

$$A_{1i} = \frac{1}{\Delta_i} det \begin{bmatrix} D_{1i} & C_{14} - \omega_i^2 C_{12} \\ D_{2i} & C_{24} - \omega_i^2 C_{22} \end{bmatrix} ;$$

$$A_{2i} = \frac{1}{\Delta_i} det \begin{bmatrix} C_{13} - \omega_i^2 C_{11} & D_{1i} \\ C_{23} - \omega_i^2 C_{21} & D_{2i} \end{bmatrix} ;$$

with

$$\Delta_i = det \begin{bmatrix} C_{13} - \omega_i^2 C_{11} & C_{14} - \omega_i^2 C_{12} \\ C_{23} - \omega_i^2 C_{21} & C_{24} - \omega_i^2 C_{22} \end{bmatrix} .$$

As to the nonlinear system represented by equation (5.9), the forced response is considered to remain the same, while the amplitude and phase of the free vibration vary slowly with θ. It is also assumed that $\tilde{\psi}'$ and u' take the same form as the amplitudes and phases of the free vibration are constant. This assumption leads to two equations involving $A_p'(\theta)$, $A_v'(\theta)$ and $\gamma_p'(\theta)$, $\gamma_v'(\theta)$. Substitution of the chosen form of the solution, i.e. equation (5.20) into equation (5.9), results in two additional equations. These four algebraic linear equations can be written as:

$$\begin{bmatrix} sin\tau_1 & cos\tau_1 & \alpha_p sin\tau_2 & \alpha_p cos\tau_2 \\ \alpha_v sin\tau_1 & \alpha_v cos\tau_1 & sin\tau_2 & cos\tau_2 \\ \omega_p cos\tau_1 & -\omega_p sin\tau_1 & \omega_v \alpha_p cos\tau_2 & -\omega_v \alpha_p sin\tau_2 \\ \omega_p \alpha_v cos\tau_1 & -\omega_p \alpha_v sin\tau_1 & \omega_v cos\tau_2 & -\omega_v sin\tau_2 \end{bmatrix} \begin{bmatrix} A_p'(\theta) \\ A_p(\theta)\gamma_p'(\theta) \\ A_v'(\theta) \\ A_v(\theta)\gamma_v'(\theta) \end{bmatrix}$$

$$= \frac{1}{C_{11}C_{22} - C_{12}C_{21}} \begin{bmatrix} 0 \\ 0 \\ C_{22} f - C_{12} g \\ C_{11} g - C_{21} f \end{bmatrix} , \tag{5.24}$$

with $\tau_1 = \omega_p \theta + \gamma_p(\theta)$; and $\tau_2 = \omega_v \theta + \gamma_v(\theta)$. Solving equation (5.24) gives:

$$A_p'(\theta) = \frac{1}{\Delta \omega_p} \left\{ (C_{22} + \alpha_p C_{21}) f - (C_{12} + \alpha_p C_{11}) g \right\} cos\tau_1 ;$$

$$A_p(\theta)\gamma_p'(\theta) = -\frac{1}{\Delta \omega_p} \left\{ (C_{22} + \alpha_p C_{21}) f - (C_{12} + \alpha_p C_{11}) g \right\} sin\tau_1 ;$$

$$A_v'(\theta) = -\frac{1}{\Delta \omega_v} \left\{ (C_{21} + \alpha_v C_{22}) f - (C_{11} + \alpha_v C_{12}) g \right\} cos\tau_2 ;$$

$$A_v(\theta)\gamma_v'(\theta) = \frac{1}{\Delta \omega_v} \left\{ (C_{21} + \alpha_v C_{22}) f - (C_{11} + \alpha_v C_{12}) g \right\} sin\tau_2 ;$$

where

$$\Delta = (C_{11}C_{22} - C_{12}C_{21})(1 - \alpha_p\alpha_v) \; .$$

Since the rates of change of $A_p(\theta)$, $A_v(\theta)$, $\gamma_p(\theta)$ and $\gamma_v(\theta)$ are small, the average values of the righthand side are used:

$$F_1 = \frac{1}{\Delta\theta}\int_0^{\Delta\theta} f\, sin\tau_1\, d\theta \; ; \qquad F_2 = \frac{1}{\Delta\theta}\int_0^{\Delta\theta} f\, cos\tau_1\, d\theta \; ;$$
$$F_3 = \frac{1}{\Delta\theta}\int_0^{\Delta\theta} f\, sin\tau_2\, d\theta \; ; \qquad F_4 = \frac{1}{\Delta\theta}\int_0^{\Delta\theta} f\, cos\tau_2\, d\theta \; ;$$
$$G_1 = \frac{1}{\Delta\theta}\int_0^{\Delta\theta} g\, sin\tau_1\, d\theta \; ; \qquad G_2 = \frac{1}{\Delta\theta}\int_0^{\Delta\theta} g\, cos\tau_1\, d\theta \; ;$$
$$G_3 = \frac{1}{\Delta\theta}\int_0^{\Delta\theta} g\, sin\tau_2\, d\theta \; ; \qquad G_4 = \frac{1}{\Delta\theta}\int_0^{\Delta\theta} g\, cos\tau_2\, d\theta \; .$$

Thus:

$$\begin{aligned}
A_p' &\approx \frac{1}{\Delta\omega_p}\left\{(C_{22} + \alpha_p C_{21})\, F_2 - (C_{12} + \alpha_p C_{11})\, G_2\right\} \; ; \\
\gamma_p' &\approx -\frac{1}{\Delta\omega_p\, A_p(0)}\left\{(C_{22} + \alpha_p C_{21})\, F_1 - (C_{12} + \alpha_p C_{11})\, G_1\right\} \; ; \\
A_v' &\approx -\frac{1}{\Delta\omega_v}\left\{(C_{21} + \alpha_v C_{22})\, F_4 - (C_{11} + \alpha_v C_{12})\, G_4\right\} \; ; \\
\gamma_v' &\approx \frac{1}{\Delta\omega_v\, A_v(0)}\left\{(C_{21} + \alpha_v C_{22}) + \alpha_v\, C_{22})\, F_3 - (C_{11} + \alpha_v\, C_{12})\, G_3\right\} \; . \qquad (5.25)
\end{aligned}$$

Now, the approximate closed form solution for the system during slewing can be written as:

$$\begin{aligned}
\begin{bmatrix} \tilde{\psi} \\ u \end{bmatrix} &= \left(A_p'\,\theta + A_p(0)\right)\begin{bmatrix} 1 \\ \alpha_v \end{bmatrix} sin\left\{(\omega_p + \gamma_p')\,\theta + \gamma_p(0)\right\} \\
&\quad + (A_v'\,\theta + A_v(0))\begin{bmatrix} \alpha_p \\ 1 \end{bmatrix} sin\left\{(\omega_v + \gamma_v')\,\theta + \gamma_v(0)\right\} \\
&\quad + \sum_{i=3}^{9}\begin{bmatrix} A_{1i} \\ A_{2i} \end{bmatrix} sin(\omega_i\,\theta + \gamma_i) \; ; \qquad (5.26)
\end{aligned}$$

where $A_p(0)$, $\gamma_p(0)$, $A_v(0)$ and $\gamma_v(0)$ are the initial conditions.

Equation (5.17) for the system response after the slewing maneuver can be solved following the same procedure with the solution as:

$$\begin{aligned}
\begin{bmatrix} \tilde{\psi} \\ u \end{bmatrix} &= A_p^*\begin{bmatrix} 1 \\ \alpha_v^* \end{bmatrix} sin\left\{(\omega_p^* + \gamma_p'^*)\,\theta + \gamma_p^*\right\} \\
&\quad + A_v^*\begin{bmatrix} \alpha_p^* \\ 1 \end{bmatrix} sin\left\{(\omega_v^* + \gamma_v'^*)\,\theta + \gamma_v^*\right\} + \begin{bmatrix} A_{13}^* \\ A_{23}^* \end{bmatrix} ; \qquad (5.27)
\end{aligned}$$

with:

$$A^*_{13} = -D^*_{23}\, C^*_{14}/(C^*_{13}\, C^*_{24} - C^*_{23}\, C^*_{14})\ ;$$
$$A^*_{23} = C^*_{13}\, D^*_{23}/(C^*_{13} C^*_{24} - C^*_{23}\, C^*_{14})\ .$$

The other parameters ω^*_p, ω^*_v and α^*_p, α^*_v are evaluated using equations (5.21), (5.22) and (5.23); and γ'^*_p, γ'^*_v through eq. (5.25). A'^*_p and A'^*_v vanish in this case. Note, A^*_p, γ^*_p and A^*_v, γ^*_v are determined by the values of the state variables right after the slewing maneuver.

5.4 Results and Discussion

The validity of the closed form solution as given by eqs. (5.26) and (5.27) is assessed, over a range of the system parameters and initial conditions, through its comparison with the numerical solutions of the exact equations of motion as given by (5.4) - (5.7). As can be expected, the amount of information obtained is literally enormous. For conciseness, only the results of eight test cases are presented here to help establish trends.

For all the cases, components of the moment of inertia of the central body are: yaw—$\tilde{J}_{01} = 0.1$; roll—$\tilde{J}_{02} = 0.5$; pitch— $\tilde{J}_{03} = 0.6$. The ratio of the appendage mass to that of the central body is taken as 1:50. The length ratio ($\epsilon_l = l/L$) is varied as 2:1, 3:1, and 5:1. In general, the duration of integration is 1/12 of an orbit; however, for the first four cases, the pitch response over the entire orbit was obtained. The analytical solutions are represented by lines, and the numerical results with dots. Except for Case 8, the two sets of results virtually coincided and hence the dots are not visible.

Case 1 may be taken as the reference. It represents slewing of the beam-type appendage, with a stiffness of 60 cycles/orbit, through 30° as the spacecraft traverses 10° of the circular orbit. All other initial disturbances are taken to be zero. The parameter affected by a change in a given case is indicated by an underline. Case 2 studies the effect of initial conditions, with all the other parameters held fixed at the values used in Case 1. Similarly, Case 3 assesses the influence of fast slew (6° per orbital degree), higher stiffness, and shorter appendage length; while Case 4 adds to this a pitch initial disturbance. Case 5 is similar to Case 2 except that the length ratio ϵ_l is larger. In Case 6, the initial orientation of the beam-type appendage

with respect to the central body is 60° instead of 0°. Case 7 shows that even if the slewing angle changes to 45°, i.e. the slewing rate increases to 4.5° per orbital degree, the correlation between the response results continues to be quite good. Perhaps a demanding situation would be represented by the faster slew of a beam with lower stiffness (compared to Case 4) in presence of a pitch disturbance. This is shown in Case 8. A small discrepancy in the pitch response appears which increases with time. However, the vibrational response of the appendage continues to be predicted accurately. Even in this extreme situation, the response results would be considered sufficiently accurate during the initial design stage.

Based on th response results, following general comments can be made:

- pitch motion has very little effect on the appendage vibration. On the other hand, the appendage vibration significantly modulates the pitch response at the appendage frequency.
- Both the magnitude of the slewing angle as well as the slewing velocity significantly affect the system response.
- As can be expected, longer and flexible appendage is more susceptible to vibration during a given slew maneuver.

Case 1 : $\epsilon_m = 0.02$; $\Delta\theta = 10°$; $\psi(0) = 0°$; $u(0) = 0.0$; $\epsilon_l = 3.0$;
$\Delta\alpha = 30°$; $\psi'(0) = 0.0$; $u'(0) = 0.0$; $r_v = 60$; $\alpha_0 = 0°$.

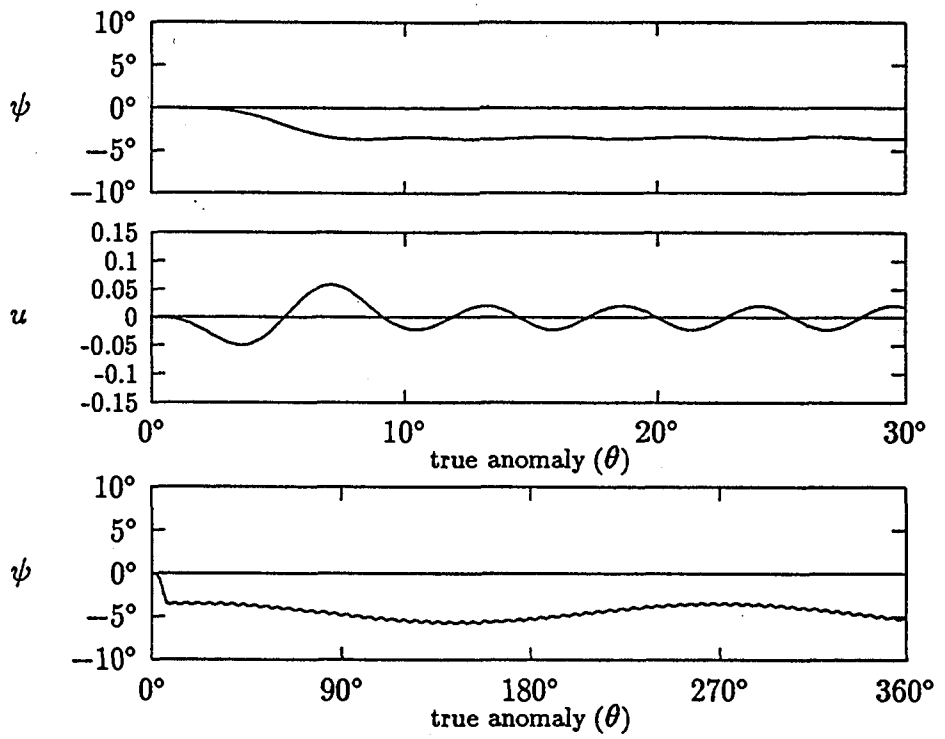

Figure 5-2 The pitch and vibrational response during the slew maneuver under the nominal conditions.

During slew:

$$\begin{aligned}
\psi = \; & (0.0297\theta + 0.0639)sin(1.4669\theta + 2.9826) - 0.0102sin(66.0212\theta - 0.0002) \\
& -0.1138sin(3.0006\theta) + 0.0175sin(3.0006\theta - 0.0823) \\
& +0.0109sin(36.0068\theta) + 0.0036sin(6.0011\theta - 0.0823) \\
& +0.0015sin(33.0062\theta) + 0.0015sin(39.0074\theta) - 0.0084 \\
u = \; & -0.0003(0.0297\theta + 0.0639)sin(1.4669\theta + 2.9826) + 0.0216sin(66.0212\theta - 0.0002) \\
& -0.0010sin(3.0006\theta) - 0.0002sin(3.0006\theta - 0.0823) \\
& -0.0424sin(36.0068\theta) - 0.0004sin(6.0011\theta - 0.0823) \\
& +0.0007sin(33.0062\theta) + 0.0022sin(39.0074\theta)
\end{aligned}$$

After slew:

$$\begin{aligned}
\psi = \; & -0.0798 + 0.0190sin(1.4431\theta + 1.0589) - 0.0021sin(66.0603\theta - 7.3535) \\
u = \; & -0.0005 + 0.0213sin(66.0603\theta - 7.3535)
\end{aligned}$$

Case 2 : $\epsilon_m = 0.02$; $\Delta\theta = 10°$; $\psi(0) = 5.7°$; $u(0) = 0.1$; $e_1 = 3.0$;
$\Delta\alpha = 30°$; $\psi'(0) = 0.0$; $u'(0) = 0.0$; $r_v = 60$; $\alpha_0 = 0°$.

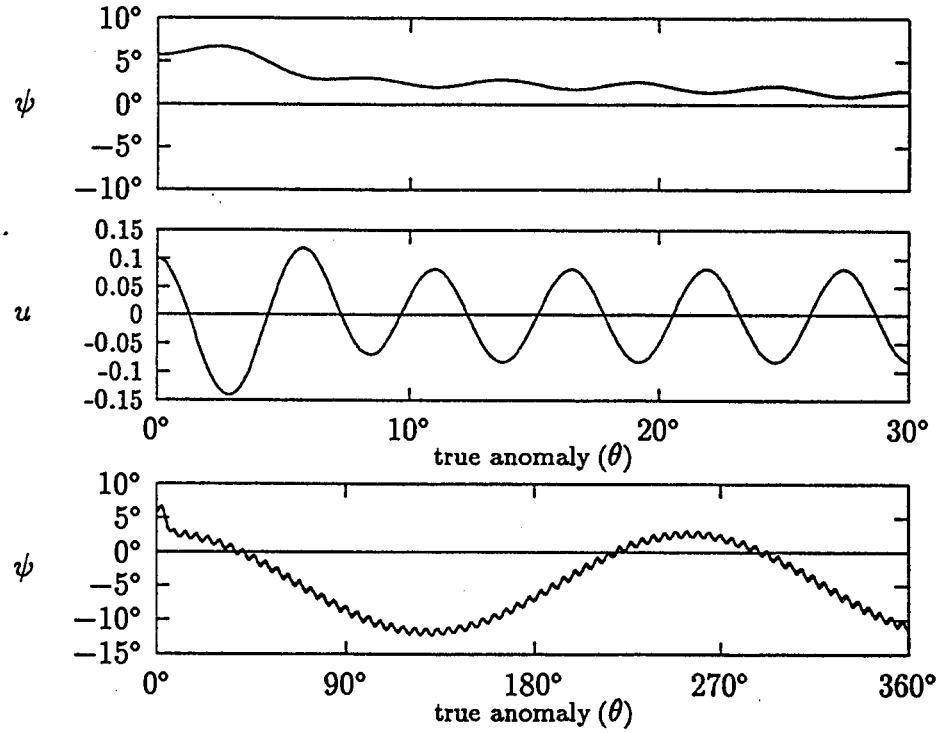

Figure 5-3 Effect of the initial pitch and the appendage disturbances on the system response as compared to Case 1.

During slew:

$$\begin{aligned}
\psi = \; & -0.0084 + (0.0037\theta + 0.1375)sin(1.5397\theta + 2.0548) \\
& -0.0995(0.0007\theta + 0.1023)sin(66.0254\theta + 1.3585) - 0.1138sin(3.0006\theta) \\
& +0.0109sin(36.0068\theta) + 0.0015sin(33.0062\theta) + 0.0015sin(39.0074\theta) \\
& +0.0175sin(3.0006\theta - 0.0823) + 0.0036sin(6.0011\theta - 0.0823) \\
u = \; & -0.0003(0.0037\theta + 0.1375)sin(1.5397\theta + 2.0548) \\
& +(0.0007\theta + 0.1023)sin(66.0254\theta + 1.3585) - 0.0010sin(3.0006\theta) \\
& -0.0424sin(36.0068\theta) + 0.0007sin(33.0062\theta) + 0.0022sin(39.0074\theta) \\
& -0.0002sin(3.0006\theta - 0.0823) - 0.0004sin(6.0011\theta - 0.0823)
\end{aligned}$$

After slew:

$$\psi = -0.0798 + 0.1257sin(1.4376\theta + 1.4557) - 0.0082sin(66.0604\theta - 11.1283)$$
$$u = -0.0005 + 0.0821sin(66.0604\theta - 11.1283)$$

Case 3 : $\epsilon_m = 0.02$; $\underline{\Delta\theta = 5°}$; $\psi(0) = 0°$; $u(0) = 0.0$; $\underline{\epsilon_l = 2.0}$;
$\Delta\alpha = 30°$; $\psi'(0) = 0.0$; $u'(0) = 0.0$; $\underline{r_v = 120}$; $\alpha_0 = 0°$.

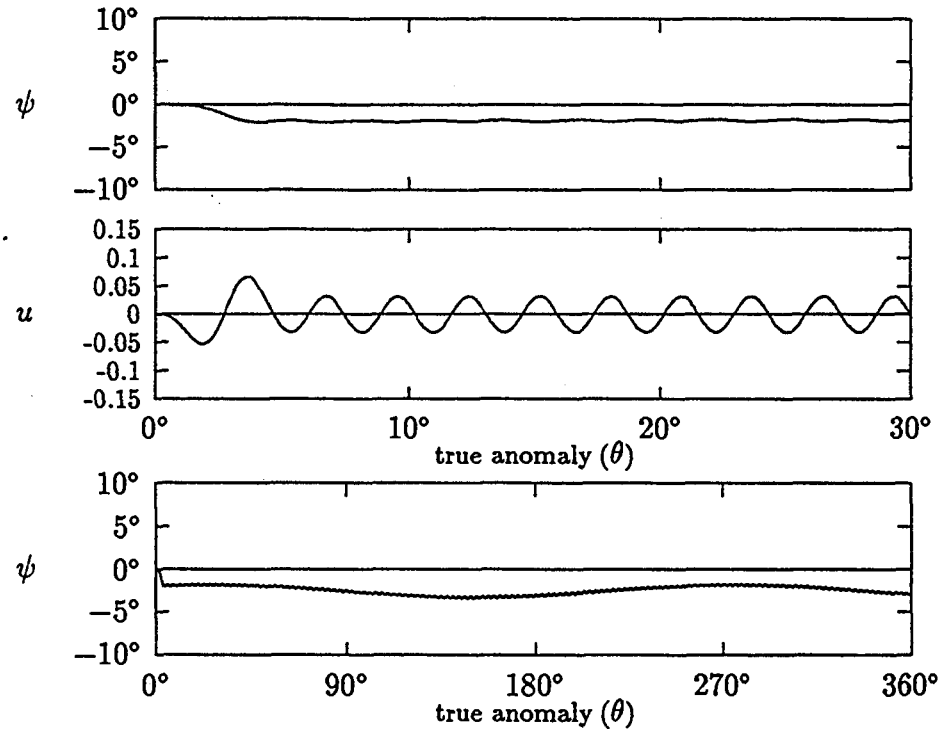

Figure 5-4 Influence of the faster slew of the appendage, with higher stiffness and shorter length, on the system response.

During slew:

$$\begin{aligned}
\psi = \; & -0.0029 + (0.0606\theta + 0.0595)sin(1.420\theta + 3.0898) \\
& -0.0551(-0.0001\theta + 0.0246)sin(127.7\theta) - 0.0558sin(5.998\theta) \\
& +0.0057sin(71.97\theta) + 0.0011sin(65.97\theta) + 0.0011sin(77.97\theta) \\
& +0.0025sin(5.998\theta - 0.0471) + 0.0004sin(12.00\theta - 0.0471) \\
u = \; & -0.0001(0.0606\theta + 0.0595)sin(1.420\theta + 3.0898) \\
& +(-0.0001\theta + 0.0246)sin(127.7\theta) - 0.0006sin(5.998\theta) \\
& -0.0461sin(71.97\theta) + 0.0007sin(65.97\theta) + 0.0018sin(77.97\theta) \\
& -0.0001sin(5.998\theta - 0.0471) - 0.0001sin(12.00\theta - 0.0471)
\end{aligned}$$

After slew:

$$\psi = -0.0453 + 0.0131sin(1.438\theta + 0.8995) - 0.0018sin(127.7\theta - 7.1555)$$
$$u = -0.0002 + 0.0320sin(127.7\theta - 7.1555)$$

Case 4 : $\epsilon_m = 0.02$; $\underline{\Delta\theta = 5°}$; $\underline{\psi(0) = 5.7°}$; $u(0) = 0.1$; $\underline{\epsilon_1 = 2.0}$;
$\Delta\alpha = 30°$; $\psi'(0) = 0.0$; $u'(0) = 0.0$; $\underline{r_v = 120}$; $\alpha_0 = 0°$.

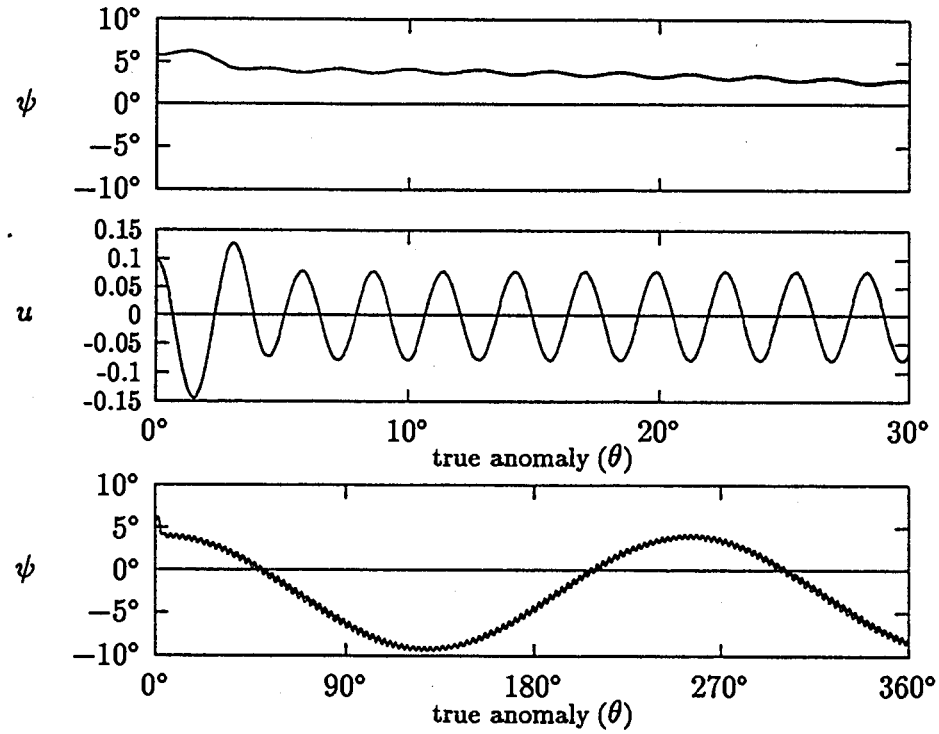

Figure 5-5 Effect of the initial pitch and the appendage disturbances on the system response as compared to Case 3.

During slew:

$$\begin{aligned}
\psi = \; & -0.0029 + (0.0151\theta + 0.1238)sin(1.687\theta + 2.0715) \\
& -0.0551(0.0004\theta + 0.1030)sin(127.7\theta + 1.3295) - 0.0558sin(5.998\theta) \\
& +0.0057sin(71.97\theta) + 0.0011sin(65.97\theta) + 0.0011sin(77.97\theta) \\
& +0.0025sin(5.998\theta - 0.0471) + 0.0004sin(12.00\theta - 0.0471) \\
u = \; & -0.0001(0.0151\theta + 0.1238)sin(1.687\theta + 2.0715) \\
& +(0.0004\theta + 0.1030)sin(127.7\theta + 1.3295) - 0.0006sin(5.998\theta) \\
& -0.0461sin(71.97\theta) + 0.0007sin(65.97\theta) + 0.0018sin(77.97\theta) \\
& -0.0001sin(5.998\theta - 0.0471) - 0.0001sin(12.00\theta - 0.0471)
\end{aligned}$$

After slew:

$$\psi = -0.0453 + 0.1157sin(1.4332\theta + 1.4599) - 0.0043sin(127.7\theta - 11.2645)$$
$$u = -0.0002 + 0.0783sin(127.7\theta - 11.2645)$$

Case 5 : $\epsilon_m = 0.02$; $\Delta\theta = 10°$; $\psi(0) = 5.7°$; $u(0) = 0.1$; $\epsilon_l = 5.0$;
$\Delta\alpha = 30°$; $\psi'(0) = 0.0$; $u'(0) = 0.0$; $r_v = 60$; $\alpha_0 = 0°$.

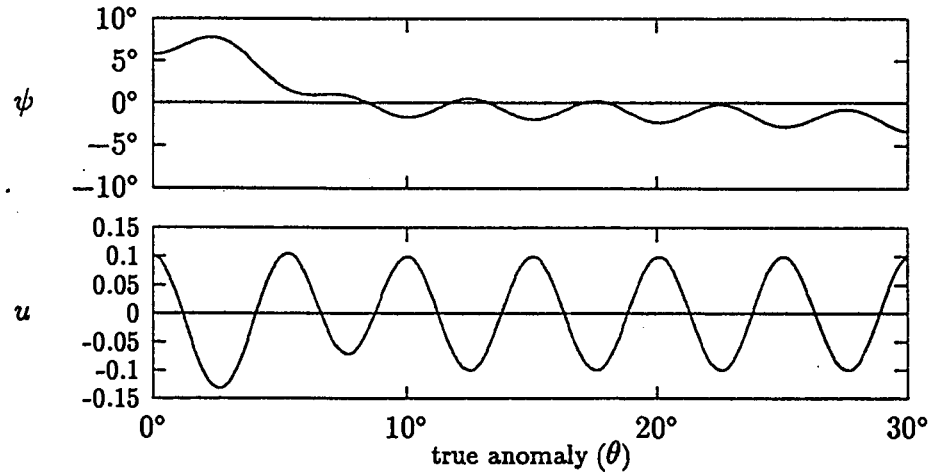

Figure 5-6 System response, during the nominal slew of the beam with its length much longer than that of the central body, in the presence of the initial pitch and appendage disturbances.

Case 6 : $\epsilon_m = 0.02$; $\Delta\theta = 10°$; $\psi(0) = 0°$; $u(0) = 0.1$; $\epsilon_l = 3.0$;
$\Delta\alpha = 30°$; $\psi'(0) = 0.0$; $u'(0) = 0.0$; $r_v = 60$; $\alpha_0 = 60°$.

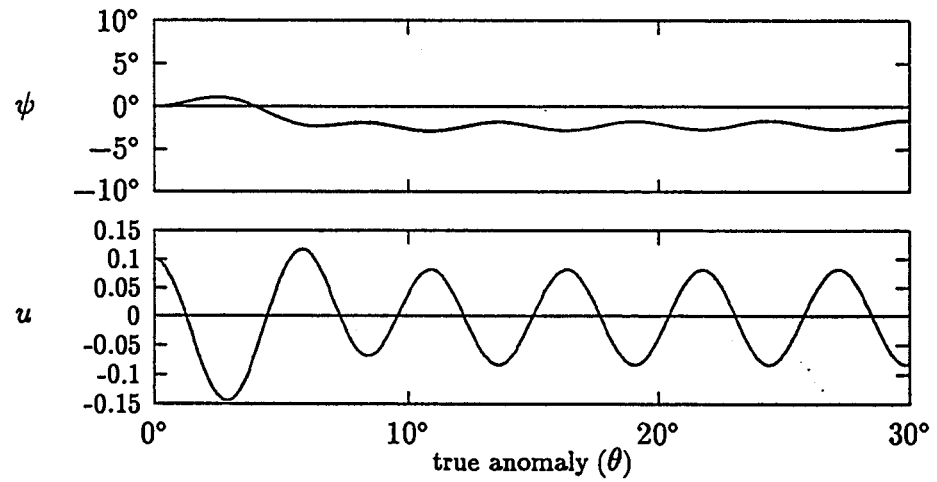

Figure 5-7 System response during the slew maneuver of the beam which initially has an 60° offset with respect to the central body.

Case 7 : $\epsilon_m = 0.02$; $\Delta\theta = 10°$; $\psi(0) = 5.7°$; $u(0) = 0.1$; $\epsilon_1 = 3.0$;
$\Delta\alpha = 45°$; $\psi'(0) = 0.0$; $u'(0) = 0.0$; $r_v = 60$; $\alpha_0 = 0°$.

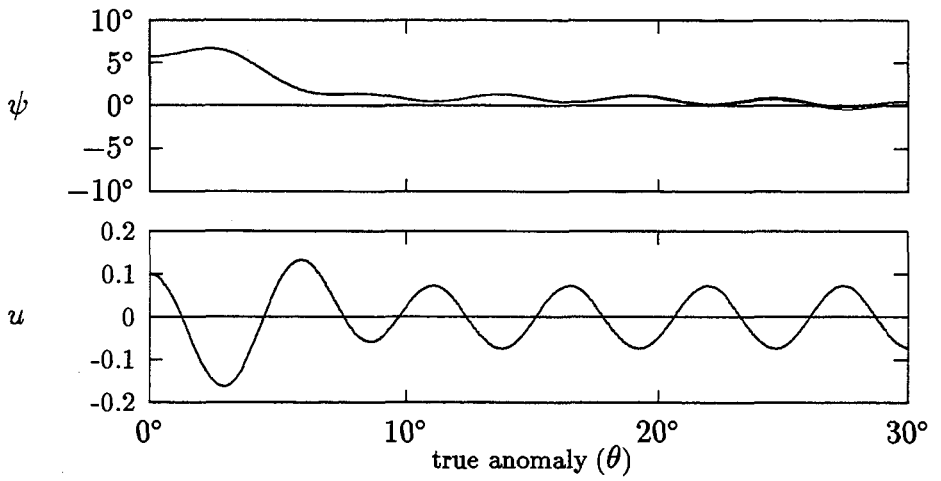

Figure 5-8 Effect of a larger slewing magnitude (45°) and higher slewing rate (4.5° per orbital degree) on the system response in the presence of a combined initial pitch and appendage disturbance.

Case 8 : $\epsilon_m = 0.02$; $\Delta\theta = 5°$; $\psi(0) = 5.7°$; $u(0) = 0.1$; $\epsilon_1 = 3.0$;
$\Delta\alpha = 30°$; $\psi'(0) = 0.0$; $u'(0) = 0.0$; $r_v = 60$; $\alpha_0 = 0°$.

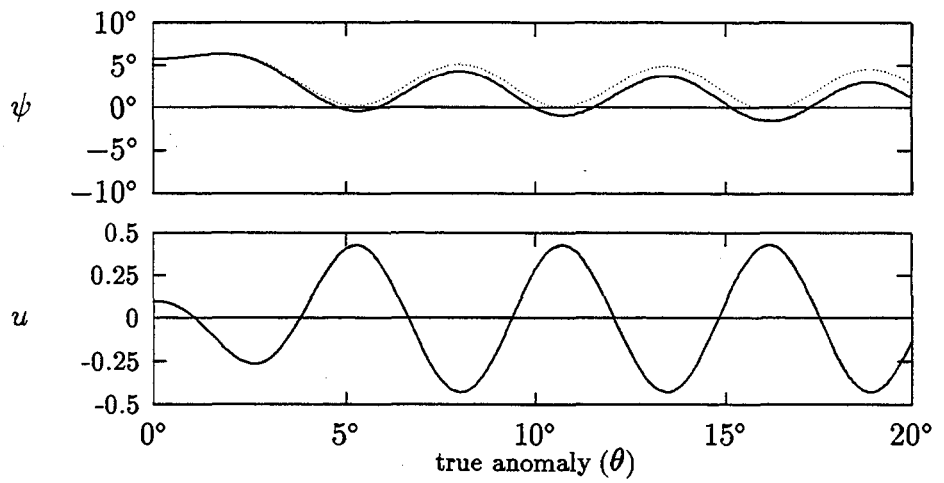

Figure 5-9 System response during the faster slew maneuver (6° per orbital degree) of the beam with a lower stiffness. Initially, the central body had a pitch disturbance and the appendage was deflected.

6. NUMERICAL IMPLEMENTATION

6.1 Computational Considerations

With the general formulation in hand, the next formidable task is the numerical integration of the governing equations of motion with acceptable accuracy as well as economy of time and effort. The computer code developed to integrate the nonlinear, nonautonomous and coupled equations of motion, is named DSDSA, standing for "Dynamics of Spacecraft with Deployable and Slewing Appendages". It was written in FORTRAN and calls NAG mathematical library subroutine D02BBF to solve the equations.

The set of equations to be integrated is of the form

$$\begin{bmatrix} & \\ U & O \\ & \\ & \\ O & M \\ & \end{bmatrix} \begin{bmatrix} y_1' \\ \vdots \\ y_r' \\ y_{r+1}' \\ \vdots \\ y_{r+r}' \end{bmatrix} = \begin{bmatrix} y_{r+1} \\ \vdots \\ y_{r+r} \\ G_1 \\ \vdots \\ G_r \end{bmatrix}, \tag{6.1}$$

where $y_1, y_2, ..., y_r$ are the dependent variables, and $y_{r+1}, y_{r+2}, ..., y_{r+r}$ represent their derivatives w.r.t. the true anomaly. M is the inertia matrix of the system and U the identity matrix.

Figure 6-1 is the computational flow chart. The program MAIN is the core routine which receives initial conditions from the subroutine INCD, calls D02BBF to integrate equations determined by FCN, and then sends the output data to the subroutine OUT for print. The subroutine FCN calculates derivatives of the variables. It uses the inverse of M prepared by the subroutine INVER, and G_i $(i = 1, 2, \ldots, r)$ obtained by the subroutines LIBRA, ELAVIB, as well as ROTAT, if there exist rotational degrees of freedom for the appendages.

The subroutines INLIB, INANMO and INRELA evaluate the inertia matrices J, $M12$, $M13$, $M14$, $M22$, $M23$, $M24$, $M33$, $M34$, $M44$ and their first derivatives. PARU and PARA give the partial derivatives with respect to the variables of the

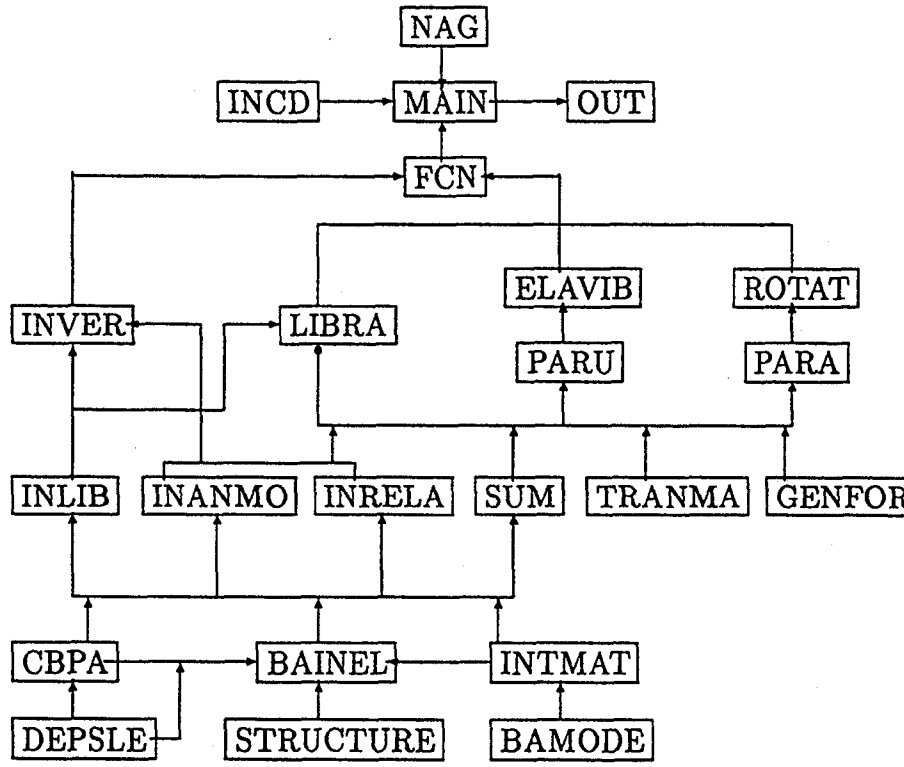

Figure 6-1 Flow chart for the program DSDSA

elastic vibration and appendage rotation (if they are free), respectively. TRANMA calculates the elements of the transformation matrix of libration, A and B_0. CBPA evaluates elements of the transformation matrix of appendage rotation, C and B, as well as their partial derivatives with respect to the rotation angles. BAMODE is a block data providing integrals of the modal functions for INTMAT; and the latter evaluates all the matrices associated with the appendage deformations. BAINEL provides the basic inertia elements, such as H, J_i, D, S, etc.

Among the family of subroutines mentioned, INCD, GENFOR, DEPSLE and STRUCTURE are developed by the user. INCD determines the initial conditions, while GENFOR gives the generalized forces, such as the free molecular reactions, solar radiation pressure, earth's magnetic field, etc. Control forces can be included in the GENFOR too. DEPSLE specifies slew maneuver and deployment or retrieval of appendages. STRUCTURE is the main input subroutine describing the configuration of the spacecraft, including masses, inertia moments, size, location and orientation of the appendages, as well as their shape and rigidity.

The computer code is relatively easy to use. The computational time involved in assessing system dynamics depends on the complexity of the problem, the precision requirement and the length of the integration period. In particular, the degree of flexibility of the appendages affects the computing time significantly.

6.2 Validity of the Program

As discussed in Chapter 3, to help assess validity of the formulation, two test configurations were analyzed. However, a question remains concerning correctness and accuracy of the computer code. One indication of its proper functioning was already obtained in Chapter 5, where the approximate analytical solution agreed quite well with the 'exact' numerical results over a range of system parameters and initial conditions. To gain further confidence in the overall functioning of the formulation and the computer code, dynamics of a different particular configuration was studied, and the results compared with those obtained by other researchers [47].

Modi and Ng [47] studied dynamics of a satellite with two beam-type appendages, nominally aligned with the local vertical. Typical response of the system, when subjected to a rather severe disturbance corresponding to the appendage excitation in the first mode of $u'_{11}(0) = 0.5$ and $u_{12}(0) = 0.025$, as obtained by them is presented in Figure 6-2. For the same system, subjected to the identical disturbance, the response results obtained by the present computer code DSDSA are shown in Figure 6-3. Note, the two sets of results are identical.

6.3 The Space Flyer Unit

With the validity of the formulation and the computer code reasonably well ascertained, the next logical step would be to demonstrate its versatility through application to several diverse configurations.

The first example pertains to the Japanese satellite called the Space Flyer Unit (SFU). It is an unmaned, reusable and free flying platform for multipurpose use, and is developed by a consortium of Japanese government agencies including the Institute of Space and Astronautical Science, the National Space Development Agency, and the Ministry of International Trade and Industry. SFU is scheduled to be launched in February, 1994.

initial condition

$$u'_{11}(0) = 0.5$$

$$u_{12}(0) = 0.025.$$

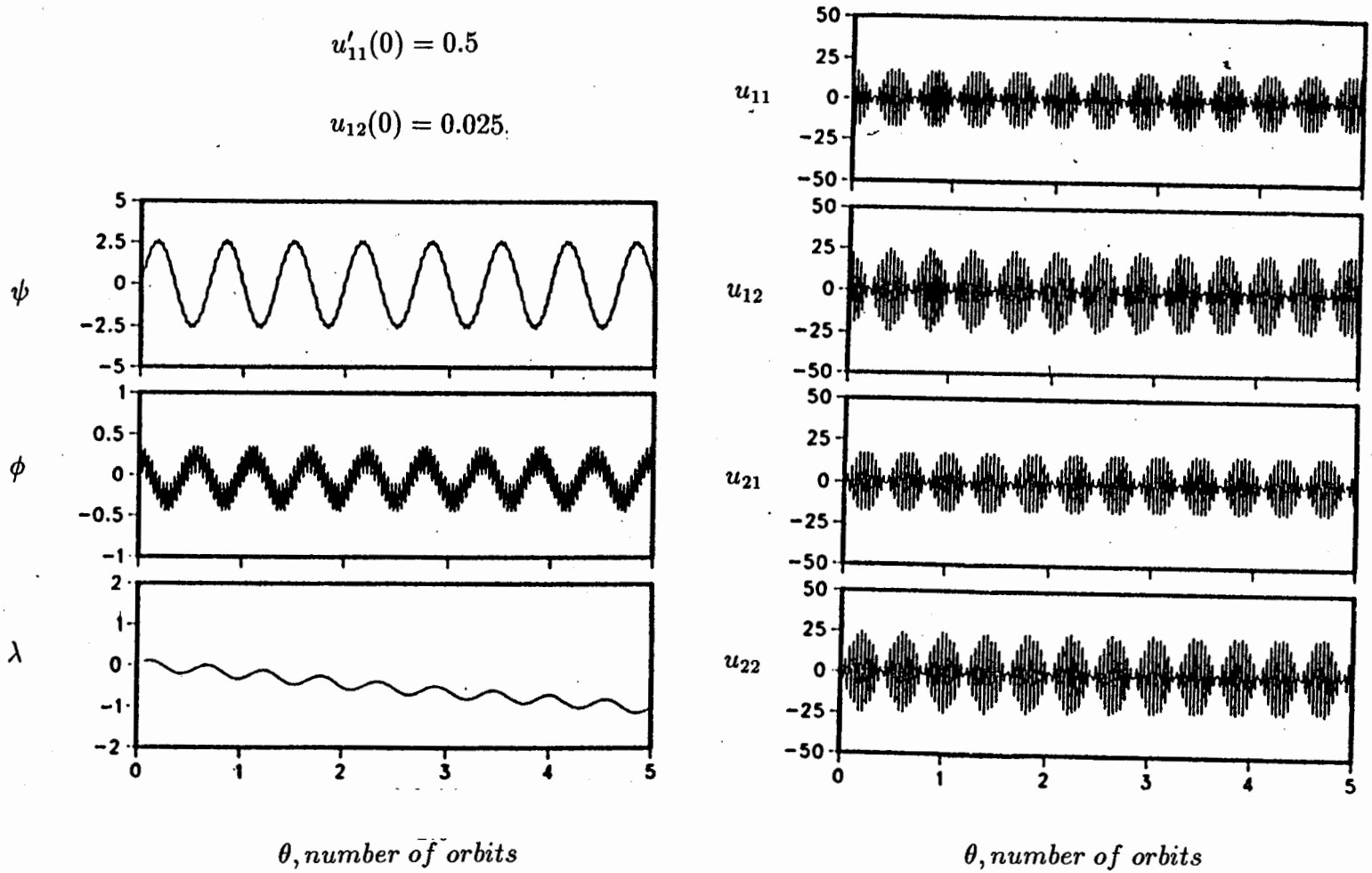

Figure 6-2 Dynamical response of a satellite with two beam-type appendages as reported by Modi and Ng [47].

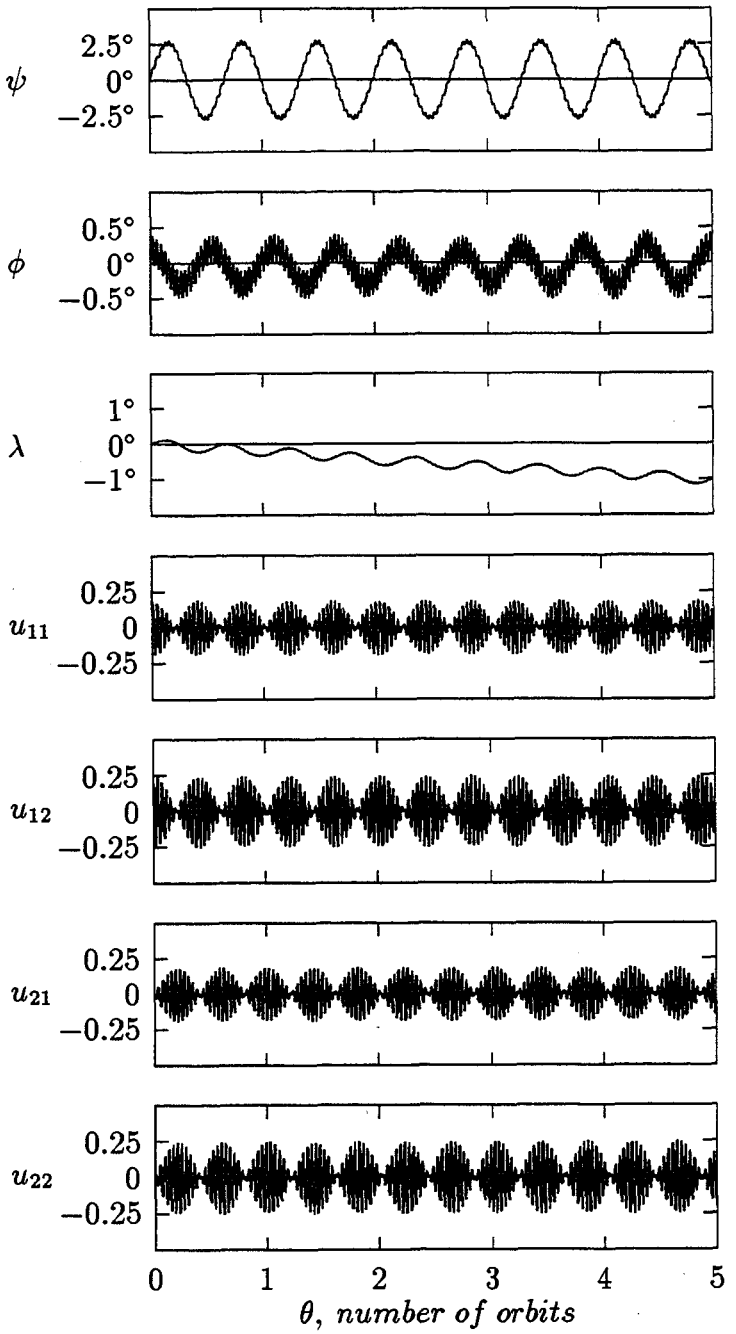

Figure 6-3 Dynamical response obtained by DSDSA for the configuration studied by Modi and Ng [47]. A comparison with their results given in Figure 6-2 showed them to be identical.

Configuration of the SFU is shown in Figure 6-4. It consists of an octagonal shaped central body which includes eight modules of scientific experiments. Two deployable solar array paddles (SAP), each $9.7m \times 2.4m$, are deployed at either end of the central body. The SAPs, besides generating power, are used for the High Voltage Solar Array (HVSA) experiment. The objectives of the experiment are to determine:

- dynamical characteristics of the unit during deployment and retrieval of the flexible SAPs;
- the upper limit of the voltage generated which would be free from surface breakdown, power drain through space plasma, and enhancement of the aerodynamic drag.

The relevant parameters used in this investigation are listed below:
Orbital motion:

$$\begin{aligned} orbit\ eccentricity(\epsilon) &= 0\ ; \\ altitude &= 300\ km\ ; \\ period &= 90\ min. \end{aligned}$$

Central body:

$$\begin{aligned} mass(m_0) &= 4000\ kg\ ; \\ J_{01} &= 4250\ kg \cdot m^2\ ; \\ J_{02} &= 9290\ kg \cdot m^2\ ; \\ J_{03} &= 11150\ kg \cdot m^2\ ; \\ length &= 5\ m\ . \end{aligned}$$

Solar array paddles:

$$\begin{aligned} mass(m_1\ or\ m_2) &= 60\ kg\ ; \\ length &= 10\ m\ (fully\ deployed)\ ; \\ width &= 2.4\ m\ ; \\ bending\ rigidity\ (EI) &= 6572\ kg \cdot m^3/s^2\ . \end{aligned}$$

Since the rigidity of the paddles is relatively large, only one bending mode is taken to represent their deformation. The corresponding generalized coordinates are

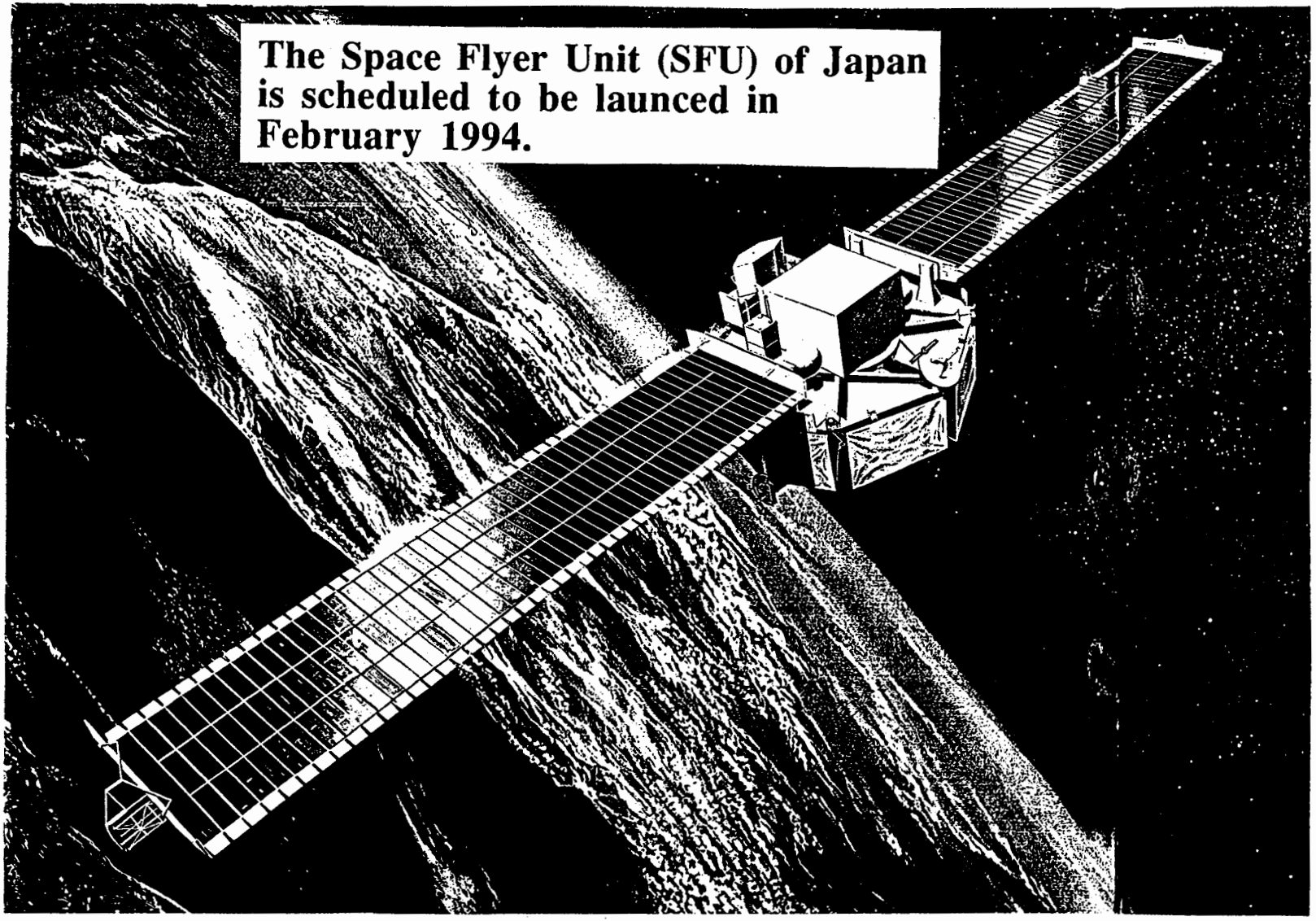

Figure 6-4 A schematic diagram of the Space Flyer Unit. The solar array extends to 24.42 m tip-to-tip with a width of 2.4 m.

(Provided by the Department of Mechanical Engineering, University of British Columbia)

u_1 (lower paddle) and u_2 (upper paddle), respectively, representing half of the tip deflections (in meter, for all the figures in this section).

Three different orientations associated with the SAP's deployment and retrieval are indicated in Figure 6-5:

(a) In the orientation B, the SAPs are deployed in 15 minutes.

(b) The SFU then undergoes a 90° roll to the orientation C.

(c) At the end of the mission, the SAPs are retrieved in 15 minutes in the same orientation as in (b).

Note, the deployment can also be carried out in the orientation indicated in 'A'. Actually, orientation A is the only stable equilibrium for the SFU. The orientation B is unstable in the yaw degree of freedom and the orientation C is unstable in all the three librational degrees of freedom. In order to get more useful results, the orientation B is purposely modified so that the major axis (with an inertia moment of 11150 $kg \cdot m^2$) of the central body is normal to the orbital plane and the minor axis (inertia moment 4250 $kg \cdot m^2$) along the local vertical giving a stable equilibrium.

In fact, the orientation A has some obvious advantages:

- The possible elastic vibrations are perpendicular to the orbital plane, hence the inplane deployment won't excite the out-of-plane motion.
- The inertia moment about the pitch axis is larger in the orientation A than that in the orientation B, hence the excited pitch motion will be smaller. Of course the effect will be more pronounced when the solar paddle is wider.

6.3.1 Solar paddle deployment or retrieval

Influence of the appendage deployment or retrieval is studied first. Both the solar array paddles are deployed in 15 minutes as in the actual situation, at a constant rate and extending from 1 m to $10m$. Effect of rapid deployment in 2.5 minutes, or some times in 7.5 minutes, is also assessed. In fact, the parametric study covers a wide range. In the following figures, λ, ϕ and ψ represent yaw, roll and pitch, respectively.

Orientation A

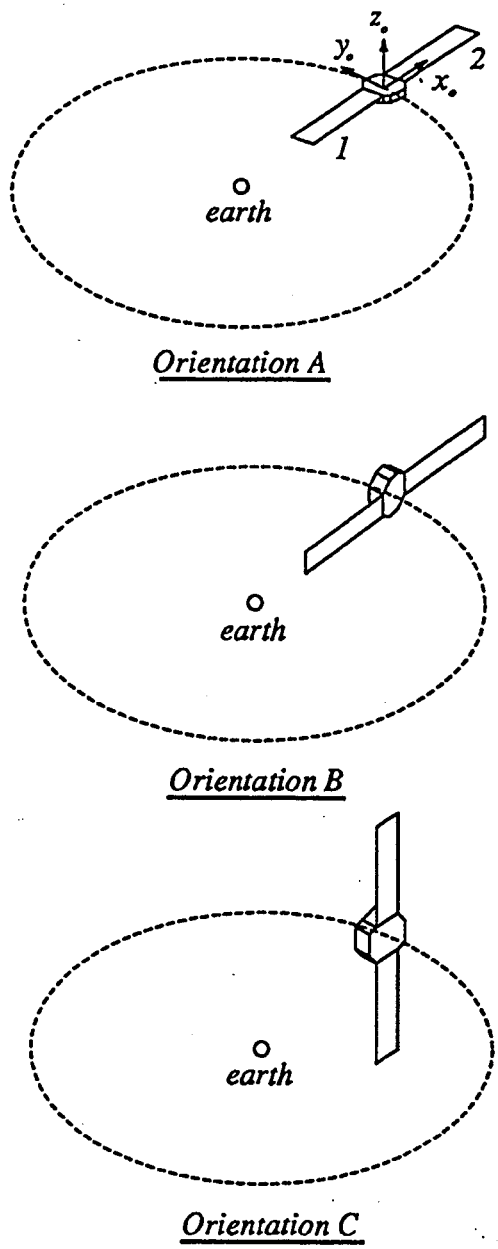

Figure 6-5 Three orientations of the Space Flyer Unit (SFU) during possible deployment and retrieval of the solar paddles.

Figures 6-6 to 6-8 pertain to the dynamical response of the SFU in the configuration A. Essentially they assess the behavior of the SFU during the solar paddle deployment. Figure 6-6 studies the effect of the solar paddle deployment rate. Several characteristic features of the response should be noticed:

- During deployment in the orbital plane, the out-of-plane degrees of freedom (roll, yaw, and appendage vibration) remain unexcited.
- The basic character of the response remains essentially the same at the higher deployment velocity except for an increase in the magnitude of the pitch motion.

Figure 6-7 shows the system behavior during the failure of one of the SAPs to deploy, i.e. only one of the solar paddles is extended in 15 minutes. Fortunately, as before in Figure 6-6*a*, only the pitch motion is excited. However, the Coriolis force induced pitch moment being small, the resulting ψ response has a smaller magnitude.

Figure 6-8 studies response of the SFU, during deployment of the paddles in 15 minutes in the presence of a roll disturbance. Note, now both the inplane and out-of-plane motions are excited. With the initial disturbance in roll of 1°, the yaw excited through coupling reaches a magnitude of around 2.5° in that many orbits. In fact, the system becomes unstable in yaw with a larger disturbance in roll (Figure 6-8*c*). The vibrational motion of the appendages, though present, was found to be quite small, and hence purposely not shown.

Orientation B

Figure 6–9 through 6–11 explore response of the SFU in the Orientation B during deployment of the solar paddles. Note, deployment is still along the local vertical, however, the two solar array paddles of SFU have now undergone a 90° yaw from their Orientation A. This results in two major changes: (a) pitch inertia reduces leading to a higher pitch response corresponding to that in the Orientation A; (b) stiffness of the solar paddles in the local horizontal direction is lower compared to that in the previous case making them susceptible to vibration, though it still remains quite small. It is of interest to recognize that during the deployment, the appendage deflect in one direction under the action of the Coriolis force. At the termination of the deployment, the deformed state acts as an initial condition for the subsequent periodic motion of the appendage. The general trends of the response in Figures 6–9 and 6–10 are similar to those for the Orientation A.

A word concerning the postdeployment beat-type response of the appendages would be appropriate. This is attributed to a slight difference in the stiffness of the solar paddles due to a difference in their position in the gravitational field, and coupling through the central body.

Figure 6-11 shows the SFU response, in the Orientation B, during a 15 minute retrieval maneuver. Note, a relatively large pitch motion is excited rather quickly. This is understandable as the angular momentum must be conserved.

Orientation C

Figure 6-12 corresponds to the SFU response in the Orientation C during retrieval of the appendages. Note, the orientation represents equilibrium, however, it is unstable. Yet the system remains unexcited during the retrieval maneuver if there is no other disturbance (Figure 6-12a). However, with a yaw disturbance of 3°, large librational motions set in, particularly in the roll and yaw degrees of freedom, which eventually drive the system unstable (Figure 6-12b). Note, the solar paddles remain unexcited by the librational instability, due to the difference in the characteristic frequencies.

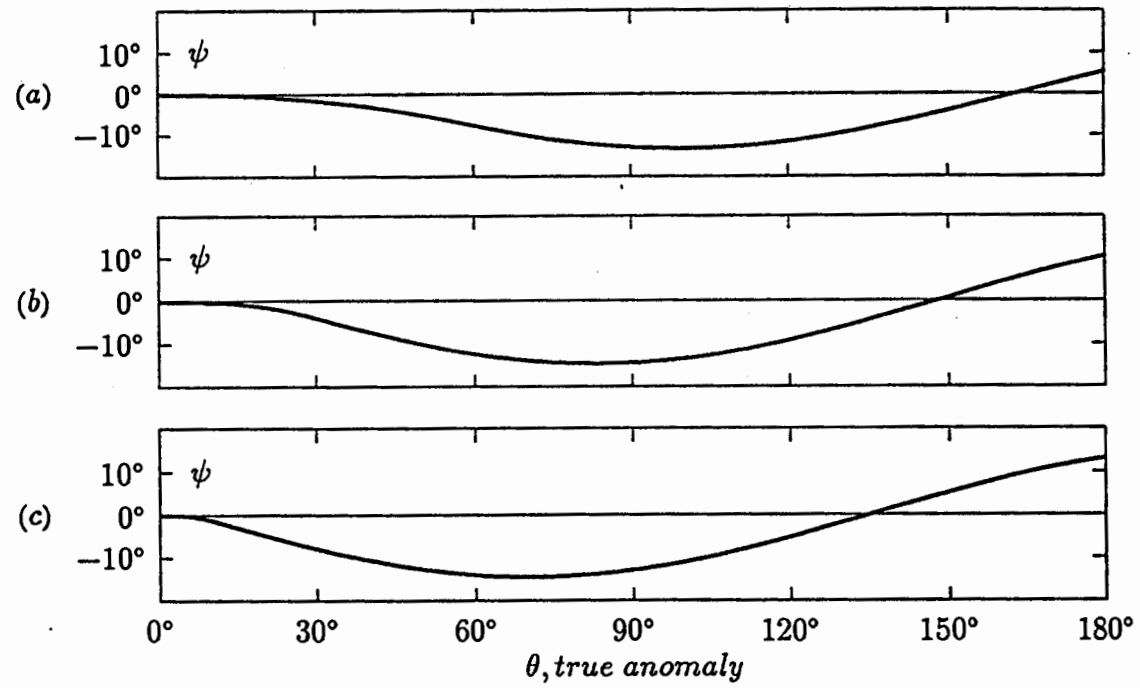

Figure 6-6 Effect of the deployment rate on the librational response of the SFU. SAP's deploy in: (*a*) 15 minutes; (*b*) 7.5 minutes; (*c*) 2.5 minutes.

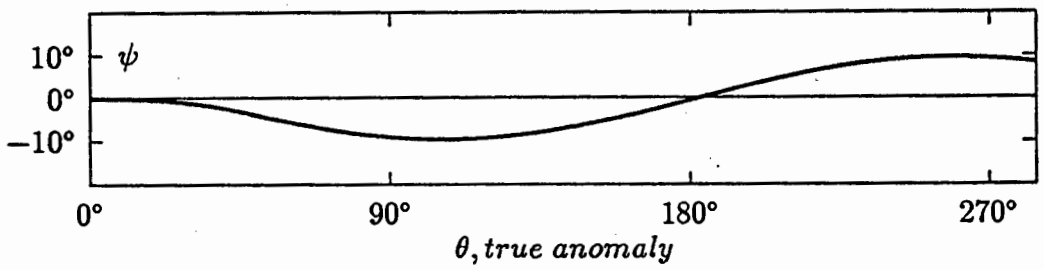

Figure 6-7 Response of the SFU when only the upper SAP deploys in 15 minutes in the Orientation A.

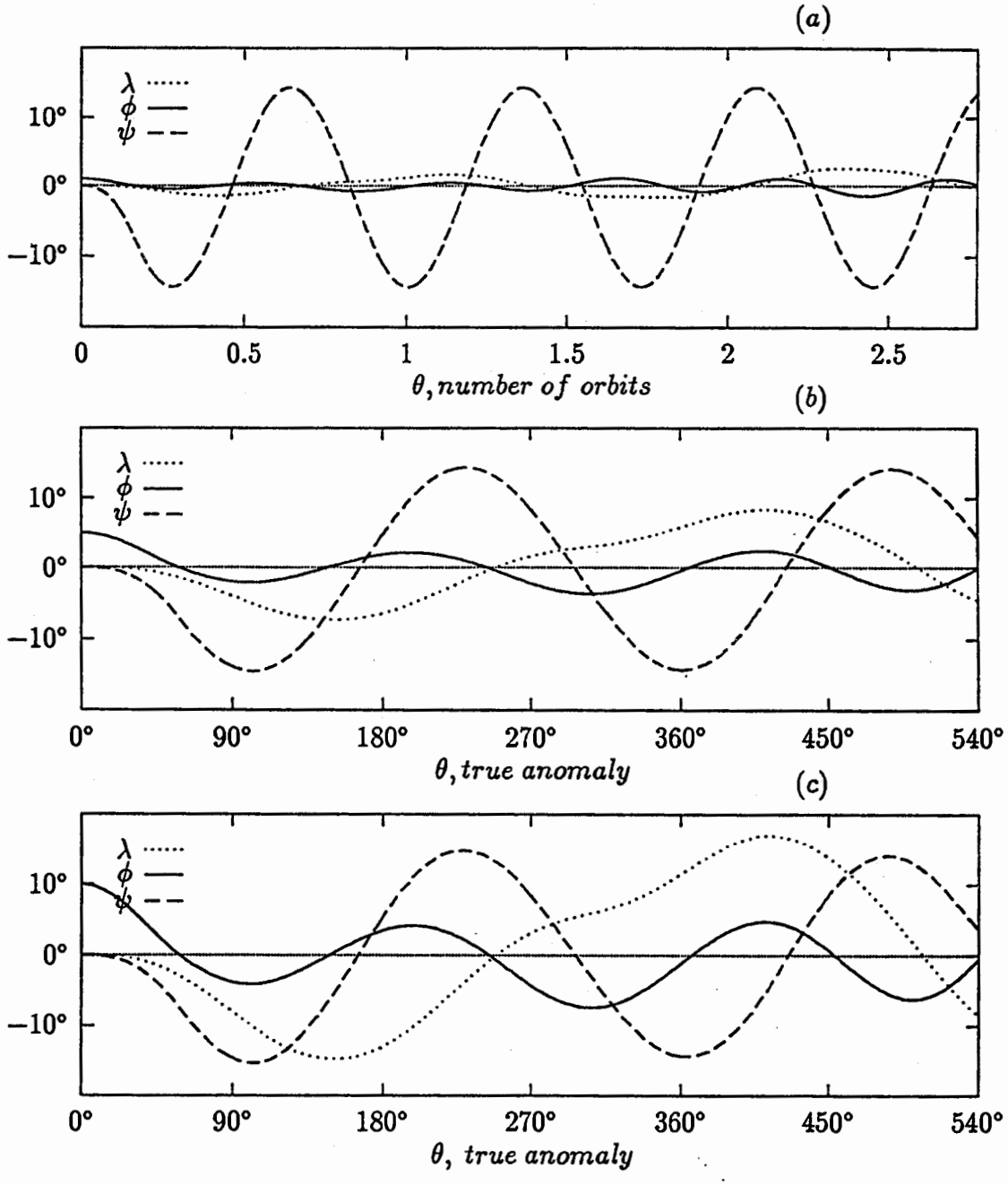

Figure 6-8 Librational response of the SFU with deploying solar paddles in the presence of a roll disturbance: (*a*) $\phi_0 = 1°$; (*b*) $\phi_0 = 5°$; (*c*) $\phi_0 = 10°$. Note, yaw becomes quite large through its coupling with roll when the initial roll disturbance is relatively large.

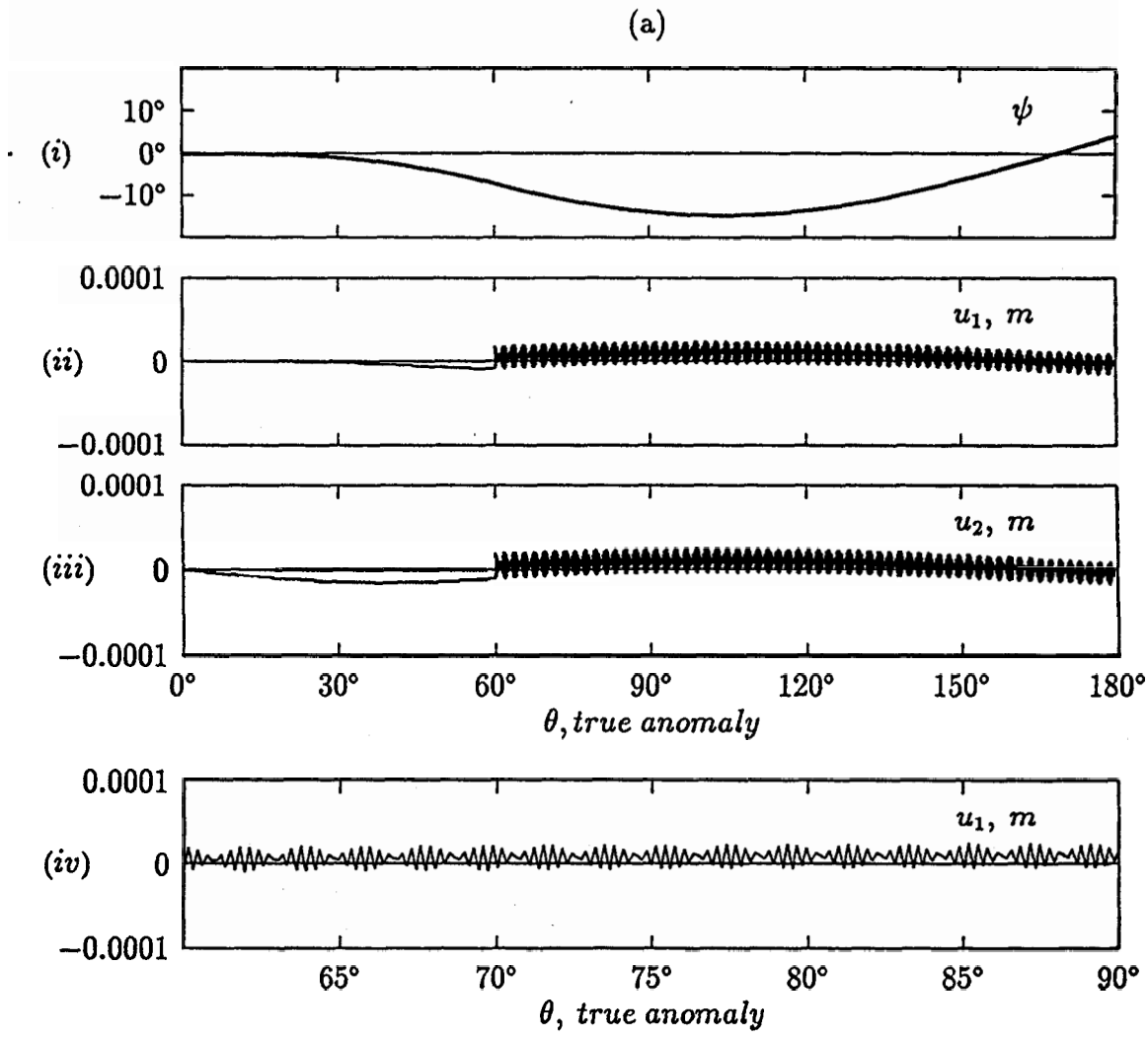

Figure 6-9 Response plots for the SFU in the Orientation B, showing the effect of velocity during the simultaneous deployment of the two solar paddles. The time of deployment is: (a) 15 minutes. Note the bottom diagram magnifies the vibrational response u_1 in (ii).

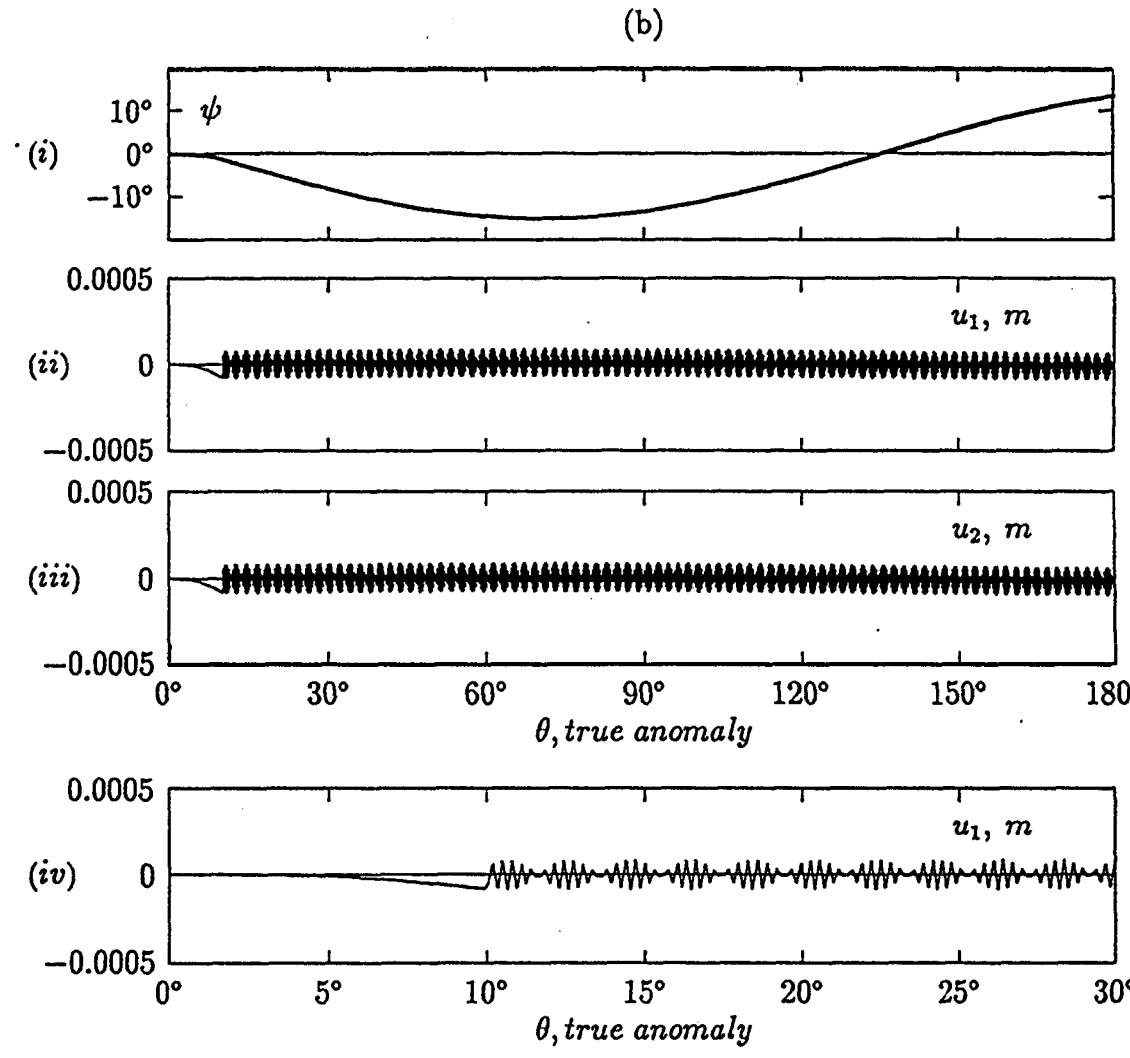

Figure 6-9 Response plots for the SFU in the Orientation B, showing the effect of velocity during the simultaneous deployment of the two solar paddles. The time of deployment is: (b) 2.5 minutes. Figure (*iv*) magnifies the u_1 response in (*ii*).

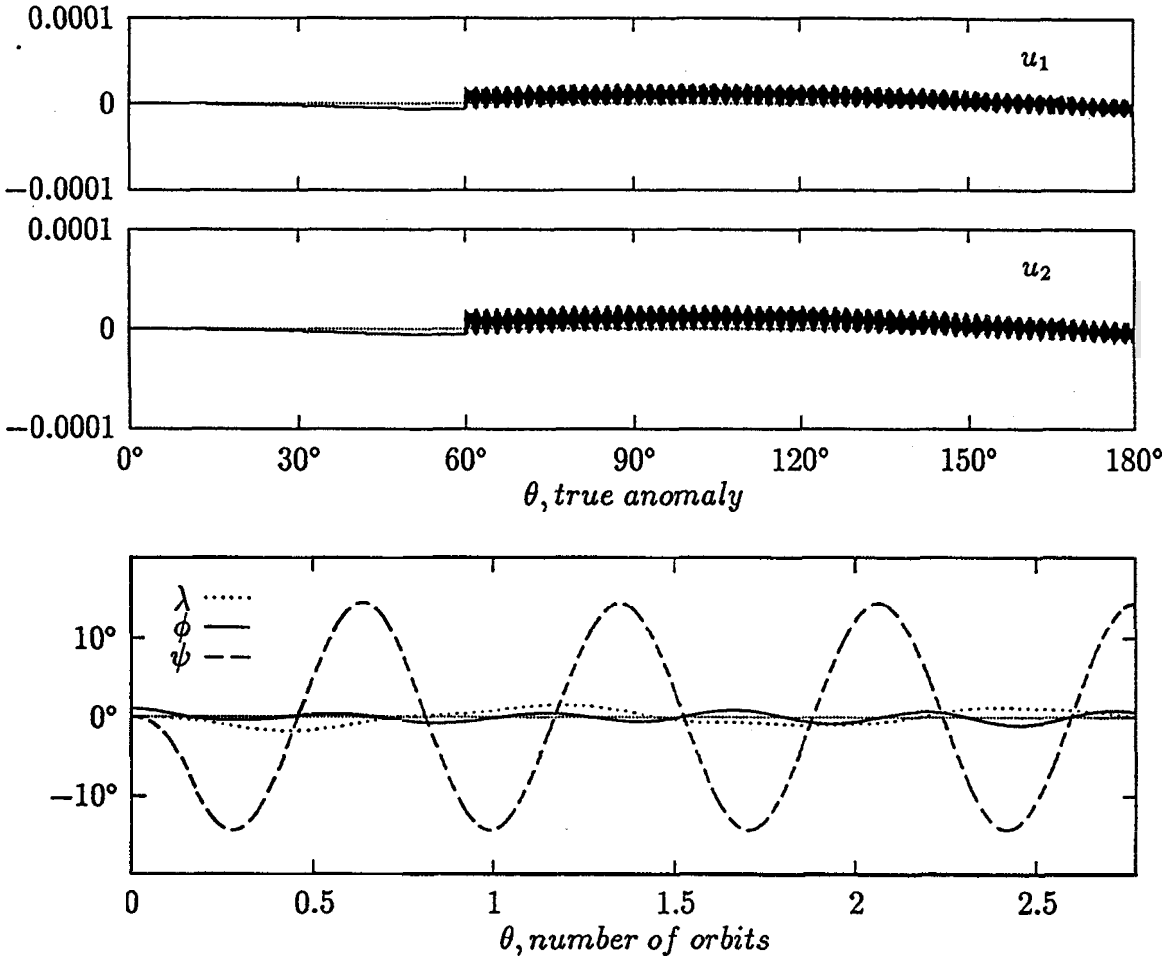

Figure 6-10 Effect of initial roll disturbance $\phi(0) = 1°$ on the response of the SFU during a 15 minute deployment maneuver of the solar paddles.

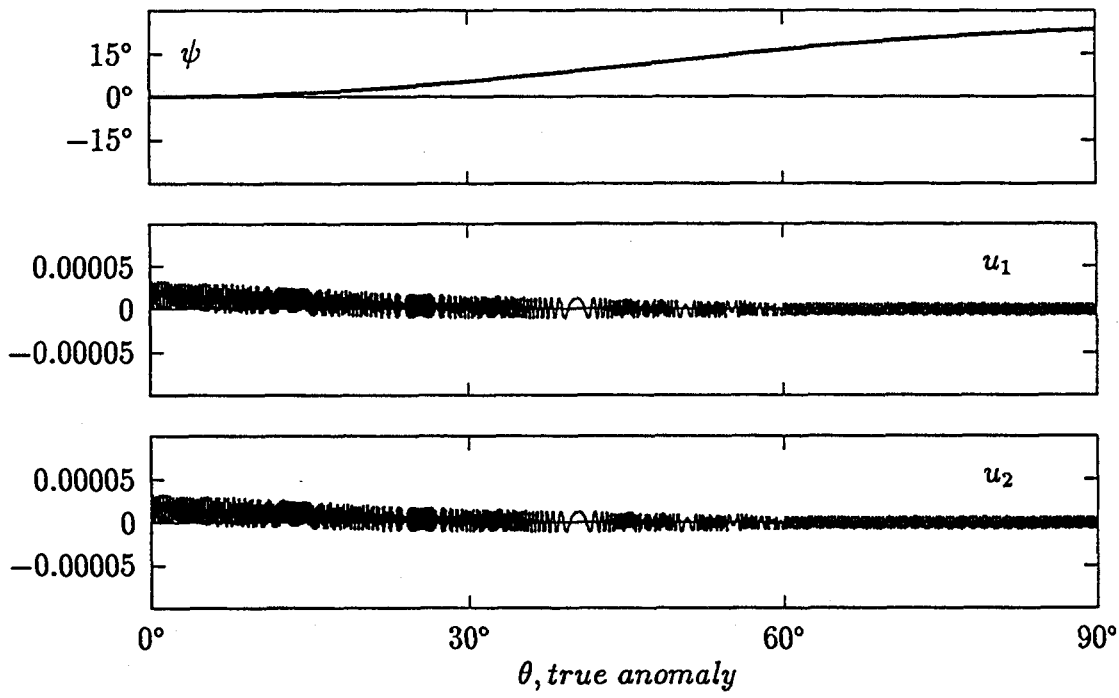

Figure 6-11 Response of the SFU in the Orientation B during retrieval of the SAPs in 15 minutes.

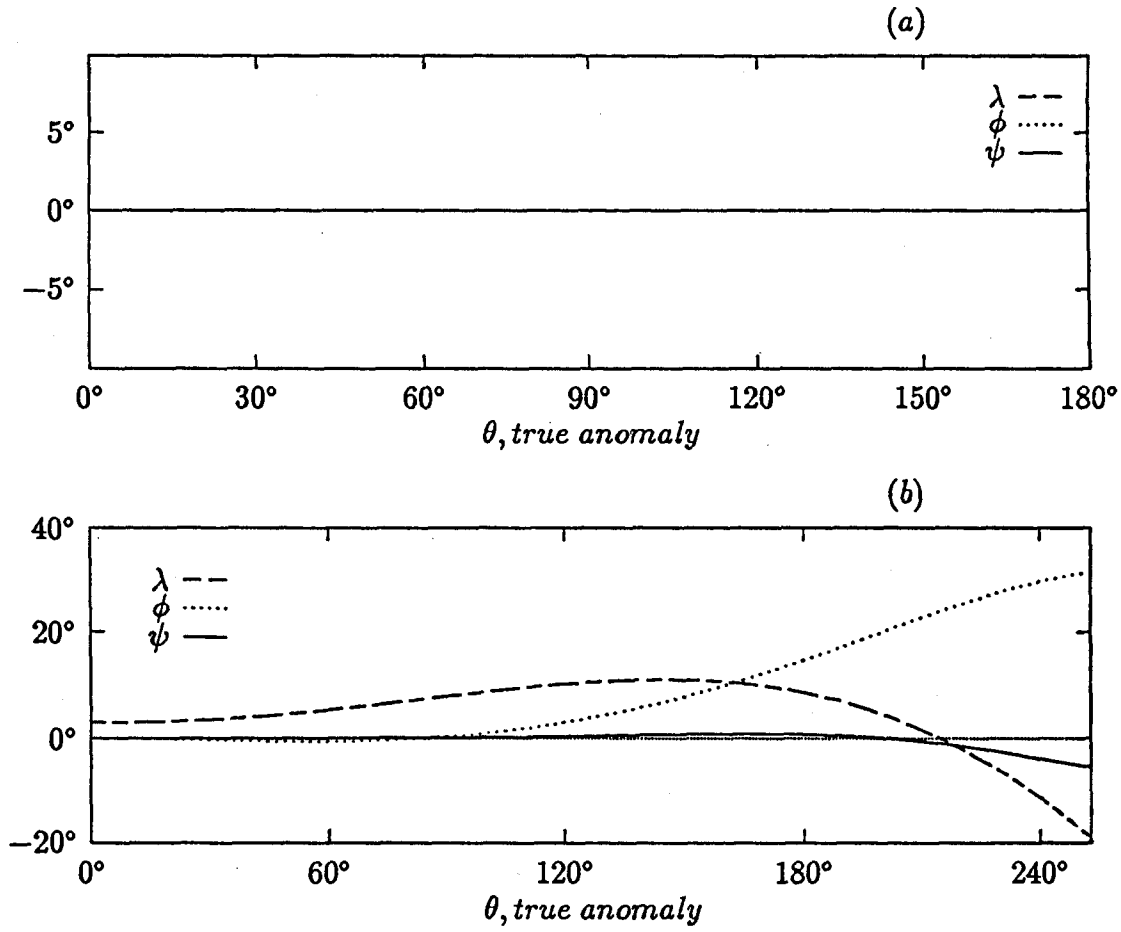

Figure 6-12 Response of the SFU in the Orientation C during the retrieval of SAPs in 12 minutes: (a) the SFU remains unexcited when there is no other disturbance; (b) the SFU reveals the unstable character of the equilibrium Orientation C under an initial yaw disturbance of 3°. Note, vibratory motion of the SAPs is not excited in both the cases.

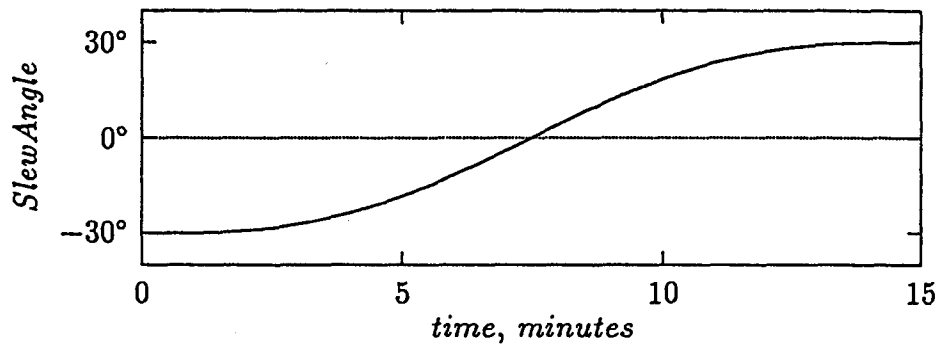

Figure 6-13 Time history of the nominal slew maneuver.

6.3.2 Slew maneuvers of the solar paddles

Next, the influence of slew maneuvers of the solar paddles is investigated. Two different slewing situations are considered: the two paddles slew together at the same time, and slew maneuver of the lower paddle alone. In each case, a typical maneuver takes place about the pin joint at the central body. Thus in the Orientation A, the slew maneuvers are perpendicular to the orbital plane and towards the positive z_o-directions. In the Orientation B, they are in the orbital plane and the two paddles slew in opposite directions (Figure 6-14). Usually, the slewing magnitude is either from $-30°$ to $+30°$ passing through the nominal equilibrium Orientation A or B, or a $+60°$ slew from the nominal Orientation B, both maneuvers completed in 15 minutes. Note, in the $-30°$ to $+30°$ slew case, neither the initial nor the post-slew orientation represents an equilibrium state. Figure 6-13 shows typical time history of the slewing maneuver. The maneuver profile is sinusoidal to avoid disturbances during initial and terminal phases of the maneuver, i.e. velocity and acceleration are zero at the beginning and end of the slew.

Orientation A

Figure 6-15 through 6-18 study behavior of the SFU, in the Orientation A, during the slewing maneuvers described earlier. Effects of faster than nominal rate of maneuver (15 minutes) as well as failure of one of the appendages to slew are also considered. At the outset it is apparent that the predominant response is in the pitch degree of freedom with roll and yaw excited, relatively, by a small amount (Figure 6-15). Vibratory response of the appendages is also quite small.

The effect of a faster slew (Figure 6-16) is somewhat surprising, particularly with reference to the pitch response which is significantly lower than that in the previous

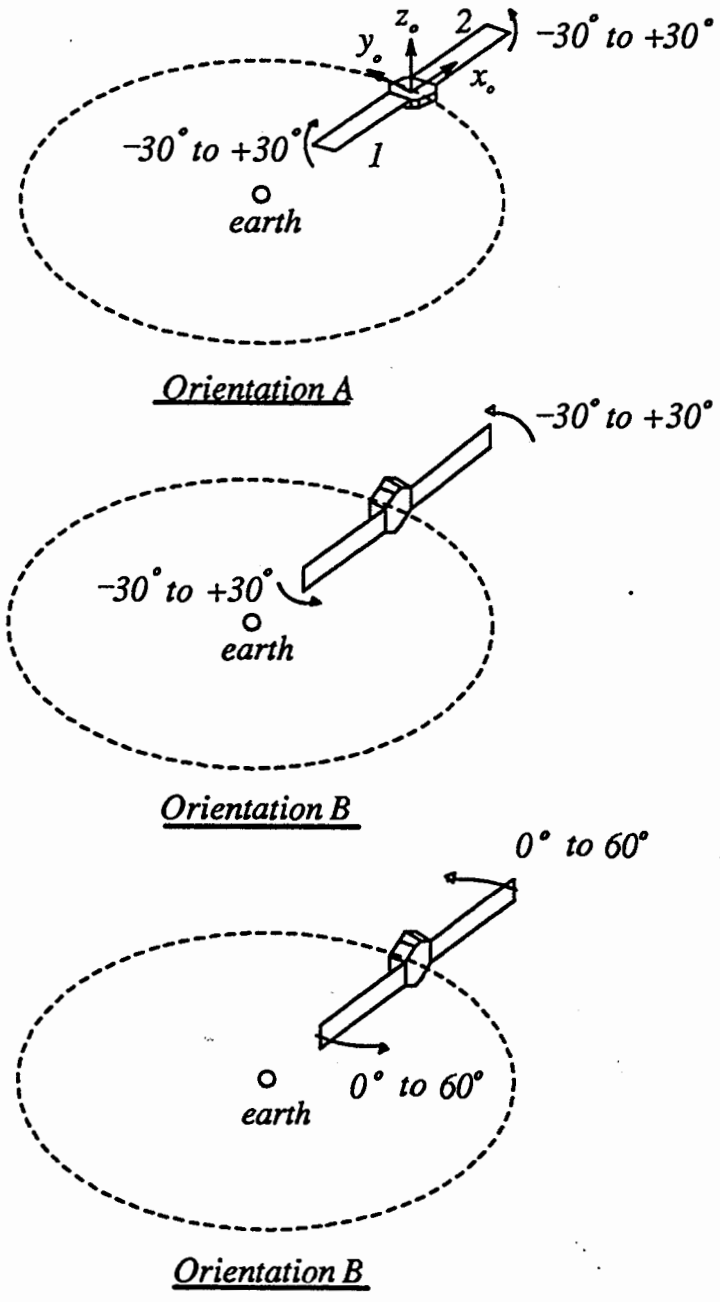

Figure 6-14 Schematic diagrams showing nominal slew maneuvers with the SFU in the Orientations A and B.

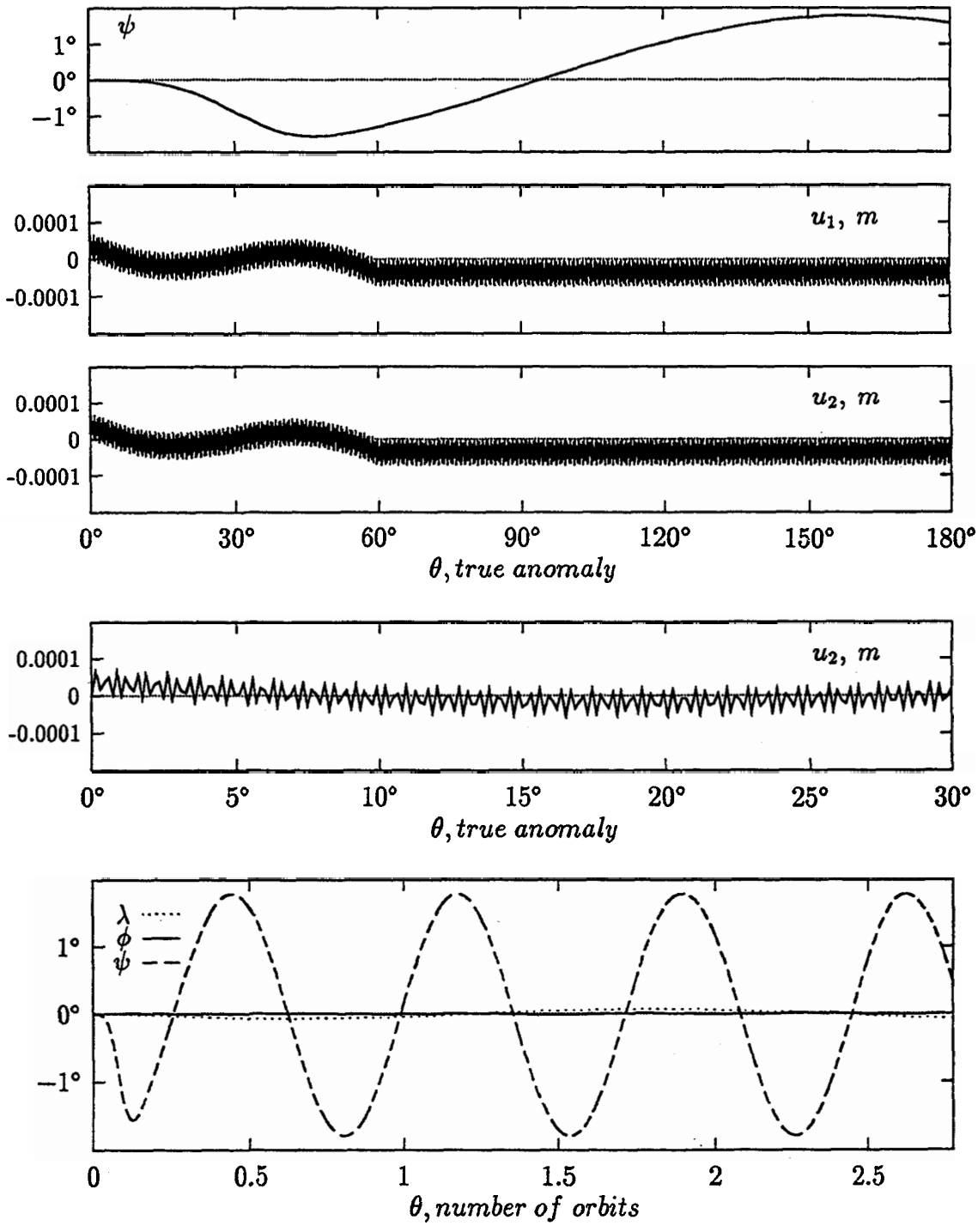

Figure 6-15 Response of the SFU, in the Orientation A, to the nominal slew maneuver of 60° with both the appendages moving in the same direction.

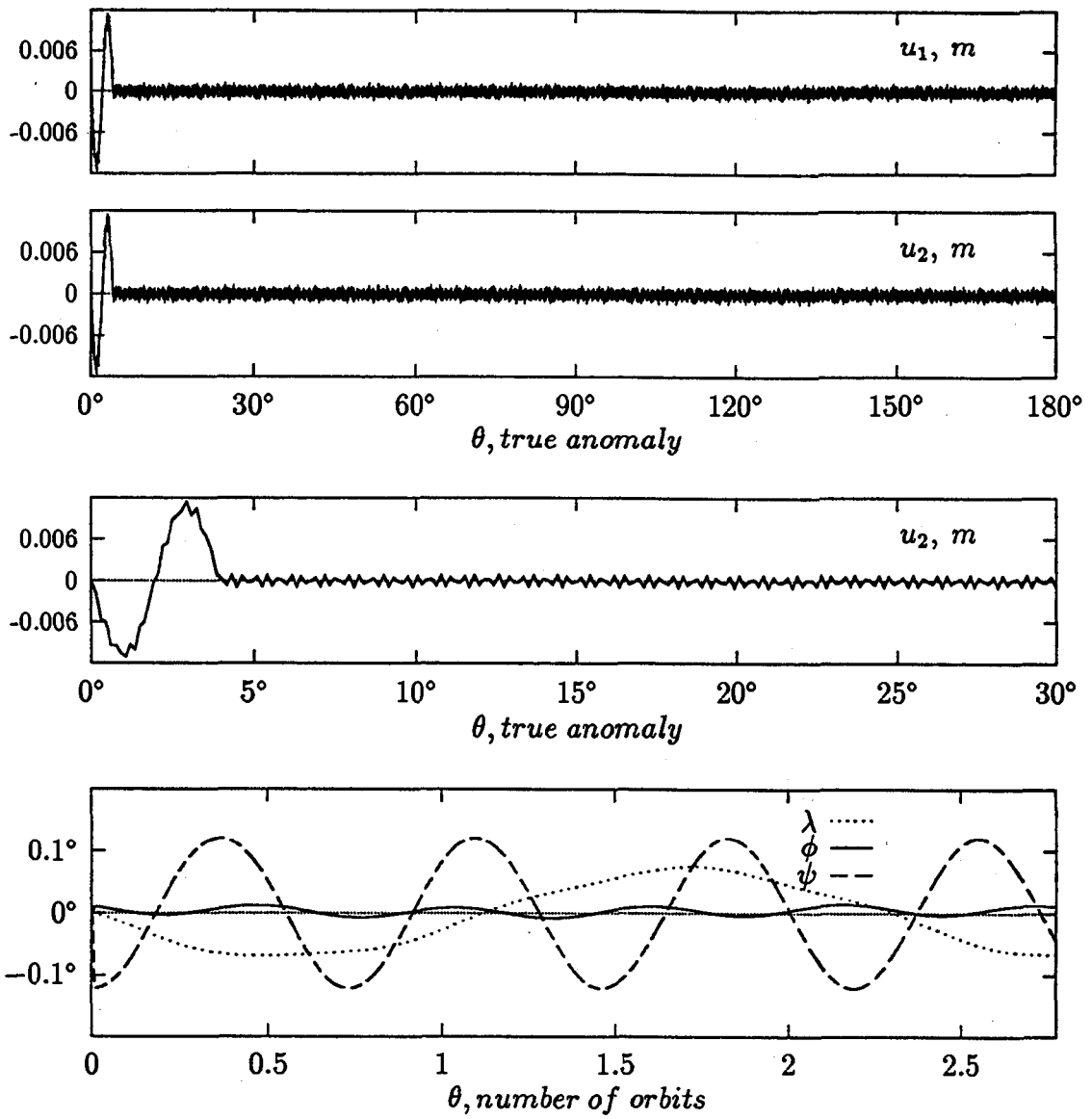

Figure 6-16 Effect of a faster slew rate of 60° in one minute on the SFU response in the Orientation A. The third plot magnifies the u_2 response in the interval $0 - 30°$.

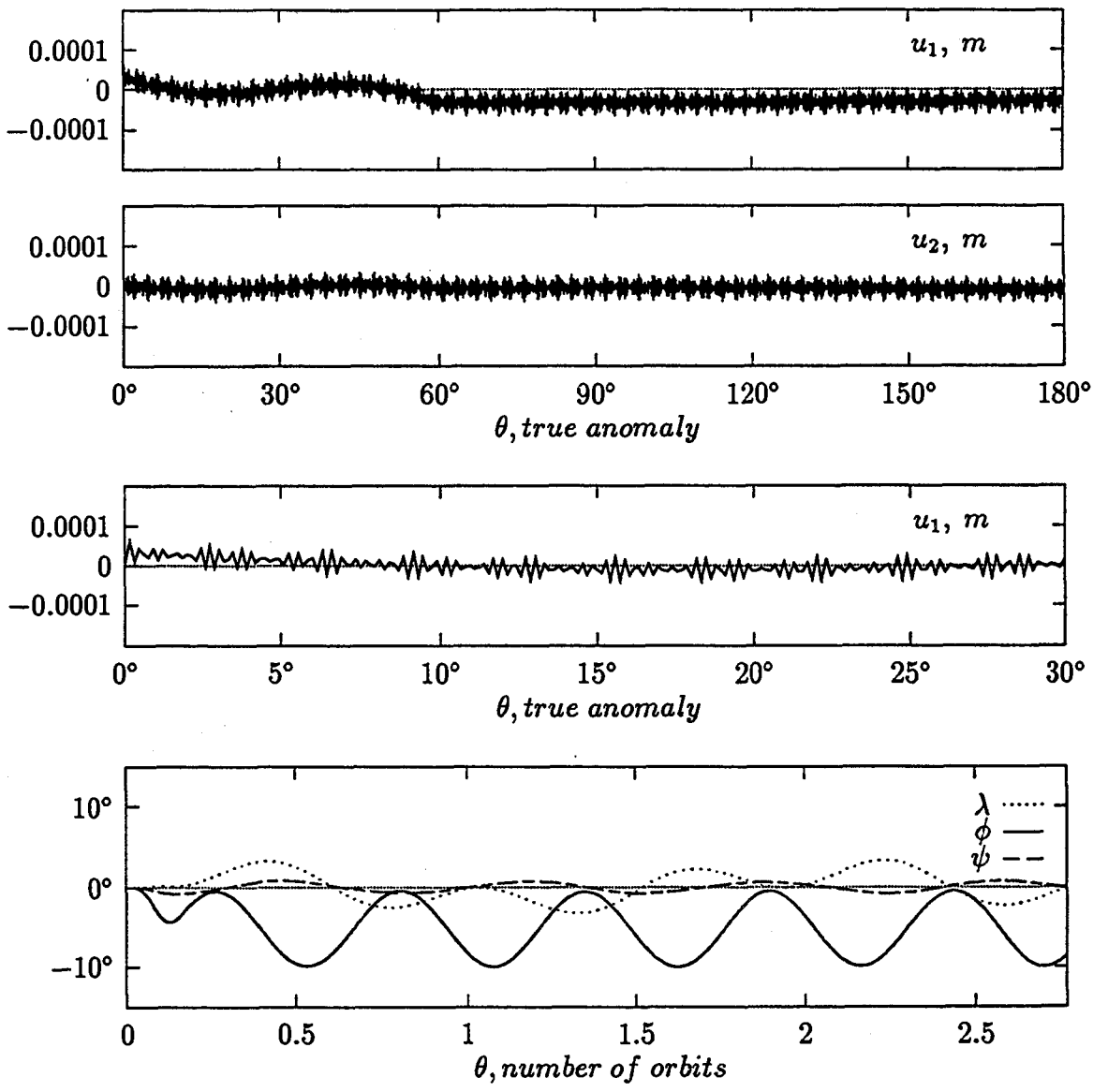

Figure 6-17 Effect of the upper appendage slew failure on the system response when occupying the Orientation A.

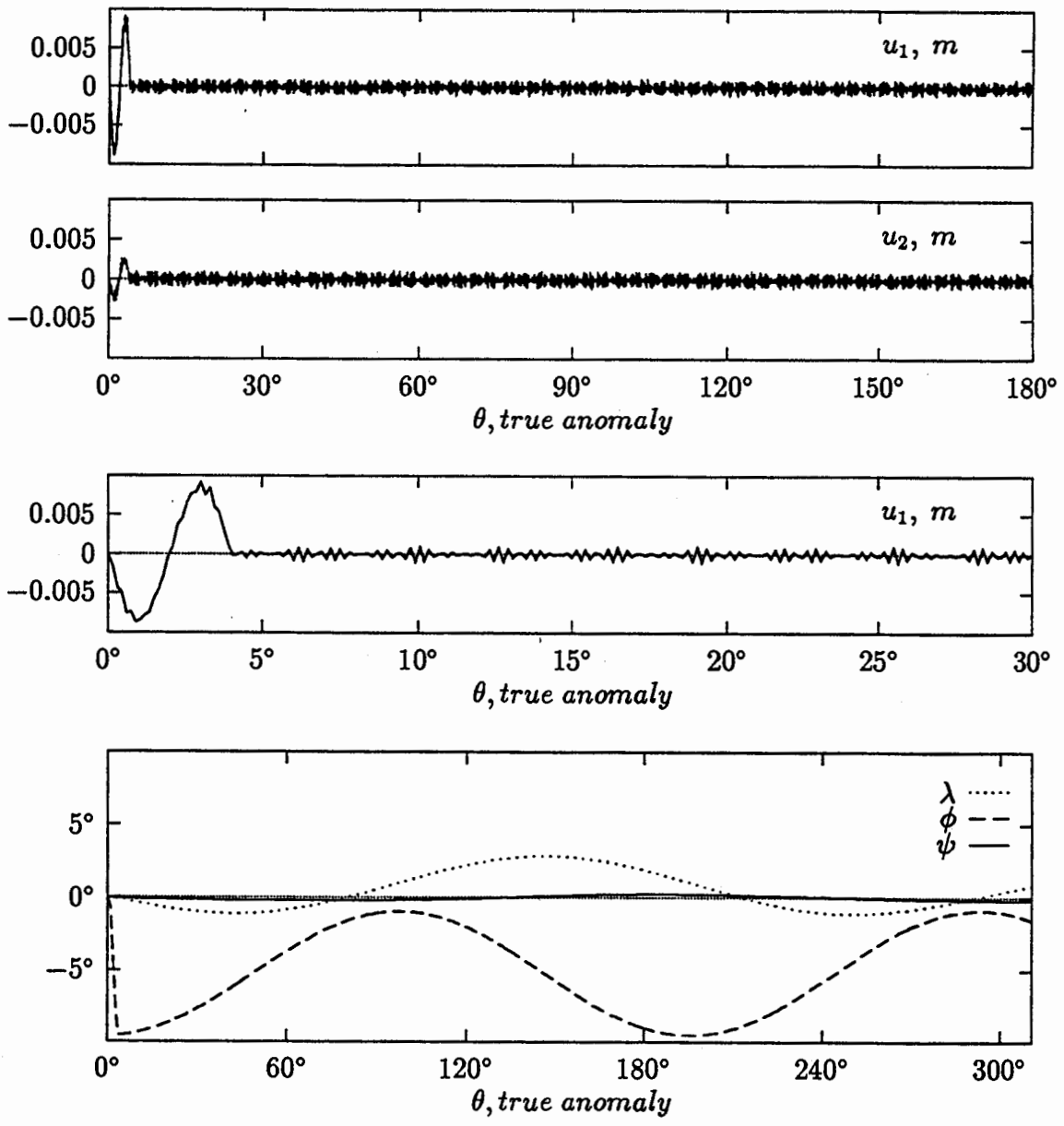

Figure 6-18 System response due to the faster 1 minute slew of the lower appendage (failed upper solar paddle).

case. On the other hand, the vibratory response is now larger at least by one order of magnitude.

With the failure of the upper appendage (the one away from the earth) to slew, the system aquires an unsymmetrical configuration and the equilibrium ϕ attains a negative value (Figure 6-17). Note, the amplitude of the steady state pitch oscillations is now significantly smaller while the out-of-plane librations (roll and yaw) are relatively larger. As can be expected, the steady state roll motion is now about the new equilibrium position. With the faster maneuver the librational response does not seem to change significantly; however, the vibratory response is considerably higher (Figure 6-18) as in the case of the two appendage slew response shown in Figure 6-16.

Orientation B

Typical response of the SFU in the B Orientation is shown in Figures 6–19 and 6–20. Note, as against the previous case (slew maneuvers in the Orientation A), now the slewing motion occurs in the orbital plane. Also the upper and lower appendages are slewing in the opposite sense (Figure 6-14). The system response with both the appendages undergoing nominal slewing motion is presented in Figures 6–19(a) ($-30°$ to $+30°$) and 6–20(a) ($0°$ to $60°$). As can be expected, the dominant motion is in the pitch about the new equilibrium position. The following observations can be made by comparing Figure 6–20(a) with 6–19(a): first, the pitch response is much larger in the $0°$ to $60°$ slew than that in the $-30°$ to $+30°$ case due to the larger deviation from the equilibrium orientation after the slew maneuver; secondly, the appendages deform inducing stress but do not vibrate after the slew, due to the absence of appendage deflection before the slew in the nominal equilibrium Orientation B. With the failure of the upper appendage to slew (Figures 6–19b), the pitch response is significantly reduced, as can be expected, and now occurs about the new equilibrium position ($\approx -6°$). Vibratory response of the appendages remains essentially the same as before. Comparing Figure 6–20(b) with Figures 6–19(b), it can be seen that the two observations mentioned above still hold, and the deformation of the upper SAP is smaller than that of the lower SAP.

6.3.3 Combined deployment and slew maneuvers

Dynamics and control during simultaneous deployment and slew for a system has not been reported in the open literature yet. Only recently its importance in efficiently

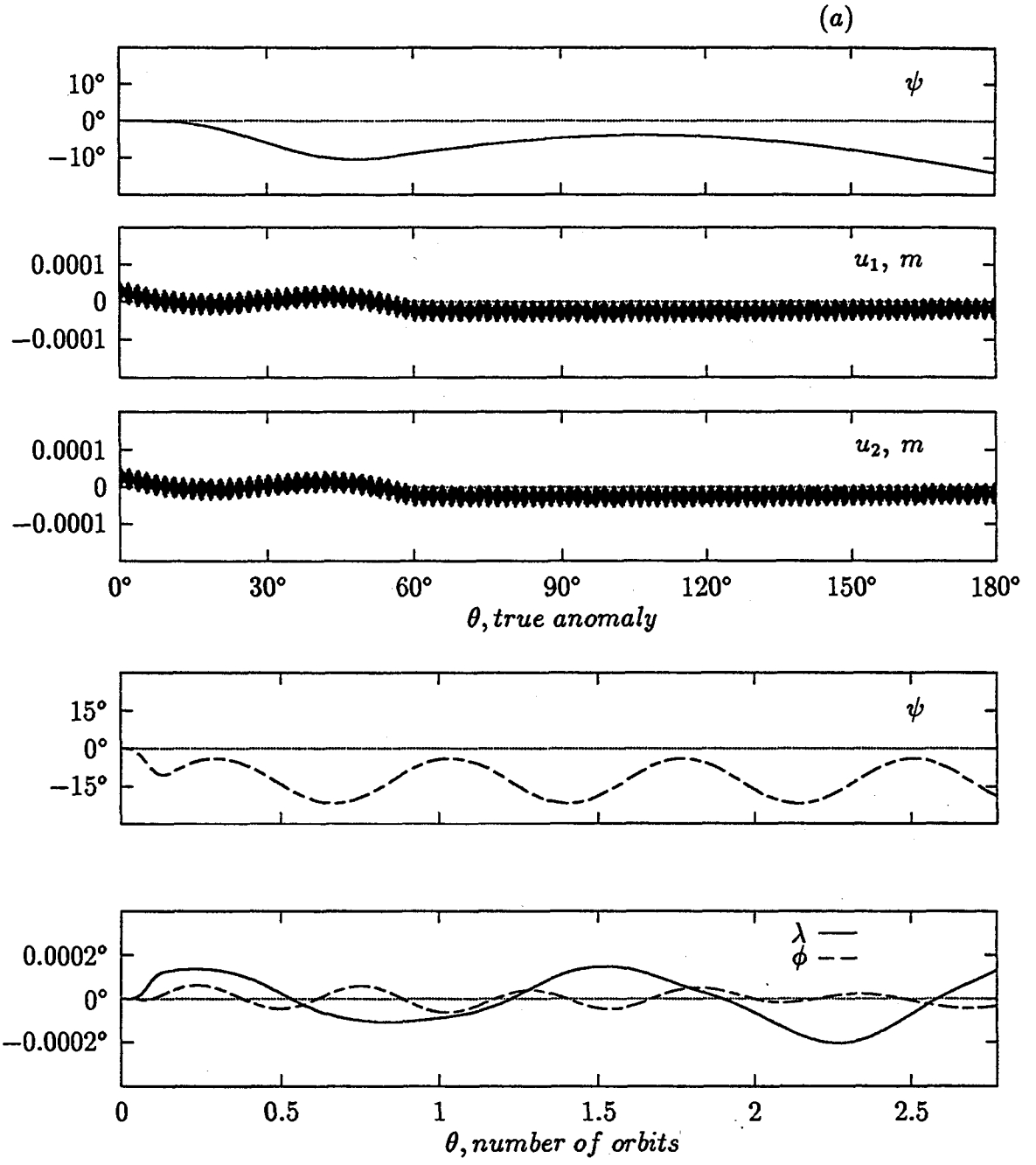

Figure 6-19 Response of the SFU to the slew maneuvers in the Orientation B: (*a*) nominal slew of both the appendages in the orbital plane.

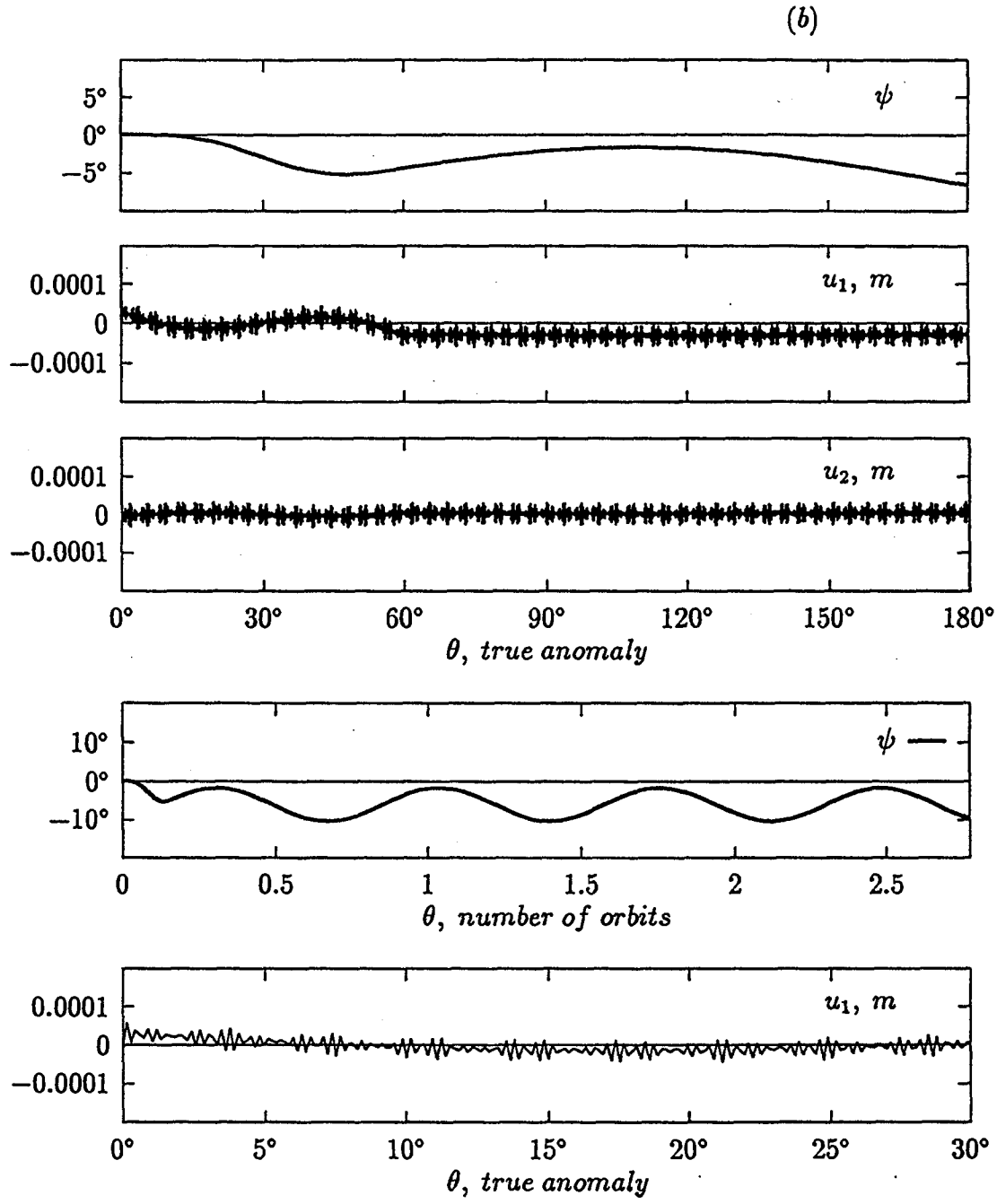

Figure 6-19 Response of the SFU to the slew maneuvers in the Orientation B: (*b*) nominal slew of the lower appendage with the upper solar paddle failed.

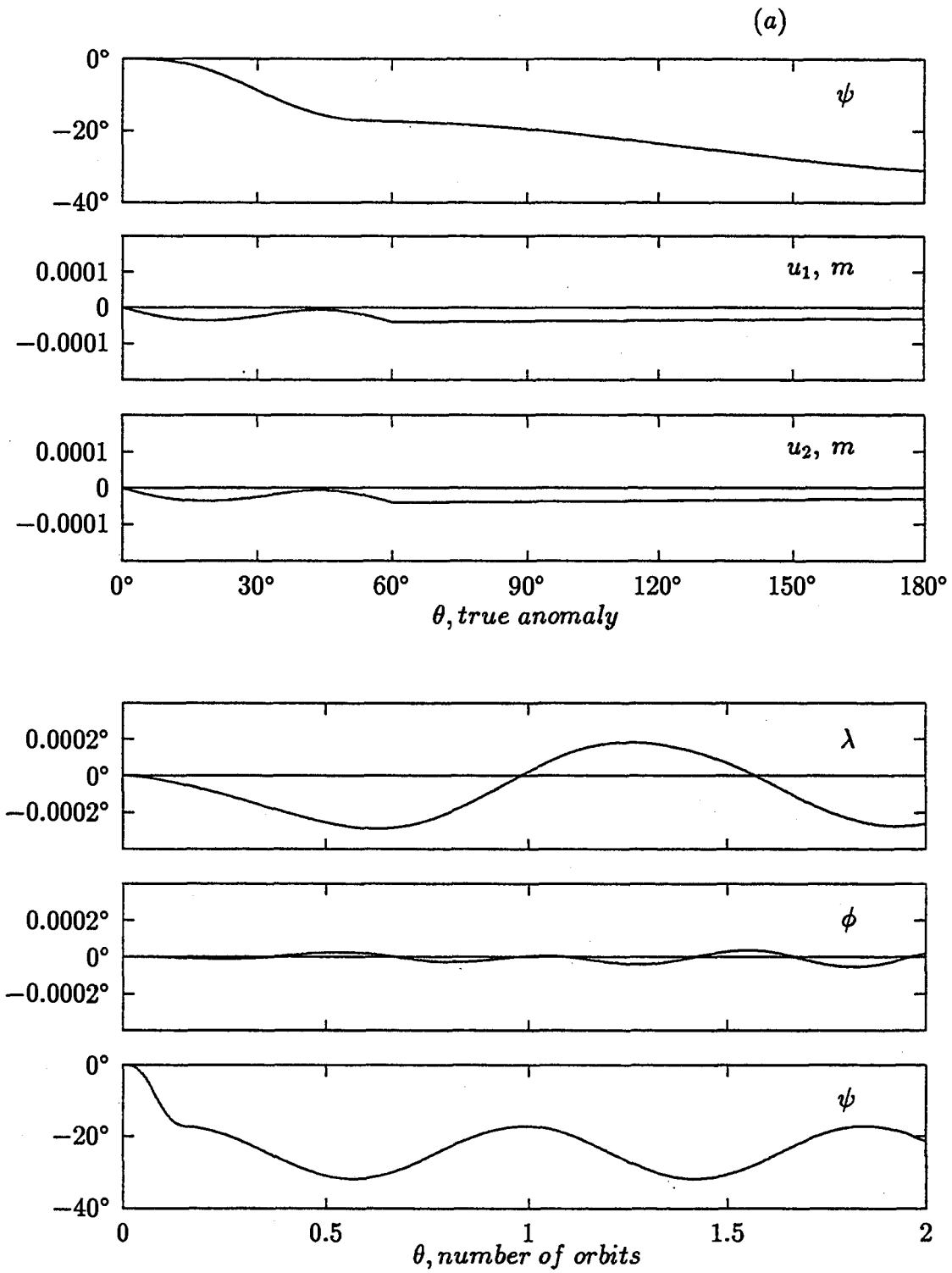

Figure 6-20 Response of the SFU to the slew maneuver, deviating from the nominal equilibrium Orientation B by 60° in 15 minutes: (*a*) both the appendages finished the maneuver.

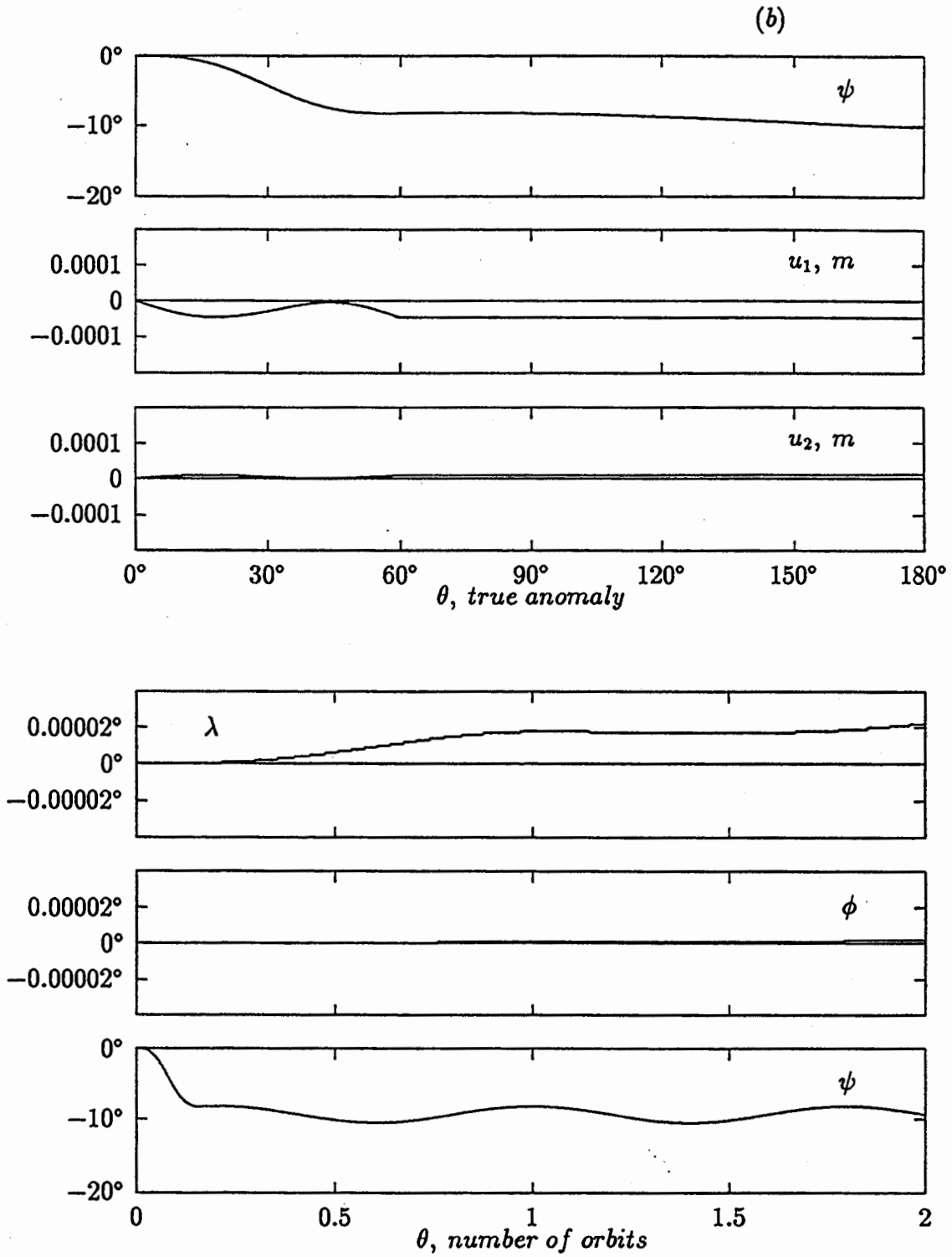

Figure 6-20 Response of the SFU to the slew maneuver, deviating from the nominal equilibrium Orientation B by 60° in 15 minutes: (*b*) the upper appendage failed to slew.

tracking a desired trajectory by a manipulator was recognized. This has led to a few investigations in that direction by several research groups around the world since 1991. It was thought appropriate to study simultaneous deployment and slew maneuvers in the present case as the algorithm can analyze this situation quite readily. As before, the SFU is taken to be either in the Orientation A or Orientation B (Figure 6-14). The nominal maneuver involves:

- deployment of the solar paddle(s) from 1 m to 10 m at a constant rate in 15 minutes; and
- slewing of the solar paddle(s) through 60° in 15 minutes following the sinusoidal time history.

Any deviation from the nominal maneuver is indicated during the discussion.

Orientation A

Figure 6–21(a) shows response of the SFU, around the equilibrium Orientation A, during the nominal maneuver. Note, the deployment is in the orbital plane; however, the slewing occurs normal to the orbital plane. The dominant response is the pitch, which is essentially the same as that during deployment ($\approx$ 13°, Figure 6-6). The out-of-plane librational motions, roll and yaw, remain relatively small by around two orders of magnitude. The maneuver has virtually no influence in exciting the vibratory motion of the appendages.

Effect of increasing the slew and deployment velocities by a factor of 6 (maneuver completed in 2.5 minutes) is shown in Figure 6–21(b). The pitch response remains essentially unchanged, so is the vibration of the appendages. The major effect appears to be on the roll and yaw librations which now increase almost by an order of magnitude.

Figure 6-22 considers the same maneuvers with one major difference: the top appendage fails to slew (although it deploys as required). The pitch and vibratory responses remain essentially the same as before, however, the out-of-plane librations, show a significant increase (Figure 6-22a; the roll from around 0.015° to 7°, and the yaw from around 0.02° to 5°!). Increasing the deployment and the slewing rate only accentuates the out-of-plane librations (Figure 6–22b).

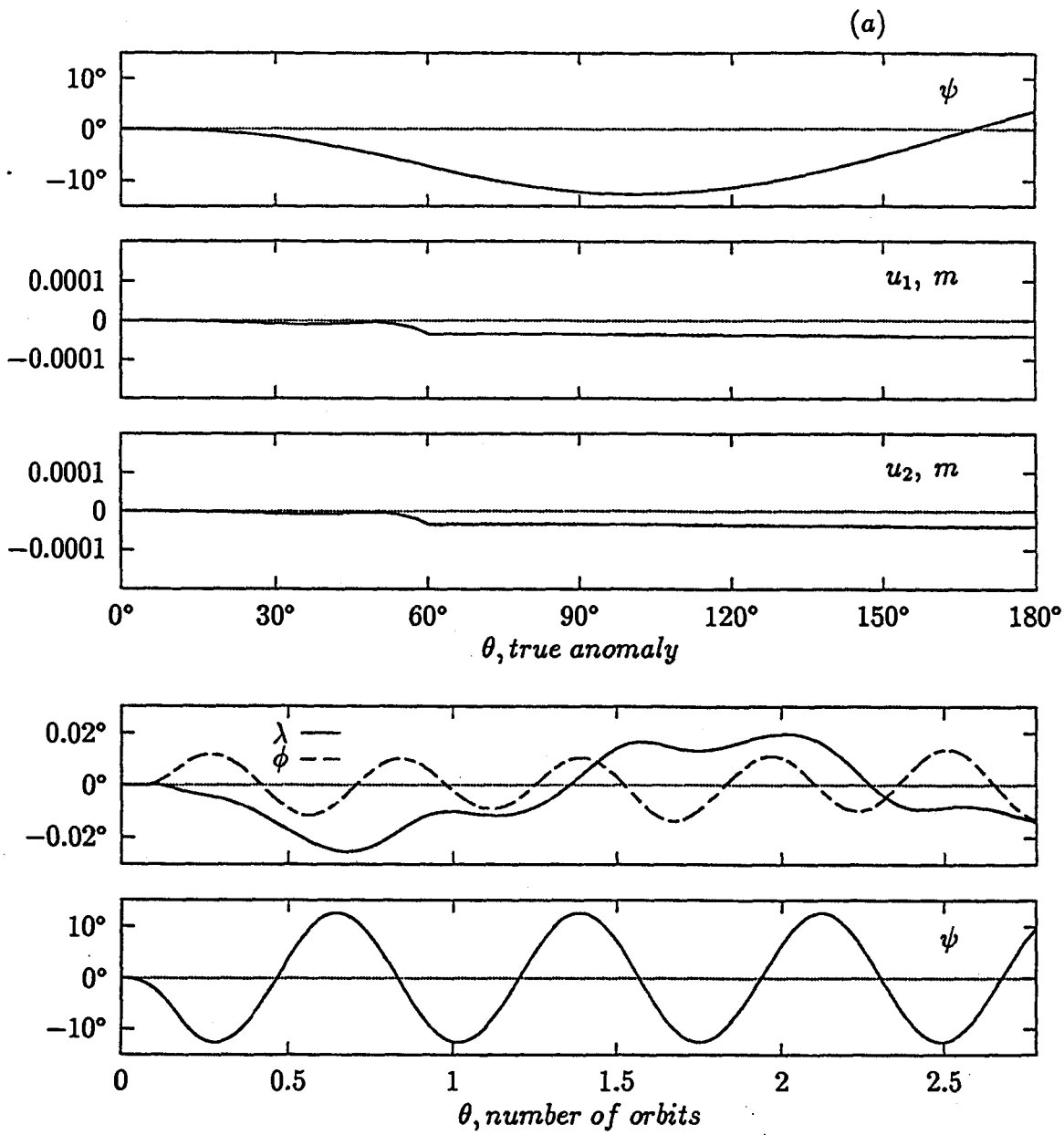

Figure 6-21 Response of the SFU, in the Orientation A, to the simultaneous deployment and slew of the solar paddles: (a) nominal maneuvers.

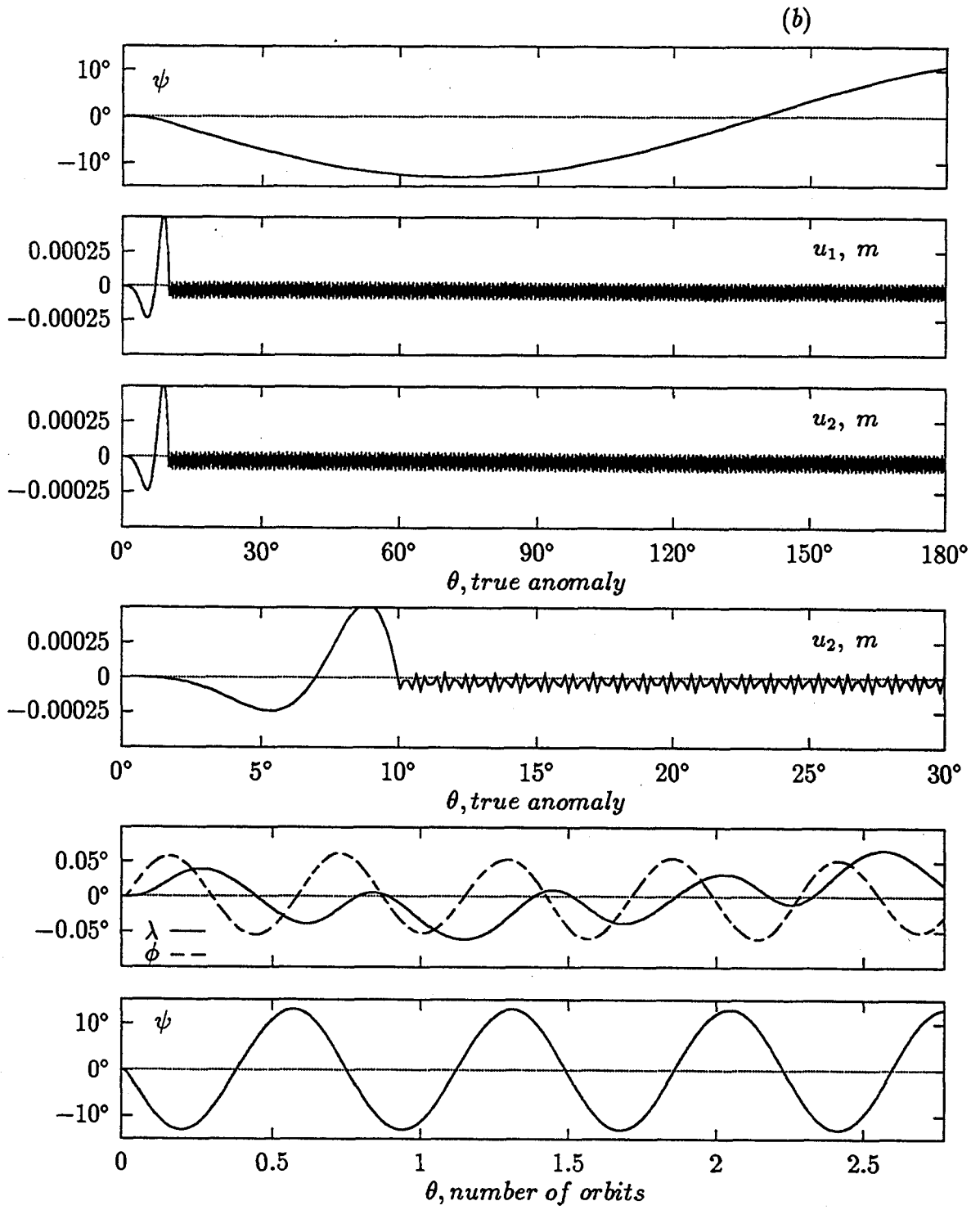

Figure 6-21 Response of the SFU, in the Orientation A, to the simultaneous deployment and slew of the solar paddles: (*b*) maneuvers completed in 2.5 minutes.

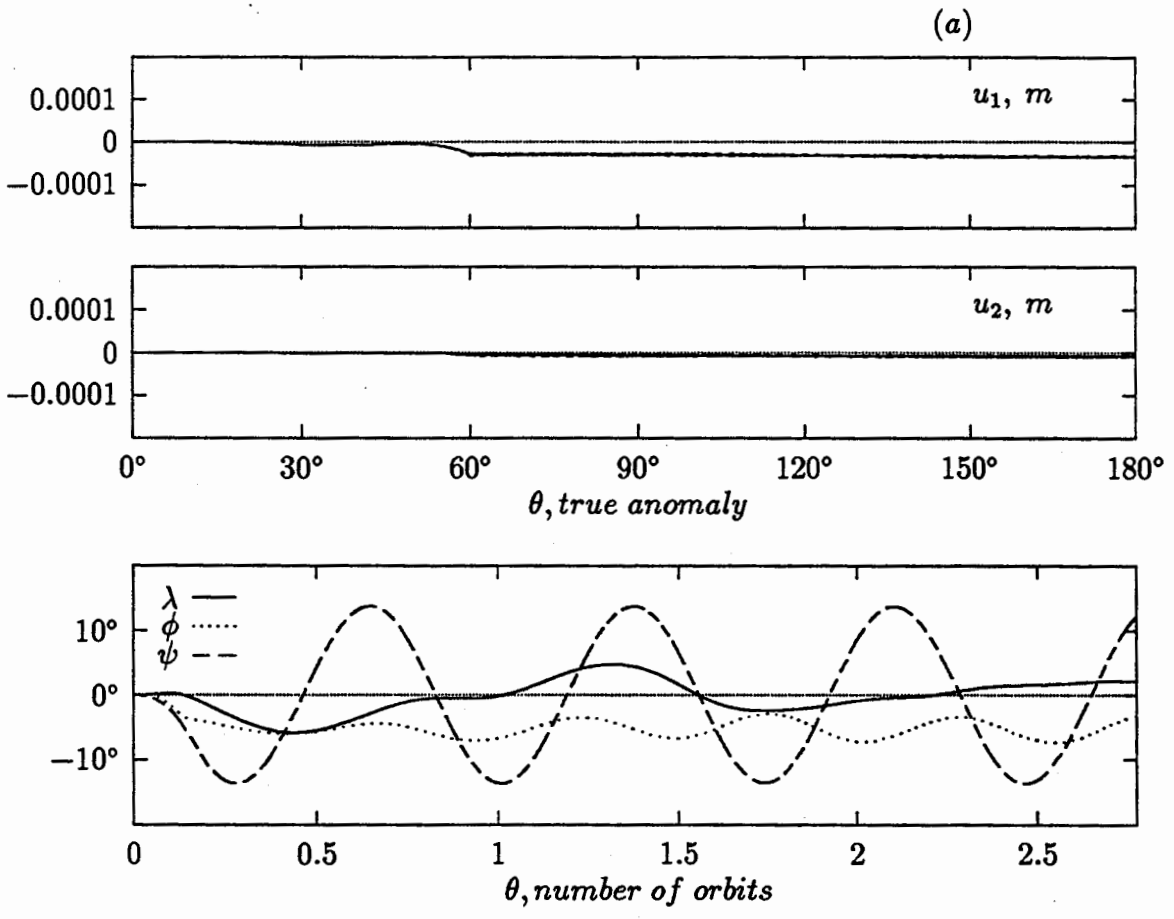

Figure 6-22 The SFU response (in the Orientation A), during failure of the upper paddle to slew: (a) nominal maneuvering rate of 15 minutes.

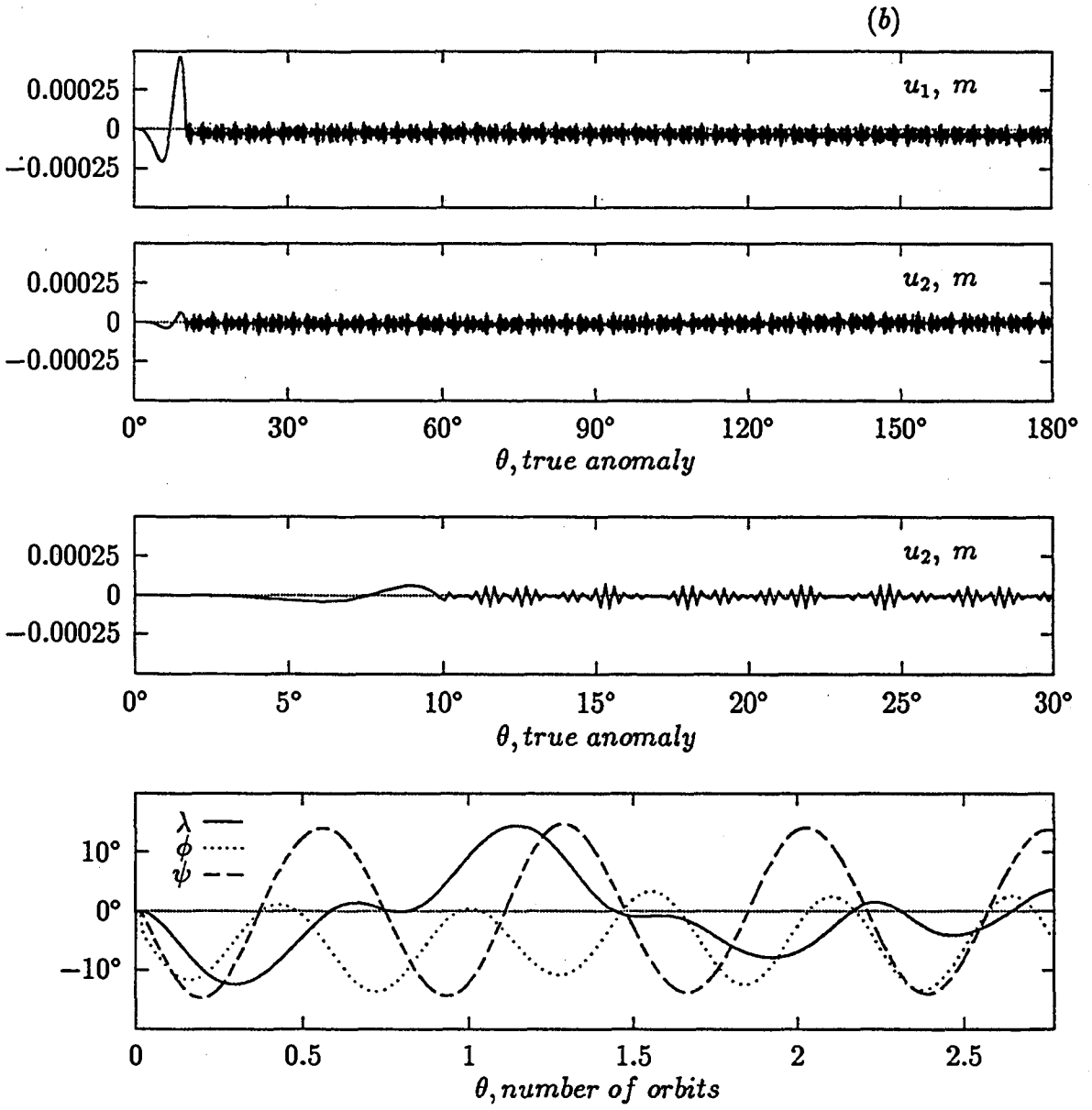

Figure 6-22 The SFU response (in the Orientation A), during failure of the upper paddle to slew: (*b*) maneuvers completed in 2.5 minutes.

Orientation B

The corresponding results were also obtained for the SFU in the Orientation B. Now both the deployment and slew of the solar paddles take place in the orbital plane. Note, the slew results in an asymmetric configuration about the local vertical leading to a new pitch equilibrium of $\psi_o \approx -13°$ (Figure 6-23*a*). The major influence of the combined deployment–slew maneuver is on the pitch response, which is essentially a synthesis of the two individual responses, corresponding to deployment (Figure 6-9) and slew (Figure 6-19). Thus the resultant response is the periodic planar librations, of approximately 17° in amplitude, around the new equilibrium position. The effect of a faster maneuver (completed in 2.5 minutes) is to more than double the pitch amplitude ($\approx 37°$, Figure 6–23*b*). In both the cases, although the out-of-plane librations are excited, they remain rather small (maximum amplitude $\approx 0.025°$) and hence are of little consequence. The same is true with the paddle vibrations which remain negligibly small.

Effect of the failure of the top Solar Array Paddle (SAP) to slew is studied in Figure 6-24. As can be expected, the system now responds in pitch around the new equilibrium position of $\psi_o \approx -7.5°$ with an amplitude of around 15° (Figure 6-24*a*). With the faster maneuver, the pitch amplitude increases to around 25° (Figure 6-24*b*). As before, both out-of-plane librations and vibrations continue to remain small and hence are of little importance.

The response of the system during deployment and a 60° slew maneuver of the beam deviating from the equilibrium Orientation B is showed in Figure 6-25. As in the combined deployment and −30° to +30° slew situation (Figure 6-23*a*), the pitch response here is a synthesis of the two individual responses. The response character and amplitude of the beam vibration are essentially the same as those in Figure 6-9(*a*) where the two appendages deployed in 15 minutes, with an equilibrium shift.

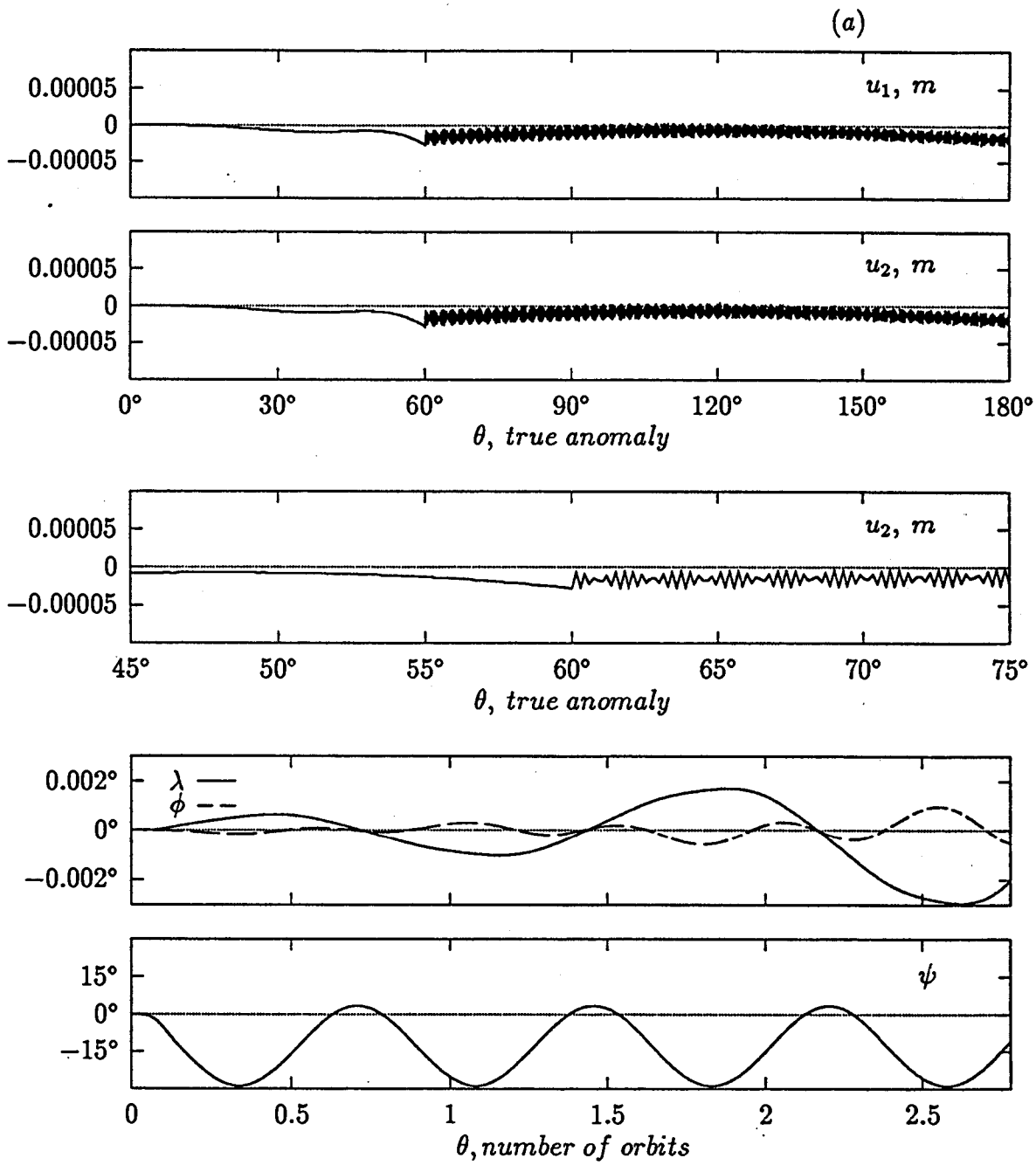

Figure 6-23 Response of the SFU, in the Orientation B, to the combined deployment and slew maneuvers completed in: (*a*) 15 minutes.

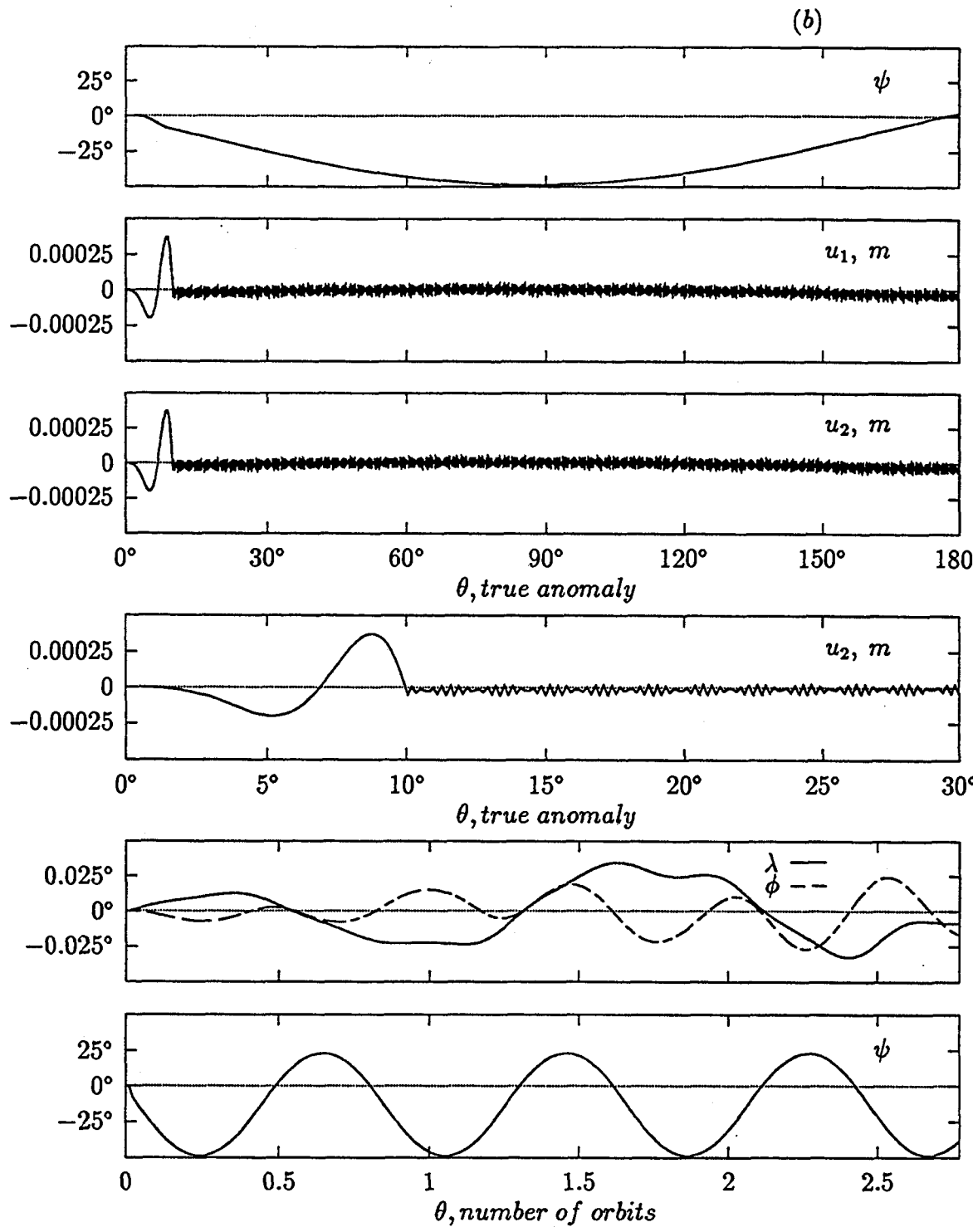

Figure 6-23 Response of the SFU, in the Orientation B, to the combined deployment and slew maneuvers completed in: (*b*) 2.5 minutes.

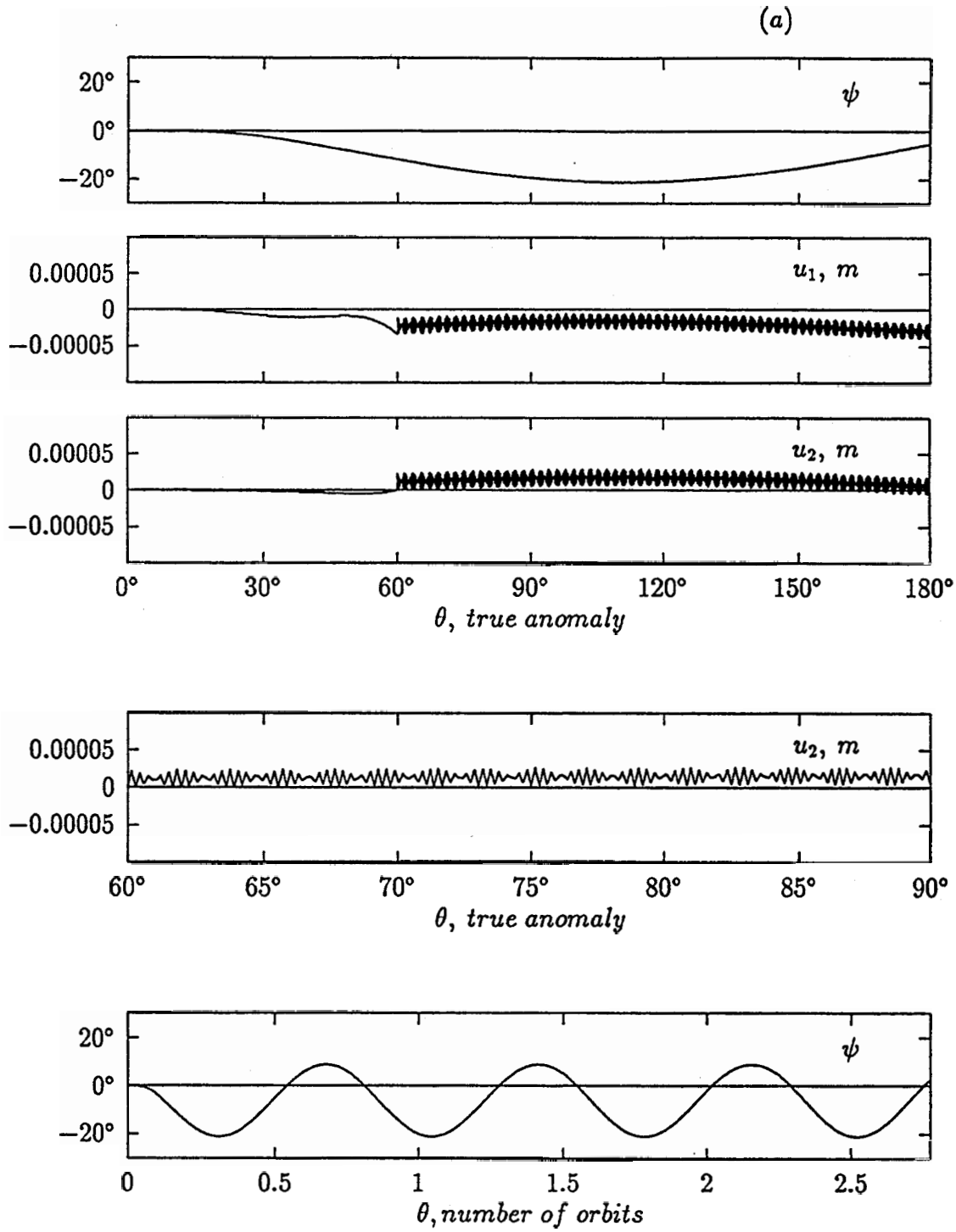

Figure 6-24 Effect of the upper SAP slew failure during the combined maneuvers completed in: (*a*) 15 minutes.

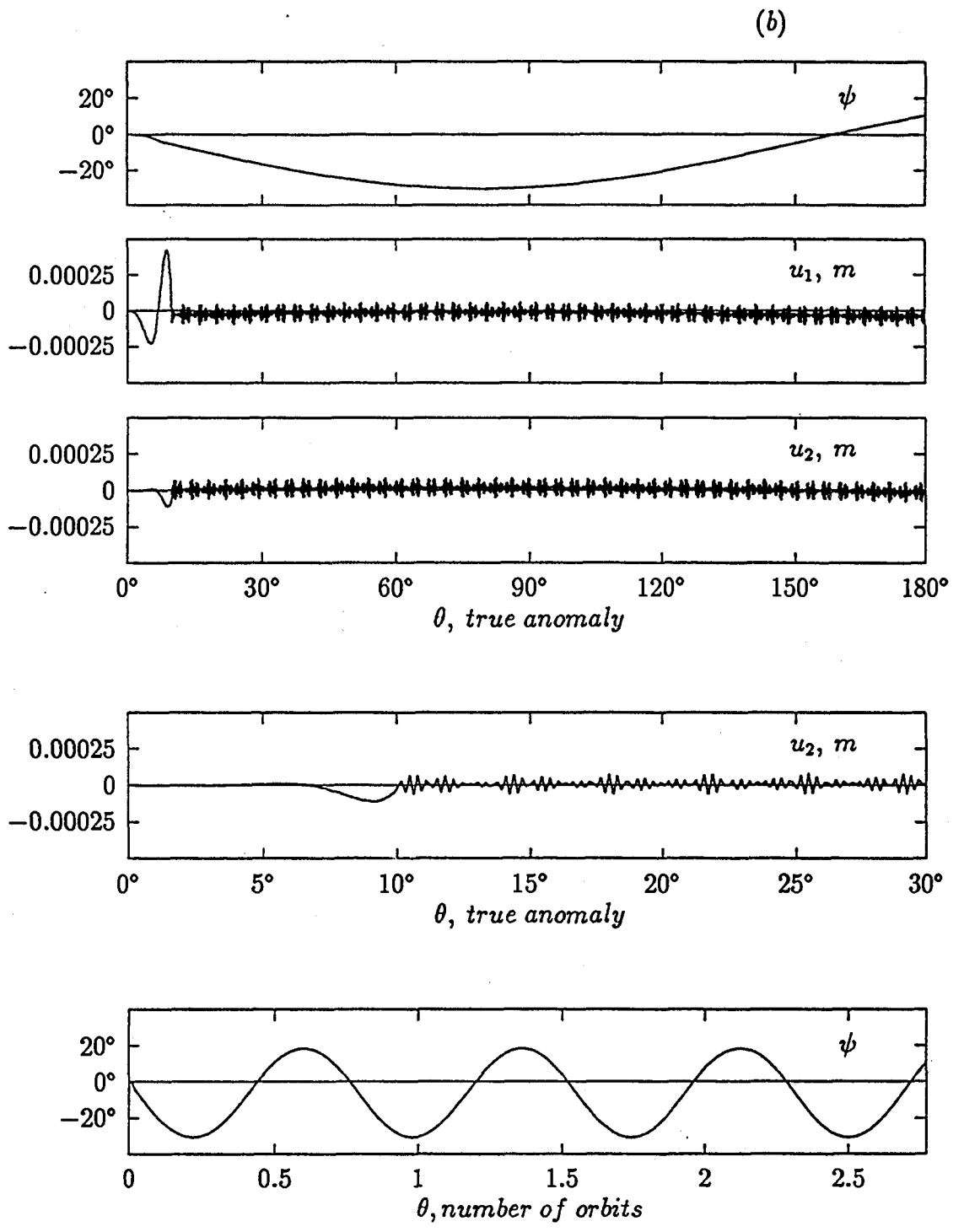

Figure 6-24 Effect of the upper SAP slew failure during the combined maneuvers completed in: (*b*) 2.5 minutes.

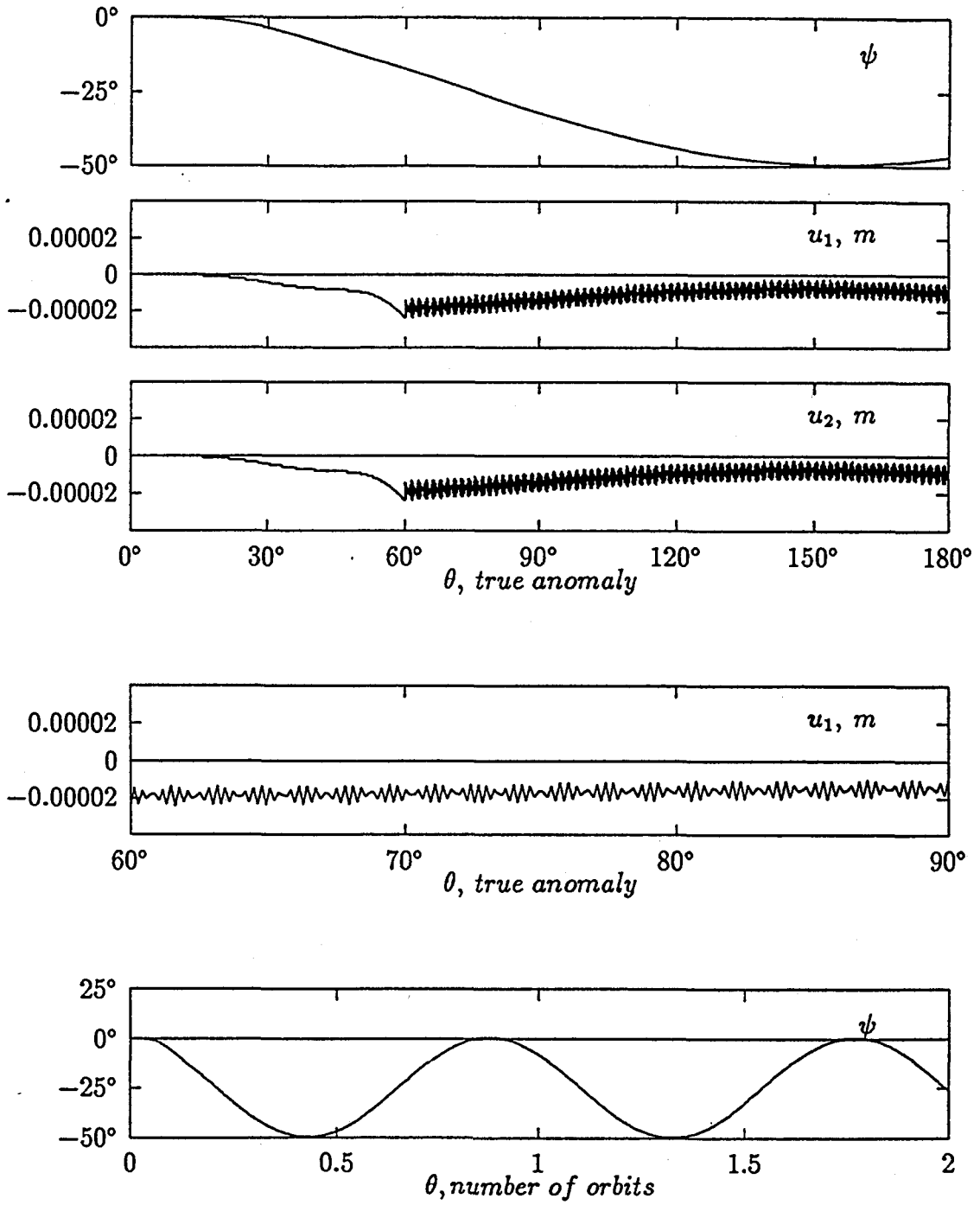

Figure 6-25 Response of the SFU during the combined deployment and slew maneuvers, deviating from the nominal Orientation B by 60° in 15 minutes.

6.3.4 Summary of results

Before closing the SFU's dynamical analysis, it would be useful to summarize salient features of its response. Based on the simulation results following general observations can be made:

Orientation A

(i) The effect of inplane deployment is to induce pitch librational motion due to the Coriolis effect. The deployment rate has little effect on the pitch amplitude in the range 15 minutes (lower deployment velocity) to 2.5 minutes (higher deployment velocity). The out-of-plane librations and paddle vibrations are not excited by the deployment.

(ii) The slew maneuver, being out-of-plane, excites all the three librational degrees of freedom. However, the pitch response is at least an order of magnitude higher ($\approx 1.8°$ amplitude) compared to the roll and yaw responses (roll amplitude$\approx$ $0.1°$, yaw amplitude $\approx 0.01°$). The large pitch response may be attributed to the reduction in the moment of inertia about the pitch axis during the slew maneuver. The increased slew rate has little effect on the out-of-plane librations. Although the slewing rate affects the vibrational motion significantly, it still remains negligibly small (tip amplitude $\approx$ 2 *cm* during slew maneuver, and 2 *mm* after slew).

(iii) Effect of the upper appendage slew failure is to shift the roll equilibrium position, as expected, with a large amplitude roll oscillations ($\approx 5°$ compared to $\approx 0.1°$ for the nominal case) about the new equilibrium position. As before, the faster slew has little effect on the response.

(iv) During the combined deployment-slew maneuver, the pitch response is dominant. It is significantly larger than that caused by the individual maneuvers. An increase in the maneuver rate affects the out-of-plane librations significantly. The same is true during the failure of the upper paddle to slew during the combined maneuver, particularly with respect to the roll. A faster maneuvering rate only accentuates the out-of-plane response.

Orientation B

(v) The dominant response during the deployment still remains the pitch and it is slightly larger in the present case compared to that for the Orientation A ($\approx 15°$ versus $\approx 13.4°$ amplitude). Other observations in (i) remain valid here also. Retrieval is essentially an unstable maneuver.

(vi) During slew, the dominant motion continues to be pitch about the new equilibrium position. However, with the failure of the upper paddle slew maneuver, the pitch response reduces significantly. This is in contrast to the roll response during the slew failure for the Orientation A as mentioned in (iii).

(vii) Dominant response continues to be pitch during the combined deployment-slew maneuver. It is rather large, of $\approx 17°$ amplitude, and occurs around the new equilibrium position. The faster maneuver accentuates the pitch response. A similar behavior is exhibited during the failure mode.

Orientation C

(viii) Although the orientation represents an equilibrium state, it is unstable.

The information is of fundamental importance in the design of a control system for the SFU, monitoring the SFU operation after launch and particularly during the conduct of the planned dynamical experiments.

6.4 The Space Shuttle 'Orbiter'

The second example considers the Space Shuttle 'Orbiter' based flexible beam extending to 33m. The Shuttle is in the Lagrange Orientation, which is relatively stable. The configuration corresponds to the Orbiter Mounted Large Platform Assembler Experiment once proposed by the Grumman Aerospace Corporation. It also resembles the SCOLE (Structural COntrol Laboratory Experiment) proposed by the NASA Langley Research Center. The Grumman experiment aimed at establishing capability of manufacturing beams in space which would serve as one of the fundamental structural elements in construction of the future space station. Objective of the SCOLE experiment is to assess dynamics and control of large flexible structures in space when excited by external disturbances including slew maneuvers.

The relevant parameters used in the numerical simulation are listed below:

Orbital motion:

$$\begin{aligned} orbit\ eccentricity(\epsilon) &= 0.1\ ; \\ altitude &= 300\ km\ ; \\ period &= 90\ min\ . \end{aligned}$$

Orbiter:

$$\begin{aligned} mass(m_0) &= 79,710\ kg\ ; \\ I_{xx} &= 1077195\ kg \cdot m^2\ ; \\ I_{yy} &= 8284868\ kg \cdot m^2\ ; \\ I_{zz} &= 8662178\ kg \cdot m^2\ . \end{aligned}$$

Beam:

$$\begin{aligned} mass(m_1) &= 129\ kg\ ; \\ length &= 33\ m\ (fully\ deployed)\ ; \\ bending\ rigidity\ (EI) &= 436\ kg \cdot m^3/s^2\ . \end{aligned}$$

The cross section of the beam is such that the area moment 'I' in both directions have the same value. The beam is free to vibrate in the two transverse directions with the deformation in each direction represented by the first two modes of a cantilever beam. $2u_{ij}$ (in meter) refers to the beam tip deflection in the ith direction and the jth mode. The plane formed by the local vertical and orbit normal is referred to as the "local vertical plane". Similarly, the plane formed by the local horizontal and the orbit normal is called the "local horizontal plane". Thus u_{11} and u_{12} represent half the tip deflections of the beam, in the local vertical plane, in the first and second modes, respectively. Similarly, u_{21} and u_{22} are half of the tip deflections in the local horizontal plane corresponding to modes one and two, respectively. In general, contribution of the second mode was found to be, relatively, quite small.

In this investigation, as in the previous example, behavior of the system during the beam deployment is considered first (Section 6.4.1). The beam deploys from 3 m to 33 m at a constant rate. This is followed by the system response during slewing maneuvers in Section 6.4.2. The slew maneuver profile is sinusoidal to avoid disturbances during initial and terminal phases of the maneuver. Finally, Section

6.4.3 addresses the question of combined deployment and slew. As before, only a few typical results are presented to help establish trends.

Figure 6–26 shows response of the orbiter, with the fully deployed 33m beam, to the orbital eccentricity induced disturbance. It serves as the reference in assessing the effects of deployment and slew. Note, only the Shuttle's pitch motion is excited, which is rather large and reaches an amplitude of around 12° in five orbits.

6.4.1 Deployment

The effect of the beam deployment in 1/2 orbit is almost negligible (Figure 6–27). The eccentricity induced disturbance appears to be quite dominant and response remains essentially the same as in the reference case. However, the things change somewhat with the beam tip excitation of 0.4 m in the first mode in the local vertical plane (Figure 6–28). Note, the vibratory motion, through coupling, excites both roll and yaw responses (in addition to pitch, of course) which are modulated at the vibration frequency. The vibratory response (Figure 6–28(b)) clearly show the reduction in frequency during deployment as expected. The beat phenomenon is attributed to the coupling between the transverse vibrational degrees of freedom. The response in the second mode is at least two orders of magnitude smaller and hence of little importance. Figure 6–28(c) shows the tip deflection of the beam during and after the deployment. Note the precessional motion due to interactions between the orbital and vibrational dynamics. u_1 represents the tip deflection in the local vertical direction and u_2 in the local horizontal direction, both in meters as stated before.

The effect of deployment of the beam in directions inclined to the orbit normal is considered in Figures 6–29, which also assesses the influence of the rate of deployment. In Figure 6–29(a) the deployment, at a rate of 1/2 orbit, is in the direction 30° to the orbit normal in the local vertical plane. There is no beam tip excitation here. Corresponding case for the beam deployment in the local horizontal plane is considered in Figure 6–29(b). The pitch motion remains essentially the same as before (Figure 6–26) except for minor changes in the local details. However, now the other librational degrees of freedom are also excited , particularly the yaw. Both the transverse components of the beam vibrations are excited with amplitude modulations contributed by the beat-type motion. Note the variation of the frequency with true

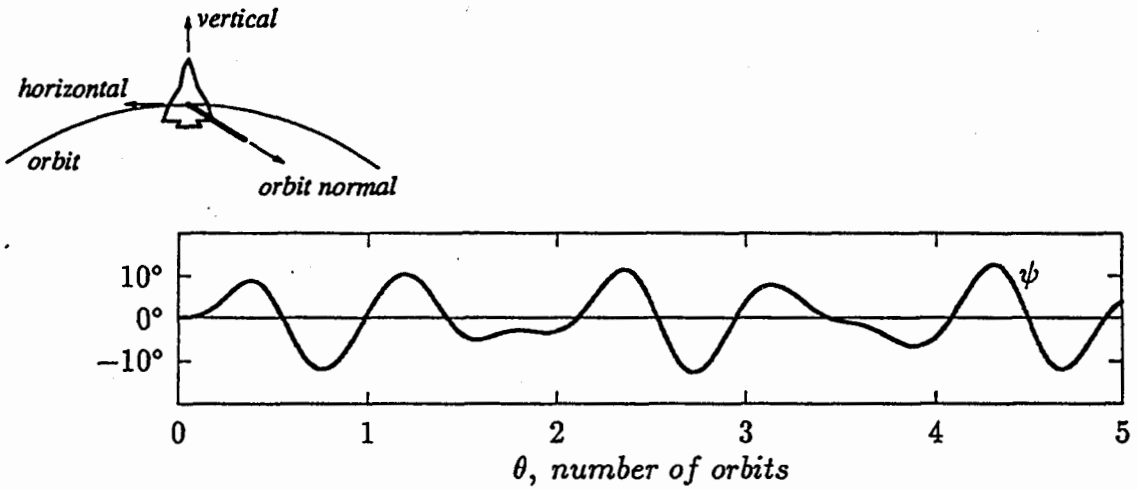

Figure 6-26 Response of the Space Shuttle, with a 33 m beam along the orbit normal, to the eccentricity induced disturbance. It serves as the reference to assess the influence of deployment and slew maneuvers. Note, only the pitch motion is excited.

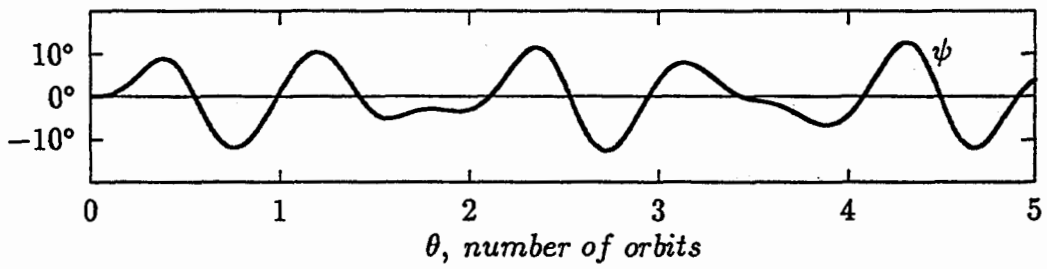

Figure 6-27 The system response with deployment of the beam in 45 minutes (1/2 orbit). The deployment has virtually no effect as the response is essentially the same as that for the reference case.

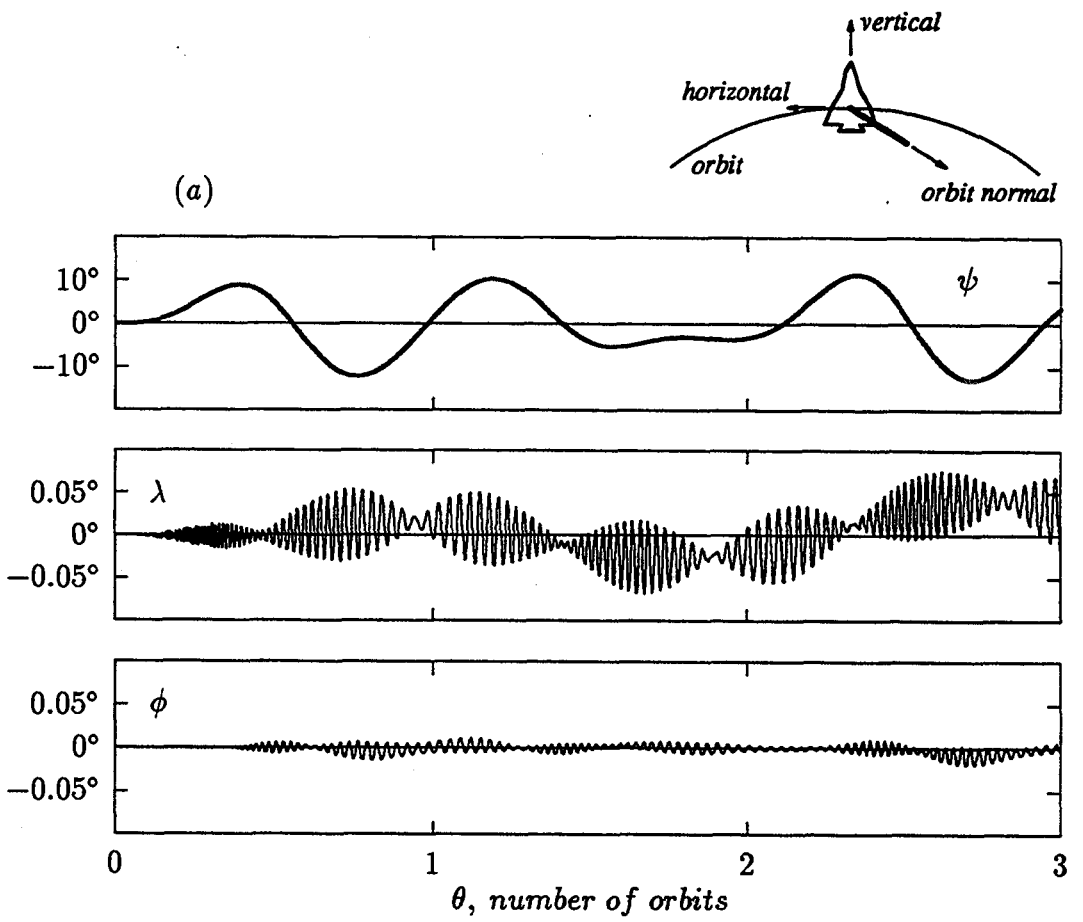

Figure 6-28 System response, during deployment of the beam along the orbit normal in 1/2 orbit, with the tip displacement of 0.4 m in the first mode along the local vertical: (a) librational response of the orbiter.

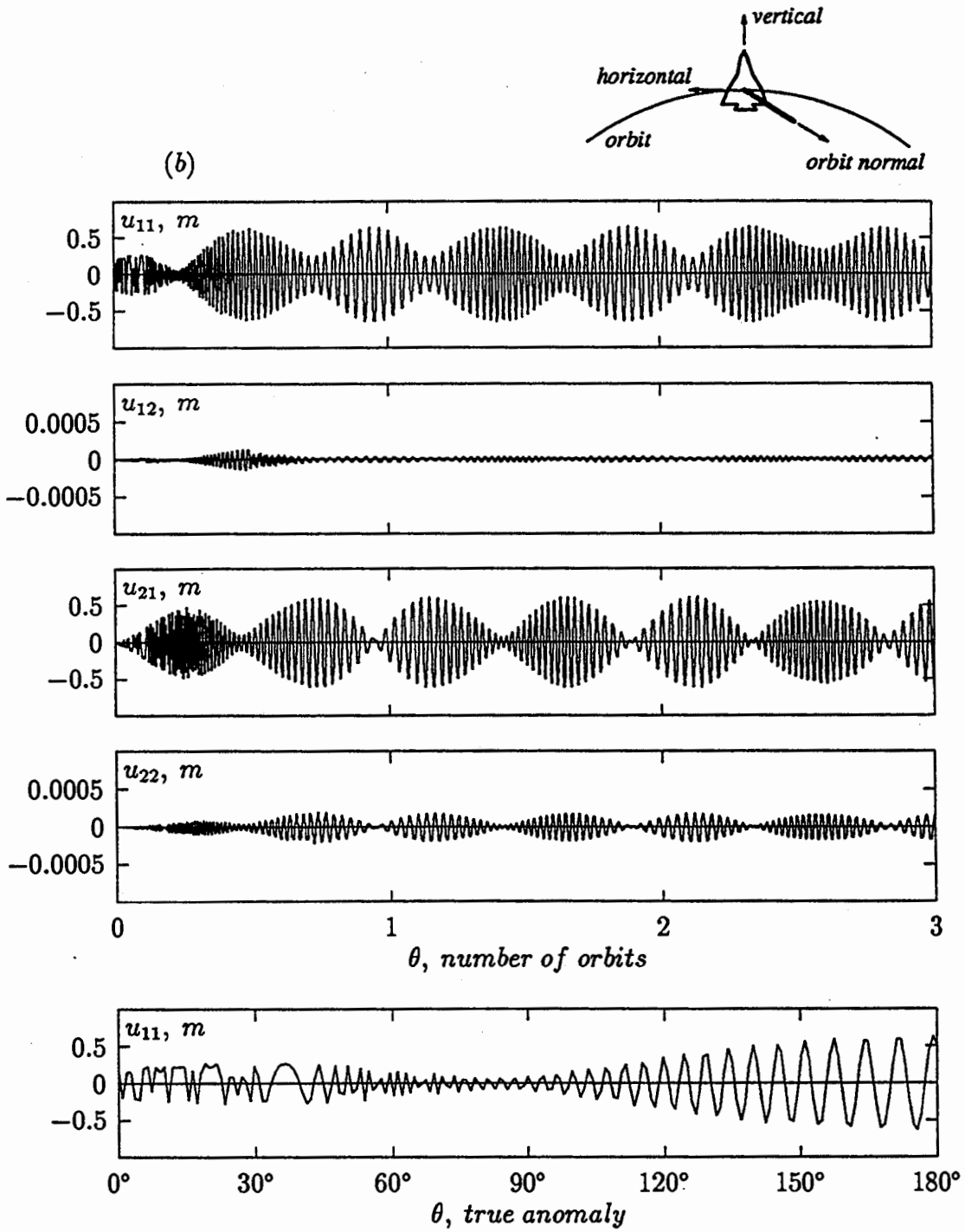

Figure 6-28 System response, during deployment of the beam along the orbit normal in 1/2 orbit, with the tip displacement of 0.4 m in the first mode along the local vertical: (*b*) vibrational response of the beam.

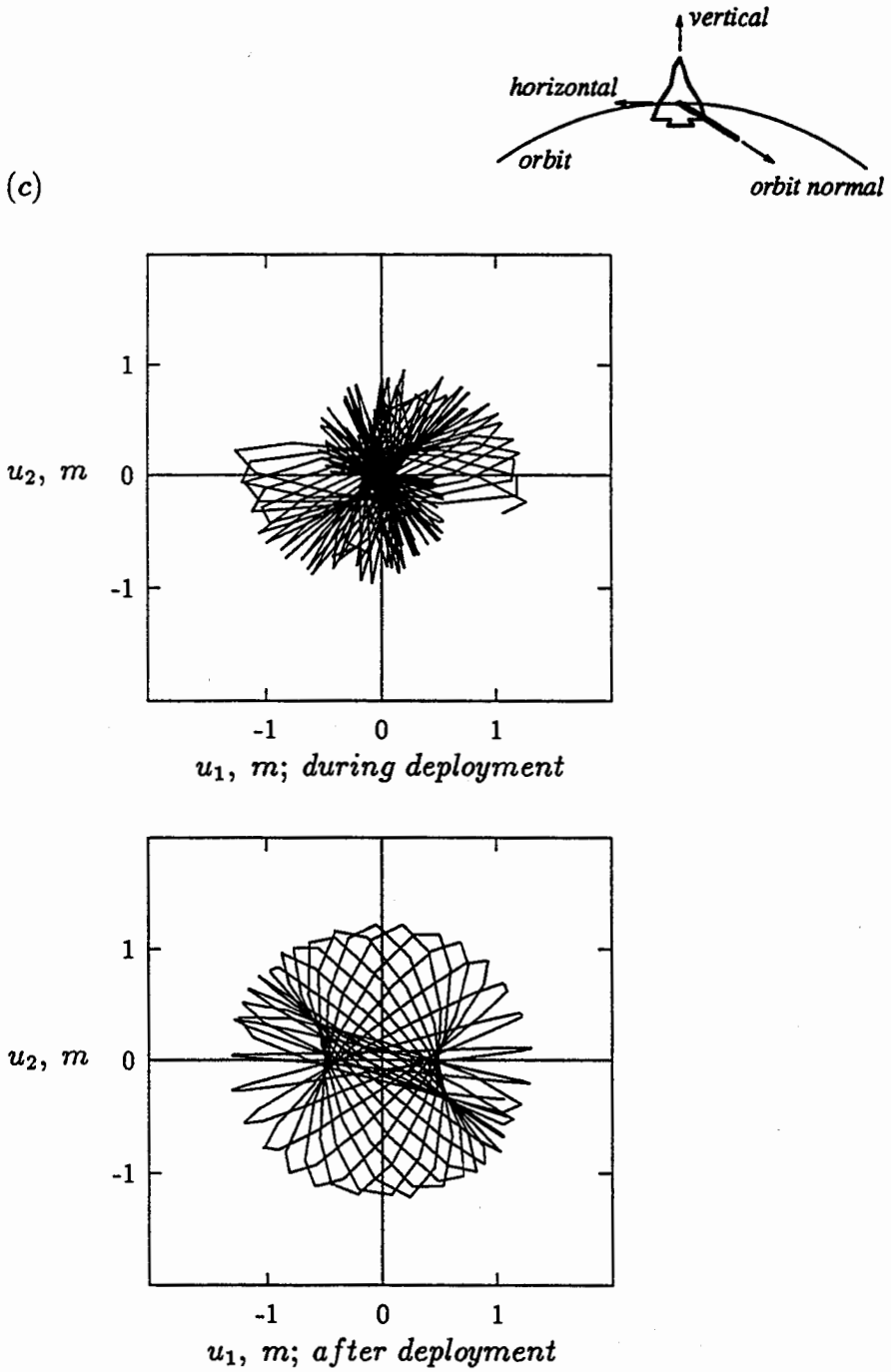

Figure 6-28 System response, during deployment of the beam along the orbit normal in 1/2 orbit, with the tip displacement of 0.4 m in the first mode along the local vertical: (*c*) tip deflection of the beam.

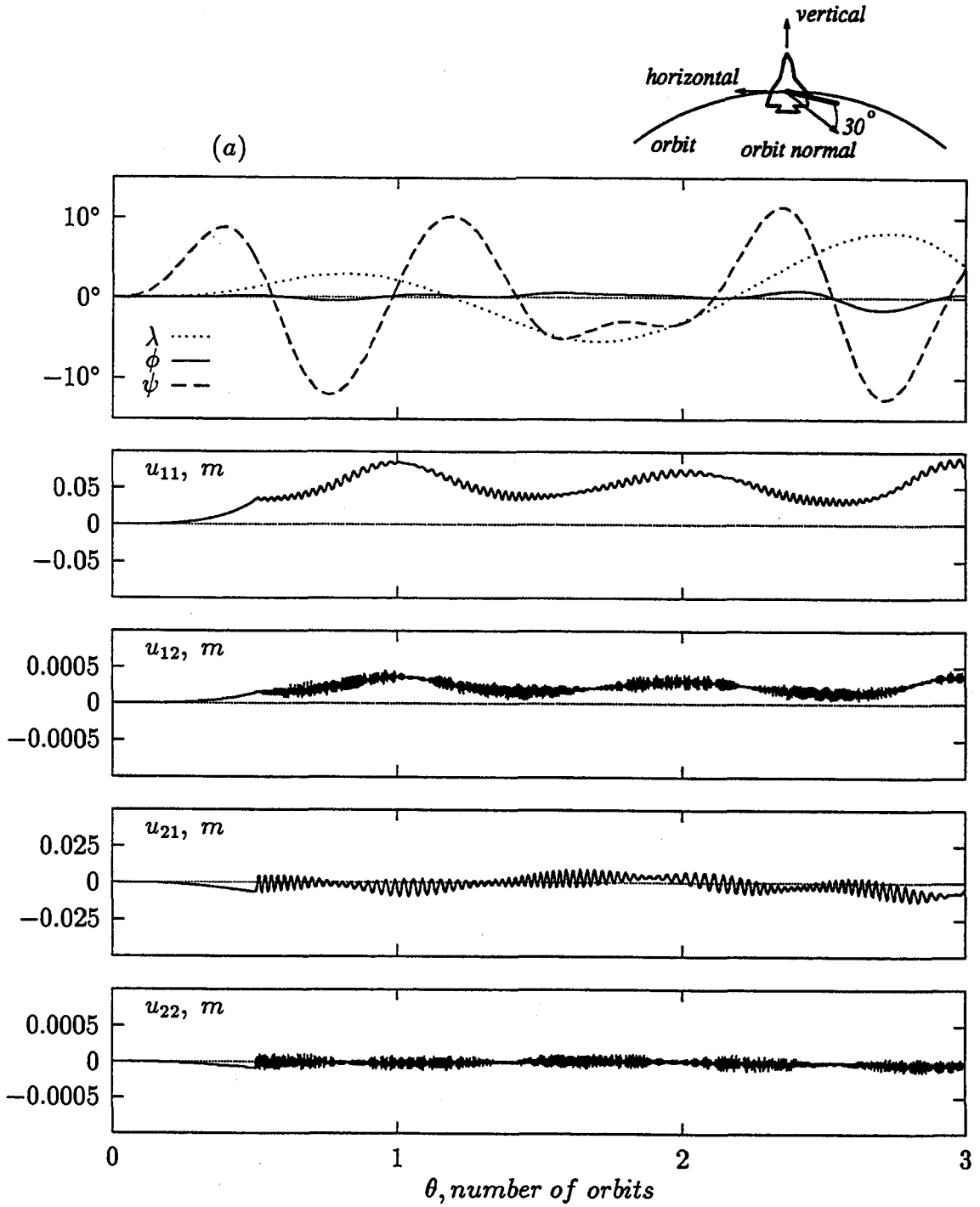

Figure 6-29 Effect of the deployment direction and rate on the system response: (*a*) deployment in 1/2 orbit at 30° to the orbit normal in the local vertical plane.

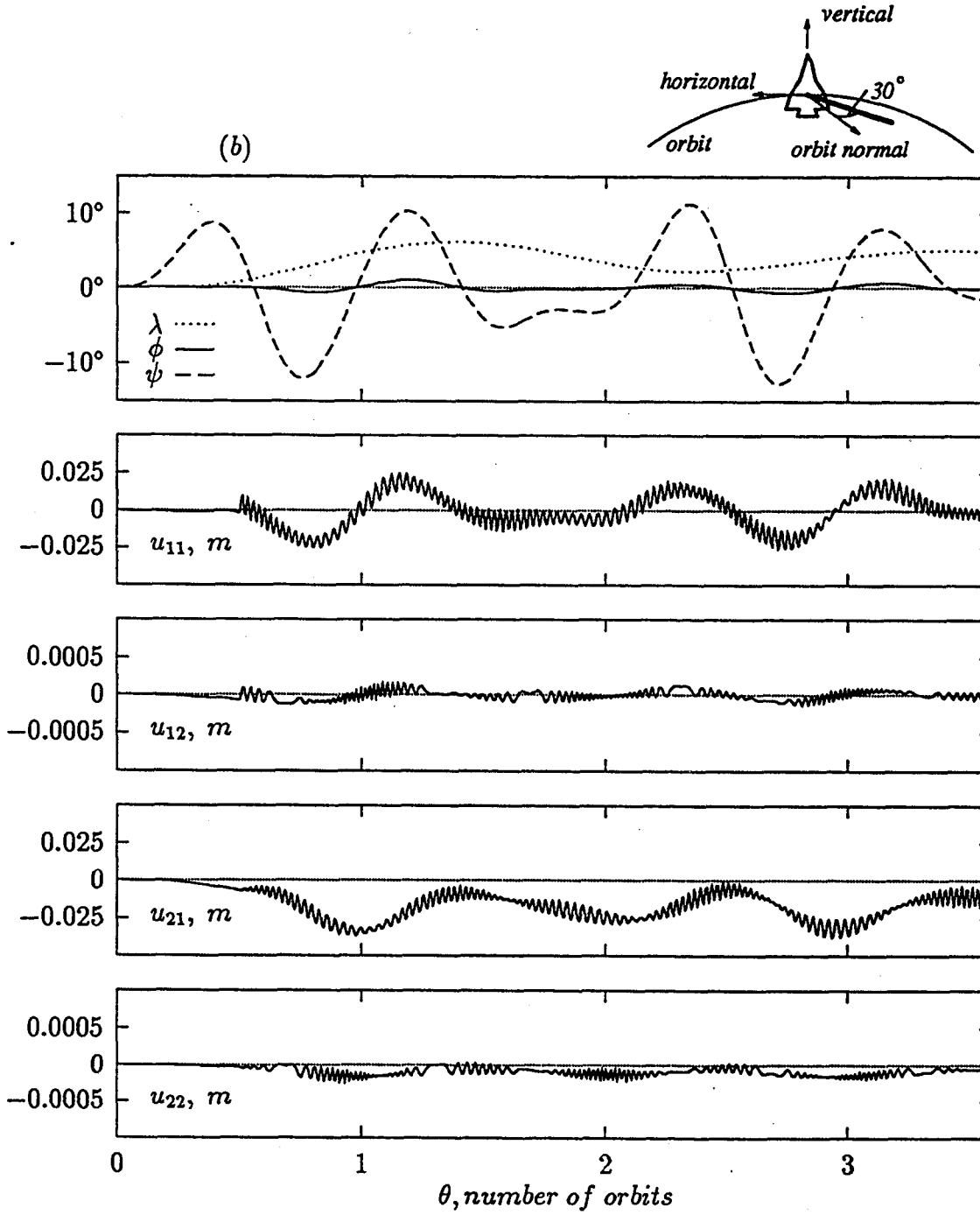

Figure 6-29 Effect of the deployment direction and rate on the system response: (*b*) deployment in 1/2 orbit at 30° to the orbit normal in the local horizontal plane.

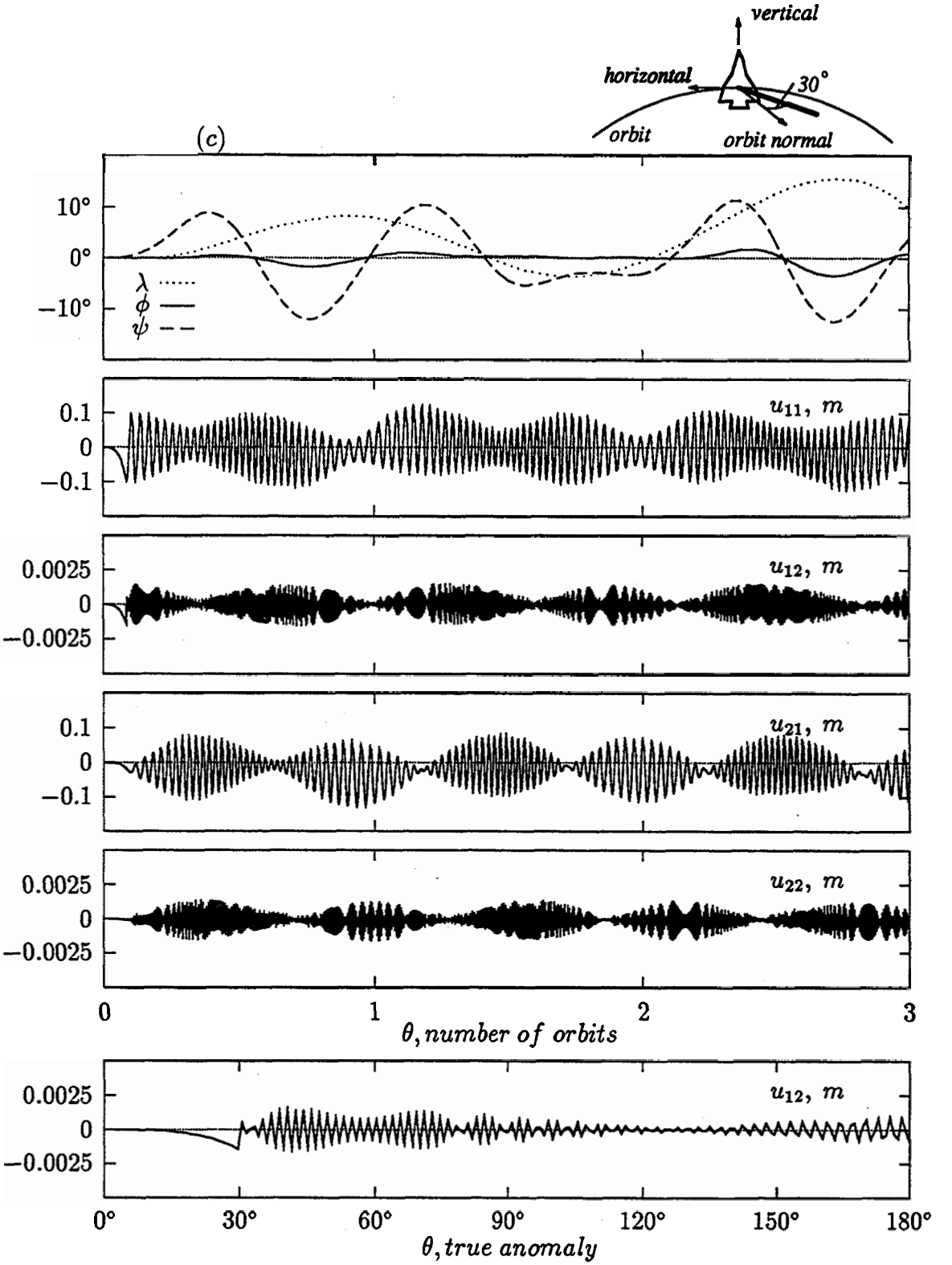

Figure 6-29 Effect of the deployment direction and rate on the system response: (*c*) faster deployment in 7.5 minutes (1/12 orbit) at 30° to the orbit normal in the local horizontal plane.

anomaly in the presence of an orbital eccentricity: higher frequency near the apogee compared to that at the perigee. Ng has also reported such 'frequency condensation'[64]. The phenomenon is associated with the $1 + \epsilon\ cos\theta$ term in the governing equations.

The effect of increased deployment rate by a factor of six (deployment completed in 7.5 minutes) for the case corresponding to (b) is presented in Figure 6-29*c*. Although the pitch motion remains essentially unchanged, all the other motions are significantly accentuated. Of particular concern would be the diverging yaw degree of freedom. Obviously, this would present a challenge in terms of design of a suitable control strategy using the Shuttle's primary and vernier engines.

6.4.2 Slew maneuvers

The proposed Space Station '*Freedom*' will be constructed using around 17–22 flights of the Space Shuttle as mentioned earlier. Integration and deployment of the structural members would involve slew maneuvers. Furthermore, orientation of the directional antenna, solar panels for optimum production of power, telescopes aiming at distant galaxies, etc. involve slewing motions. Thus slewing maneuvers are important aspects of the space based system.

Here two different slewing motions of the beam were considered:

- the beam, originally along the local vertical, going through the 90° slew (about the local horizontal) to occupy the orbit normal position;
- the beam, originally along the local horizontal, going through the 90° slew (about the local vertical) to occupy the orbit normal position.

Both the maneuvers nominally take place in half-orbit. Effects of the faster slew maneuvers (completed in 1/12 of an orbit) are also investigated.

Figure 6–30(a) shows response results during the 90° slew in the local vertical plane for the nominal slew duration of 45 minutes (1/2 orbit). The corresponding tip deflection is shown in Figure 6-30*b*). Here u_2 represents the tip deflection in the local horizontal direction and u_1 is perpendicular to u_2, both in centimeter. Note, the sense of u_1 is changing, from normal to the orbit plane at the begining of the slew, to the local vertical at the end of it. Effect of the faster slew (1/12 orbit) is presented in Figure 6–30*c*. Corresponding results for the slew maneuver in the local horizontal plane are given in Figure 6–31. It is apparent that:

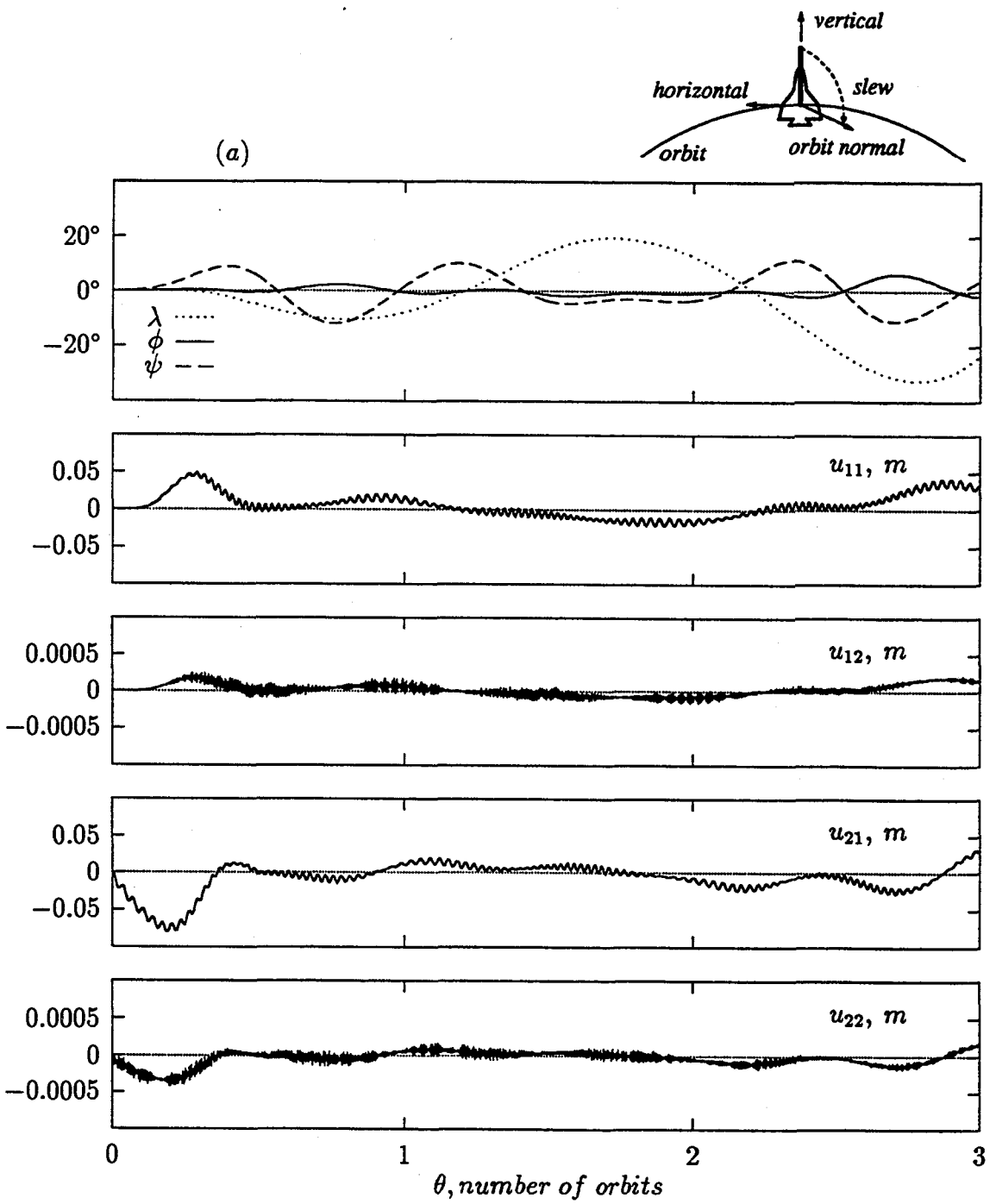

Figure 6-30 The system response during a 90° slew maneuver in the local vertical plane: (*a*) the maneuver completed in 1/2 orbit.

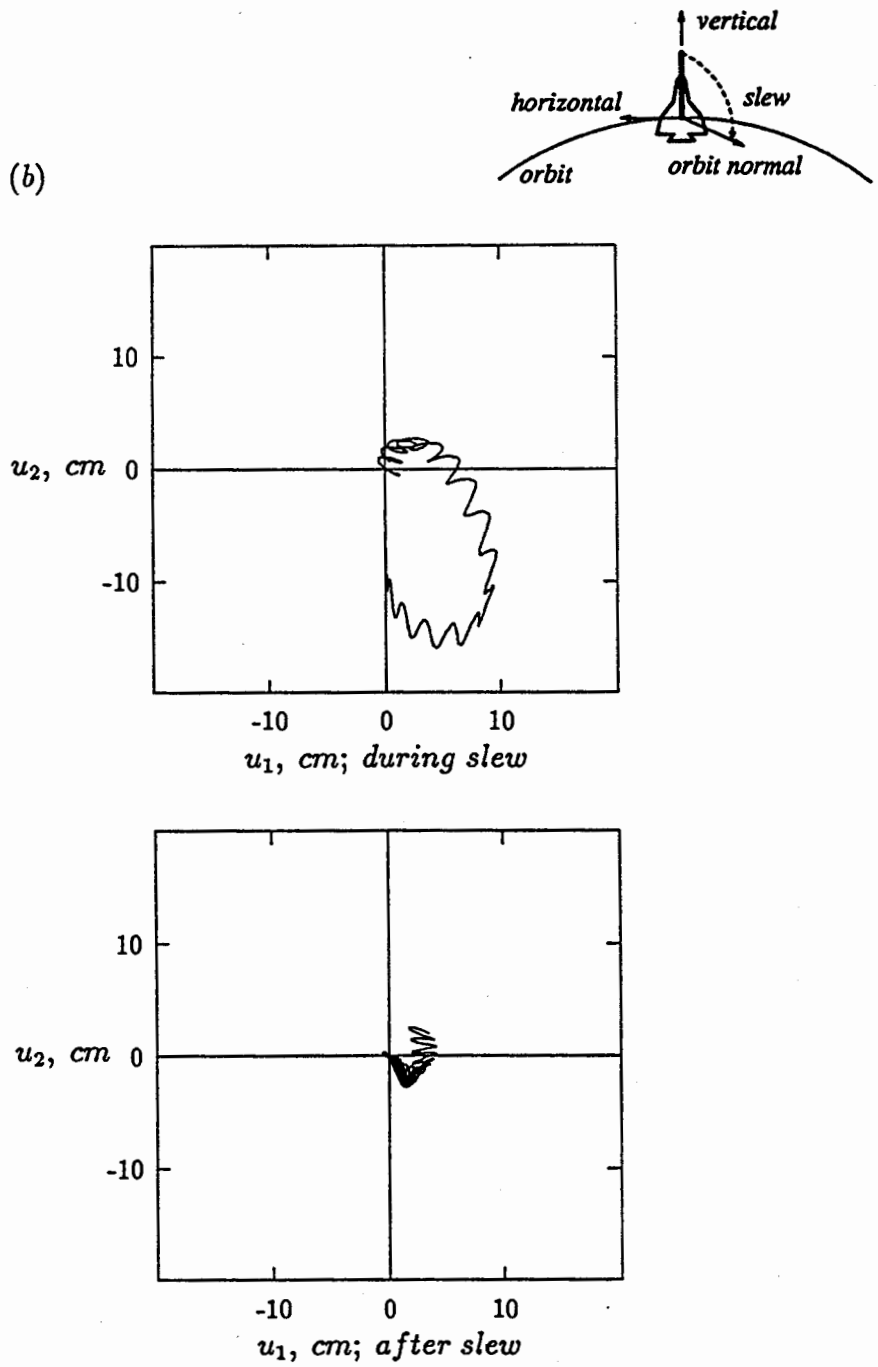

Figure 6-30 The system response during a 90° slew maneuver in the local vertical plane: (*b*) tip deflection.

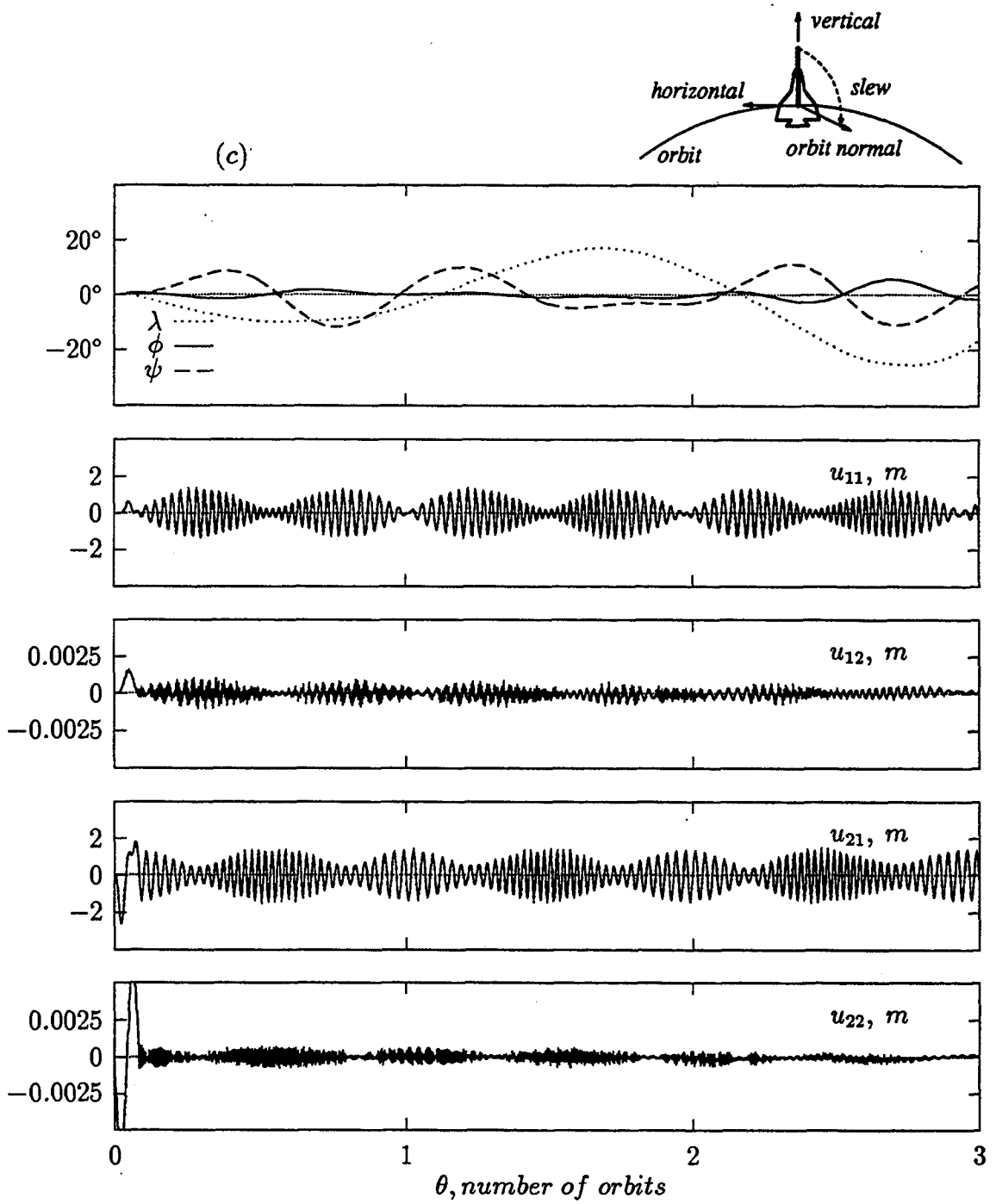

Figure 6-30 The system response during a 90° slew maneuver in the local vertical plane: (c) the maneuver completed in 1/12 orbit.

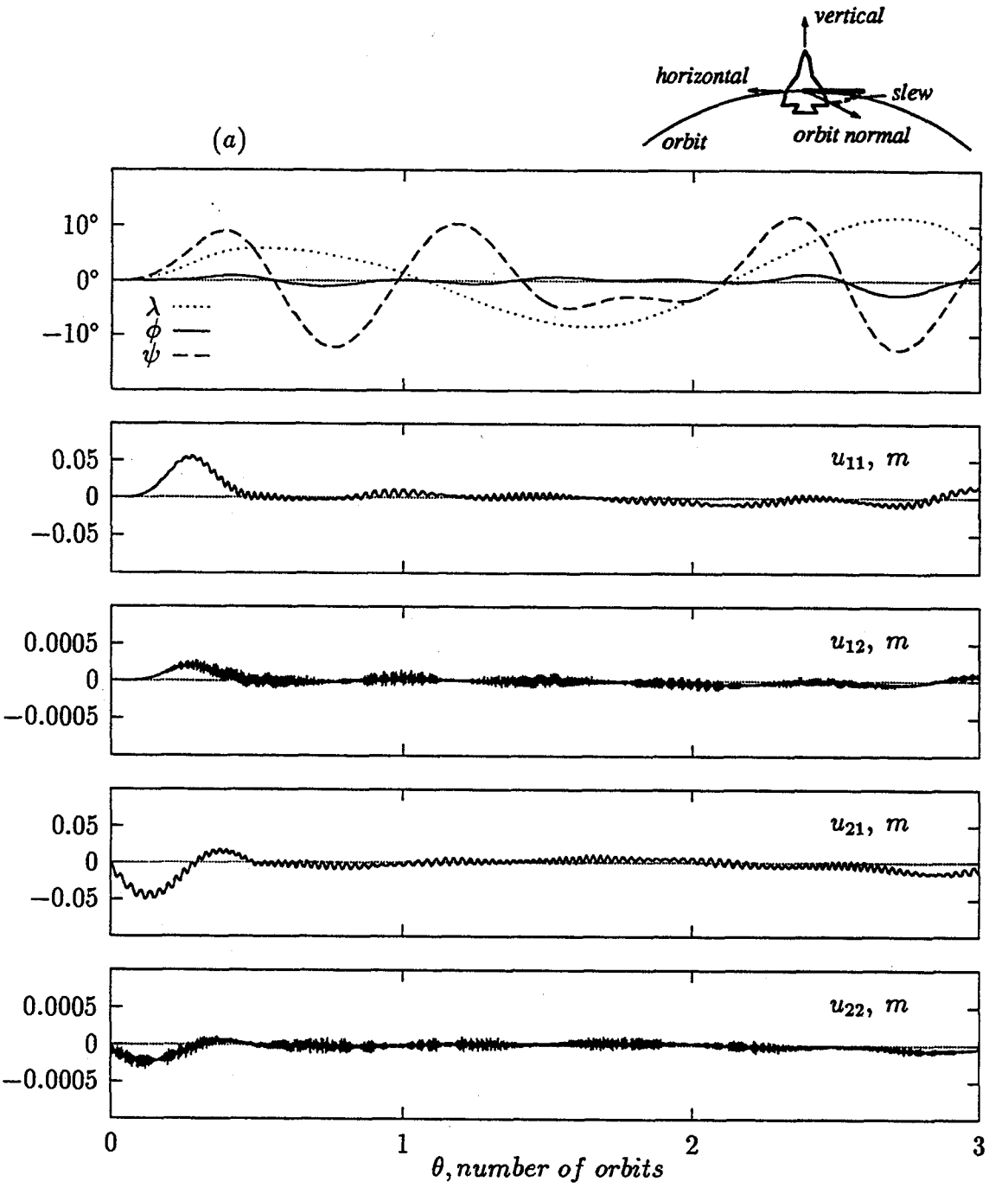

Figure 6-31 Effect of a 90° slew maneuver, of the Space Shuttle based beam, in the local horizontal plane. The maneuver completed in: (a) 1/2 orbit.

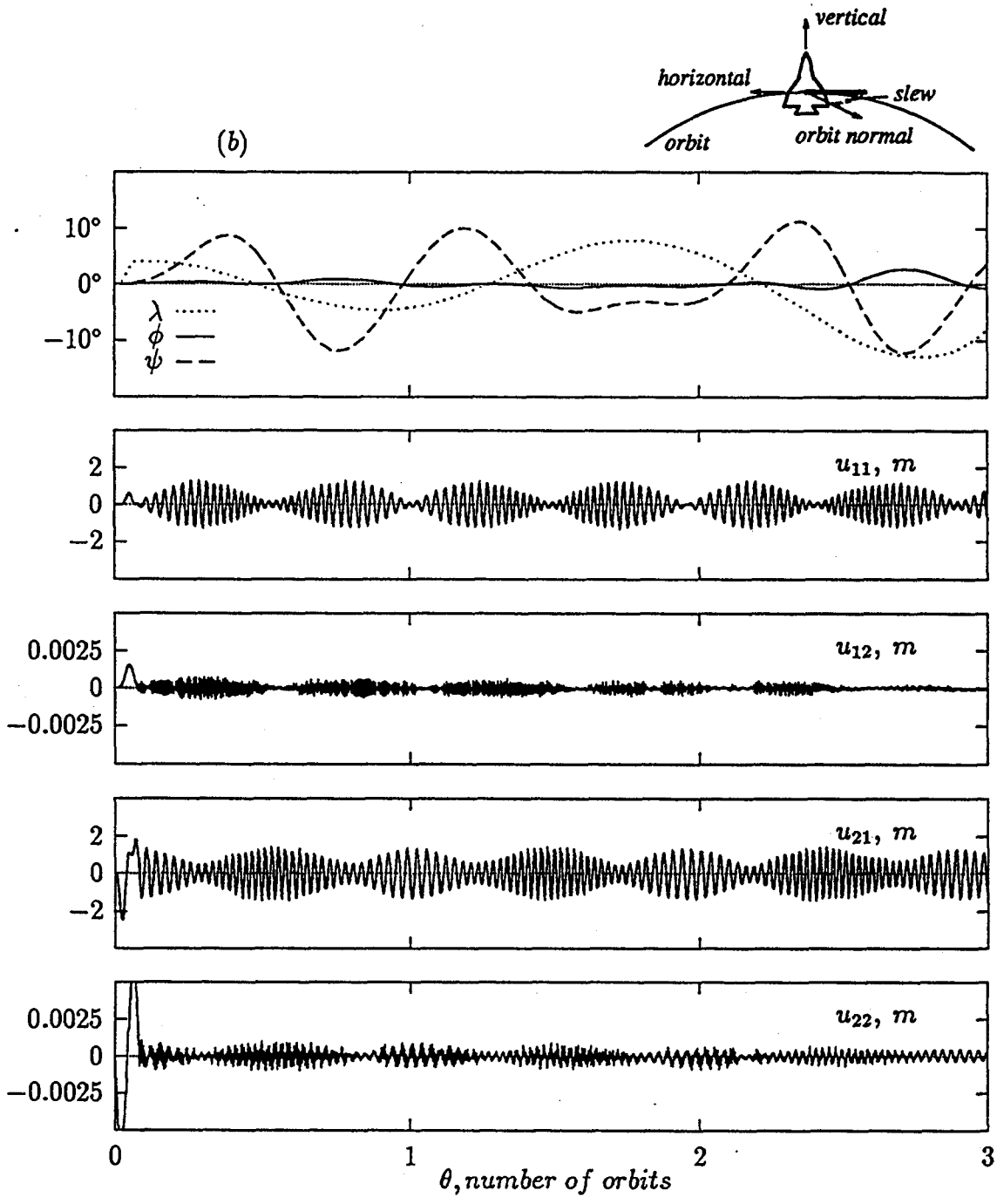

Figure 6-31 Effect of a 90° slew maneuver, of the Space Shuttle based beam, in the local horizontal plane; the maneuver completed in: (*b*) 1/12 orbit.

- The maneuvers excite relatively large motion in yaw, particularly during the slew in the local vertical plane.
- Vibrational response of the beam, in general, is small. It is almost negligible in the second mode. The faster maneuver accentuates the response, significantly, by at least an order of magnitude.
- As in the case of the deployment, the beat response is present due to coupling between the transverse vibrations.

6.4.3 Combined deployment and slew

Figure 6–32 shows the system response during the combined deployment and slew maneuvers. Two cases are considered:

(a) simultaneous deployment from 3 m to 33 m and a 90° slew from the local vertical to the orbit normal;

(b) simultaneous deployment from 3 m to 33 m and a 90° slew from the local horizontal to the orbit normal.

In both the cases, the deployment and slew maneuvers are completed in 1/2 orbit.

The pitch response is virtually the same as in the case of pure deployment (Figure 6-27), however the out-of-plane librations (roll, yaw) and vibrations are distinctly smaller (Figures 6–30(a) and 6–31(a)). The response in the second mode is too small and hence purposely not shown. Figure 6-33 presents the tip deflection for both the cases, (a) and (b).

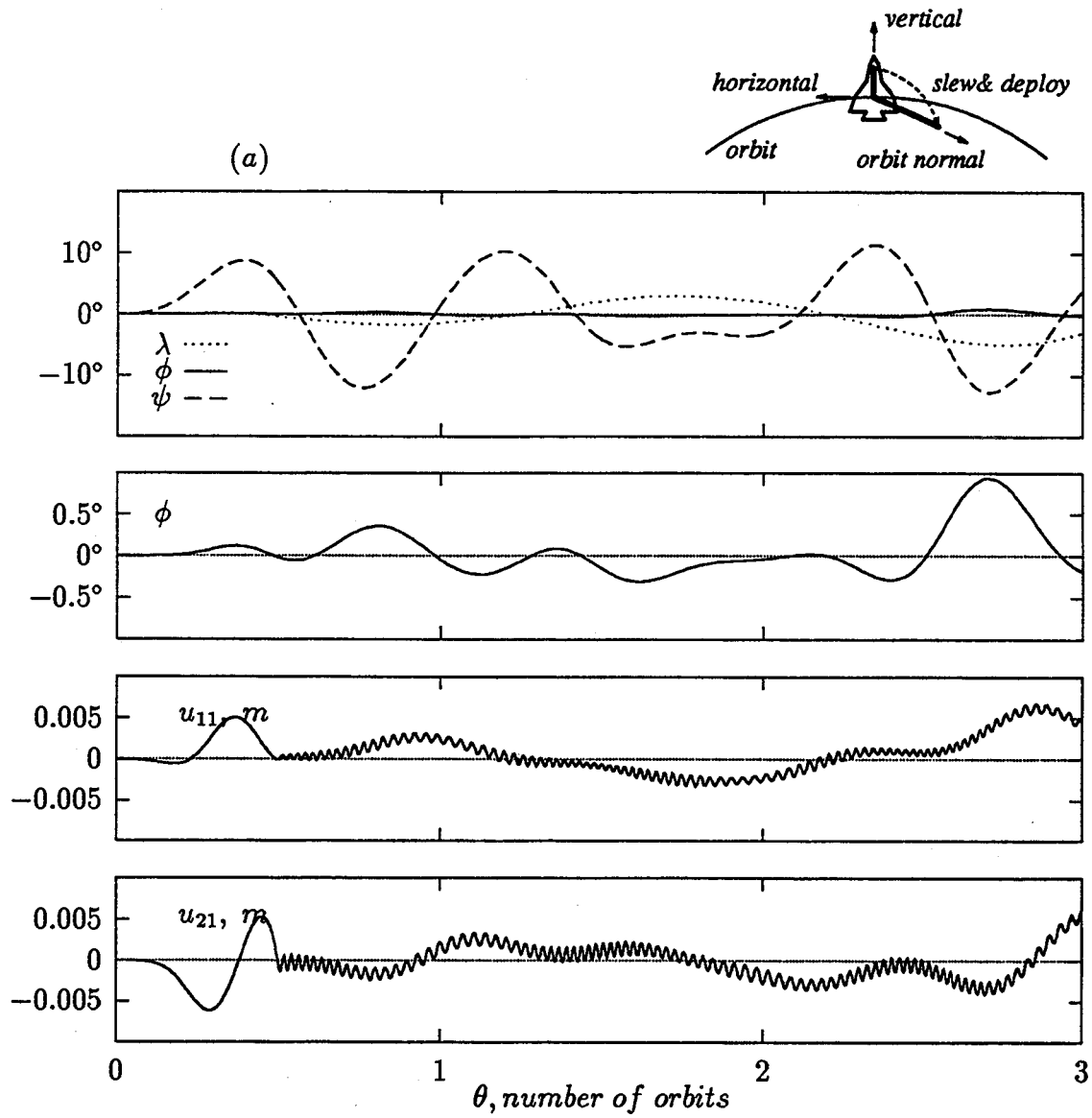

Figure 6-32 System Response during the combined deployment and slew in 1/2 orbit: (*a*) from local vertical to orbit normal.

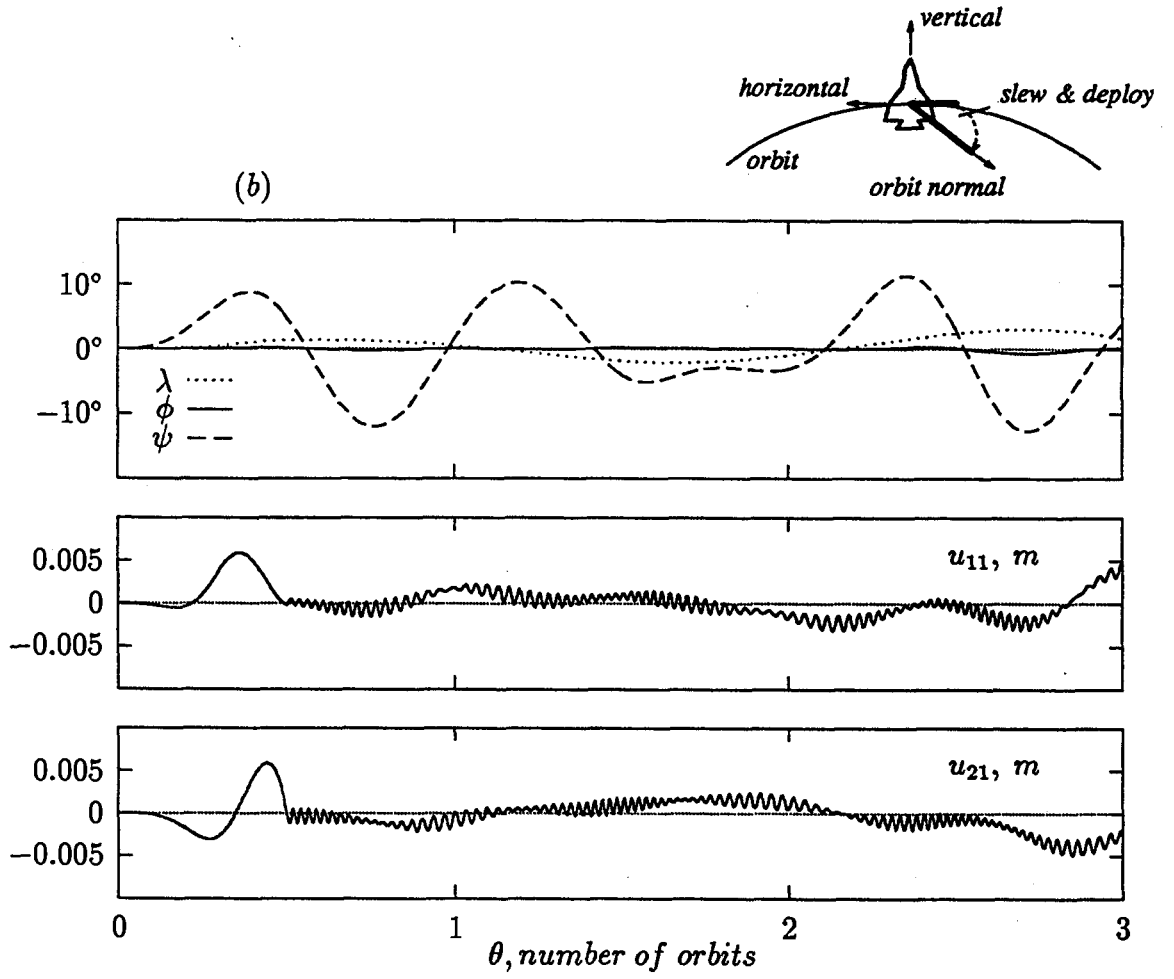

Figure 6-32 System Response during the combined deployment and slew in 1/2 orbit: (b) from local horizontal to orbit normal.

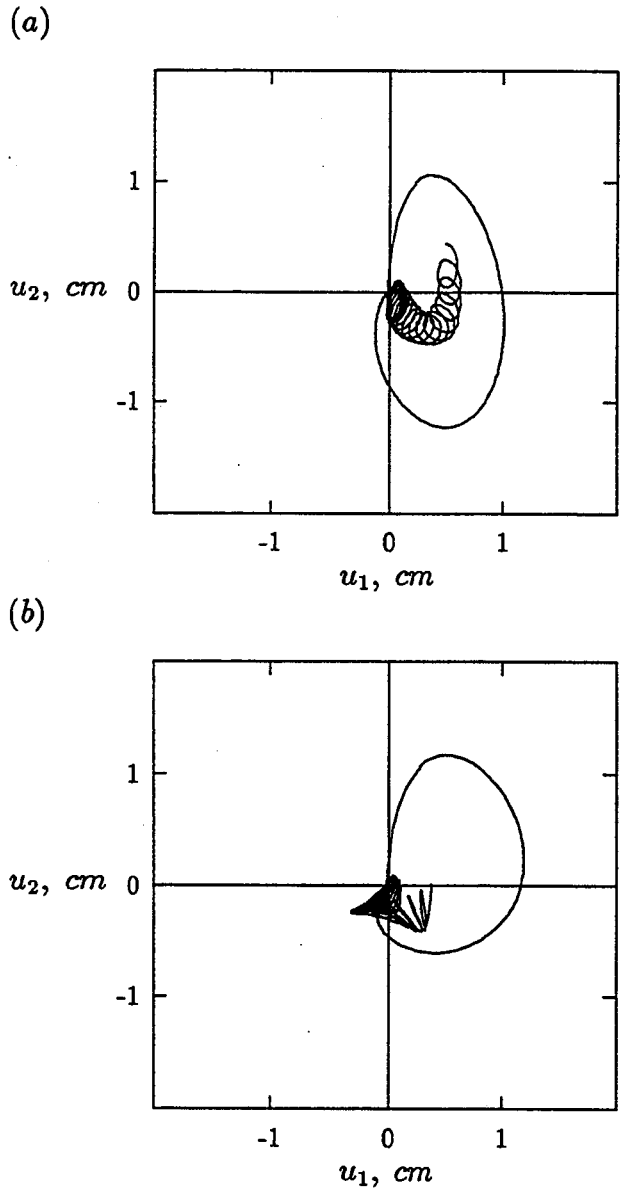

Figure 6-33 Tip deflection of the beam during the simultaneous deployment and slew maneuvers in 1/2 orbit: (a) from local vertical to orbit normal; (b) from local horizontal to orbit normal. The response is over one orbit.

6.5 Two–Dimensionally Deployable Array Experiment: Slew Maneuvers

The third example pertains to an experiment to be conducted using the Space Flyer Unit mentioned earlier. It is one of the first experiments aimed at dynamics and control of flexible structural members in space. Referred to as the Two–Dimensionally Deployable Array Experiment, it involves deployment of an initially stowed membrane like structure, strengthened by a grid of cables and supported through a pair of orthogonal deployable truss-type members (Figure 6-34). Unfolding of the membrane like structure is brought about through simultaneous deployment, in two directions, along the diagonal of the 6 m square array. Objective is to study vibration characteristics, damping properties and control of flexible structures in space. Eventually, one would like to predict their performance through numerical simulation. Thus development of the algorithm in present thesis is ideally suited for application to the proposed experiment of considerable contemporary interest.

The numerical values used in the simulation are listed below:

Orbital motion:

$$\begin{aligned} \textit{orbit eccentricity } (\epsilon) &= 0\ ; \\ \textit{altitude} &= 300\ km\ ; \\ \textit{period} &= 90\ min.\ . \end{aligned}$$

Central body:

$$\begin{aligned} \textit{mass } (m_0) &= 4000\ kg\ ; \\ I_{xx} &= 4250\ kg\text{-}m^2\ ; \\ I_{yy} &= 9290\ kg\text{-}m^2\ ; \\ I_{zz} &= 11150\ kg \cdot m^2\ ; \\ \textit{length} &= 5\ m\ . \end{aligned}$$

Array structure:

$$\begin{aligned} \textit{mass } (m_1) &= 90\ kg\ ; \\ \textit{length of each side} &= 6\ m\ ; \\ \textit{flexural rigidity } (D) &= 1643\ kg \cdot m^2/s^2\ . \end{aligned}$$

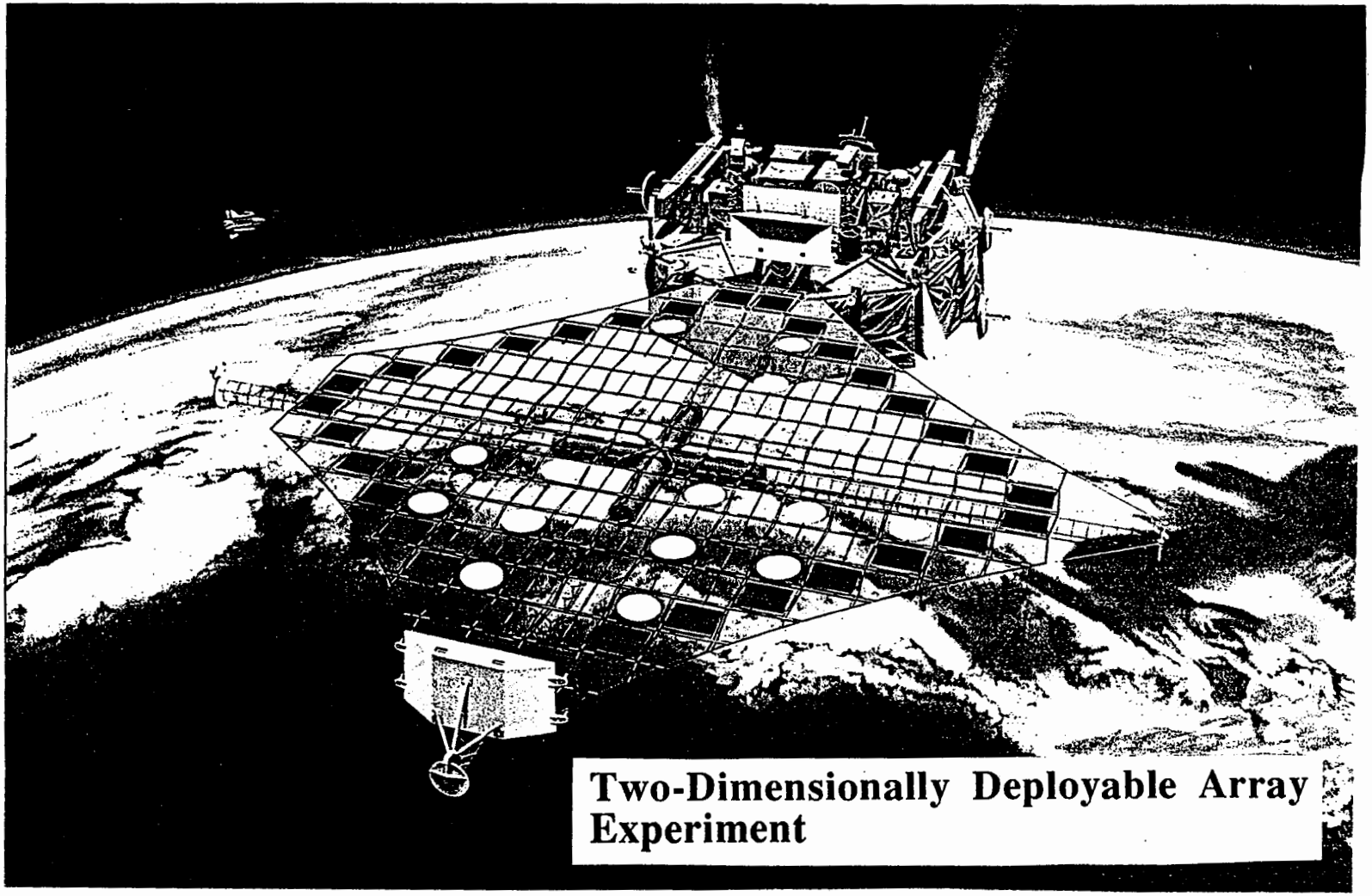

Figure 6-34 A schematic diagram of the two–dimensionally deployable array experiment to be carried out by the Space Flyer Unit (SFU) in late 1994.

(Provided by the Department of Mechanical Engineering, University of British Columbia)

The array structure is assumed to have uniform thickness. The first bending mode of a cantilever rectangular plate is used to represent the deformation of the array structure. Note, the modal integrals are different here from those for the rectangular plate case. The generalized coordinate is u, representing half the tip deflection.

The objective here is to predict the response of the system during slew maneuvers of the array. The slew maneuvers take place about the pin joint at the central body, which is in the plane of the array structure. Five nominal orientations and slew maneuvers examined are summarized below:

Orientation A:

The array structure is perpendicular to the orbital plane and slews about the diagonal truss aligned with the orbit normal at an orbital rate of 4°/minute to track the sun (Figure 6-35). This may be referred to as the sun tracking maneuver.

Orientation B:

The array is nominally in the local vertical, local horizontal-plane LV,LH-plane, i.e. the orbital plane) with its diagonal truss along the local vertical and directed towards the earth. The slew maneuvers take place in the direction normal to the orbital plane and about the local horizontal.

Orientation C:

Nominally, the array is in the local vertical, orbit normal LV,ON-plane with its diagonal truss towards the earth (i.e. aligned with the local vertical). The slew maneuvers take place in the orbital plane and about the orbit normal.

Orientation D:

The nominal position of the array is in the LV,LH-plane with its diagonal truss along the local horizontal. The slew maneuver is normal to the orbital plane and about the local vertical.

Orientation E:

The array is in the local horizontal, orbit normal LH,ON-plane with its diagonal truss along the local horizontal. The slew maneuvers take place in the orbital plane through rotation about the orbit normal.

The Orientations B, C, D and E are shown in Figure 6-36. Except for the Orientation A, the major axis of the central body is aligned with the orbit normal, and the minor axis with the local vertical; i.e. it is in a stable equilibrium.

Two types of slewing maneuvers are considered for the Orientations B to E:

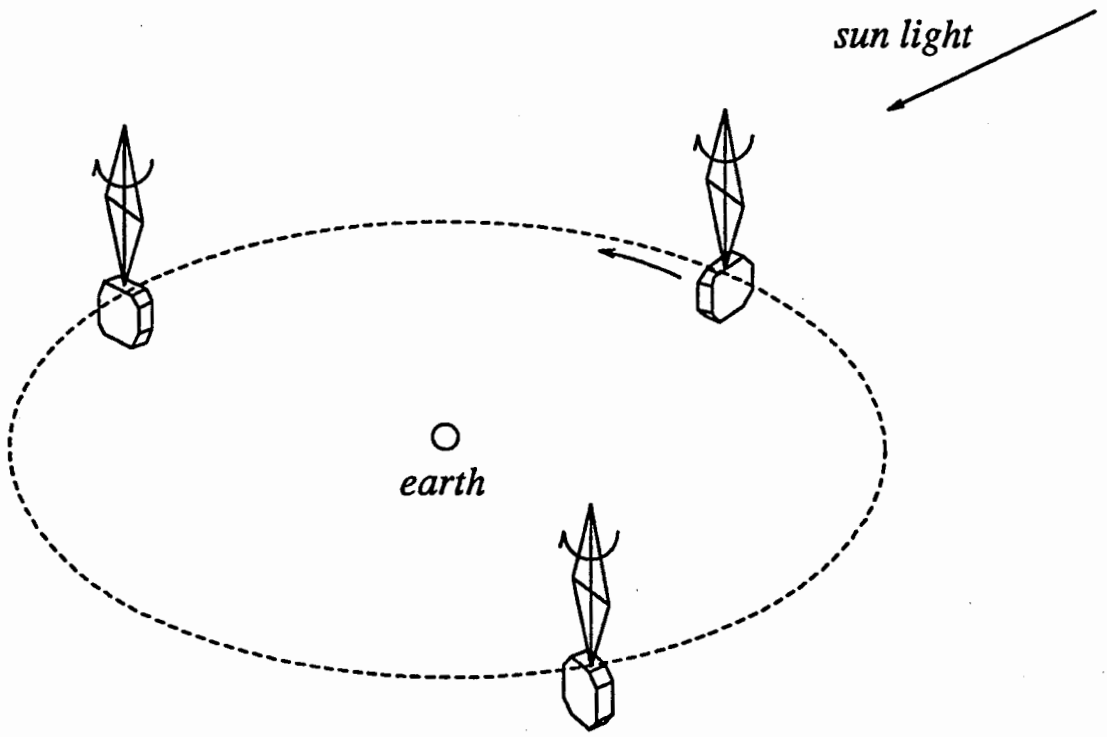

Figure 6-35 The sun-pointing structural array involving slewing around the orbit normal at the orbital rate.

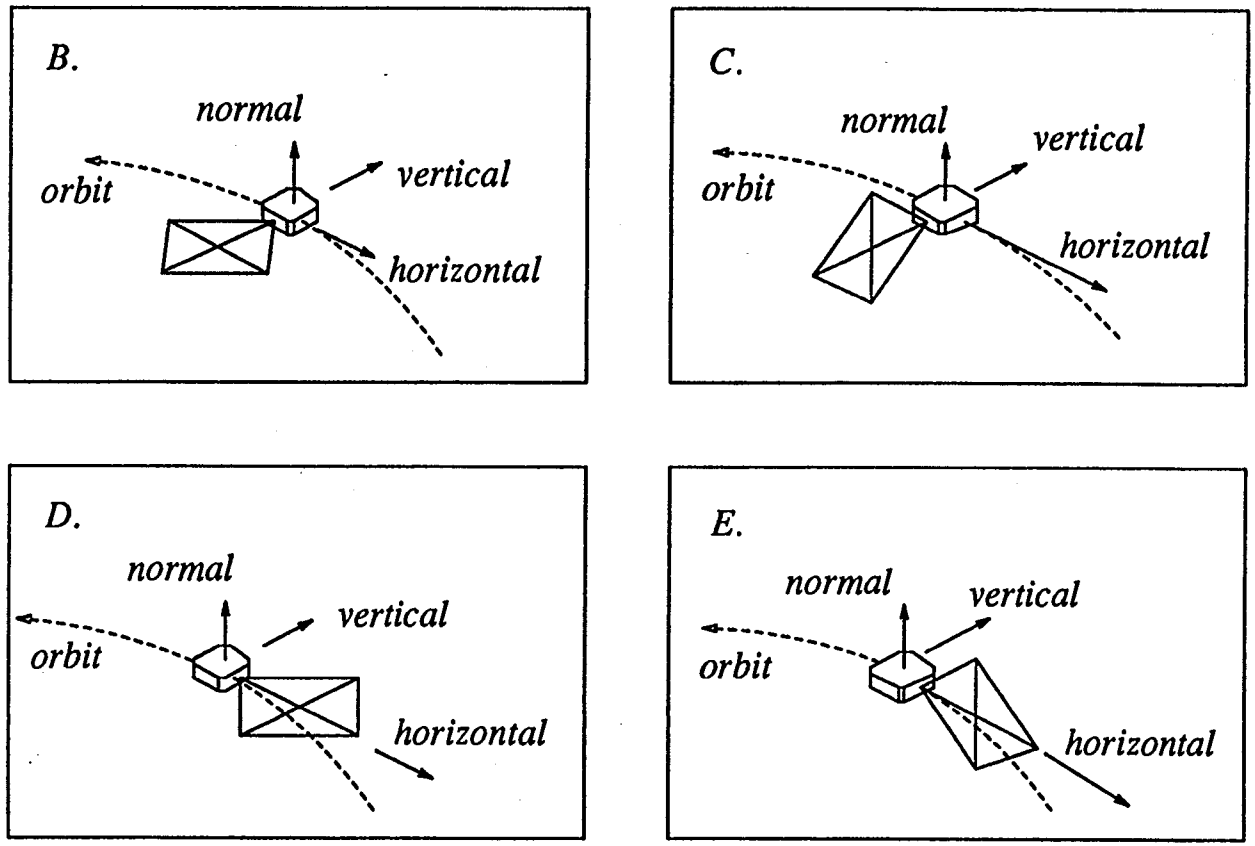

Figure 6-36 Schmatic diagrams showing the B, C, D, E Orientations of the Space Flyer Unit with the two–dimensionally deployable array.

- The array originally has a 90° deviation from its nominal position and slews through 90° to return to the nominal position.

- The array initially oriented at −30° from its nominal position, slews through 60° to occupy +30° position w.r.t. the nominal configuration. Thus neither the initial nor the post-slew orientation represents the equilibrium state.

.The slew maneuvers are nominally completed in 15 minutes (1/6 orbit). To study the influence of faster slew, maneuvers completed in 1 minute (4° variation of the true anomaly) are also considered .

Orientation A:

Figure 6-37 shows response of the array under two different disturbances. During tracking of the sun (Figure 6-37*a*), only the librational motion in the pitch, with a relatively large amplitude of 5°, is excited. The roll, yaw degrees of freedom as well as the elastic deformation of the array are zero. The situation changes dramatically when a small initial disturbance (i.e. in addition to the sun tracking slew maneuver) through the array tip deflection of 0.4 m ($2u = 0.4$) transverse to its plane is introduced. Now all the three librational degrees of freedom are excited with system becoming unstable in yaw due to its coupling with the roll generalized coordinate. This also emphasizes inherently unstable character of the equilibrium in Orientation A, where the maximum moment of inertia axis is in the orbital plane and the minimum moment of inertia axis is along the orbit normal.

Orientation B:

Response of the system, occupying the Orientation B, to slew maneuvers normal to the orbital plane is shown in Figures 6-38 and 6-39. The array maneuvers from −30° to +30° in 15 minutes, passing through the nominally stable equilibrium Orientation B, as explained before. As in the case of the Orientation A, two cases are considered: response in absence of the initial array tip disturbance (Figures 6-38*a*); and with the transverse tip disturbance $2u$ of 0.4 m (Figure 6-38*b*). The following observations can be made:

- Slew maneuvers normal to the orbital plane excite all the three librational degrees of freedom. In particular, the roll, yaw responses are relatively larger in magnitude compared to the pitch. This is understandable as the maneuver is about the roll axis (local horizontal) and a strong coupling exists between the

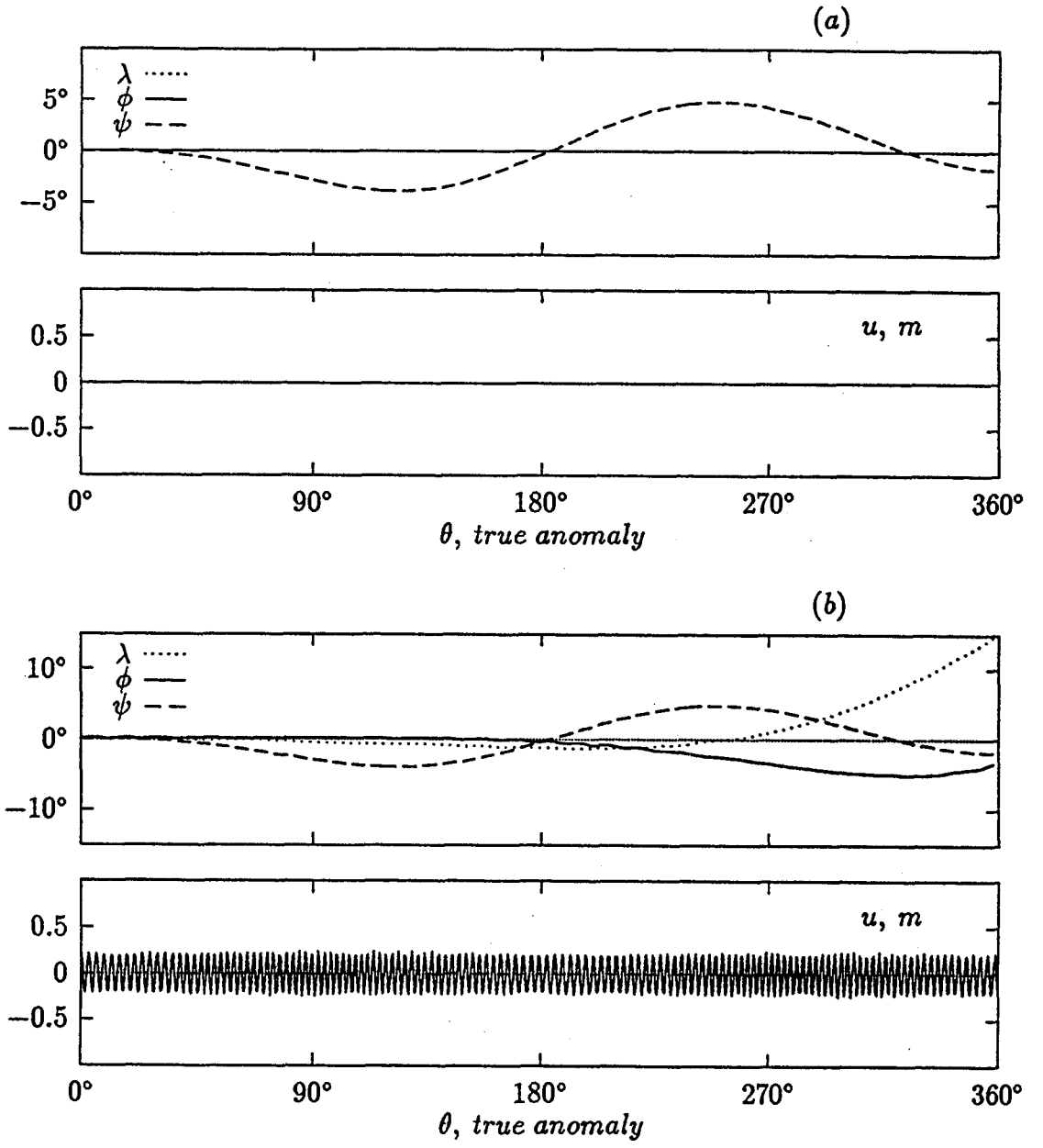

Figure 6-37 System response during the sun tracking maneuver at a constant rate of 4°/minute: (*a*) in absence of any initial array tip disturbance; (*b*) the array subjected to an initial tip deflection of 0.4 m.

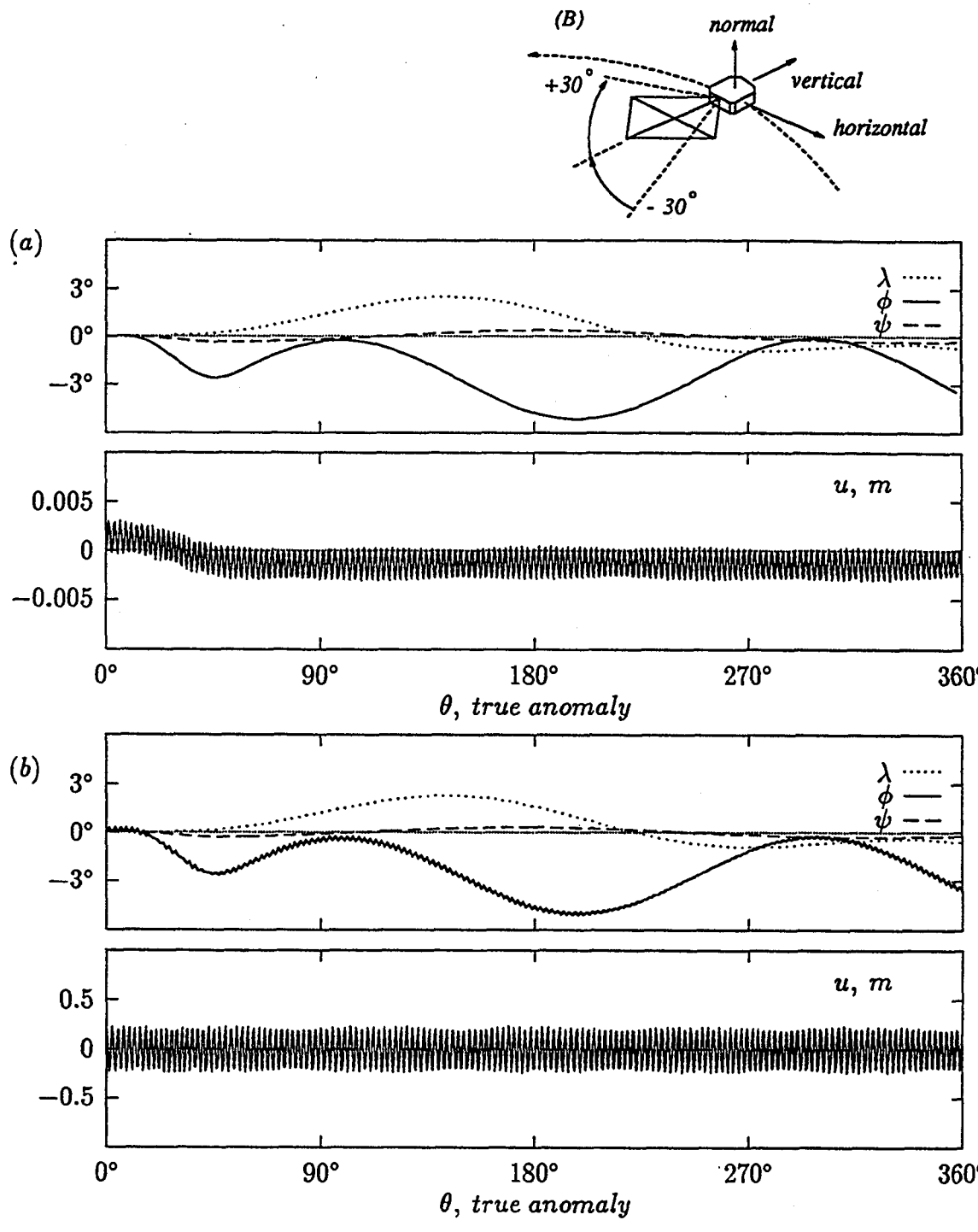

Figure 6-38 Response of the system to the array slew maneuver normal to the orbital plane. The array slews from $-30°$ to $+30°$ passing through the nominal equilibrium of the Orientation B: (a) in absence of a tip disturbance; (b) the tip of the array displaced transversely by 0.4 m initially.

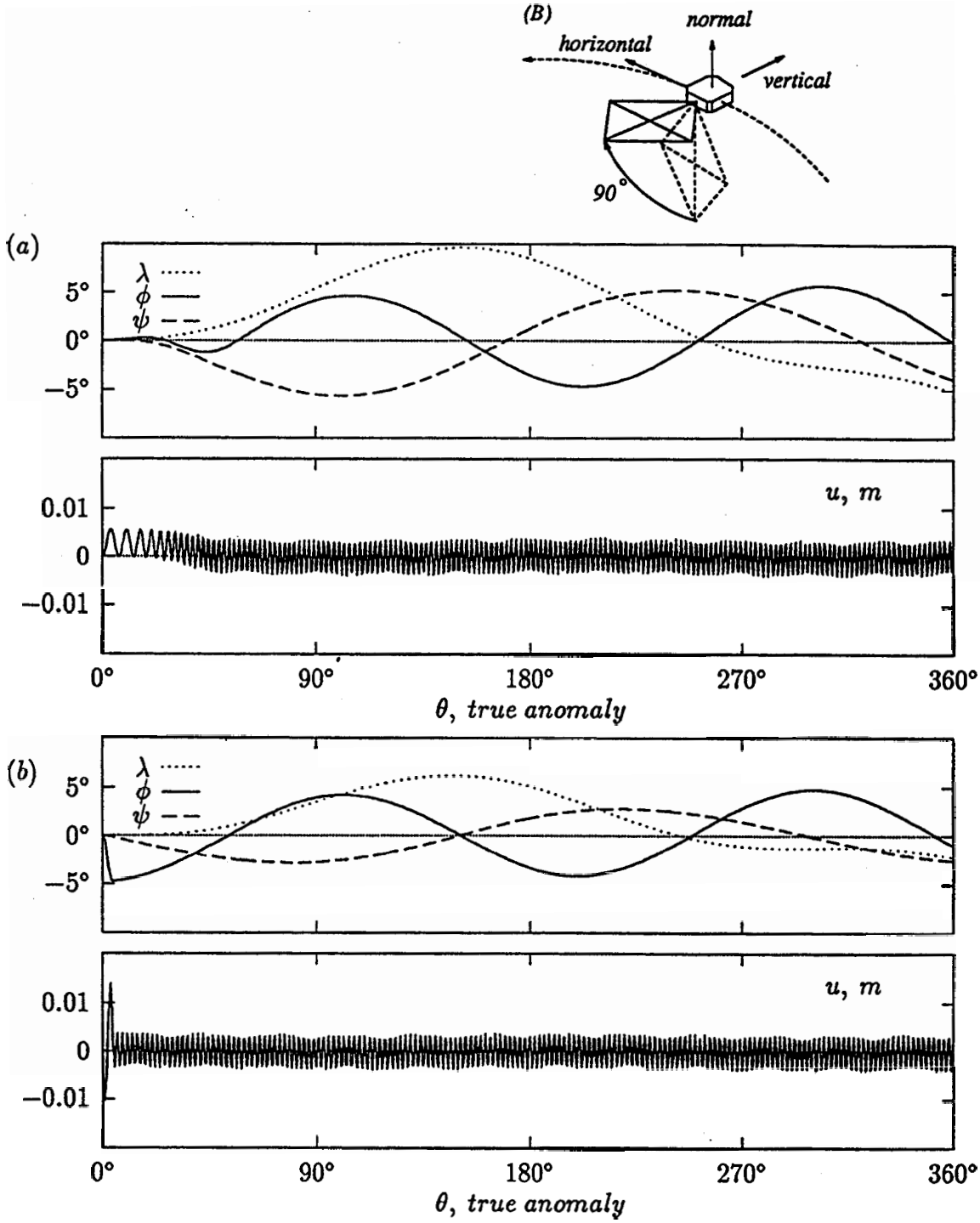

Figure 6-39 Response of the system to 90° slew maneuvers of the array towards the nominal Orientation B. The maneuver is completed in: (*a*) 15 minutes; (*b*) 1 minute.

roll and the yaw degrees of freedom. The vibratory motion of the panel is extremely small (Figure 6-38a) due to widely separated librational and vibrational frequency spectra.

- Vibratory disturbance of the panel does not affect, significantly, overall character of the response, except for the small high frequency modulations of the roll libration.

Effect of the slewing rate on the system response is studied in Figure 6-39. The array, initially in the LH,ON-plane, slews through 90° to return to the nominal Orientation B. Two slewing rates are considered: maneuver completed in 15 minutes (i.e. 1/6 of the orbit, Figure 6-39(a)); and a faster rate with the maneuver completed in 1 minute (i.e. in 4° of the orbital motion, Figure 6-39(b)). As can be expected, the larger magnitude of the slewing angle (90° compared to 60° in the previous case) leads to both increased librational and vibrational amplitudes. This may affect the system mission suggesting a need for active control. In fact, the system may become unstable in yaw through its coupling with roll as seen before in Figure 6–37(b). However, for that information, response results will have to be obtained over a longer duration. This will demand higher computational effort and cost.

The effect of the faster rate is to reduce the librational response as the system quickly returns to the nominal equilibrium state.

Of particular interest is the change in frequency during the slewing maneuver. It is interesting to see how the gravitational force stiffens the panel as it approaches the LV,LH-plane.

Orientation C

Performance of the system during the inplane slew maneuvers is indicated in Figures 6-40 and 6-41. Figure 6-40 considers the effects of the extent of the maneuver: (a) from $-30°$ to $+30°$; and (b) from $-90°$ to $0°$, i.e. returning to the nominal equilibrium orientation from the LH,ON-plane. The effects of the speed of the maneuver and the initial panel tip deflection are studied in Figure 6-41, for the 90° slew case. Based on the results following general comments can be made:

- Maneuver in the orbital plane (inplane slew) excites only the librational motion in pitch. Vibratory motion of the panel remains rather small. Even for a 90° slew the tip amplitude is around 1 cm (Figure 6-40(b)).

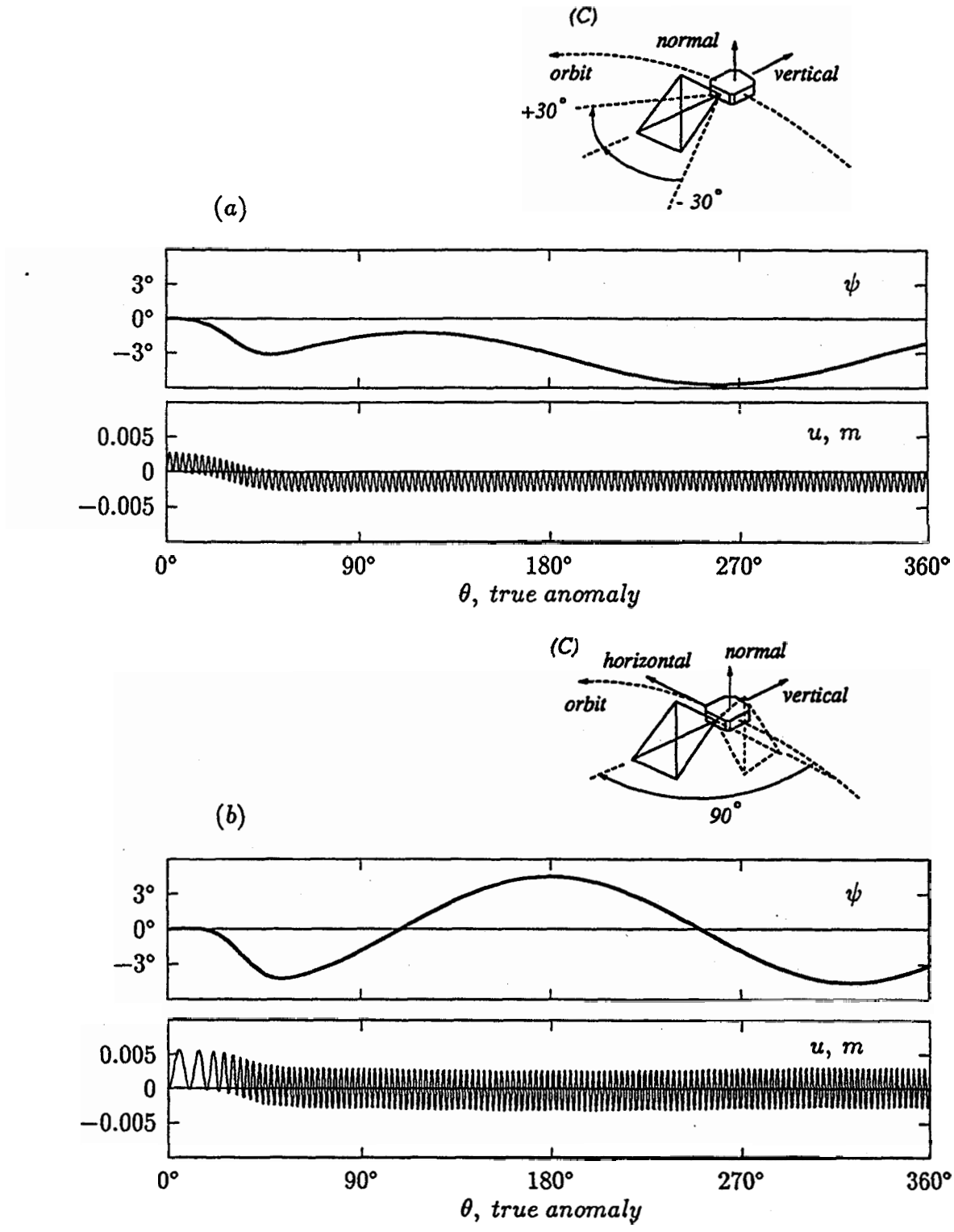

Figure 6-40 Typical response of the system, in the nominal Orientation C, to inplane slew maneuvers: (a) the array slews from $-30°$ to $+30°$ passing through the Orientation C: (b) the array slews through 90° to occupy the nominal Orientation C. Both the maneuvers are completed in 15 minutes.

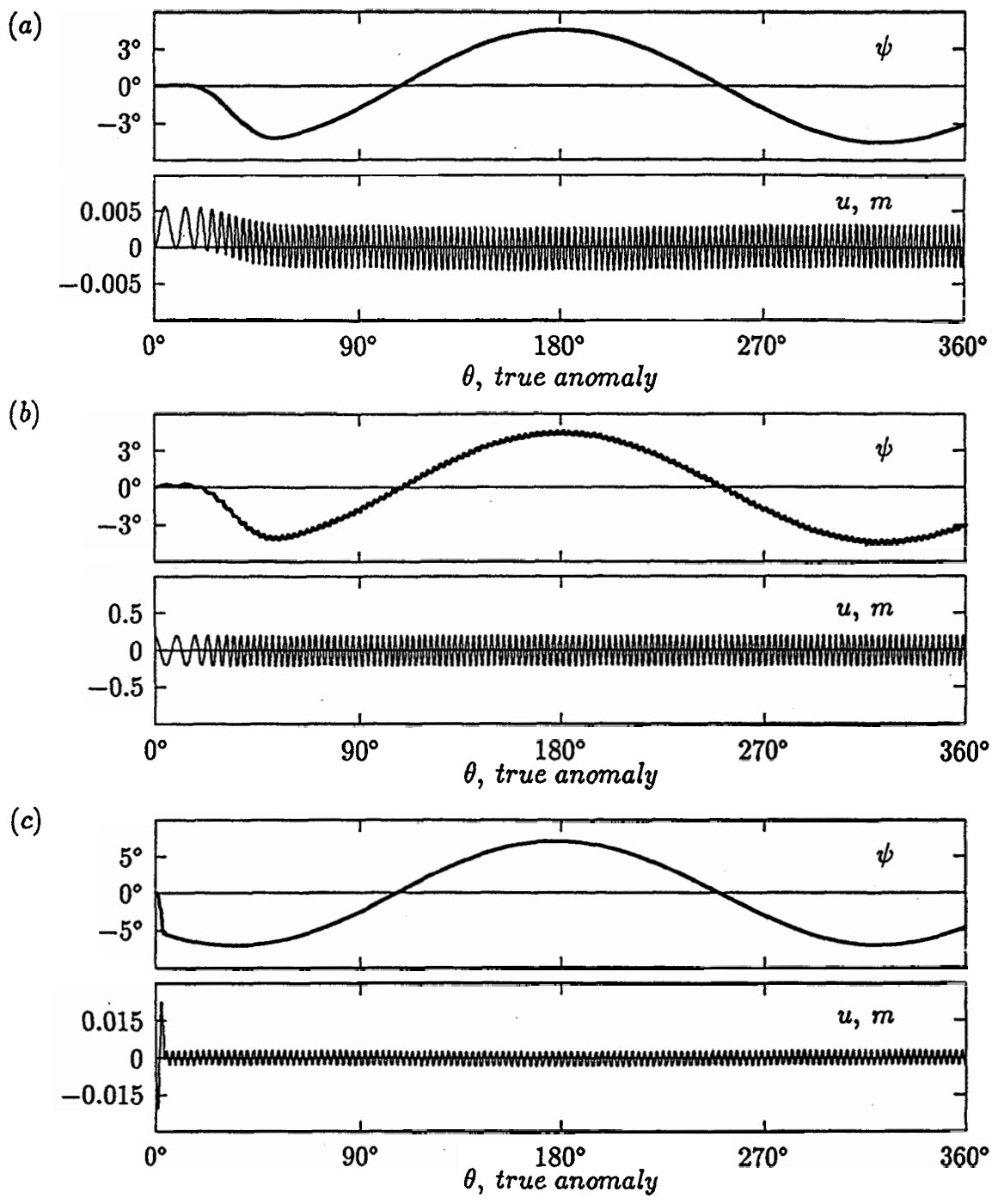

Figure 6-41 Effect of speed and tip deflection during a 90° slew of the panel with the system in the Orientation C: (*a*) the maneuver completed in 15 minutes; (*b*) the maneuver completed in 15 minutes with the tip of the array deflected by 0.4 m initially; (*c*) the maneuver completed in 1 minute.

- Stiffening of the panel due to gravitational field is again apparent (as in the case of the Orientation B) when the panel approaches the LV,ON-plane.

- A comparison of the results in Figures 6-41(a) and 6-41(c) suggests that faster slew maneuvers lead to larger amplitude pitch, however the vibratory response is not significantly affected.

- The effect of the panel tip disturbance is confined to small amplitude high frequency modulations of the pitch response.

Orientation D

To recollect, in the Orientation D, the array is in the LH,LV-plane with the diagonal truss along the local horizontal. Figures 6-42 and 6-43 show the system response during out of the orbital plane maneuvers about the local vertical. As seen before, the out-of-plane maneuvers excite all the three librational degrees of freedom: pitch, roll and yaw. As before, the two different slewing maneuver magnitudes are considered in Figure 6-42: $-30°$ to $+30°$ about the nominal equilibrium position (Figure 6-42a); and 90° from the LV,ON-plane to regain the nominal Orientation D (Figure 6-42b). Figure 6-43b considers the same 90° maneuver completed at a faster rate (15 times faster; in 1 minute instead of a nominal time of 15 minutes). Effect of initial tip displacement of the array is also assessed (Figure 6-43a). The results suggest the following trends:

- As the maneuvers are around the local vertical, the dominant librational motion is the yaw. On the other hand, the pitch inertia being the highest, the corresponding motion about the orbit normal is the least sensitive.

- The large magnitude yaw response in the presence of significant roll suggests a possibility of instability.

- The faster maneuver can lead to, during the period of the maneuver, reasonably large panel tip deflection (Figure 6-43b). In the present case, with the 90° maneuver completed in 1 minute, the displacement reached an amplitude of around 3.5 cm before reaching a steady state value of 0.4 cm.

- The effect of initial tip displacement during the slew maneuver is to superpose high frequency, negligibly small amplitude modulations on the yaw response.

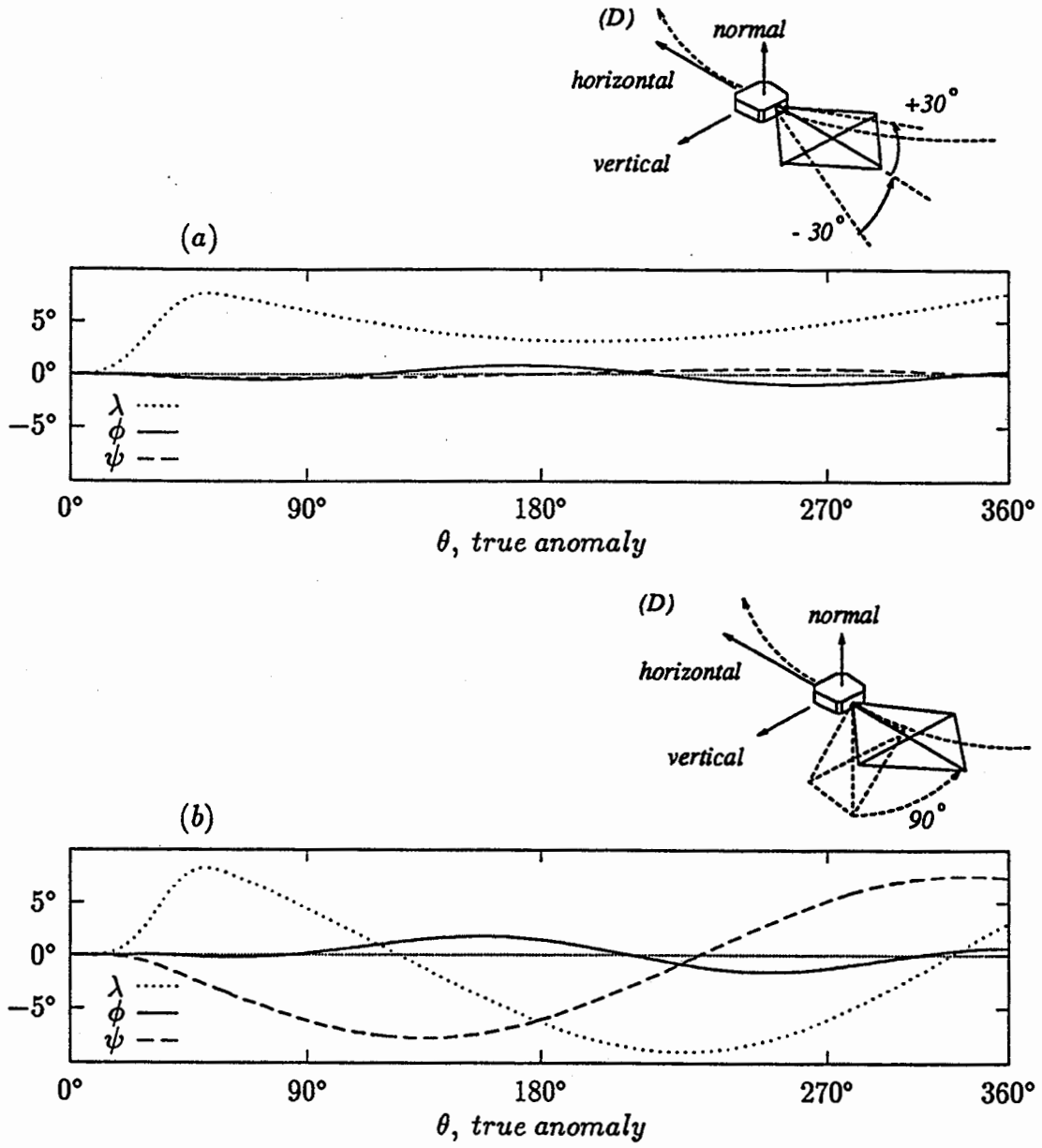

Figure 6-42 Librational response during two typical slew maneuvers completed in 15 minutes: (*a*) the array slews from −30° to +30° about the local vertical; (*b*) 90° slew normal to the orbital plane to regain the nominal equilibrium of the D Orientation. The vibratory response, being negligible, is purposely not shown.

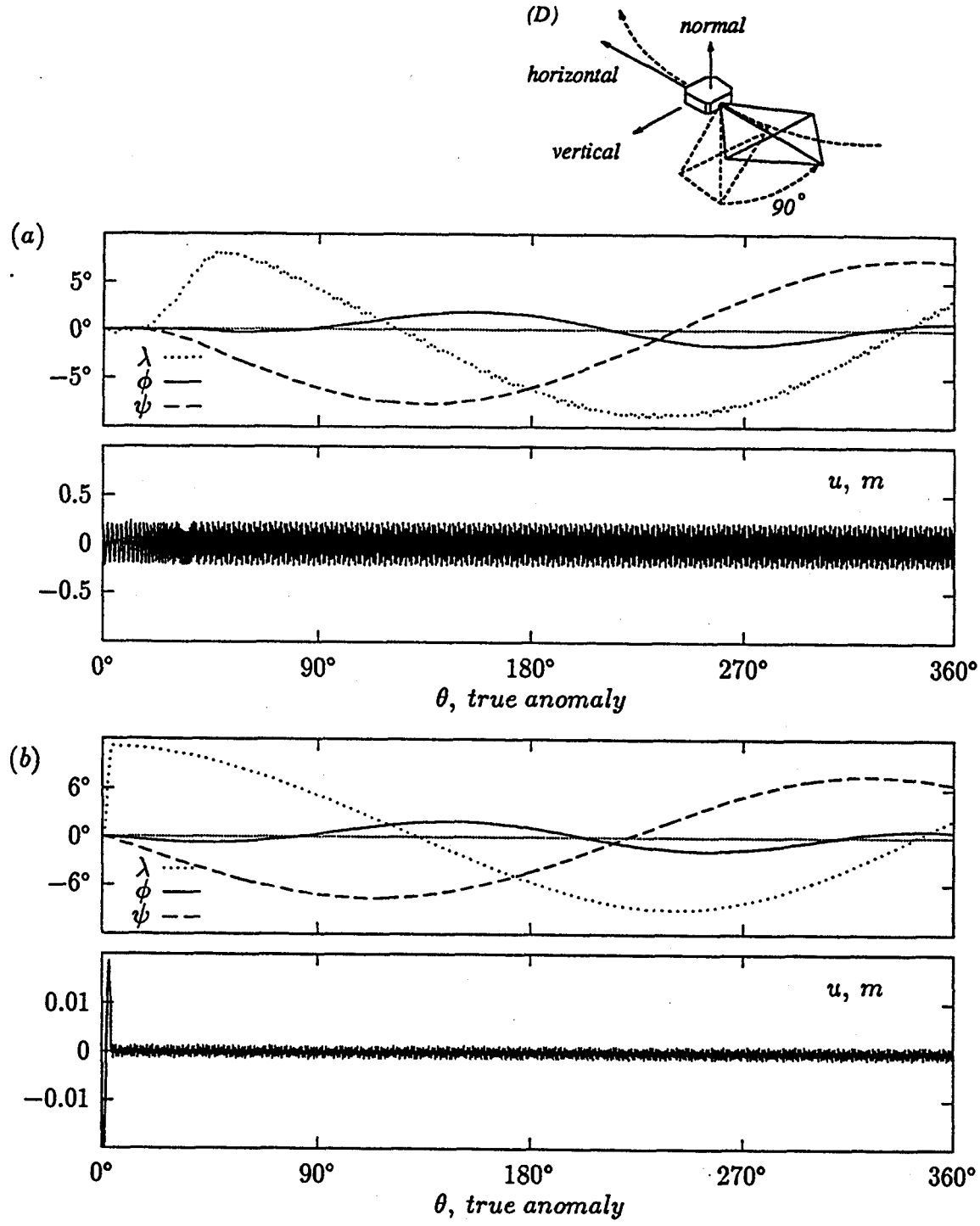

Figure 6-43 Response of the system to 90° slew maneuvers normal to the orbital plane to occupy the nominal D Orientation: (*a*) the maneuver completed in 15 minutes and the array subjected to an initial tip deflection of 0.4 m; (*b*) the maneuver completed in 1 minute without the tip disturbance.

Orientation E

In this case, the array nominally in the LH,ON-plane, undergoes slew maneuvers about the orbit normal, i.e. in the orbital plane. The results are presented in Figures 6-44 and 6-45. As can be expected, the inplane slew excites only the pitch motion, rather large in amplitude ($\approx 17°$). It serves as the forcing function for the panel which oscillates at the same frequency as the pitch libration with the minute modulations at the panel frequency superposed.

In Figure 6-44*a*, the array slews from $-30°$ to $+30°$ thus passing through the nominal E Orientation. Figure 6-44*b* attempts to assess the effect of a large 90° maneuver, with the array initially in the LV,ON-plane and slewing to regain the nominal Orientation E, by comparison with the response in (*a*). Note, both the maneuvers are completed in 15 minutes, so the 90° slew represents both larger as well as faster rotation. As can be expected, the response is larger both in librational (pitch) and vibrational (panel tip deflection, $2u$) degrees of freedom, with a phase difference. However, essential character of the response remains virtually the same. It is of interest to recognize that the peak response is reached, in both the cases after the completion of the maneuver; and relatively earlier for the faster slew (Figure 6-44(*b*)).

Figure 6-45 investigates the effects of initial tip deflection and faster slew. The array slews from $-30°$ to $+30°$. The faster slew maneuver results in larger amplitude of the panel vibration, however, the pitch response remains essentially the same (Figure 6-45*c*).

Influence of the initial panel tip displacement during the slew maneuver is rather interesting. Note, the vibratory motion is essentially periodic with the initial disturbance as the amplitude. Its effect is to superpose very small amplitude, high frequency modulations on the pitch response (Figure 6-45(*b*)). This is in contrast to the response in Figure 6-45(*a*). Thus the vibratory response, when small, is modulated at the pitch frequency; however when relatively large, it modulates the pitch response at the vibration frequency.

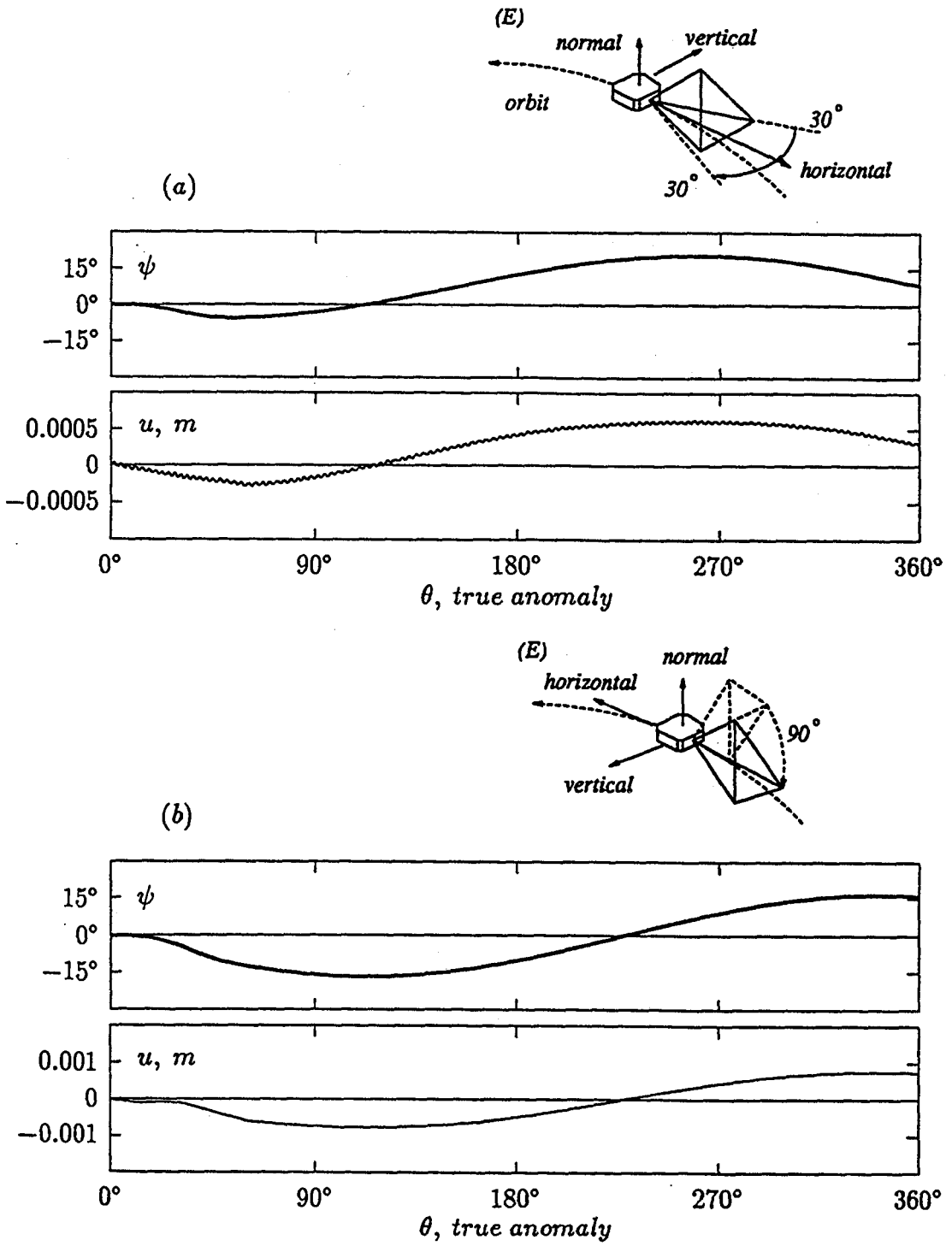

Figure 6-44 A comparative response study, for the Configuration E, to assess the effect of magnitude and speed of the slew maneuvers: (a) $-30°$ to $+30°$ slew passing through the nominal Orientation E; (b) $90°$ slew to occupy the nominal Orientation E, the array originally in the LV,ON-plane. Both the maneuvers are completed in 15 minutes.

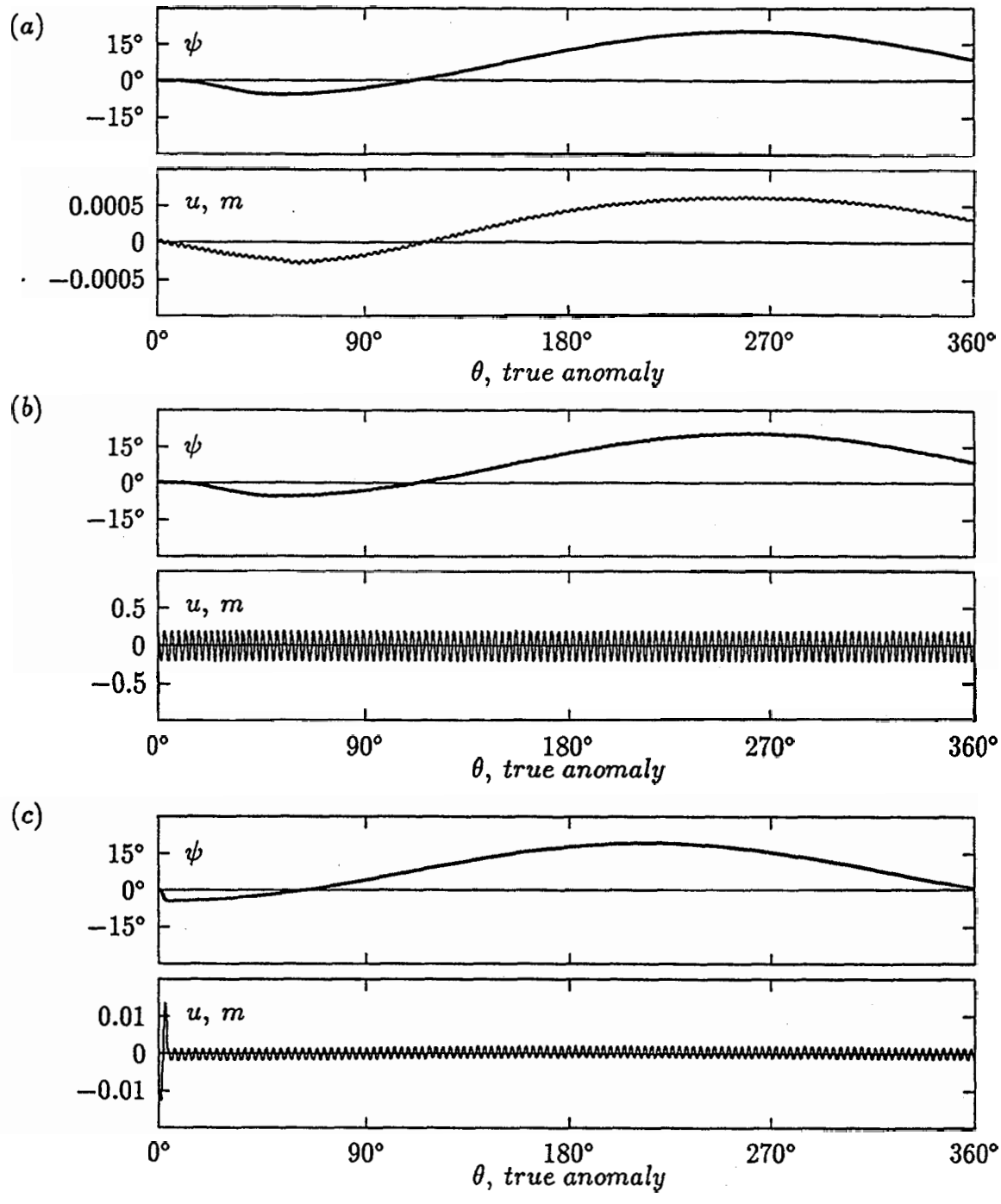

Figure 6-45 The system response during a slew maneuver from −30° to +30° passing through the nominal E Orientation in the orbital plane: (*a*) the maneu ver completed in 15 minutes; (*b*) effect of the initial 0.4 m tip deflection of the array during the maneuver; (*c*) the maneuver completed in 1 minute (in absence of the tip disturbance).

6.6 Conclusions

The main objective of this chapter was to investigate the influence of deployment and slew maneuvers on the system using three spacecraft of contemporary interest as examples. More significant and common features of the system performance as suggested by the results may be summarized as follows:

(a) The effect of deployment in the orbital plane is to induce pitch and inplane vibration due to the Coriolis effect. In general, the out-of-plane deployment, along the direction inclined to the orbit normal, excites all the three librational degrees of freedom as well as inplane and out-of-plane vibrations. As can be expected, no motion is excited when the spacecraft is in the stable Lagrangian configuration and the appendage deploys along the orbit normal.

(b) Slew maneuvers induce librational and vibrational motions. As in the case of deployment, inplane slew leads to inplane motions only, while the out-of-plane slew excites all the three librational as well as vibrational degrees of freedom.

(c) The vibrational response excited by deployment and slew maneuvers, in general, is small. For the cases considered, the tip deflection of the appendage varied in the range of a few millimeters to a couple of centimeters. This may appear small, however, can be quite critical depending on the mission objective. The vibrational response in the second mode is at least two orders of magnitude smaller and hence of little consequence.

(d) The deployment and slewing rates do not affect the librational response significantly. On the other hand, vibrational motion is accentuated by faster maneuvers. The magnitude of a slew maneuver has some effect on the response, however, the general trends remain essentially the same.

(e) The pitch response during the combined inplane deployment and slew maneuvers is essentially a synthesis of the two individual responses.

(f) Deployment and slew maneuvers change the ellipsoid of inertia of the spacecraft. The librational response after the maneuver is around the new equilibrium. In the new equilibrium, the appendages, if not aligned with the local vertical, local horizontal or orbital normal, will deform inducing the undesirable stresses.

7. CLOSING COMMENTS

7.1 Concluding Remarks

The objective of the thesis has been to develop a relatively general formulation and the associated computer code applicable to a large class of systems characterized by a rigid central body with flexible, deployable, slewing beam and/or plate type appendages. There is no restriction as to the number of appendages, their orientations and character of the orbit. The Lagrangian approach with its built-in advantages is used in the matrix form, introduced early during the formulation, which leads to relatively compact set of governing equations even for such a complex system. Such general approach to the problem has not been reported before and represents a versatile tool of far-reaching consequence.

As can be expected, the highly nonlinear, nonautonomous and coupled equations of motion, in general, do not admit any closed form solution. Furthermore, the governing equations as well as the numerical code developed for their integration have to be validated. Particular cases involving rigid as well as flexible systems are used to this end. Besides substantiating the equations of motion and the computer program, dynamical studies themselves, using the Liapunov direct method and Butenin's variation of parameter approach as applied to the systems considered, represent useful contributions to the field.

It should be emphasized that purpose of the thesis is not to generate vast amount of response data for a specific system, but to indicate the methodology in approaching studies aimed at dynamics of a large class of systems. Of course, with the formulation in hand and the program operational, it can easily provide the necessary design information pertaining to dynamics, if called upon. However, what is important is to recognize the potential of this versatile tool as demonstrated through its application to three different situations of contemporary interest. The objective here is to illustrate the capability of the algorithm in accounting for the interactions between librational and vibrational responses as affected by the orbital eccentricity, deployment and slew induced disturbances. Though preliminary in character, such studies

of the Space Shuttle and Space Flyer Unit represent important information that has not been reported in the literature.

A comment concerning the damping would be appropriate. It was purposely not included here as the damping model and its level are still a matter of controversy. Most of the damping information obtained so far has been through ground based experiments. The only on-orbit study during the NASA/Lockheed Solar Array Flight Experiment (SAFE, 1984) showed discrepancy ranging to several orders of magnitude! Once the accurate model is identified, it can be incorporated quite readily as a generalized force in the present formulation.

7.2 Recommendation for Future Work

Like many scientific pursuits, the thesis represents a small step in approaching the everwidening horizon of knowledge. Although it establishes a sound foundation, considerable challenge exists in building the superstructure. Some of the avenues for further studies, which are likely to be satisfying, are indicated below:

(a) Perhaps the following three items need immediate attention in terms of further generalizing the model:

  (i) inclusion of joint flexibility;

  (ii) specified translational motion (in addition to slew);

  (iii) torsional degree of freedom for the appendages (in addition to transverse vibrations).

(b) Environmental effects, particularly due to the free molecular reaction forces and solar radiation induced thermal deformations, can be significant and hence should be accounted for.

(c) In the case of the proposed Space Station, the central body (main mast) is indeed quite flexible. It would be useful to incorporate this aspect through further generalization of the model.

(d) Perhaps one of the most exciting aspects of the present study is its possible extension to an adaptive structure capable of assuming desired shape in space. By considering a series of deployable, slewing, connected links, each

one of a desired length, a robotic arm can be created to assume and track any spatial trajectory as indicated in Figure 7-1.

(e) A challenging extension of the above development could be to the closed loop system. This, of course, would involve introduction of appropriate constraint relations.

(f) Obviously, the final objective would be the control of this class of systems, once the dynamics is understood. Particularly attractive would be the control, using the Feedback Linearization Technique (FLT) accounting for the complete nonlinear dynamics. Control of even a simple slewing, deploying system has not been attempted yet. If successful, this would represent a major contribution towards evolution and utilization of adaptive structures in space.

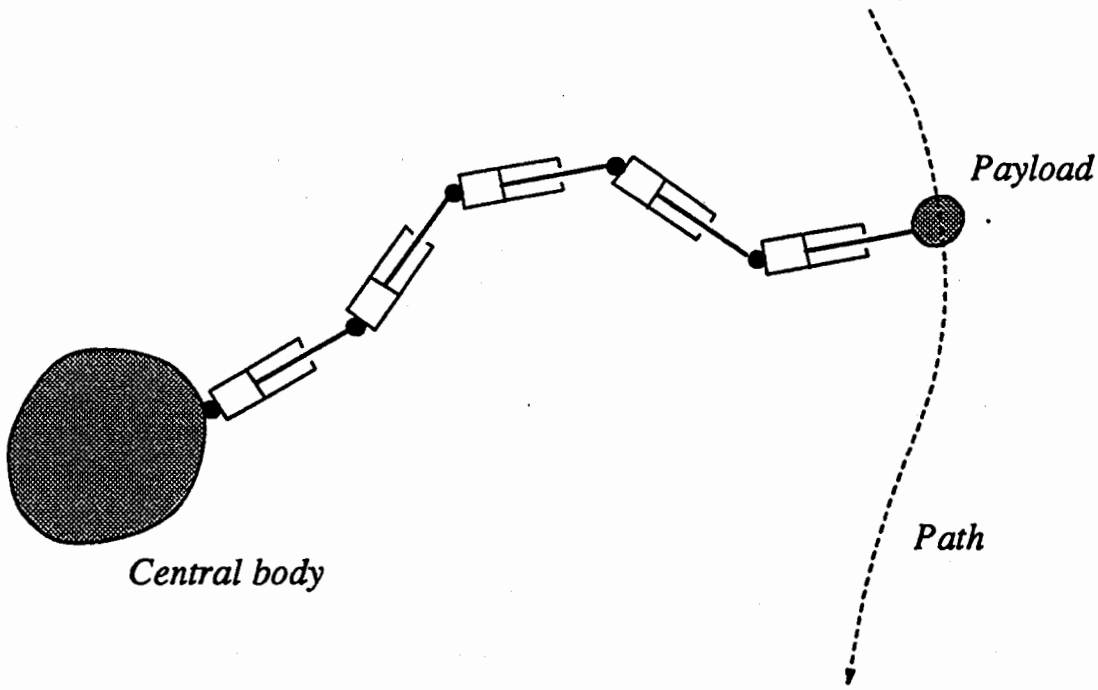

Figure 7-1 A schematic diagram of a robotic arm capable of assuming desired shape in space to track any spatial trajectory.

BIBLIOGRAPHY

[1] Hughes, P.C., *Spacecraft Attitude Dynamics*, John Wiley and Sons, New York, 1986, pp. 233–239, 246–248, 280–318.

[2] Roberson, R.E., "Two Decades of Spacecraft Attitude Control", *Journal of Guidance and Control*, Vol. 2, Jan.–Feb., 1979, pp. 3–8.

[3] Chetty, P.R.K., *Satellite Technology and its Application*, TAB Books Inc., U.S.A., 1988, pp. 64–78, 154–203, 264–284.

[4] Taylor, L., "The SCOLE Desigh Challenge—An Overview", *Proceedings of the 2nd Annual SCOLE Workshop*, Hampton, Virginia, Dec. 1985, NASA Publisher, pp. 1–13.

[5] Taylor, L., and Balakrislnan, A.V., "A Mathematical Problem and a Spacecraft Control Laboratory Experiment (SCOLE) Used to Evaluate Control Laws for Flexible spacecraft," *NASA/IEEE Design Challenge*, June 1984.

[6] Yu, E.Y., "A Long-Term Coupling Effects Between the Librational and Orbital Motions of a Satellite", *AIAA Journal*, Vol. 2, No. 3, March 1964, pp. 535–555.

[7] Likins, P., "Spacecraft Attitude Dynamics and Control-A Personal Perspective on Early Developments", *Journal of Gidance, Control and Dynamics*, Vol. 9, No. 2, March-April 1986, pp. 129–134.

[8] Modi, V.J., "Attitude Dynamics of Satellite with Flexible Appendages—A Brief Review", *Journal of Spacecraft and Rockets*, Vol. 11, No. 11, Nov. 1974, pp. 743–751.

[9] Modi, V.J., and Shrivastava, S.K., "Satellite Attitude Dynamics and Control in the Presence of Environmental Torques—A Brief Survey", *Journal of Guidance, Control and Dynamics*, AIAA, Vol. 6, No. 6, Nov.–Dec. 1983, pp. 461–471.

[10] Shrivastava, S.K., Tschann, C., and Modi, V.J., "Librational Dynamics of Earth Oriented Satellite—A Brief Review", *Proceedings of 14th Congress on Theoretical and Applied Mechanics*, Kurukshetra, India, 1969, pp. 284–306.

[11] Bainum, P. M., "A review of Modeling Techniques for the Open and Closed Loop Dynamics of Large Space Structures", *Large Space Structures: dynamics and Control*, Springer Series in Computational Mechanics, Editors: Atluri, S.N. and Amos, A.K., Springer-Verlag, Berlin, 1988, pp. 165–177.

[12] Lips, K.W., *Dynamics of a Large Class of Satellites with Deploying Flexible Appendages*, Ph.D. Thesis, The University of British Columbia, Sept. 1980.

[13] Ibrahim, A.M., *Mathematical Modelling of Flexible Multibody Dynamics with Applications to Orbiting Systems*, Ph.D. Thesis, The University of British Columbia, April 1988.

[14] Chan, J.K., *Dynamics and Control of an Orbiting Space Platform Based Mobile Flexible Manipulator*, M.A.Sc. Thesis, The University of British Columbia, April 1990.

[15] Ng, C.A., *Dynamics and Control of Orbiting Flexible Systems: A Formulation with Applications*, Ph.D. Thesis, The University of British Columbia, April 1992.

[16] Junkins, J.L., (Ed.) *Mechanics and Control of Large Flexible Structures*, AIAA Inc., Washington, D.C., 1990, pp. 3–16, 71–85, 349–371.

[17] Fletcher, H.J., Rongved, L., and Yu, E.Y., "Dynamic Analysis of a Two-Body Gravitationally Oriented Satellite", *Bell System Technical Journal*, Vol. 42, Sept. 1963, pp. 2239–2266.

[18] Hooker, W.W., and Margulies, G., "The Dynamical Attitude Equations for an n-Body Satellite", *The Journal of the Astronautical Science*, Vol. 12, No. 4, 1965, pp. 123–128.

[19] Roberson, R. E., and Wittenburg, J., "A Dynamical Formulation for an Arbitrary Number of Interconnected Rigid bodies, with reference to the problem of Satellite Attitude Control", *Proceedings of the Third Congress of the International Federation for Automotic Control*, London, Paper No. 46D, 1966.

[20] Wittenburg, J., "Nonlinear Equations of Motion for Arbitrary Systems of Interconnected Rigid Bodies", *Proceedings of the Symposium on Dynamics of Multibody Systems*, IUTAM, Munich, Germany, Aug.–Sept. 1977, Editor: K. Magnus, Spinger-Verlag, 1978.

[21] Shen, Q., "Formulation of Equations of Motion for Multi-Rigid-Body Systems", *Acta Mechanica Sinica*, No. 3, May 1983, pp. 259–266.

[22] Hooker, W.W., "Equations of Attitude Motion of a Topological Tree of Bodies, the Terminal Members of which may be Flexible", Technical Report LMSC-D354938, Lockheed Missles and Space Company, 1973.

[23] Hooker, W.W., "Equations of Motion for Interconnected Rigid and Elastic Bodies: A Derivation Independent of Angular Momentum", *Celestial Mechanics*, Vol. 11, No. 1, 1975, pp. 337–359.

[24] Likins, P.W. "Dynamics and Control of Flexible Space Vehicles", Technical Report 32–1329, Jet Propulsion Laboratory, 1970.

[25] Likins, P.W., "Dynamic Analysis of a System of Hinge Connected Rigid Bodies With Flexible Appendages", *International Journal of Solids and Structures*, Vol. 9, 1973, pp. 1473–1487.

[26] Ho, J.Y.L., "Direct Path Method for Flexible Multibody Spacecraft Dynamics", *Journal of Spacecraft and Rockets*, Vol. 14, No. 2, Feb. 1977, pp. 102–110.

[27] Hughes, P.C., "Dynamics of a Chain of Flexible Bodies", *The Journal of the Astronautical Sciences*, Vol. 27, No. 4, Oct.–Dec. 1979, pp. 359–380.

[28] Hughes, P.C., "Deployment Dynamics of the Communication Technology Satellite—A progress Report", *Proceedings of ESA Symposium on Dynamics and Control of Non-Rigid Spacecraft*, ESA SP 117, 1976, pp. 335–340.

[29] Lips, K.W., and Modi, V.J., "Transient Attitude Dynamics of Satellites with Deploying Flexible Appendages", *Acta Astronautica*, Vol. 5, No. 10, 1978, pp. 797–815.

[30] Ibrahim, A.M., and Misra, A.K., "Attitude Dynamics of a Satellite During Deployment of Large Plate-Type Structures", *Journal of Guidance, Control and Dynamics*, Vol. 5, No. 5, Sept.–Oct. 1982, pp. 442–447.

[31] Modi, V.J., and Ibrahim, A.M., "A General Formulation for Librational Dynamics of Spacecraft with Deploying Appendages", *Journal of Guidance, Control and Dynamics*, Vol. 7, No. 5, Sept.–Oct. 1984, pp. 563–569.

[32] Ibrahim, A.M., and Modi, V.J., "On the Orbiter Based Deployment of Flexible Members", *36th Congress of the International Astronautical Federation*, Stockholm, Sweden, Paper No. IAF–85–230; also Acta Astronautica, Vol. 13, No. 10, 1986, pp. 319–331.

[33] Turner, J. D., and Junkins, J. L., "Optimal Large-Angle Single Axis Rotational Maneuver of Flexible Spacecraft", *Journal of Guidance and Control*, Vol. 3, No. 6, 1980, pp. 578–585.

[34] Mah, H.W., and Modi, V.J., "Dynamics and Control During Slew Maneuvers", *Acta Astronautica*, Vol. 19, No. 2, 1989, pp. 125–143.

[35] Meirovitch, L., and Quinn, R.D., "Equations of Motion for Maneuvering Flexible Spacecraft", *Journal of Guidance, Control and Dynamics*, Vol. 10, No. 5, Sept.–Oct. 1987, pp. 453–465.

[36] Meirovitch, L., and Kwak, M.K., "On the Maneuvering and Control of Space Structures", in *The Dynamics of Flexible Structures in Space*, C.L. Kirk and J.L. Junkins (eds.), Springer Verlag, Berlin, 1990, pp. 3–17.

[37] Huston, R.L., and Passarello, C.E., "Multibody Structural Dynamics Including Translation Between the Bodies", *Computers and Structures*, Vol. 12, No. 5, Nov. 1980, pp. 713–720.

[38] Modi, V.J., and Ibrahim, A.M., "Dynamics of the Orbiter Based Construction of Structural Components for Space Platform", Acta Astronautica, Vol. 12, No. 10, 1985, pp. 879–888.

[39] Spenny, C.H., and Williams, T.E., "Librational Instability of Rigid Space Station Due to Translation of Internal Mass", *Journal of Guidance, Control and Dynamics*, Vol. 14, No. 1, 1991, pp. 31–35.

[40] Hooker, W.W., "A Set of r Dynamical Attitude Equations for an Arbitrary n-Body Satellite having r Rotational Degrees of Freedom", *AIAA Journal*, Vol. 8, No. 7, July 1970, pp. 1205–1207.

[41] Russell, W.J., "On the Formulation of Equations of Rotational Motion for a n-Body Spacecraft", Report TR–0200 (4133)–2, 1969, Aerospace Corp., EI Segundo, CA, U.S.A.

[42] Frisch, H.P., "A Vector-Dyadic Development of the Equations of Motion of N Coupled Rigid Bodies and Point Masses", NASA TN D–7767, Oct. 1974.

[43] Wu, Z., *Analytical Mechanics*, Shanghai Jiaotong University, 1984, pp. 44–49.

[44] Kane, T.R., and Wang, C.F., "On the Derivation of Equations of Motion", *Journal of the Society for Industrial and Applied Mathematics*, Vol. 13, 1965, pp. 487–492.

[45] Huston, R.L., "Multibody Dynamics Formulations via Kane's Equations", *AIAA Dynamics Specialist Conference*, Long Beach, CA, U.S.A., April 1990, Paper No. AIAA–90–1248–CP.

[46] Ibraham, A.M., and Modi, V.J., "A Formulation for Studying Dynamics of N Connected Flexible Deployable Members", *Acta Astronautica*, Vol. 16, 1987, pp. 151–164.

[47] Modi, V.J., and Ng, A.C., "Dynamics of Interconnected Flexible Members in the Presence of Environmental Forces: A Formulation with Applications", 39th Congress of the International Astronautical Federation, Bangalore, India, Oct. 1988, Paper No. IAF–88–318; also *Acta Astronautica*, Vol. 19, No. 6/7, 1989, pp. 561–571.

[48] Kane, T.R., and Levinson, D.A., "Formulation of Equations of Motion for Complex Spacecraft", *Journal of Guidance and Control*, Vol. 3, No. 2, March–April 1980, pp. 99–112.

[49] Shen, Q., *Derivation of Equations of Motion for Multi-Rigid-Body Systems*, M.Eng. Thesis, Beijing University of Aeronautics and Astronautics, Dec. 1981.

[50] Prescott, J., *Applied Elasticity*, Dover Publications Inc., New York, 1924, pp. 204–209.

[51] Hughes, P.C., "Space Structrue Vibration Modes: How Many Exist? Which Ones Are Important?", *Proceedings of the Workshop on Applications of Distributed System Theory to the Control of Large Space Structures*, Jet Propulsion Laboratory, California Institute of Technology, Pasadena, CA, U.S.A., TR 83–46, 1983, pp. 31–47.

[52] Kim, S.S., and Haug, E.J., "Selection of Deformation Modes for Flexible Multibody Dynamics", *Mechanics of Structure and Machine*, Vol. 18, No. 4, 1990, pp. 565–586.

[53] Spanos, J.T., and Tsuha, W.S., "Selection of Component Modes for Flexible Multibody Simulation", *Journal of Guidance, Control and Dynamics*, Vol. 14, No. 2, 1991, pp. 278–286.

[54] Modi, V.J., and Suleman, A., "System Modes and Dynamics of the Proposed Space Station Type Configuration", *Dynamics of Flexible Structures in Space*, Eds: Kirk, C.L., and Junkins, J.L., Computational Mechanics Publications, Springer-Verlag, 1990, pp. 645–659.

[55] Schiehlen, W., *Multibody Systems Handbook*, Spinger-Verlag, Berlin Heidelberg, 1990.

[56] Ho, J.Y.L., Herber, D.R., Clapp, B.R., and Schultz, R. J., "ALLFLEX Program—Simulation Methodology", *Proceedings of the Workshop on Multibody Simulation*, JPL, Pasadena, CA, U.S.A., April 1988, Editors: G. Man and R. Laskin, Report No. JPL D–5190, Vol. 2, pp. 811–856.

[57] Frisch, H.P., "A Digital Computer Program for the Dynamic Interaction Simulation of Controls and Structures", *Proceedings of the Workshop on Multibody Simulation*, JPL, Pasadena, CA, U.S.A., April 1988, Editors: G. Man and R. Laskin, Report No. JPL D–5190, Vol. 2, pp. 478–481.

[58] Sherman, M., "SD/EXACT and SD/FAST—Symbolic Manipulation Codes", *Proceedings of the Workshop on Multibody Simulation*, JPL, Pasadena, CA,

U.S.A., April 1988, Editors: G. Man and R. Laskin, Report No. JPL D-5190, Vol. 2, pp. 692–726.

[59] Singh, R.P., and Vandervoort, R.J., "Dynamics of Flexible Bodies in Tree Topology—A Computer Oriented Approach", *Journal of Guidance, Control and Dynamics*, Vol. 8, No. 5, Sept.–Oct. 1985, pp. 584–590.

[60] Mah, H.W., Modi, V.J., Morita, Y., and Yokota, H., "Dynamics during Slewing and Translational Maneuvers of the Space Station Based MRMS", *The Journal of the Astronautical Sciences*, Vol. 38, No.4, 1990, pp. 557–579.

[61] Modi, V.J., and Misra, A.K., "On Deployment Dynamics of Tether Connected Two-Body Systems", *Acta Astronautica*, Vol. 6, No.9, 1979, pp. 1183–1197.

[62] Modi, V.J., Ng, A.C., and Suleman, A., "Dynamics of Orbiting Multibody Systems: A Formulation with Application", AIAA 32nd Structures, Structural Dynamics, and Materials Conference, Baltimore, MD, April 1991.

[63] Morita, Y., and Modi, V.J., "Dynamics of a Flexible Orbiting Platform with MRMS", Report No. 625, The Institute of Space and Astronautical Science, Tokyo, Feb. 1988.

[64] Ng, A.C., *Dynamics of Gravity Oriented Axi-Symmetric Satellites with Thermally Flexed Appendages*, M.A.Sc. Thesis, Department of Mechanical Engineering, University of British Columbia, Nov. 1986.

[65] Golla, D.F., Buhariwala, K.J., Hughes, P.C., and D'eleuterio, G.M.T., "Efficient Algorithms for the Dynamical Simulation of Structurally Flexible Manipulators", *Transections of the Canadian Society for Mechanical Engineers*, Vol. 13, No. 4, 1989, pp. 97–102.

[66] Butenin, N.Y., *Elements of Nonlinear Oscillations*, Blaisdell, New York, 1965, pp. 102–137, 201–217.

[67] Wittenburg, J., *Dynamics of Systems of Rigid Bodies*, B.G. Teubner Publisher, Stuttgart, Germany, 1977, pp. 19–31.

[68] Likins, P.W., and Roberson, R.E., "Uniqueness of Equilibrium Attitudes for Earth Pointing Satellite", *The Journal of the Astronautical Sciences*, Vol. 13, No. , 1966, pp. 87–88.

[69] Karapetyan, N.V., "Stability of Steady Motions of Systems of a Certain Type", *Mechanics of Solids*, Vol. 18, No. 2, 1983, pp. 41–47.

[70] Yu, E.Y.,"Optimum Design of a Gravitationally Oriented Two-Body Satellite", The Bell System Technical Journal, Vol. 44, Jan. 1965, pp. 49–76.

[71] Gao, W., *Stability of Motion*, Beijing University of Aeronautics and Astronautics, 1984, pp. 297–316, 331–346.

[72] Soudack, A C., Modi, V.J., Ng, A.C., "Analytical Solution of a Gravity Gradient Axisymmetric Satellite in Eccentric Orbits", *International Journal of Control*, Vol. 50, No.6, 1989, pp. 2187–2203.

[73] Kryloff, N., and Bogoliuboff, N., *Introduction to Nonlinear Mechanics*, Princeton University Press, Princeton, 1947, pp. 8–14, 79–87.

[74] Kalaycioglu, S., and Misra, A.K., "Approximate Solutions for Vibrations of Deploying Appendages" *Journal of Guidance, Control and Dynamics*, Vol. 14, No. 2, March–April, 1991, pp. 287–293.